1969

Studies of solid compounds of group IV and V transition metals formed at high temperature: I. The crystal structures of Ti2S, Nb21S8, and Nb2Se; II. The metal-rich region of the zirconium-sulfur system

Bruce Randolph Conard
Iowa State University

This dissertation has been
microfilmed exactly as received 70-7683

CONARD, Bruce Randolph, 1942-

Iowa State University, Ph.D., 1969
Chemistry, physical

University Microfilms, Inc., Ann Arbor, Michigan

STUDIES OF SOLID COMPOUNDS OF GROUP IV AND V TRANSITION METALS FORMED AT HIGH TEMPERATURE

I. THE CRYSTAL STRUCTURES OF Ti_2S, $Nb_{21}S_8$, AND Nb_2Se

II. THE METAL-RICH REGION OF THE ZIRCONIUM-SULFUR SYSTEM

by

Bruce Randolph Conard

A Dissertation Submitted to the
Graduate Faculty in Partial Fulfillment of
The Requirements for the Degree of
DOCTOR OF PHILOSOPHY

Major Subject: Physical Chemistry

Approved:

Signature was redacted for privacy.

In Charge of Major Work

Signature was redacted for privacy.

Head of Major Department

Signature was redacted for privacy.

Dean of Graduate College

Iowa State University
Of Science and Technology
Ames, Iowa

1969

TABLE OF CONTENTS

LIST OF TABLES

List of Tables (Continued)

List of Tables (Continued)

List of Tables (Continued)

List of Tables (Continued)

LIST OF FIGURES

List of Figures (Continued)

List of Figures (Continued)

List of Figures (Continued)

List of Figures (Continued)

List of Figures (Continued)

PREFACE

The crystalline state of matter, from snowflakes in our infancy to gold or diamonds in our youth, has amazed men for centuries. This thesis concerns the solid state of matter. Specifically, the research was performed to prepare and to characterize new solid compounds of titanium, zirconium, and niobium. More specifically, the investigations reported here concern metal-rich chalconide compounds; "metal-rich" means that the number of metal atoms in the compound is approximately equal to or is greater than the number of chalcogen atoms, and the word "chalcogen" refers to the family of elements sulfur, selenium, and tellurium.

The thesis is in two parts. The first chapter of Part I, the Introduction, is intended also to serve as an introductory chapter for Part II. This introduction discusses the general techniques used in the investigations, namely, high temperature techniques in preparative work and x-ray diffraction techniques in the characterization of the compounds. The remarks in the introduction regarding x-ray diffraction and, in particular, crystal structure analysis, are necessarily brief and incomplete; they are included so that the neophyte might understand the overall procedure rather than being included to elucidate experimental and theoretical details, items which are adequately discussed in many texts on this subject. Chapters II, III and IV discuss the structure determinations and possible bond-

ing interpretations for Ti_2S, $Nb_{21}S_8$, and Nb_2Se, respectively. Other metal-rich chalconide compounds are reviewed in these chapters.

Part II presents a discussion of results obtained in an investigation of the metal-rich region of the Zr-S system. The discussion of this system, however, is based upon the proposed bonding interpretations presented in the previous chapters and, for that reason, is not exclusive. Indeed, just the opposite is true: the two parts of the thesis may be viewed as being dependent with regard to the interpretation of results, but they are organized so as to reflect differences in scope.

The last chapter proposes further research activities to broaden the understanding and applicability of the bonding interpretations suggested herein and to survey other metal-rich compounds which are structurally related to the chalconides.

The author wishes to express his gratitude to Dr. H. F. Franzen who consistently and enthusiastically provided stimulation, advice, help and friendship during the course of this research.

The author is indebted to many of the personnel of the Ames Laboratory, particularly: James Owens, who obtained the data for Ti_2S and who performed much of the superposition work on that structure; Joseph Graham for his initial x-ray work on Nb_2Se and Lars-Johan Norrby for his help in determining the structure of Nb_2Se; Vernon DeJong who first prepared $Nb_{21}S_8$; Harlan Baker who photographed the single crystals; Donald

Bailey and James Benson for their advice in the procedural details of data collection; and members of Dr. Fitzwater's and Dr. Jacobson's groups who helped in computer orientation: Peter Hansen, Al Schlueter, Dale Nimrod, Don Dahm, Marv Hackert, Jim Rodgers and others.

Also, the author wants to express appreciation to the members of Dr. Franzen's high temperature laboratory who provided both working and recreational atmospheres which were truly enjoyable.

The most difficult acknowledgment results from the most subtle but most significant influence in this work: for Audrey, whose understanding and devotion is beyond description.

PART I. THE CRYSTAL STRUCTURES OF Ti_2S, $Nb_{21}S_8$, AND Nb_2Se

I. INTRODUCTION

A. High Temperature Techniques

The high temperatures used in this work to prepare several new metal-rich compounds were between 1000-2000°C. The majority of attempts by previous investigators to synthesize metal-rich compounds at temperatures lower than 1000°C resulted in failure, e.g., see work on the Zr-S system by Strotzer, et al. (1). It is important to try to understand why low temperature methods failed.

One possible reason for the failure was that at temperatures of about 500-1000°C the rate of diffusion of the non-metal into the metal or metal-rich phase was too low to attain equilibrium within an experimentally feasible time. Some workers recognized that higher temperatures were needed to reach equilibrium, but they were plagued at temperatures over 1000°C with interaction of samples with the silica reaction containers. For example, in a study of the Ti-S system by Bartram (2), Ti reacted with a fused silica tube container to yield Ti_5Si_3 and Ti_2O_3 as products, resulting in serious contamination of the sulfide product.

Another possible reason for the failure of low temperatures in the preparation of a metal-rich phase was that, at equilib-

rium, the standard change in Gibbs free energy for metal-rich compound formation from the metal and a more non-metal-rich phase was positive.

$$\Delta F^{o} = \Delta H^{o} - T\Delta S^{o} \qquad (1)$$

For positive changes in standard enthalpy and standard entropy and low temperatures, ΔF^{o} would be positive and the equilibrium so established would favor the reactants. However, for an increase in temperature, a temperature might be reached such that the entropy term would become dominant and the change in the standard free energy would be negative, resulting in an equilibrium which would favor the products. The metal-rich phases so formed, if this were the case, would be higher entropy and higher energy phases than the reactant phases. Thermodynamic data for metal-rich chalconides are at present lacking and, consequently, the changes in heats and entropies for formation are unknown. A definite answer to the question as to whether the compounds are unstable with respect to disproportionation at low temperatures will have to await further work, but the results of structure determinations of several of these chalconides (see below) show that many metal-rich phases have high coordination of metal and of non-metal atoms and, in addition, have narrow ranges of solid solution, both of which suggest that they are not high entropy phases.

The technical problems in this work were (a) to achieve sufficiently high temperature environments, (b) to measure the temperature accurately, and (c) to contain the samples in inert environments during the high temperature treatments. The first problem was handled by inductively heating a metal crucible using high frequency current; the second problem was surmounted by optical pyrometric temperature measurement with $\pm 5^{\circ}$ precision at $1500^{\circ}C$. The third problem was solved for most cases in this work by using tungsten as the container material under high vacuum but, as will be discussed in detail in Chapter V, to avoid the formation of W_2Zr in the metal-rich zirconium sulfide preparations, a zirconium liner for the tungsten container was used.

A schematic diagram of the vacuum line used in the preparation of the metal-rich compounds is shown in Figure 1. The oil diffusion pumps used were capable of maintaining 10^{-6}- 10^{-7} mmHg residual pressure. The work coil was 1/4" copper tubing with 11 turns. A Lepel High Frequencies Laboratories, Inc., unit was used to drive the coil. A diagram of the tungsten crucible used to contain 0.5-1.0 gram samples is shown in Figure 1. The pyrometer used to measure the temperature of the crucible was a Leeds and Northrup three-scale instrument which was calibrated at Argonne National Laboratory using a procedure described in Appendix A; the calibration curves for the three scales also appear in Appendix A.

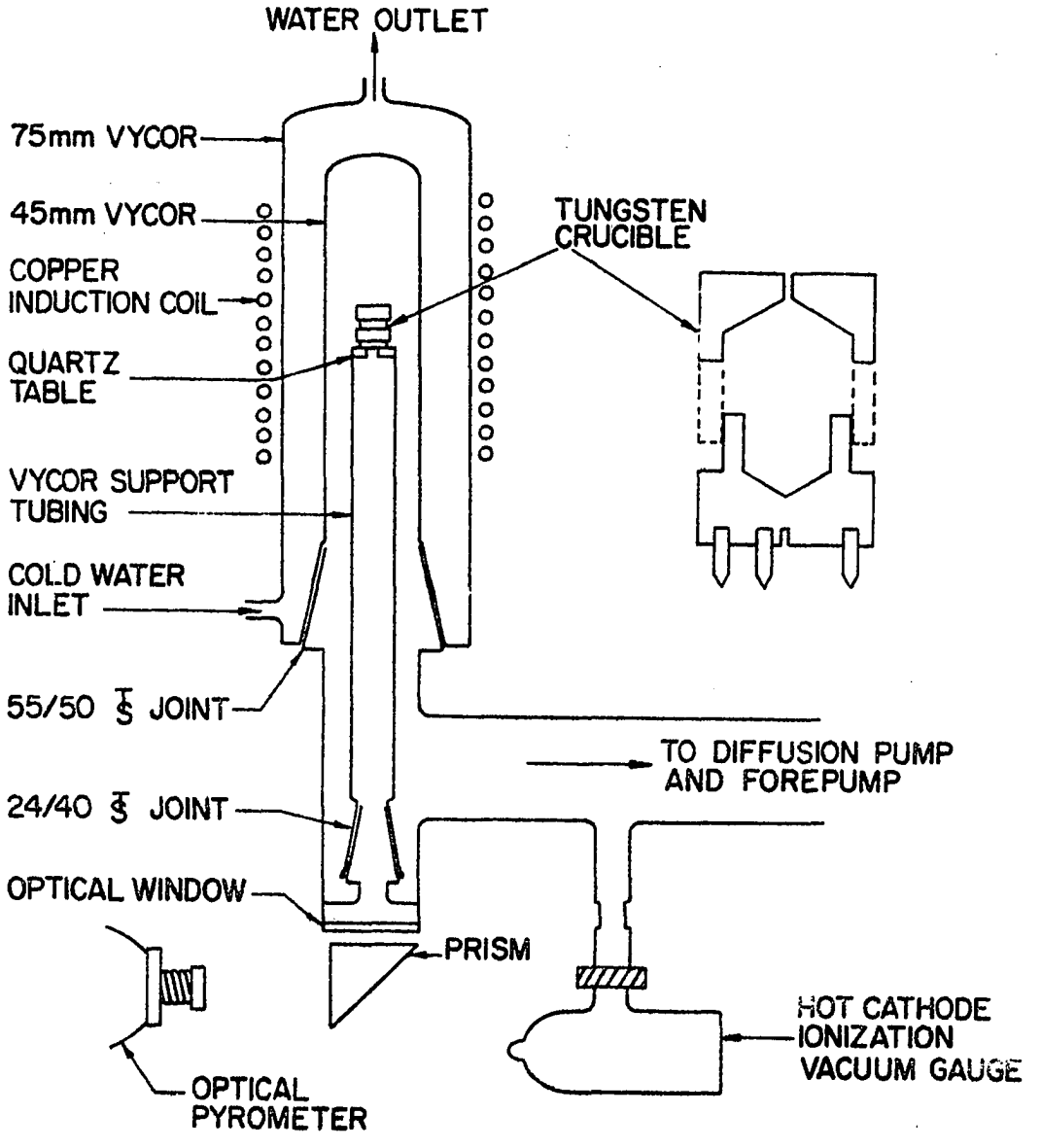

Figure 1. Schematic diagram of vacuum line used for high temperature annealing treatments

The general procedure used in this work for the preparation of the metal-rich chalcogen compounds is given below. More specific conditions are considered for each in their respective sections.

The metal bars or sheets were filed under an argon atmosphere with coarse, clean files. A strong magnet was used to remove file chips from the metal filings. The metal filings and the elemental sulfur or selenium were weighed for the desired atomic ratios of Ch/M, Ch/M = chalcogen at. %/metal at. %, and were inserted into Vycor tubes. The tubes were evacuated to about 50 microns residual pressure, sealed, and placed in a furnace at 400-500°C until the chalcogen vapor was no longer visible in the tubes. The purpose of these low temperature reactions was merely to cause the chalcogen to enter into a combined state with the metal. The products of these reactions were generally polyphasic and were characterized as higher sulfides coating the metal filings.

The polyphasic samples which resulted from the reaction at 400-500°C were pelletized to aid in the diffusion of the components, were placed in the tungsten container in a vacuum and were annealed at high temperature. The equilibrium or near equilibrium states achieved at high temperatures were brought to room temperature by rapid cooling of the crucible, primarily by radiative heat loss.

The possibility of attaining an equilibrium state within an hour or two varied for the various systems and compositions under study. Usually a lack of equilibrium was indicated by the presence of more than two phases in the product of a high temperature treatment. The Gibbs Phase Rule limits the number of phases which may coexist in equilibrium to two for a two-component bivariant system. That is,

$$f = c - p + 2, \qquad (2)$$

where f is the number of independent intensive variables, c is the number of components in the system, and p is the number of phases in the system. For a two-component system in which there are two independent variables (T and X), then $p=2$. The compounds prepared in this work, due to the high temperature of preparation, are probably in equilibrium with respect to change of phase.

Arc-melting was also used to prepare samples. These syntheses were made using a water-cooled Cu hearth and a W electrode contained in an Ar-He atmosphere. Reproducible conditions were difficult to achieve using the arc-melter due to the fact that the temperature used for the melting and the rate of cooling of the sample after melting were not measured or precisely controlled.

B. X-ray Diffraction Techniques

There are excellent texts available which treat both theoretical and practical problems of x-ray crystallography, e.g. Buerger (3), Crystal Structure Analysis and Stout and Jensen (4), X-Ray Structure Determination. In addition to referencing these texts, it is desirable to present a survey of the experimental techniques and interpretive procedures to be encountered in this thesis.

A three-dimensional solid acts like a three-dimensional diffraction grating for electromagnetic radiation of wavelength of the same order of magnitude as the distances between electron density maxima in the solid. The condition under which diffracted radiation in particular directions constructively interferes is

$$\lambda = 2d_{hk\ell}\sin\theta, \tag{3}$$

which is Bragg's Law. This equation relates the angle of diffraction, θ, from a set of equidistant parallel planes of electron density within the crystal to the distance between the planes and the wavelength of the radiation. The position of the diffracted beam is 2θ degrees from the undiffracted primary beam and is dependent only on λ and $d_{hk\ell}$. The convention for indexing planes in a unit cell is according to Miller indices.

The intensity of the diffracted radiation is dependent on the amount and distribution of electron density within the unit

cell. A factor proportional to the square root of the intensity, called the structure factor, is given by

$$F(hk\ell) = \sum_{j=1}^{N} f_j e^{2\pi i(hx_j+ky_j+\ell z_j)}, \qquad (4)$$

where F is indexed by the set of planes which are in diffracting position, i.e., which fulfill the Bragg condition, f_j is the scattering factor of the j^{th} atom located at fractional coordinates x_j, y_j, z_j, and the summation is over all atoms, N, in the unit cell.

The structure factors are Fourier transforms of the electron density.

$$\varrho(XYZ) = \frac{1}{V} \sum_{hk\ell} \sum \sum F(hk\ell) e^{-2\pi i(hX+kY+\ell Z)}. \qquad (5)$$

In order to obtain the electron density one must know both the magnitude and the phase of $F(hk\ell)$. The phase problem in crystallography arises from the fact that $F^2(hk\ell)$ is proportional to the intensity, which is the quantity observed, but that the phase of $F(hk\ell)$ is not experimentally observed.

1. Powder methods

X-ray investigation of solids is usually carried out on powder samples or single crystal samples.

In a powdered crystalline sample equivalent sets of planes are randomly oriented. Since the radiation diffracted by the sample is dependent only on $d_{hk\ell}$ and λ, the rays diffracted by a given set of planes define the surface of a cone with the

apex of the cone at the sample and the apical angle equal to 4θ. The portion of the diffracted radiation which is intercepted by a cylindrical film appears as a curved line.

a. Debye-Scherrer method The geometry of the Debye-Scherrer camera is as follows. The powder sample is attached to a rotatable mount in the middle of a cylinder of specified radius. The diffracted radiation is recorded for $0 < \theta < 90^{\circ}$ by a film wrapped on the inside of the cylinder. In the high θ region, $0<45^{\circ}$, separation of K_{α_1} and K_{α_2} radiation is observed. Many of the samples prepared in this research, however, had diffuse lines in the high θ region and therefore accurate lattice parameters were not obtained using this method. The Debye-Scherrer method was used primarily for identification of solid phases.

b. Guinier method For accurate lattice parameter determination in this work, the Guinier powder photographic method was employed. The geometry of the camera is different from that of the Debye-Scherrer. A thin layer of powdered sample is placed on a piece of clear tape in a rotating holder which is located on the circumference of a cylindrical film. The primary x-ray beam is monochromatized by a bent quartz crystal before striking the sample. Low angle, $0<\theta<50^{\circ}$, diffraction lines are recorded on the film. A primary beam is also exposed on the film, together with a scale, so that the diffraction angle may be measured to within $\pm 0.01^{\circ}$. To account for shrinkage of film

in developing, an internal standard may be mixed with the powder sample. The internal standard used in this work was KCl, $\underline{a}$=6.2930Å at 25°C, as determined by Hambling (5).

2. Single crystal methods

A single crystal which is bathed completely by a beam of x-radiation gives rise to diffracted x-ray beams, the directions of which are dependent on λ and $d_{hk\ell}$ and the intensities of which are dependent upon the placement and kind of atoms within the crystal. The collection of single crystal x-ray data is the term used to describe the procedure of measuring the intensities of the diffracted radiation.

a. The concept of the reciprocal lattice A convenient geometrical construct used in crystallography is the reciprocal lattice. It is defined as the lattice of points described by the endpoints of vectors which originate at a common origin, are directed normal to all possible sets of planes ($hk\ell$), and which have respective magnitudes of $1/d_{hk\ell}$. Thus, planes in real space (crystal space) are represented as points in reciprocal space.

The convenience of the reciprocal lattice is found in the relation

$$\sin \theta = \frac{\lambda}{2} d^*, \quad d^* = \frac{1}{d} \tag{6}$$

which is a direct proportionality between the length of the reciprocal lattice vector and the sine of the Bragg angle. It is also convenient to view the reciprocal lattice in conjunction

with a "sphere of reflection", defined as an imaginary sphere of radius $1/\lambda$. It is shown in standard texts (4) that if the "sphere of reflection" is imagined such that the real crystal is at its center and the origin of the reciprocal lattice is on the surface of the sphere at the point where the primary x-ray beam exits the sphere, then the condition for diffraction is met when a reciprocal lattice point lies on the surface of the sphere and the diffracted beam is in the direction of a line drawn from the crystal to the reciprocal lattice point on the surface of the sphere.

b. Photographing the reciprocal lattice The Weissenberg and Buerger precession cameras are instruments used for recording the intensities of diffracted radiation which, as discussed above, can be associated with reciprocal lattice points. Both cameras rotate an otherwise stationary crystal and move a photographic plate to obtain many intensities on one record. The Weissenberg instrument records reciprocal lattice layers which are perpendicular to a rotation axis of the real crystal. For example, if the crystallographic c axis coincides with the rotation axis, then it is possible to photograph hk0, hk1, hk2, etc., layers. The term "alignment" is used to describe the procedure whereby a real crystallographic axis is made to coincide with the rotation axis of the crystal. The Buerger precession instrument, on the other hand, photographs reciprocal lattice layers which are parallel to the rotation axis.

The intensities of diffracted radiation on photographs are estimated either with a densitometer or by visual comparison with a standard set of intensities. Photographic data collection was employed as a part of all single crystal studies described in this thesis, except $Zr_{1-x}S$.

c. Recording intensities by scintillation counter methods

A single crystal orienter (SCO) is an instrument used to position a crystal by means of four space variables such that a scintillation detector may measure the intensity of the diffraction maxima by scanning in θ or 2θ. An equatorial plane of the SCO is defined by the x-ray source, the crystal and the detector, and the crystal is positioned for each measurement so as to bring the diffracted beam into the equatorial plane. For a manually operated SCO the only motor drive on the instrument is the detector 2θ drive. The positioning of the crystal is done by manual adjustment. Standard maxima are usually monitored periodically during the data collection so that a correction for x-ray tube intensity drift or crystal shift may be made. This technique of data collection was used in the determination of the structures of $Nb_{21}S_8$ and $Zr_{1-x}S$.

Another more recent innovation in data collection is to have all manual operations described above done automatically by utilization of a computer and computer-to-diffractometer interface. In this case routines may be programmed for finding maximum intensities of three diffracted beams, for calculating other diffracting positions, for moving the four space coor-

dinates to properly position the diffraction maxima, for scanning the maxima and for checking the standard peaks and recalculating diffracting positions periodically. A Hilger-Watts four circle device coupled to an SDS 910/1401 computer was made operational by Dahm, Benson, Nimrod, Fitzwater, and Jacobson (6). This device was used for the Nb_2Se data collection.

d. Solution of the phase problem The intensities of diffracted radiation are generally corrected for absorption and polarization effects to obtain values of F_{obs}, the observed magnitudes of the structure factors.

To construct the electron density as observed via the experimental intensities one needs to know the sign of the $F(hk\ell)$ for a centrosymmetric structure. Basically two methods for obtaining signs of structure factors were used in this work: superposition techniques and direct method techniques. The superposition technique is explained briefly in connection with the solution of the crystal structure of Ti_2S, Chapter II. The direct method, applied to both $Nb_{21}S_8$ and Nb_2Se, is described in Chapter III.

e. Refinement The parameters which describe the positions of atoms in the unit cell and the thermal motion of the atoms are usually obtained by fitting the observed quantities, F_o, to calculated quantities, F_c, by a least squares procedure. The function minimized is $D = \sum_{hk\ell} w_{hk\ell} \left(|F_o| - k|F_c| \right)^2$, where $w_{hk\ell}$ is the weight of observation $F_o(hk\ell)$ and k is a scale

factor. Depending upon the complexity of the structure (number of variable parameters), the initial parameters (the trial structure) must be more or less close to those of the refined structure in order for the refinement to converge in less than five cycles, and the most suitable number of observations to be used in the refinement is about ten times the number of parameters being varied.

Structures for which there is no evidence of extensive defects usually are refined by varying atomic positions, either isotropic or anisotropic temperature factor coefficients, and the scale factor. In the refinement of structures which occur over a wide range of solid solution, however, one also has to take into account the number of vacancies or interstitial atoms in the unit cell. In this research two non-stoichiometric compounds were investigated.

One of the compounds was ZrS_{1-x} which has a randomly distributed number of vacancies which can be accounted for by a simple fractional multiplier in the expression for F_c. The second compound investigated was $Zr_{1-x}S$, x=0.33, which has Zr vacancies as defects. In this second case the vacancies are ordered in three dimensions such that the lattice repeat distances are longer and the symmetry of the structure is different from that for the stoichiometric compound, ZrS. $Zr_{0.77}S$ is a superstructure of the ZrS structure, where by superstructure is meant a structure for which the space group of the atom posi-

tions, termed the substructure space group, is different from the space group of the structure arising from the incomplete occupancy of one or more atom positions. The superstructure has additional diffraction maxima relative to the fundamental (or substructure) maxima due to the changes in repeat distances and electron density. The additional maxima are called superstructure reflections; the parent structure gives rise to substructure reflections. The refinement of superstructures may involve independent fractional occupancy parameters for independent atom positions.

An indication of the accuracy of the determination of a structure is given by the residual factor, or R factor, defined as $R = \frac{\sum_{hk\ell} \left| |F_o| - k|F_c| \right|}{\sum_{hk\ell} |F_o|}$, where the summation is over all observed reflections.

3. Computer usage

Two computers have been used for the calculations in this work, the IBM 7074 and three versions of the IBM 360, models 40, 50 and 65. Many of the programs used were written by other people. An attempt to acknowledge those people is made in Table 1.

Table 1. Compilation of computer programs obtained from outside sources

Program name	Language	Description	Authors	Reference
ABCOR	Fortran	Absorption correction	W. R. Busing and H. A. Levy	(7)
DUTCH	Fortran	General Fourier synthesis	D. J. Dahm[a]	
FOURIER	PL/I	General Fourier synthesis	J. Rodgers[b]	
LCR-2	Fortran	Lattice constant refinement	D. E. Williams	(8)
OMEGA	Fortran	Weights adjusted by least squares procedure	S. Porter[c]	
ORFLS	Fortran	Oak Ridge cryst. least squares procedure	W. R. Busing, K. O. Martin, and H. A. Levy	(9)
ORTEP	Fortran	Oak Ridge Thermal Ellipsoid Plot	C. K. Johnson	(10)
SCO-6	Fortran	Generation of single crystal orienter settings	D. E. Williams[d]	

[a]Dahm, D. J., Department of Chemistry, Iowa State University of Science and Technology, Ames, Iowa. General crystallographic Fourier program. Private communication. 1965.

[b]Rodgers, J., Department of Chemistry, Iowa State University of Science and Technology, Ames, Iowa. General crystallographic Fourier program. Private communication. 1969.

[c]Porter, S., Department of Chemistry, Iowa State University of Science and Technology, Ames, Iowa. Crystallographic weights adjustment program. Private communication. 1968.

[d]Williams, D. E., Department of Chemistry, Iowa State University of Science and Technology, Ames, Iowa. Generation of single crystal orienter angles. Private communication. 1966.

Table 1 (Continued)

Program name	Language	Description	Authors	Reference
TABLE	Fortran	Structure factors printed in table	M. L. Hackert[e]	
TABLEA	Cobol	Structure factors printed in table	C. Sage[f]	
-----	Fortran	Calculation of bond distances	D. Bailey[g]	
-----	Fortran	Cryst. least squares procedure	D. R. Fitzwater and J. E. Benson[h]	
-----	Fortran	Sharpening program	B. Granoff[4]	
-----	Fortran	Intensity calculation for powder patterns	K. Yvon, W. Jeitschko, and E. Parthé	(11)

[e]Hackert, M. L., Department of Chemistry, Iowa State University of Science and Technology, Ames, Iowa. Program for printing structure factors. Private communication. 1969.

[f]Sage, C., Ames Laboratory, Iowa State University of Science and Technology, Ames, Iowa. Program for printing structure factors. Private communication. 1966.

[g]Bailey, D., Department of Metallurgy, Iowa State University of Science and Technology, Ames, Iowa. Program for the calculation of bond distances. Private communication. 1967.

[h]Fitzwater, D. R. and Benson, J. E., Department of Chemistry, Iowa State University of Science and Technology, Ames, Iowa. Crystallographic least squares program. Private communication. 1965.

II. CRYSTAL STRUCTURE OF Ti_2S

A. Introduction

1. Survey of the metal-rich region of the Ti-S system

The condensed phases observed in the metal-rich region of the titanium-sulfur system, S/Ti $\leqslant$ 1, are listed in Table 2. In addition, Table 2 also includes some phases (in parentheses) which were reported as metal-rich sulfides of titanium, but which have been established as impurity phases by other, later investigations.

Biltz, Ehrlich and Meisel (12) performed the first systematic study on the Ti-S system in 1937. In the metal-rich region they reported the existence of TiS and a volatile subsulfide. The subsulfide they reported has since been established by Hahn and Ness (13) to be Ti_5Si_3, which is a product of reaction of Ti metal with the quartz preparative tube used by the early workers. In another systematic investigation Hägg and Schönberg (14) also observed TiS and a metal-rich phase which they labeled Ti_2S. Jellinek (15), however, expressed the opinion, after comparing Hägg and Schönberg's data for Ti_2S with those data from Abendroth and Schlechten (16) for a subsulfide labeled Ti_5S_4 and finding that the two sets of data were similar, that impurities from metal-sample tube interaction were present in the metal-rich preparations of these workers. Generally, problems of this sort have plagued many investigators

Table 2. Condensed phases in the Ti-S system for $0 < S/Ti < 1.1$

Phase	Range of solid solution	Symmetry or space group
$Ti_{1-x}S$	x=0.04-0.20	rhombohedral $R\bar{3}m$
TiS_{1-x}-I	x=0.04-(-0.03)	hexagonal $P6_3/mmc$
TiS-ht	-	?
TiS_{1-x}-II	-	hexagonal $P6_3/mmc$
TiS_{1-x}-III	-	hexagonal $P\bar{6}m2$
(Ti_5S_4)	-	-
TiS_x	x=0.5-0.75	hexagonal $P\bar{6}m2$
(Ti_2S)	-	-
$(\tau\text{-}Ti_2S)$	-	-
Ti_2S	-	orthorhombic Pnnm
Ti_3S	-	-
Ti_6S	-	hexagonal

[a] Jellinek (15)

[b] Kudielka and Rohde (20)

Lattice Parameters	Comments	References
$\underline{a}$= 3.424Å $\underline{c}$=24.493Å	-	(2),(28)
$\underline{a}$= 3.299Å $\underline{c}$= 6.380Å	NiAs-type structure	(2),(12),(14), (15),(22),(28)
-	-	(22)
$\underline{a}$= 3.287Å $\underline{c}$= 6.421Å	Disordered NiAs	(2)
$\underline{a}$= 3.272Å $\underline{c}$= 6.440Å	WC or disordered NiAs	(2)
-	Jellinek[a] suggested impurities present in this preparation.	(34)
$\underline{a}$= 3.279Å $\underline{c}$= 3.210Å	WC-type structure; probably NiAs-type.	(13),(29)
-	Jellinek[a] suggested impurities present in this preparation.	(14)
-	Found to be Ti_2CS by Kudielka and Rohde[b]	(17),(18),(19)
$\underline{a}$=11.367Å $\underline{b}$=14.060Å $\underline{c}$= 3.326Å	-	(21),(23),(24), (26), this research
-	Ti_3P-like	(26)
$\underline{a}$= 2.967Å $\underline{c}$=14.495Å	Expanded Ti metal with $\underline{c}$ axis tripled.	(2)

who synthesized compounds at high temperature in sealed silica tubing, as was previously discussed in Chapter I.

Bartram (2) studied the complete system in 1958. Bartram's contribution was primarily in the monosulfide region. In the region $0 < S/Ti < 0.66$ he found a phase labeled Ti_6S for which the structure is not yet known, but the unit cell is like that of Ti saturated by sulfur with the c axis tripled in length.

Hahn and Ness (13) reported a metal-rich titanium sulfide to have the WC-type structure with a range of homogeneity $TiS_{0.75}$ - $TiS_{0.50}$, but there is some doubt as to whether this structure is correct. Jellinek (15) pointed out that the densities measured for TiS_{1-x} (WC) were high and that faint powder diffraction lines were observed indicating a doubling of the c axis which would be consistent with the NiAs-type structure reported previously. Jellinek suggested, therefore, that the sample prepared by Hahn and Ness was TiS_{1-x} (NiAs-type) plus Ti or some Ti-rich phase which was not present in a sufficient amount to be observed in the powder diffraction pattern.

The situation in the $0 < S/Ti \leqslant 1$ region was further complicated by the report by Filonenko and Kudryavtsev (17) of a hexagonal phase, τ-Ti_2S; the same phase was observed by Brown et al. (18) and by Frick and Rohde (19). Kudielka and Rohde (20), however, determined the τ-Ti_2S phase to be Ti_2CS. Also in the region in the neighborhood of $TiS_{0.5}$ Franzen and Gilles (21) prepared a phase, Ti_2S, by arc-melting TiS and Ti in

equimolar amounts. They observed the new compound to melt at 1760±20°K. Franzen (22) reported that Ti_2S appeared to be unstable at 1000°C with respect to formation of TiS and another more metal-rich phase. Franzen and Gilles (21) also found that Ti_2S loses Ti preferentially upon vaporization at elevated temperatures to form TiS which vaporizes congruently. Stone (23) used the Ti_2S sample prepared by Franzen and Gilles to attempt a structural analysis by single crystal methods. Stone determined the space group to be Pnnm (#58) or Pnn2 (#34), the lattice parameters to be

$$\underline{a} = 11.36\text{Å}$$
$$\underline{b} = 14.06\text{Å}$$
$$\underline{c} = 3.32\text{Å},$$

and the density, determined by both a buoyancy method and a pycnometric method, to be 4.80g/cc. Stone's density corresponded to 11.97 Ti_2S formula units per unit cell. A combustion analysis performed by Stone yielded S/Ti = 0.498. He was, however, unable to solve the structure. Owens, Conard, and Franzen (24) prepared Ti_2S and confirmed the lattice parameters and space group determined by Stone. They also reported that Ti_2S was isostructural with Ta_2P reported by Nylund (25). Eremenko and Listovnichii (26) also reported the existence of Ti_2S. In addition, these workers reported a new phase, Ti_3S, to have a structure similar to the ϵ(Fe-P-B)-type structure reported by Rundqvist (27).

2. Specific purposes of this research

The purposes of the research described in this section were to confirm the existence of Ti_2S, to determine its crystal structure using single crystal x-ray diffraction techniques, to discuss the structure in terms of other known metal-rich chalconide compounds, and to attempt to understand, in a qualitative way, the bonding in Ti_2S.

3. Preparation of samples

The dititanium sulfide samples were prepared in a manner similar to the procedure discussed in Chapter I. The 99.93% Ti metal was obtained from the Chicago Development Corporation. The 99.999% sulfur was obtained from the Gallard-Schlesinger Chemical Manufacturing Corporation. Equimolar amounts of elemental Ti and S were sealed in evacuated Vycor tubes and were heated in a resistance furnace at 450°C for 2 days. The products, a mixture of Ti metal, TiS, and higher sulfides, were mixed with equimolar amounts of Ti metal filings, compressed into a pellet and annealed at ca. 1490°C for two hours in a tungsten crucible. The vacuum line and crucible are diagrammed in Figure 1. The use of high temperature techniques for preparing solid compounds in an inert container has been discussed in Chapter I. Arc-melting procedures were also employed for the preparation of Ti_2S from Ti and TiS.

A sample of Ti_2S was analyzed for metal content by ignition to TiO_2. Assuming that titanium and sulfur were the only constituents, the S/Ti ratio was 0.514 ±0.002, which was close

to Stone's value of 0.498.

4. Physical properties of Ti_2S

Ti_2S is metallic in appearance. Very rough resistivity measurements performed using a vacuum tube ohmeter showed Ti_2S to be a good conductor of electricity. The compound is very hard, but brittle. The melting point of Ti_2S was found to be 1505 $\pm 10^{\circ}C$, in good agreement with Franzen and Gilles's value 1490 $\pm 20^{\circ}C$.

B. Investigation by X-ray Diffraction; Data Collection

X-ray examination of Ti_2S was performed using Guinier and Debye-Scherrer powder photograph techniques and Weissenberg and precession single crystal techniques. These methods have been briefly touched upon in Chapter I. Accurate lattice parameters, determined by a least squares treatment of the 2θ values from a Guinier powder diffraction pattern, were:

$$\underline{a} = 11.367 \pm 0.003\text{Å}$$

$$\underline{b} = 14.060 \pm 0.004\text{Å}$$

$$\underline{c} = 3.326 \pm 0.001\text{Å}.$$

Table 3 lists the observed and calculated $\sin^2\theta$ values and the relative intensity of each reflection observed in the Guinier powder pattern. These parameters were in good agreement with those found by Stone, as reported above.

A single crystal of Ti_2S was selected from the annealed sample and was aligned by J. Owens on a Charles G. Supper Company Weissenberg camera such that the $\underline{c}$ axis was coincident

Table 3. Guinier x-ray powder diffraction data for Ti_2S[a]

CuK_α radiation, Orthorhombic $\underline{a}$=11.367Å, $\underline{b}$=14.060Å, $\underline{c}$=3.326Å							
hkℓ	I/I_o	$\sin^2\theta(\text{obs}) \times 10^5$	$\sin^2\theta(\text{calc}) \times 10^5$	2θ(obs)	2θ(calc)	d(obs)	d(calc)
400	1	31.42	31.45	7332	7345	2.845	2.842
221	1	33.67	33.69	8388	8398	2.660	2.658
301	60	35.90	35.89	9498	9493	2.499	2.500
311	10	36.50	36.48	9807	9797	2.460	2.461
141	50	38.04	38.04	10621	10621	2.363	2.363
060	10	38.37	38.38	10799	10804	2.344	2.343
350	100	39.89	39.89	11636	11636	2.258	2.258
510	5	40.17	40.14	11793	11776	2.243	2.245
331	100	40.89	40.88	12202	12196	2.205	2.206
520	5	41.75	41.72	12698	12680	2.162	2.163
051	60	42.03	42.04	21860	12866	2.148	2.147
151	5	42.81	42.82	13319	13325	2.111	2.110
421	50	43.76	43.79	13888	13906	2.067	2.066
170	10	45.86	45.84	15179	15167	1.977	1.978
540	10	47.58	47.59	16272	16278	1.909	1.909
501	5	48.42	48.46	16817	16843	1.878	1.877
511	20	48.94	48.91	17820	17800	1.825	1.826
002	60	55.19	55.18	21457	21450	1.663	1.663

[a]In the list above the line 241 does not appear because it superimposes on a KCl standard line: $\sin^2\theta(241, Ti_2S) = 0.11978$; $\sin^2\theta(220, KCl) = 0.11985$.

with the rotation axis of the Weissenberg instrument. A photograph of the crystal is shown in Figure 2. The dimensions of the approximately parallelepiped crystal were 50μ x 30μ x 30μ. The conditions for reflections observed on Weissenberg and precession photographs were

$hk\ell$	= no conditions
$0k\ell$	= $k + \ell = 2n$
$(0k0),(00\ell)$	= $(k = 2n,\ \ell = 2n)$
$h0\ell$	= $h + \ell = 2n$
$(h00)$	= $(h = 2n)$
$hk0$	= no conditions.

These conditions indicated two possible space groups: Pnn2 (C_{2v}^{10} - #34) and Pnnm (D_{2h}^{12} - #58), where Pnnm is the centrosymmetric group. The Laue group was observed to be mmm (D_{2h}). These observations were in agreement with those of Stone (23).

Three-dimensional intensity data were collected in four Weissenberg layer photographs using MoK_{α} radiation, filtered by Zr. The observed structure factors were obtained from the intensities, $I_{hk\ell}$, on the photographic record using

$$|F|_{hk\ell} = \sqrt{I_{hk\ell} \cdot \overline{Lp} \cdot A}, \qquad (7)$$

where $|F|_{hk\ell}$ is the absolute magnitude of the structure factor for the set of crystal planes denoted by Miller indices h, k, and ℓ, $\overline{Lp}$ is the Lorentz-polarization correction factor, and A is the absorption factor. The intensities were estimated visually by J. Owens by multiple film techniques using an intensity scale obtained from timed oscillations of the 4,0,0 re-

Figure 2. Photograph of single crystal of Ti_2S (X500)

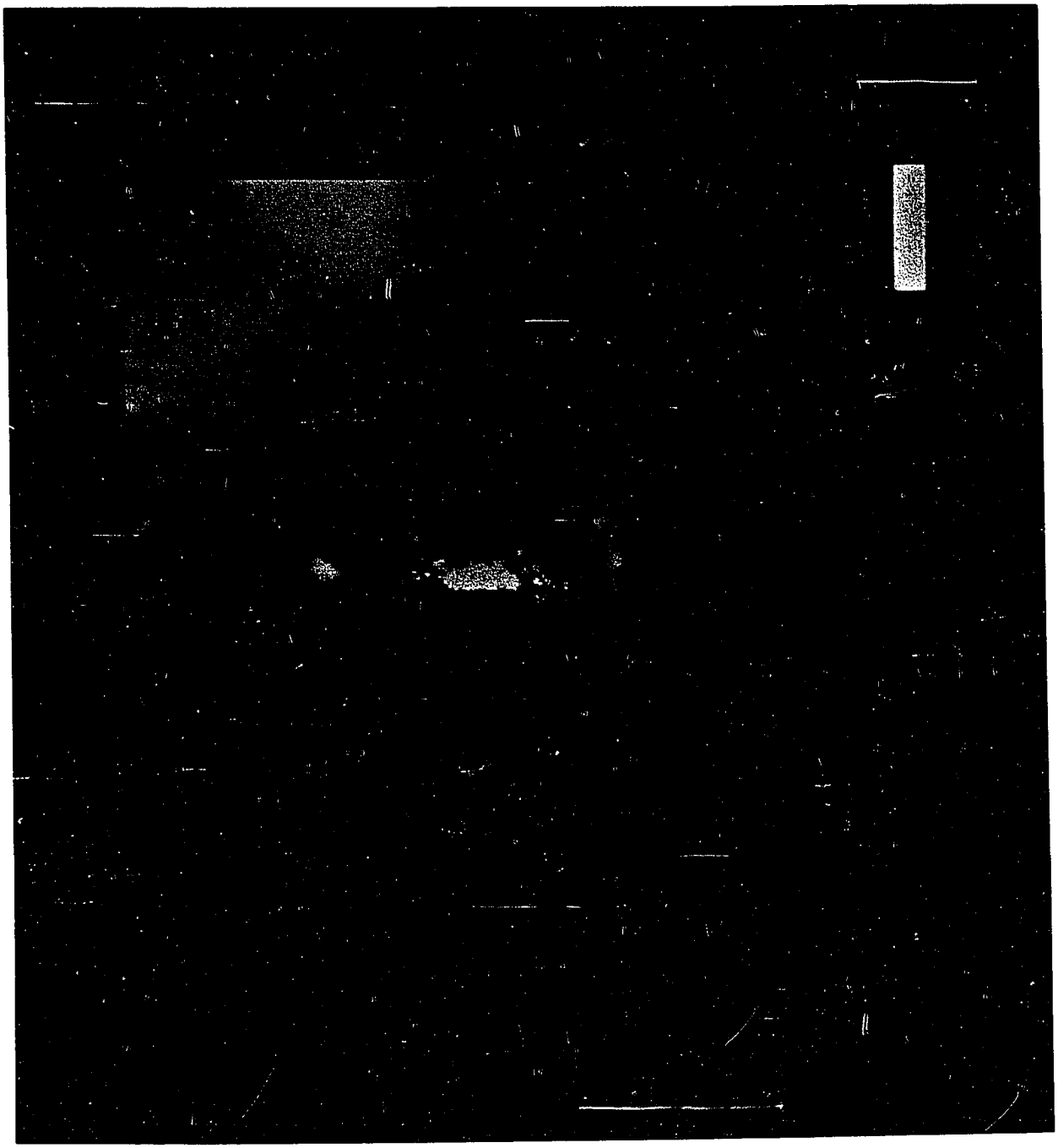

flection. No absorption corrections were deemed necessary due to the small size of the crystal. Lorentz-polarization corrections were obtained graphically from the International Tables of X-ray Crystallography (30). All intensities were corrected to unresolved K_α intensities using a linear approximation in the range of K_{α_1} - K_{α_2} overlap. Standard deviations for the observed |F|'s were obtained using the method of Hughes (31) (see below). No extinction corrections were made.

C. Structure Determination

The positions for possible atomic occupation in the centric space group, Pnnm, under the general conditions for reflection were: 8-fold general positions (h) x, y, z; $\bar{x}$, $\bar{y}$, z; 1/2 + x, 1/2 - y, 1/2 - z; 1/2 - x, 1/2 + y, 1/2 - z; $\bar{x}$, $\bar{y}$, $\bar{z}$; 1/2 - x, 1/2 + y, 1/2 + z; x, y, $\bar{z}$; 1/2 + x, 1/2 - y, 1/2 + z; and 4-fold special positions (g) x, y, 0; $\bar{x}$, $\bar{y}$, 0; 1/2 + x, 1/2 - y, 1/2; 1/2 - x, 1/2 + y, 1/2. It was noted that the general positions were not likely to be occupied by either Ti or S atoms since the short c lattice parameter of 3.32Å would not allow Ti atoms or S atoms at both x, y, z and x, y, $\bar{z}$ positions. In addition, the ratio $|F_o(hk0)| / |F_o(hk2)|$ was constant, indicating that the atoms were contained in layers separated by 1/2 of the c axis. Accordingly, the fourfold positions (g) x, y, 0 were chosen as the positions of lowest symmetry for both the Ti and S atoms. As discussed below, the Patterson synthesis had maxima only at z = 0 and z = 1/2, in agreement with this choice.

1. The solution of the phase problem

As discussed in Section B, Chapter I, the structure factors are known from the intensities of diffracted x-radiation only as an absolute quantity; the phases are not known. Since the phases of the structure factors are needed for an electron density Fourier synthesis in which the phased structure factors are proportional to the Fourier coefficients, the phases must be determined, at least for some of the larger structure factors, as the first step in the structure determination. The phase problem in Ti_2S was solved by means of a Patterson function (32) using superposition techniques. An excellent discussion of the Patterson function and of superposition techniques is given by Buerger (33). The purpose of the discussion below is to provide a brief introduction to these subjects and to discuss their application to Ti_2S.

a. The Patterson function The Patterson function (32) is fairly easily constructed; its usefulness is somewhat more difficult to understand. Patterson's function uses the information directly resulting from the knowledge of the intensities of diffracted radiation, namely the $|F|^2$. It will be recalled from Chapter I that a periodic function of electron density within a crystal may be represented by a Fourier series,

$$\varphi(XYZ) = \frac{1}{V} \sum_{hk\ell} F_{hk\ell} e^{-2\pi i(hX + kY + \ell Z)}, \qquad (8)$$

where the letter representations have been defined previously, and

$$F_{hk\ell} = \sum_{j=1}^{N} f_j e^{2\pi i(hx_j + ky_j + \ell z_j)}. \qquad (9)$$

One possible Patterson function, as given for the "squared crystal" by Buerger (33), is:

$$P(UVW) = \frac{1}{V} \sum\sum\sum_{hk\ell} |F_{hk\ell}|^2 e^{-2\pi i(hU + kV + \ell W)}. \qquad (10)$$

It may be noticed that the differences between $\rho(XYZ)$ and P(UVW) are merely the Fourier coefficients. In the latter case the $|F_{hk\ell}|^2$ are known from the intensities of diffracted radiation. The forms of the coefficients, $|F_{hk\ell}|^2$, in this function are

$$|F_{hk\ell}|^2 = [\sum_{j=1}^{N} f_j e^{2\pi i(hx_j+ky_j+\ell z_j)}][\sum_{j=1}^{N} f_j e^{-2\pi i(hx_j+ky_j+\ell z_j)}]. \qquad (11)$$

Buerger points out that a convenient way to view $|F_{hk\ell}|^2$ is in matrix notation

$$|F_{hk\ell}|^2 = \sum_{r=1}^{N} f_r^2 + \sum_{\substack{r=1 \\ r\neq s}}^{N} \sum_{s=1}^{N} f_r f_s e^{2\pi i[h(x_r-x_s)+k(y_r-y_s)+\ell(z_r-z_s)]}, \qquad (12)$$

where the terms under the first summation are diagonal matrix elements and the double summation represent a summation of all non-diagonal elements.

The usefulness of this particular Patterson function is seen by investigating the requirements under which maximum values of P(UVW) occur. In the same way that the electron density function $\rho(XYZ)$ has a maximum at $X=x_j$, $Y=y_j$, $Z=z_j$ when

the j^{th} atom is located at positional coordinates x, y, z, the Patterson function P(UVW) has a maximum at $U=x_r-x_s$, $V=y_r-y_s$, $W=z_r-z_s$ for two atoms r and s located at different positions in the unit cell, x_r, y_r, z_r and x_s, y_s, z_s, respectively.

A Patterson synthesis is therefore alternatively termed a vector synthesis. It is so termed because the maxima occurring in the synthesis can be viewed as being located at the endpoints of vectors between pairs of atoms in the unit cell as demonstrated above. There are two other significant aspects of the maxima in a Patterson map:

1) A very large maximum appears at the origin. This maximum results from the vector being very small which implies that r=s, i.e., it is a vector between the atom and itself. The maximum is large because every atom in the cell contributes f_r^2 to it, as is obvious from the first summation of Equation 12.

2) The magnitudes of non-origin maxima are the products of the pairs of atomic scattering factors, $f_r f_s$. The multiplicity of such vectors, however, must also be taken into account when dealing with these magnitudes.

The Ti_2S Patterson map located in the (X,Y,0) plane is shown in Figure 3. Contour lines were drawn in increments of 5 $(\text{electrons})^2/\text{Å}^3$ in P(UVW) with a minimum of 30. The Patterson synthesis was calculated in sections along the z axis in increments of 0.25Å. The only other maxima were located in the (X, Y,1/2) plane, in agreement with atomic positions at z=0 and z=1/2 as suggested above.

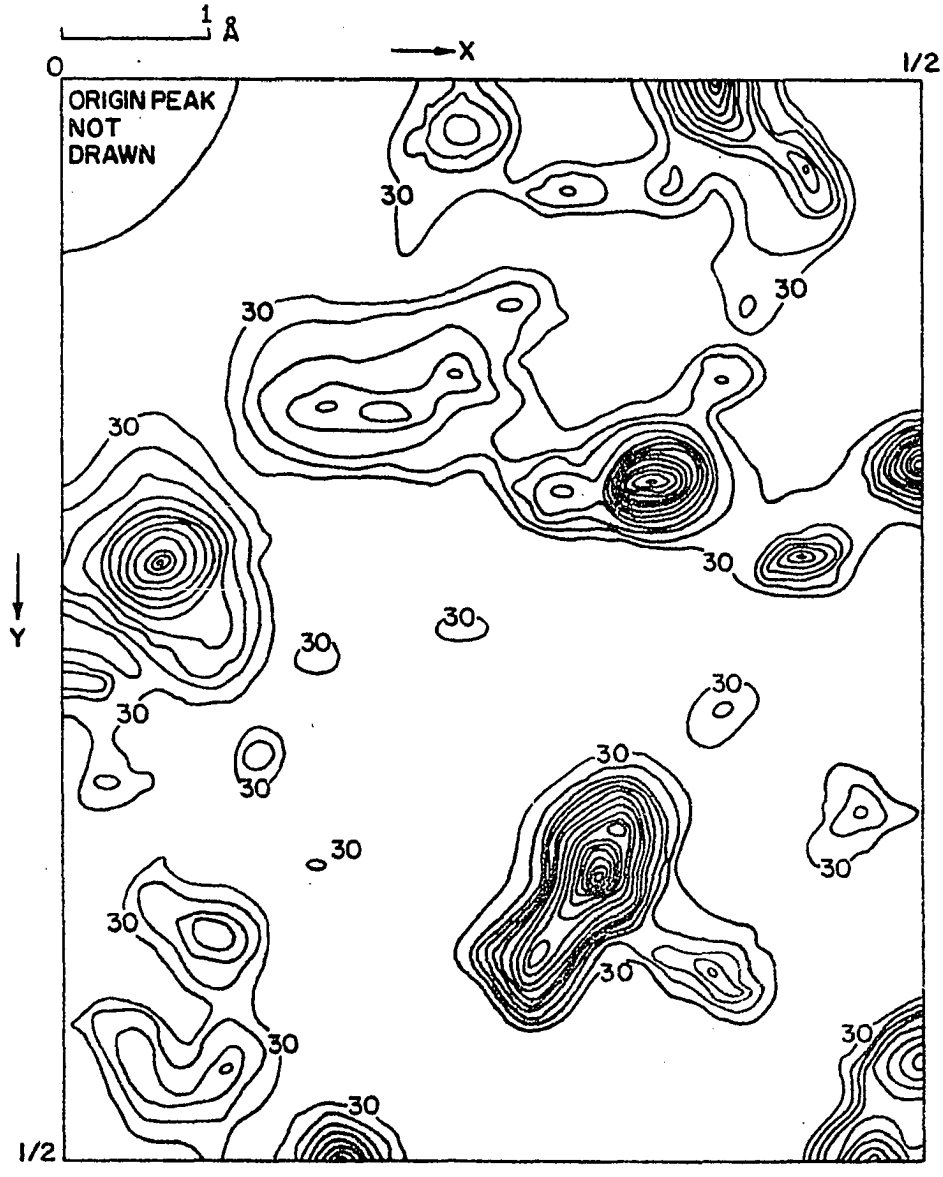

Figure 3. Patterson section (X, Y, 0) for Ti_2S

b. The use of superposition techniques Once the Patterson has been synthesized, it can be used in a variety of ways. The advantages and disadvantages of methods and the applicability of certain methods to particular structural features, such as symmetry and kinds of atoms, are thoroughly discussed by Buerger (33). The method used for the Patterson solution for Ti_2S was the superposition or vector-shift method. This method was selected for application to the data of Ti_2S because of its utility in resolving planar images. For example, superposition methods are usually most successful in resolving a projected structure from a projected Patterson. Since all the structural information is contained in a plane in Ti_2S, i.e., all atoms occur in x,y,0 positions, superposition techniques were used on the Z=0 section of the Ti_2S Patterson.

The superposition method consists of constructing two identical Z=0 Patterson maps (map A and map B), positioning the origin of map B on a maximum in map A, and recording all maxima which are coincident between the maps A and B. The vector set which results from this superposition may contain an image of the structure (see Buerger), but sometimes such an image is difficult to see because of the large area of coincidence of maxima between the two maps. This difficulty in the superposition technique is usually caused by poorly resolved Patterson peaks, that is, peaks which do not have sharply defined positions. Such was the case in Ti_2S. An attempt to diminish this problem was made by synthesizing a sharpened

Patterson. "Sharpening" is a term for a procedure which adjusts $|F_o|$ or $|F_o|^2$ by assuming that the scattering matter is located at points in the cell rather than volume elements in the cell. The sharpened Patterson map of Ti_2S for the (X,Y,0) plane is shown in Figure 4. This map should be compared with the one in Figure 3 in order to see the difference in peak resolution between the sharpened Patterson and the regular Patterson. Even with the more highly resolved map, however, random superpositions were only mildly successful.

c. The use of Harker lines Because superposition techniques resulted in generally complicated images, it was decided to attempt to gain more information from Harker (34) lines. Harker suggested that vectors between symmetrically related atoms could be found in a Patterson synthesis and that atomic positions could be deduced from the coordinates of the endpoints of such vectors.

There are two n-glides in space group Pnnm (Ti_2S). Upon performing the glide operations, positions at x, y, 0 become 1/2 + x, 1/2 - y, 1/2 and 1/2 - x, 1/2 + y, 1/2. If a position x, y, 0 is occupied by an atom, then so are the symmetrically related positions. In the Patterson synthesis, therefore, there should be a vector between these two atoms, located at

$$[1/2+x,\ 1/2-y,\ 1/2]-[x,y,0] = 1/2,\ 1/2-2y,\ 1/2. \qquad (12)$$

Thus, examining the Harker line located in the Patterson at Z=1/2 and X=1/2, it was possible to locate maxima along this

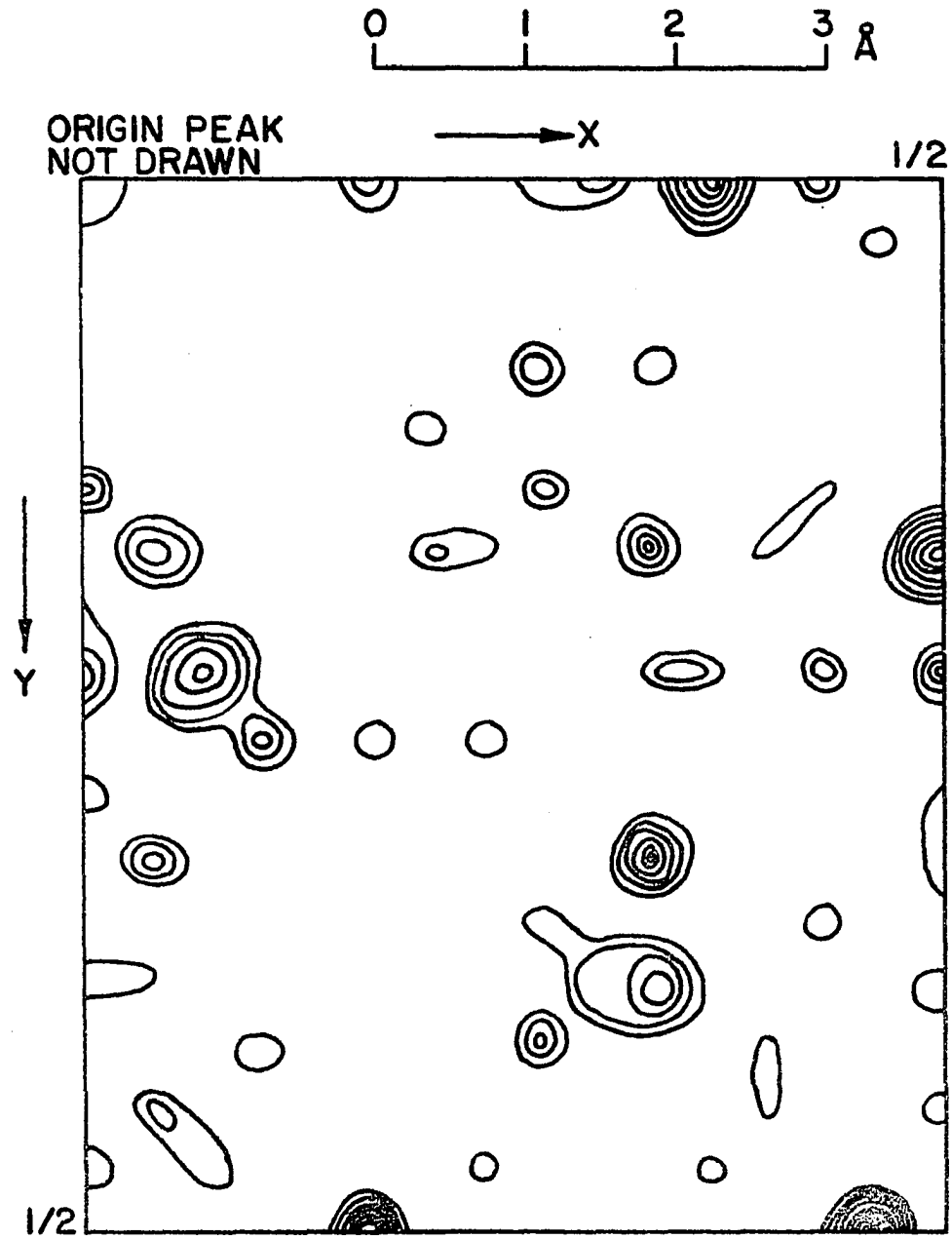

Figure 4. Sharpened Patterson section (X, Y, 0) for Ti_2S

line and to calculate y-coordinates of atoms at x, y, 0. The same argument applied to the x-coordinates:

$$[1/2-x,\ 1/2+y,\ 1/2]-[x,y,0] = 1/2-2x,\ 1/2,\ 1/2, \qquad (13)$$

and the Harker line in this case was Y=1/2, Z=1/2. Both the Harker lines which were of interest in Ti_2S were located in the Z=1/2 Patterson section; that section is shown in Figure 5, where the contours have been drawn in increments of 5 $(\text{electrons})^2/\text{Å}^3$ starting at 30. Again it was necessary to sharpen this Patterson section in order to obtain more precise peak positions. From the peak positions the possible values of the atomic x and y positional parameters were calculated; these calculations are summarized in Table 4.

It was possible to obtain information about the most probable x and y atomic coordinates from the list of possible positions by considering another kind of vector between symmetrically related pairs of atoms, namely, those atoms related by the center of symmetry. For example, if an atom occupies position x, y, 0, then an equivalent atom occupies $\bar{x}$, $\bar{y}$, 0; the vector between these atoms is 2x, 2y, 0. This vector occurs in the Z=0 Patterson section. Every possible combination of the x and y values calculated and presented in Table 4 was subjected to the criterion that a 2x, 2y, 0 peak be present. This procedure, when combined with further superpositions on these 2x, 2y, 0 peaks, resulted in the location of six out of nine atoms in the

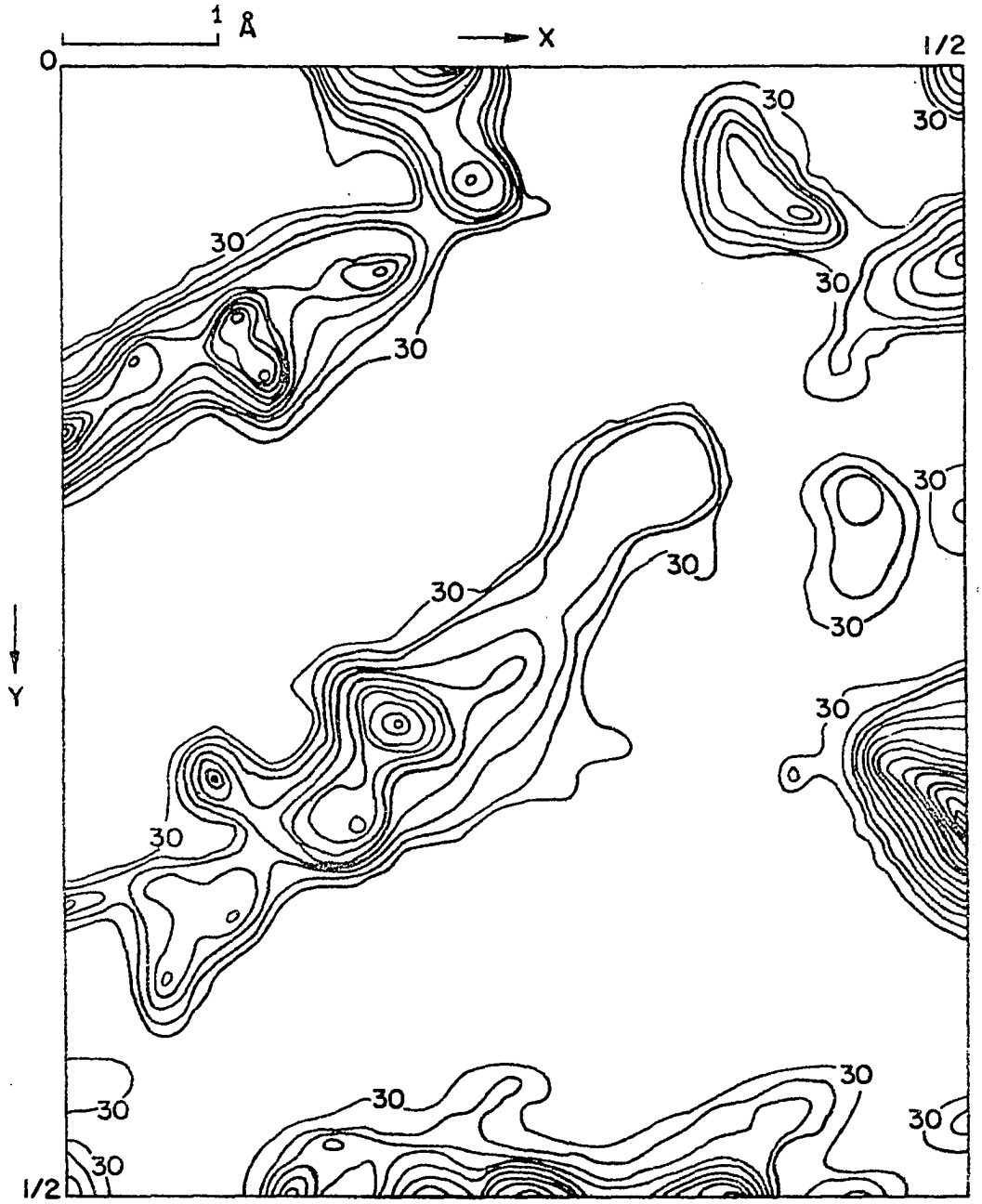

Figure 5. Patterson section (X, Y, 1/2) for Ti_2S

Table 4. Calculation of possible atomic parameters, x and y, for Ti_2S from Harker lines of the sharpened Patterson

Peak position x'=1/2-2x	-2x	x	Comments
0.4325	-0.0675	0.0337	
0.358	-0.1420	0.0710	
0.267	-0.233	0.1165	
0.200	-0.300	0.1500	Ti(1),x=0.1543
0.133	-0.367	0.1835	
0	-0.500	0.2500	S(2),x=0.2451
-0.133	-0.633	0.3165	
-0.200	-0.700	0.3500	
-0.267	-0.767	0.3835	
-0.358	-0.858	0.4290	S(1),x=0.4320
-0.4325	-0.9325	0.4662	Ti(4),x=0.4696
-0.567	-1.067	0.5335	
-0.641	-1.141	0.5705	
-0.733	-1.233	0.6165	
-0.800	-1.300	0.6500	
-0.867	-1.367	0.6835	S(3),x=0.6841
-1.000	-1.500	0.7500	
-1.133	-1.633	0.8165	
-1.200	-1.700	0.8500	
-1.267	-1.767	0.8835	Ti(6),x=0.8797
-1.358	-1.858	0.9290	
-1.4325	-1.932	0.9662	

Peak position y'=1/2-2y	-2y	y	Comments
0.470	-0.030	0.0150	Ti(1),y=0.0206
0.412	-0.088	0.0440	
0.353	-0.1570	0.0735	Ti(3),y=0.0797
0.264	-0.2360	0.1180	
0.206	-0.2940	0.1470	
0.147	-0.3530	0.1765	
0.0588	-0.4412	0.2206	
0	-0.500	0.2500	Ti(2),y=0.2553
-0.0588	-0.5588	0.2794	
-0.147	-0.647	0.3235	
-0.206	-0.706	0.3530	S(3),y=0.3498
-0.264	-0.764	0.3820	
-0.353	-0.853	0.4265	Ti(6),y=0.4221
-0.412	-0.912	0.4560	
-0.470	-0.970	0.4850	

asymmetric unit cell[1].

The remaining three atomic positions were located by Fourier synthesis.

2. Refinement of the structure

The atomic positions and isotropic temperature factor coefficients were refined by four cycles of least squares computation using the computer program written by Busing, Martin, and Levy (9). For this computation, atomic scattering factors were obtained from Hansen, Herman, Lea and Skillman (35). The weighting scheme adopted for the initial refinement was the one suggested by Hughes (31). Hughes' proposal for weighting was:

$$\sqrt{w} \propto \frac{1}{4F_{min}} \quad \text{for } |F_o| < 4|F_{min}| \tag{14}$$

$$\sqrt{w} \propto \frac{1}{F_o} \quad \text{for } |F_o| > 4|F_{min}|\,, \tag{15}$$

where F_{min} is the minimum F_o. Hughes stated:

> This corresponds to taking the percentage probable error in the intensities as constant for intensities more than sixteen times the background and the absolute probable error constant for smaller intensities, an approximation justified chiefly by the simplicity in application (36).

The Hughes weights for Ti_2S were checked in the final stages of refinement by plotting $\overline{w(F_o-F_c)^2}$ versus $\overline{|F_o|}$ for groups of 75 reflections with increasing $|F_o|$ values. That plot is shown in Figure 6. The slope of Line 1 (Hughes weights) was 0.14. Re-

---

[1] James Owens' patience and perseverance with nearly all the superposition trials for Ti_2S is gratefully acknowledged.

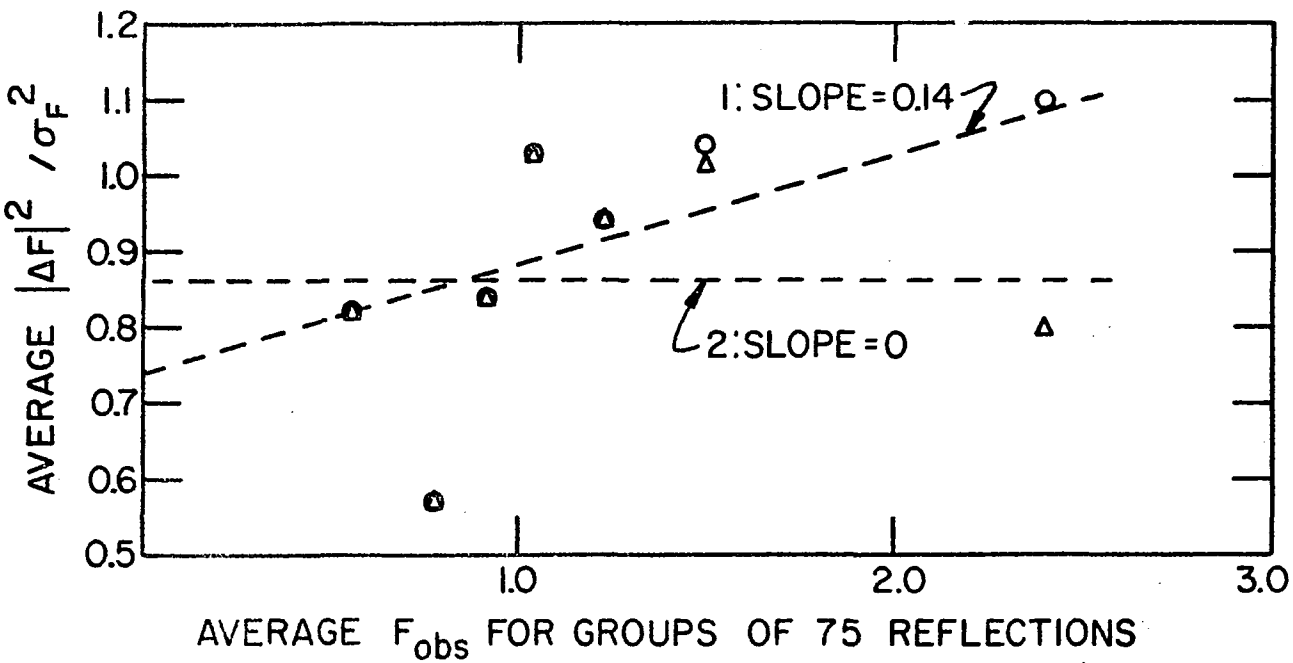

Figure 6. Plot of $\overline{w(F_o - F_c)^2}$ vs. $\overline{|F_o|}$ in groups of 75 reflections for weights check for Ti_2S

vised weights were assigned such that the line would have approximately zero slope. A final cycle of least squares computation with the revised weights yielded an agreement factor, $R = \Sigma||F_o| - k|F_c||/\Sigma|F_o|$, equal to 0.10. Table 5 contains a listing of the positional parameters and isotropic temperature factor coefficients obtained. Table 6 lists the observed and calculated structure factors for all 535 observed reflections. The "goodness of fit," defined by $\Sigma w(F_o-F_c)^2/n-s$, was 0.94.

A final Fourier electron density synthesis was calculated at z=0 and is shown in Figure 7(a). An electron density difference Fourier was calculated and is shown in Figure 7(b). The residual electron densities located at the atom position on this map corresponded to less than one electron.

Another refinement of the structure was performed using four anisotropic temperature factors: β_{11}, β_{22}, β_{33}, β_{12}. The other two anisotropic coefficients, β_{23}, and β_{13}, were set equal to zero following the procedure by Levy (37), due to the fact that the atoms were in a mirror plane. The positional parameters were not significantly altered, nor was the R factor; the anisotropic temperature factors are listed in Table 7.

D. Description of the Ti_2S Structure

Ti_2S is isostructural with Ta_2P which was reported in 1966 by Nylund (25). It is an interesting coincidence that the structures of these two compounds were determined independently and approximately concurrently; Ta_2P was solved three months before

Table 5. Final refined atomic parameters for Ti_2S. All atoms occupy fourfold positions (g) x,y,0 of space group Pnnm

Atom	x	σ(x)	y	σ(y)	B	σ(B)
Ti(1)	0.1543	0.0004	0.0206	0.0003	0.51Å^2	0.06
Ti(2)	0.0867	0.0004	0.2553	0.0003	0.55	0.06
Ti(3)	0.5881	0.0004	0.0797	0.0003	0.44	0.06
Ti(4)	0.4696	0.0004	0.3904	0.0003	0.55	0.06
Ti(5)	0.8073	0.0004	0.2078	0.0003	0.46	0.06
Ti(6)	0.8797	0.0004	0.4221	0.0003	0.57	0.06
S(1)	0.4320	0.0005	0.2068	0.0004	0.56	0.08
S(2)	0.2451	0.0006	0.4124	0.0005	0.68	0.08
S(3)	0.6841	0.0005	0.3498	0.0004	0.34	0.07

Table 6. Observed and calculated structure factors for Ti_2S

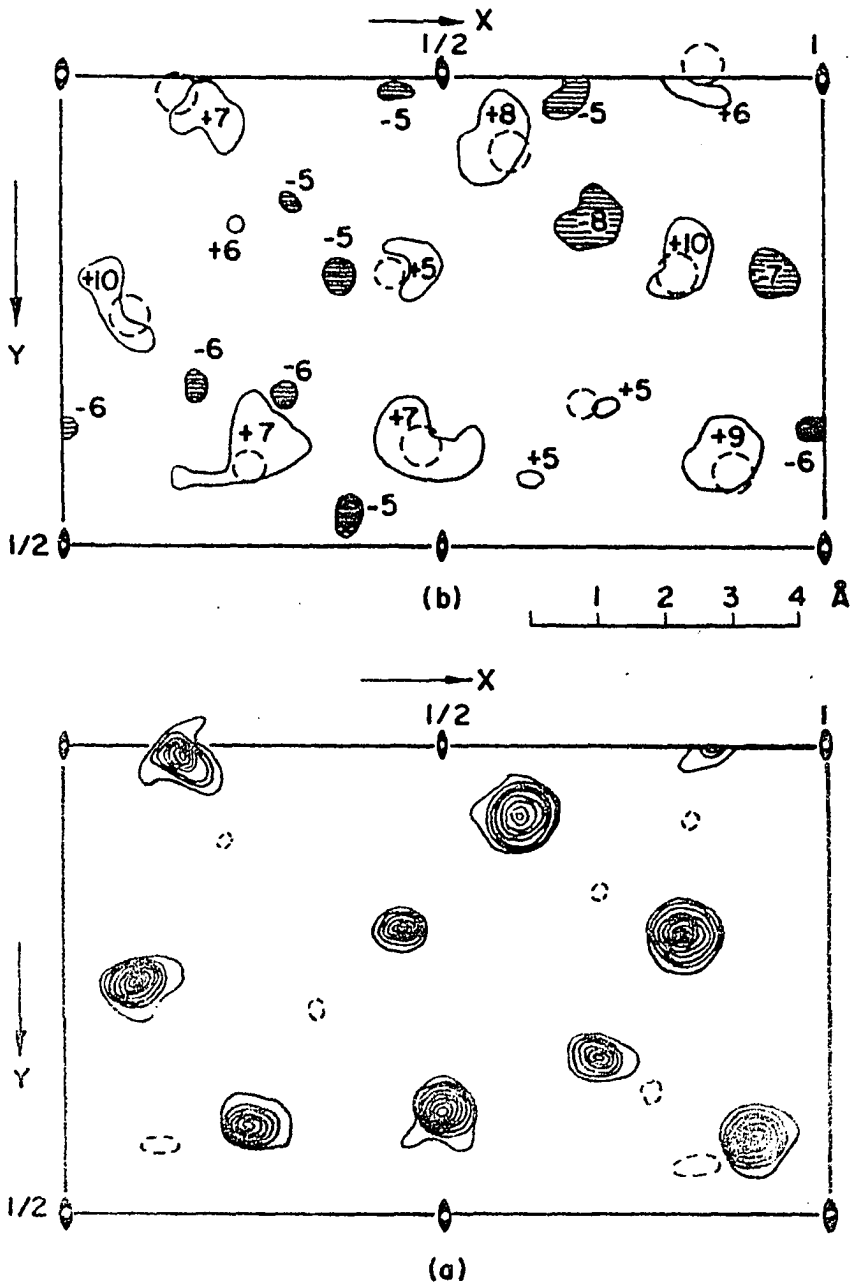

Figure 7. (a) Final Fourier electron density section at (X, Y, 0) for Ti_2S; (b) final difference electron density section at (X, Y, 0) for Ti_2S

Table 7. Refined anisotropic temperature factor coefficients for Ti_2S, $\beta_{13} = \beta_{23} = 0$

Atom	β_{11}	β_{22}	β_{33}	β_{12}
Ti(1)	0.0016(3)	0.0005(2)	0.026(4)	-0.0000(2)
Ti(2)	0.0011(2)	0.0010(2)	0.020(4)	0.0002(2)
Ti(3)	0.0011(3)	0.0007(1)	0.019(4)	-0.0002(2)
Ti(4)	0.0013(3)	0.0010(2)	0.022(5)	0.0002(2)
Ti(5)	0.0008(2)	0.0008(2)	0.023(4)	0.0001(2)
Ti(6)	0.0012(3)	0.0010(2)	0.021(4)	0.0001(2)
S(1)	0.0014(4)	0.0006(2)	0.032(6)	-0.0004(2)
S(2)	0.0011(4)	0.0009(2)	0.021(6)	0.0000(2)
S(3)	0.0009(3)	0.0008(2)	0.019(5)	0.0000(2)

Ti_2S and therefore the structure-type is appropriately termed the Ta_2P structure-type. To avoid confusion, however, in the subsequent discussion of the metal-rich chalconide compounds of the Group IVB transition metals, the structure-type to which Ti_2S belongs is referred to as the Ti_2S-type.

The Fourier electron density map reproduced in Figure 7(a) shows the z=0 asymmetric unit cell, the volume of which is one-fourth of the volume of the crystallographic unit cell. Figure 8 shows the entire z=0 section of Ti_2S. The atomic positions are those which resulted from the final cycle of least squares refinement. The atom boundaries are drawn using Slater's (38) atomic radii. A complete list of these atomic radii is presented in Appendix B, and a justification for the use of these particular radii is given in the discussion section which follows immediately. It is important, however, in the present endeavor to describe the Ti_2S structure to point out a feature of the structure which is illustrated in Figure 8. The feature is the amount of bonding in the (x,y,0) plane. Slater's prerequisite for bonding between two atoms is that the internuclear distance between atomic centers be approximately equal to the sum of the Slater atomic radii for those atoms. The word "approximately" allows a range of distances over which two atoms can be considered as bonded. The greater the distance between atomic centers compared with the sum of Slater's atomic radii, the less likely that the two atoms will be bonding and/or the weaker will be the bond formed. Figure 8 provides a pictorial

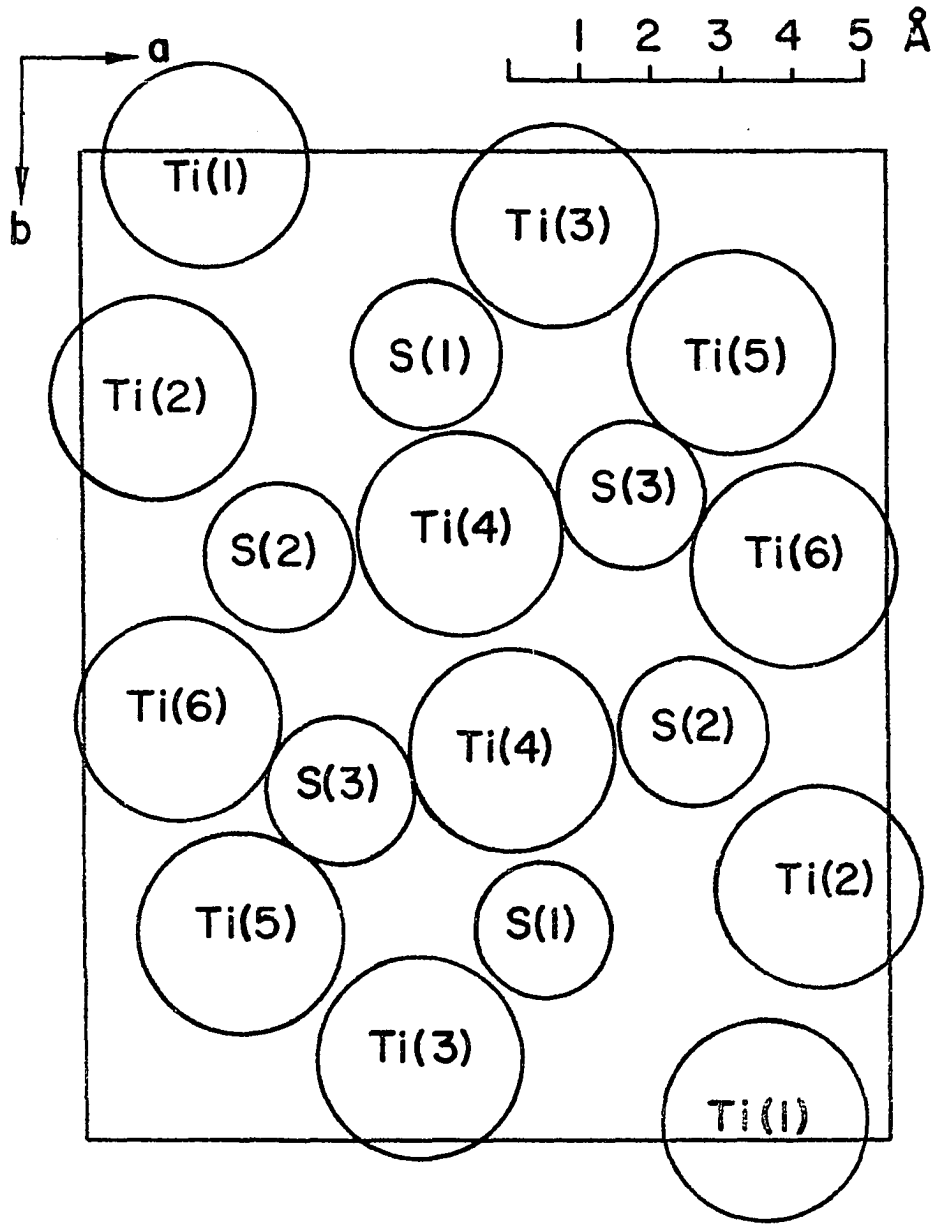

Figure 8. The structure of Ti_2S at section z = 0. Atom boundaries are drawn using Slater's atomic radii

representation of the Slater viewpoint. For example, the circle representing the radius of S(3) is almost exactly tangent to three other circles representing Ti(4), Ti(5) and Ti(6). The use of Slater's criteria for bonding does not include consideration of the directional nature of atomic orbitals. Directional bonding may necessitate a modification of Slater's criteria, as discussed in the next section. According to Slater's criteria S(1) is bonded to Ti(3) and Ti(4) in the z=0 section. The situation is somewhat less clear for S(2), but as can be judged by looking at the figure, S(2) is probably bonded to Ti(4), and possibly bonded to both Ti(2) and Ti(6).

A computer program written by Johnson was used to obtain a stereoscopic drawing of the Ti_2S structure shown in Figure 9; Slater's radii were again used. Special glasses are needed to view this illustration in order to see the structure in three-dimensions.

A complete schematic representation of the Ti_2S structure projected down the c axis is shown in Figure 10. In this figure the atomic radii are arbitrary in an attempt to make the drawing less cluttered and, moreover, to show some features of the coordination present in this compound. The figure also contains the symmetry elements present in space group Pnnm. It is important to the interpretation of this figure that it be understood that there are mirror planes parallel to the plane of the paper at z=0, z=1/2, z=1, etc. In the final structure the atoms are located in the mirror planes and therefore the slashed Ti

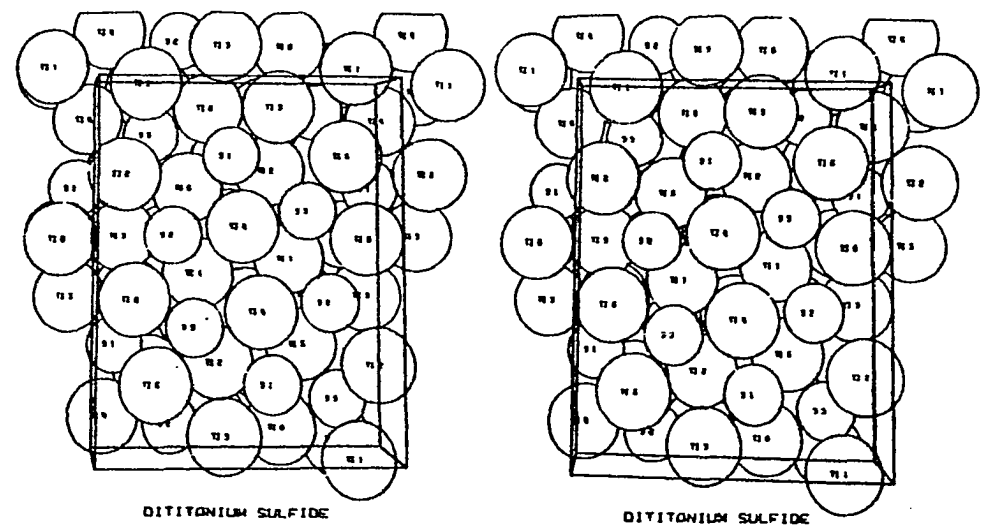

Figure 9. Stereoscopic illustration of the Ti_2S structure viewed along the c axis. The box represents one unit cell

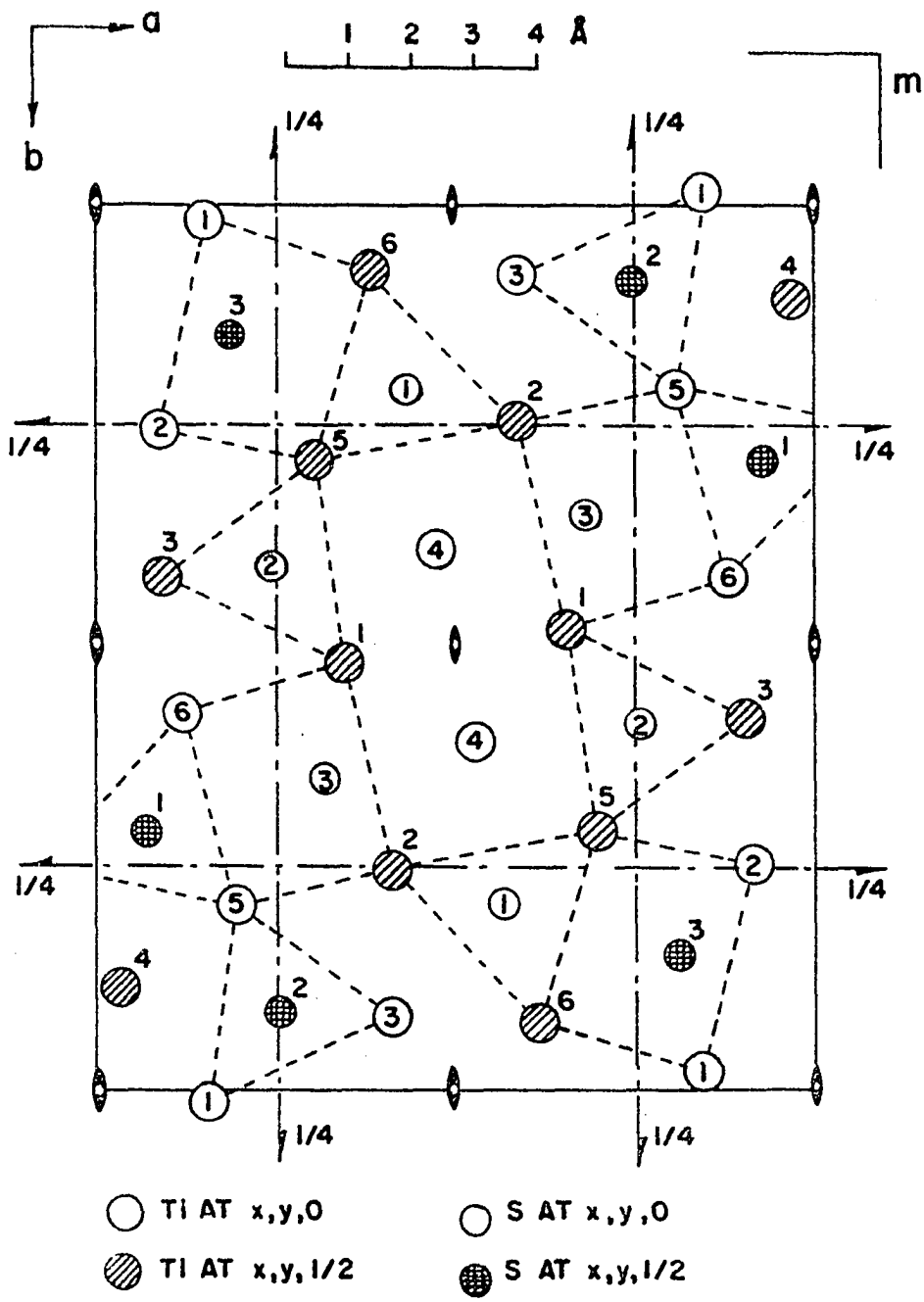

Figure 10. Projection of the Ti_2S structure along the c axis. Symmetry elements of Pnnm are shown. Dashed lines show projected coordination polyhedra of the sulfur atoms

atoms and the crosshatched S atoms occurring in the figure at z=1/2 also are present at the z=-1/2 section. The clear circles in this figure are located at z=0.

There are three crystallographically independent sulfur positions in Ti_2S. All three sulfur atoms are coordinated by six Ti atoms in a slightly distorted trigonal prismatic arrangement. Consider the coordination of S(1), and focus attention on the S(1) which lies in the z=0 section with coordinates $x \tilde{=} 1/2$, $y \tilde{=} 1/4$. One can see in the projected structure that Ti(5), Ti(6), and Ti(2) lie at z=1/2 and z=-1/2 and can be considered as being located at the corners of a trigonal prism. This coordination of S(1) is seen in perspective in Figure 11 (a). It is clear that the approximate threefold axis of the trigonal prism is parallel to the c axis of the unit cell. But this is not the whole story for S(1). By observing interatomic distances, listed in Table 8, one finds Ti(3) at a distance of 2.52Å, which is of the same order as the six distances to the corners of the trigonal prism. Ti(3) is located in the z=0 section, i.e., in the same plane as S(1), as is also Ti(4) which is 2.62Å from S(1). It was seen in Figure 8 that both Ti(3) and Ti(4) could be considered as bonded to S(1) on the basis of Slater's criterion for bonding. From a consideration of only interatomic distances it becomes necessary to discuss the coordination of S(1) as "augmented" trigonal prismatic. The augmentation is by additional coordinated metal atoms which are adjacent to the rectangular faces of the trigonal prism.

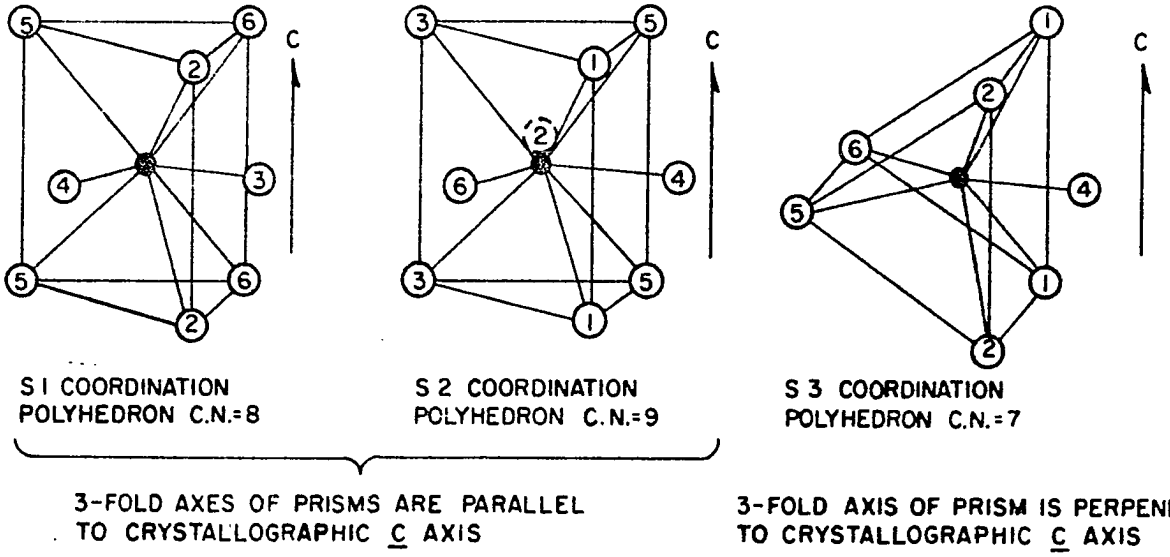

Figure 11. Coordination polyhedra of the three independent sulfur atoms in Ti_2S: (a) S(1), (b) S(2), and (c) S(3)

Table 8. Interatomic distances and bond orders for Ti_2S. All distances less than or equal to 3.16Å are listed

Reference atom	Neighbor atom	Number of neighbors	Distance (Å)	Bond order
S(1)	Ti(2)	2	2.48	0.64
	Ti(5)	2	2.49	0.62
	Ti(3)	1	2.52	0.54
	Ti(6)	2	2.53	0.52
	Ti(4)	1	2.62	0.37
S(2)	Ti(3)	2	2.44	0.74
	Ti(5)	2	2.48	0.64
	Ti(1)	2	2.53	0.53
	Ti(4)	1	2.58	0.44
	Ti(6)	1	2.71	0.26
	Ti(2)	1	2.85	0.15
S(3)	Ti(6)	1	2.44	0.74
	Ti(5)	1	2.44	0.74
	Ti(2)	2	2.49	0.61
	Ti(1)	2	2.49	0.61
	Ti(4)	1	2.51	0.57
Ti(1)	S(3)	2	2.49	0.61
	S(2)	2	2.53	0.53
	Ti(4)	2	2.84	0.47
	Ti(4)	2	2.95	0.30
	Ti(6)	2	3.16	0.14
Ti(2)	S(1)	2	2.48	0.64
	S(3)	2	2.49	0.61
	S(2)	1	2.85	0.15
	Ti(3)	2	2.86	0.44
	Ti(4)	2	2.95	0.30
	Ti(5)	2	3.06	0.20
Ti(3)	S(2)	2	2.44	0.74
	S(1)	1	2.52	0.54
	Ti(6)	2	2.79	0.56
	Ti(2)	2	2.86	0.44
	Ti(6)	2	2.89	0.38
	Ti(3)	1	3.00	0.26
	Ti(5)	1	3.08	0.18

Table 8 (Continued)

Reference atom	Neighbor atom	Number of neighbors	Distance (Å)	Bond order
Ti(4)	S(3)	1	2.51	0.57
	S(2)	1	2.58	0.44
	S(1)	1	2.62	0.37
	Ti(5)	2	2.83	0.48
	Ti(1)	2	2.84	0.47
	Ti(1)	2	2.95	0.30
	Ti(2)	2	2.95	0.30
	Ti(4)	1	3.16	0.14
Ti(5)	S(3)	1	2.44	0.74
	S(2)	2	2.48	0.64
	S(1)	2	2.49	0.62
	Ti(4)	2	2.83	0.48
	Ti(2)	2	3.06	0.20
	Ti(3)	1	3.08	0.18
	Ti(6)	1	3.12	0.16
Ti(6)	S(3)	1	2.44	0.74
	S(1)	2	2.53	0.52
	S(2)	1	2.71	0.26
	Ti(3)	2	2.79	0.56
	Ti(3)	2	2.89	0.38
	Ti(5)	1	3.12	0.16
	Ti(1)	2	3.16	0.14

These additional atoms, specifically Ti(3) and Ti(4) coordinated to S(1), are termed "waist" atoms since they are positioned halfway along the principal threefold axis of the prism.

S(2) also has trigonal prismatic coordination: 2 Ti(1), 2 Ti(3) and 2 Ti(5), and like S(1) it is augmented by waist atoms, namely Ti(2), Ti(4) and Ti(6). Unlike S(1), which had a coordination number of 8, S(2) is coordinated to nine metal atoms. Figure 11(b) contains a perspective drawing of this coordination for S(2).

The coordination symmetry of S(3) is also augmented trigonal prismatic, but the trigonal prism in this case no longer has its (approximate) threefold axis parallel to the c axis. Instead, the threefold axis is perpendicular to the short crystallographic axis; that is, the trigonal prism is lying on its side. The seven-coordinated S(3) is shown in Figure 11(c) where it is evident that the waist atom is Ti(4).

Refer once again to Figure 10. In this drawing the dashed lines outline the projections of the trigonal prisms just described. It is fairly easy to see the trigonal prism when it is projected down its threefold axis, but when the threefold axis of the prism is perpendicular to the direction of the projection, the result is more difficult to see. Figure 12 shows the projection of two prisms, oriented differently with respect to a mirror plane. The mirror is at z=1/2; the projection is down z. All slashed atoms are in the mirror plane. The results in the two cases are (a) a triangle in the

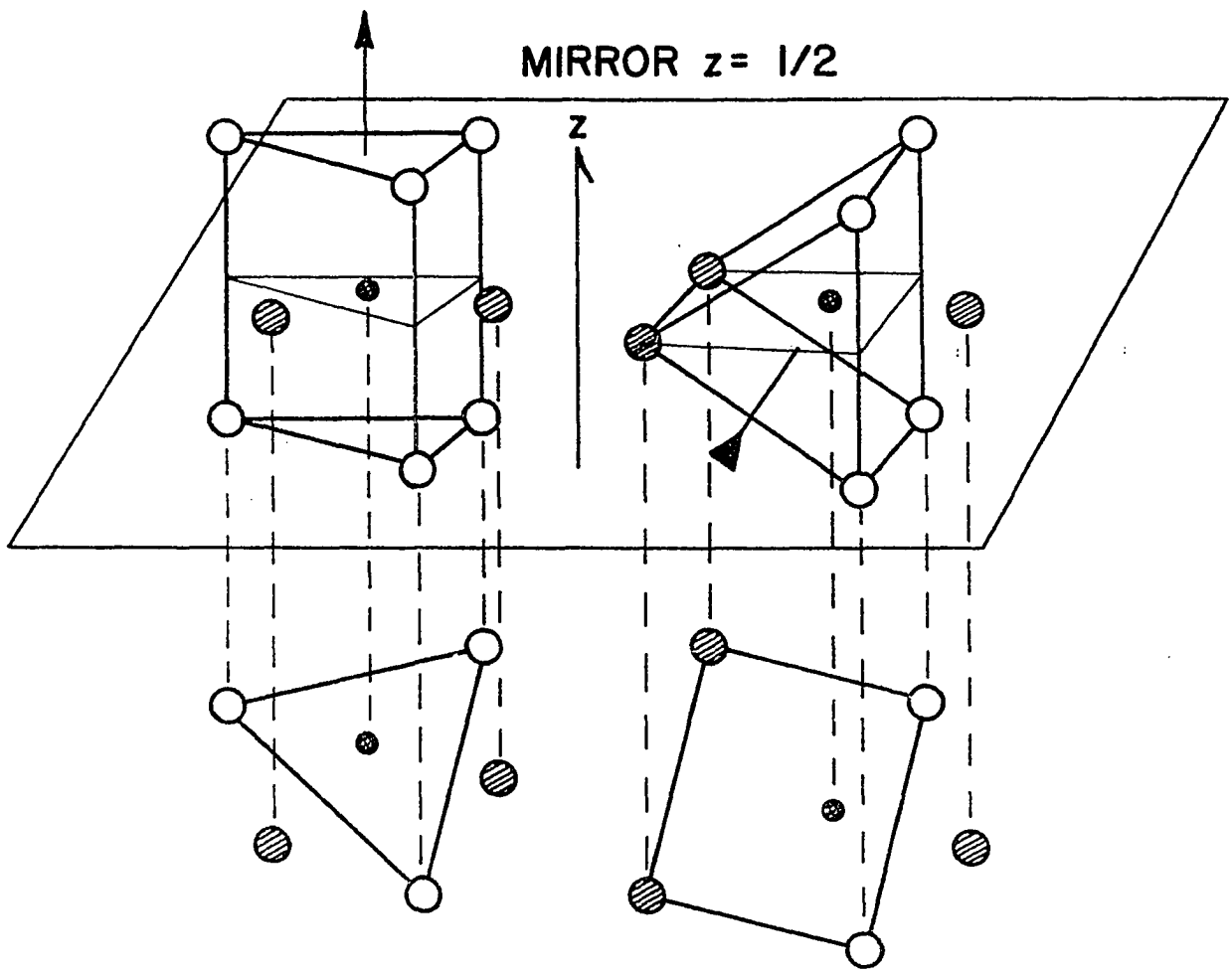

Figure 12. Orientations of two augmented trigonal prisms relative to a mirror plane: (a) threefold axis of the prism is perpendicular to the mirror; (b) threefold axis of the prism lies in the mirror plane

case of projection down the threefold, and (b) a rectangle in the case of the threefold axis of the prism being perpendicular to the axis of projection.

Now shift attention to the Ti atoms. The titanium coordination is difficult to describe for there does not seem to be as striking a coordination characteristic among the six different Ti positions as there appeared in the sulfur cases. One feature of the coordination of Ti should be mentioned; the feature is perhaps best described as a tendency for Ti to have cubic coordination, i.e., to be situated in the center of a cube of both Ti and S atoms. For example, for Ti(1) the cube is 4 Ti(4) atoms, 2 S(2), and 2 S(3) atoms. In most cases such a cubic arrangement of atoms around the titanium atoms in Ti_2S is very much distorted. The Ti atom with the smallest distortion of its coordination geometry is Ti(4), which exhibits, in part, cubic coordination to eight Ti metals at distances ranging from 2.83Å to 2.95Å. In addition, Ti(4) is bonded to sulfur atoms, S(1), S(2), and S(3), which are located adjacent to the approximately square faces of the slightly distorted cube.

In view of the fact that the three sulfur coordination polyhedra are nearly perfect trigonal prisms, whereas the titanium coordination polyhedra are not similar to each other or are greatly distorted when viewed as similar, it is interesting to describe the structure of Ti_2S as a collection of interconnected sulfur coordination polyhedra. Figure 13 is a

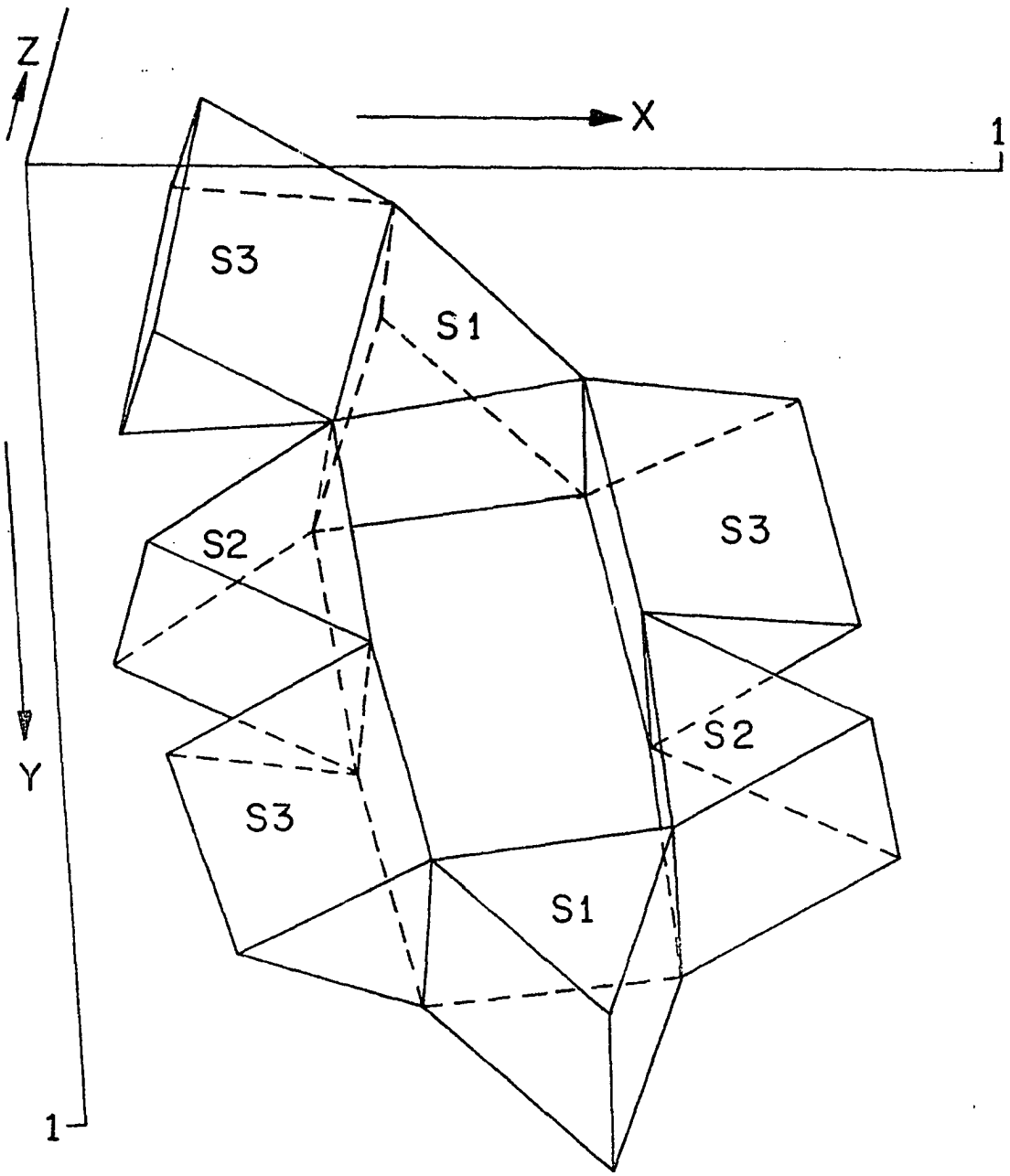

Figure 13. Linkage of sulfur coordination polyhedra in Ti_2S. Only trigonal prisms are drawn

computer (13) drawing which shows the trigonal prisms and their linkage for one unit cell. Titanium atoms are located at all corners of the prisms. The polyhedra are labeled with the labels of the sulfurs which are located at their respective centers. Figure 14 is again the same kind of drawing, but the prisms have been augmented to include waist atoms. The drawing shows how a waist atom of one prism may be a corner atom in another trigonal prism. This description of Ti_2S in terms of the coordination polyhedra of the non-metal atoms is different from the "usual" description of transition-metal compounds. The usual description is made in terms of the metal atom coordination polyhedra. The use of non-metal coordination polyhedra, however, is not new. For example, Caro (39) described the rare-earth oxides and oxysalts in terms of the OM_4 (M=rare-earth metal) coordination tetrahedra of oxygen. In Ti_2S the polyhedra are different, being augmented prisms STi_6, STi_7, STi_8, or STi_9. The motivations behind these descriptions are the same--to provide a way of viewing the structures using fairly simple building blocks, although the building block may change from one non-metal to another. The occurrence of similar coordination polyhedra throughout a particular structure and the differences between the polyhedra for different central atoms in different structures may be important in considering the nature of the bonding in such compounds displaying these features.

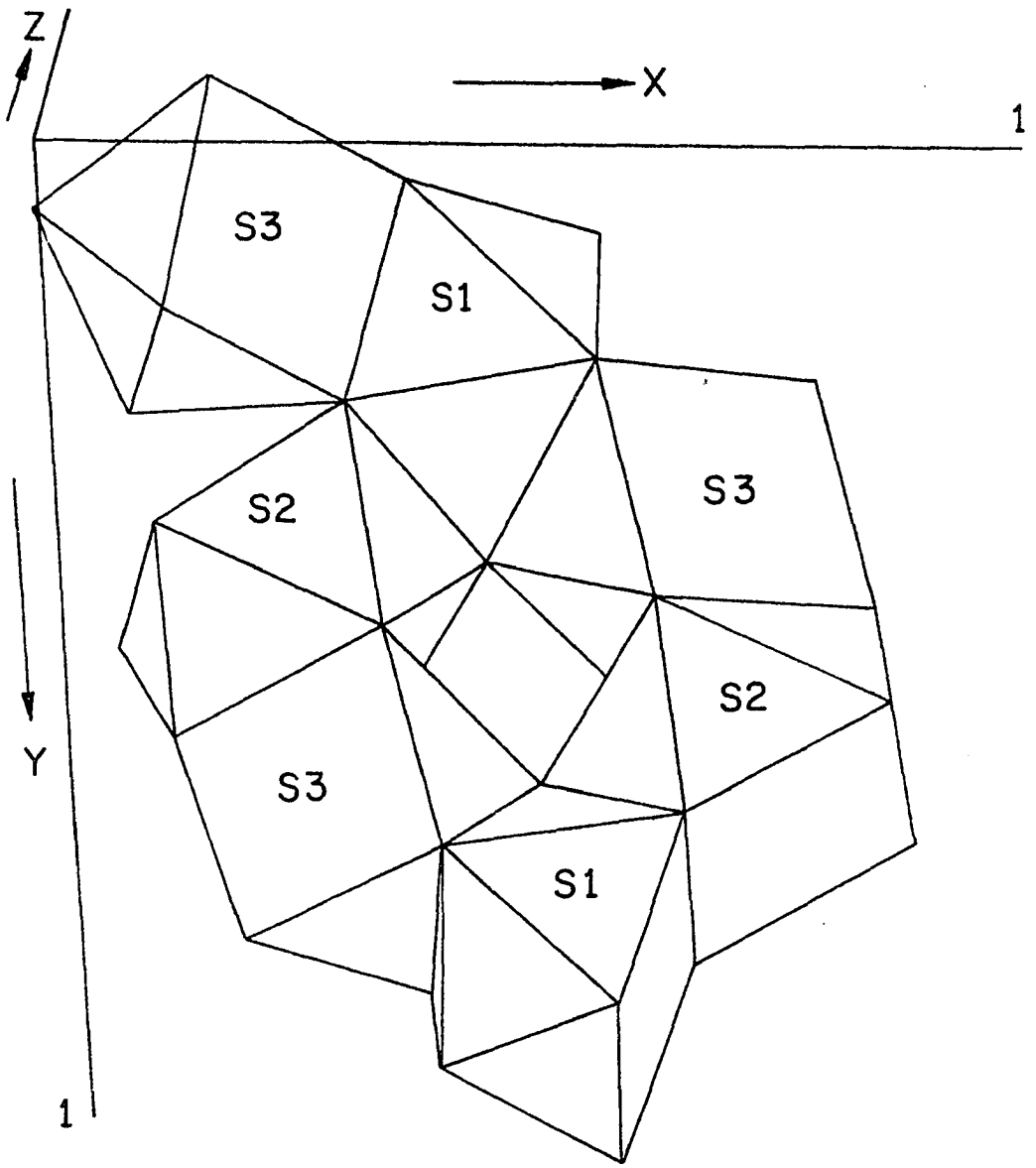

Figure 14. Linkage of sulfur coordination polyhedra in Ti_2S. Augmented trigonal prisms are drawn

E. Discussion

1. General remarks

It is indeed difficult, if not impossible with present techniques, to obtain a quantitative understanding of the bonding in a solid compound such as Ti_2S; either (a) the approximations to simplify the problem are very severe, as is, for example, the muffin-tin potential used in augmented-plane-wave calculations or (b) necessary information for a sophisticated calculation is not known or, if known, computer core sizes cannot handle the complexity of the problem. It is therefore important at this time to try to qualitatively understand the bonding in solid compounds with the aid of such information as physical properties, local atomic environment, interatomic distances, and bond angles, and from investigations of changes in these quantities with changing elemental constituents. It is hoped that a bonding proposal for compounds exhibiting related characteristics will provide a basis for a more quantitative understanding in the future.

The discussion which follows is divided into three sections. In the first section a basis is selected for viewing the bonding in Ti_2S; the basis is an extension of the ideas of Franzen (40) on the bonding of chalcogens in transition-metal monochalconides. Franzen's discussion is based on three more general propositions: Slater's (38) view of covalent binding in solids, Pauling's (41) valence bond approach to intermetallic compounds, and an application of directionality of bonding

orbitals by Rundle (42). The employment of these propositions in the discussion of Ti_2S warrants a consideration of their development and applicability, and this will be done in Section A. The next section deals specifically with the bonding in Ti_2S. The last section provides a survey of other metal-rich compounds of Group IVB (M/Ch > 1) in an attempt to correlate the structural differences and similarities of these compounds with an appropriate qualitative bonding proposal.

2. Basis of the discussion

a. Slater's view of bonding in solids

Slater's (38) discussion of atomic radii in 1964 dealt with three points important to the discussion which follows: 1) he provided experimentalists with a single set of atomic radii which are consistent with the empirical interatomic distances observed in approximately 1200 solids; 2) he pointed out that the differences between the previous sets of ionic radii [e.g., Wasastjerna (43), Goldschmidt (44), Pauling (45), and Zachariasen (46)] and his own atomic radii are compatible with the view that they result from different ways of looking at the same bonding situations; and 3) he concluded that compounds which are conventionally viewed as ionic in their interatomic interactions can be described in terms of covalent interactions and, indeed, it is appropriate to consider bonding in all solids as being predom-

inantly covalent in nature.[1]

The basis for the empirical set of Slater's atomic radii is given in detail in Quantum Theory of Molecules and Solids (47). The radii are listed for reference in Appendix B.

The significance of an atomic radius as presented by Slater is that the radius describes the maximum radial charge density of the outermost shell of the atom. The formation of a bond depends on the overlapping of the wavefunctions of two bonding atoms. The nature of a covalent bond is that, due to partially filled orbitals, the wavefunctions of the bonding atoms are able to overlap considerably before the exclusion principle prevents further overlap; by "considerably" is meant up to the distance at which the maxima of radial charge density of the two bonding atoms coincide. If the bond is considered to be ionic in nature, then electrons are conceptually transferred from one species to another at infinite separation, thereby filling the outer orbitals. Then with decreasing interatomic distance, the Coulombic attraction and electronic repulsion of filled orbitals compete to yield the minimum energy configuration, the re-

---

[1] A distinction between conventional covalent and ionic bonds is perhaps necessary at this point. The term "covalent bonding" is usually used to describe the interaction between semi-atomic species which share an electron(s) as opposed to the quasi-classical interaction which persists when the atoms are infinitely separated in "pure" atomic states. Semi-atomic is used above because the atoms are not in "pure" states when interacting at bonding distances. Ionic bonding is a term used to describe the strictly classical interaction between species which are formally charged.

sult being that only the tails of the wavefunctions overlap when the electronic repulsion is large enough to balance the attraction. Thus, an atomic radius can be viewed as the position of maximum radial charge density of the outermost shell, while an ionic radius can be viewed as the position of the tail of the wavefunction of the outermost shell.

The third significant point raised by Slater has to do with the nature of bonding in all solids. Slater considered KCl and argued that neutral atoms can be brought from infinity to their separation in the crystal and, depending upon how the chlorine radius is drawn, the chlorine can attain a negative charge relative to the potassium. A linear combination of atomic wavefunctions and ionic wavefunctions describes the true final wavefunction, but Slater maintained that covalent contributions to the wavefunction are dominant. Accordingly he formulated one set of atomic radii to be used for all solid compounds in determining whether a distance could be viewed as a bonding distance.

The great success of lattice energy calculations, for which charge density is localized, is an indication of the degree to which the final description is appropriately an ionic one for some compounds. For example, recent calculations of bond energies including energy terms for both neutral and electrostatic bonded species by Sanderson (48) show good agreement with existing experimental results. On the other hand, some electrostatic models for calculating lattice energies are in

serious disagreement with experiment. Moody and Thomas (49), using an electrostatic model, for example, calculated the stability of Ti_2S, with a hypothetical structure-type, with respect to disproportionation to TiS and Ti. Their calculations yielded, for the reaction $Ti_2S \rightleftharpoons Ti+TiS$, $\Delta H=-22$ kcal/mole. This value for ΔH was shown to be in error by an order of magnitude by the preparation of Ti_2S at 1400°C as reported by Franzen and Gilles (21) and by Owens, Conard and Franzen (24).

b. Bond orders in metallic substances Linus Pauling has been one of the leading figures in the development of the valence-bond theory of chemical bonding. Rundle (50) has provided an excellent summary of Pauling's arguments with regard to metals and alloys. For metals and intermetallic compounds Pauling (41) used fractional bonding electron pairs resonating (delocalized) among bonding species to account for the valences, the interatomic distances, the metallic properties and the cohesive energies observed for such solids. An empirical equation proposed by him,

$$D(n) = D(1) - 0.6 \log n, \qquad (16)$$

relates a bond distance of order n to the bond distance of order 1, a single electron pair bond. A set of metallic radii, Pauling's metallic radii, was derived on the basis of this equation from a consideration of interatomic distances and valence electron configurations of metals. Furthermore, Equation 16 provides a consistent way of calculating valences of species in intermetallic compounds. One merely adds all bond orders

associated with an atom to find the number of electron pairs participating in the bonding of that atom to its neighboring atoms.

The application of Pauling's proposal has suffered from a lack of accuracy and consistency in relatively few cases. Such a case of failure was noted by Geller (51) for intermetallic compounds of composition A_3B having the β-W-type structure for which the valences, calculated using Pauling's metallic radii with Equation 16, were generally too high from a chemical point of view. Failures of the valence-bond approach for specific structures, such as β-W-type, suggests that atoms at close distances in some structures may be non-bonded due to the directional nature of the bonding.

c. Directional bonding The third contribution, which is important to the understanding of Franzen's presentation which follows and of which the discussion of Ti_2S is an extension, was made by R. E. Rundle (42). Rundle proposed a bonding scheme for MX compounds (M is a transition element and X is C, N, or O) which was consistent with their physical properties. Rundle noted that the MX compounds formed predominantly the NaCl-type structure regardless of the structure of the metal or the atomic (ionic) radii or electronegativities of the components, and that, accordingly, it was difficult to consider these MX compounds as interstitials, as suggested by Hägg (52). Rather, the preference for octahedral coordination by C, N, and O, when considered in conjunction with physical properties and bond dis-

tances, led Rundle to focus his attention on this coordination symmetry in proposing a bonding description. The description involved delocalized electrons to account for electrical and thermal conductivity and luster. It involved directed bonds between metal and non-metal to account for the brittleness of MX compounds and strong metal/non-metal bonds to account for high melting points of MX compounds, compared with the melting points of the constituent metals, in spite of increased metal-metal distance from M to MX. Rundle proposed that six bonds could form from three 2p orbitals or one 2s and three 2p orbitals to give 1/2 to 2/3 electron pairs per bond. Pauling's bond orders calculated for MX compounds using Equation 16 were consistent with this proposal.

A discussion of more recent proposals for the bonding in NaCl-type structures of MX compounds by Bilz (53) and by Denker (54) will be delayed until Chapter V.

d. A proposal for the bonding in monochalconides by Franzen In a discussion of the bonding in MX compounds where M is a transition metal and X is a chalcogen element, Franzen (40) proposed that a delocalized, directional, covalent bonding description for such compounds was consistent with their observed metallic conductivity, brittleness, and Pauli paramagnetic behavior. An application of Pauling's bond order equation to these compounds yielded high valences for the chalcogens--between three and four in most cases--and indicated that chalcogen d orbitals were participating in the bonding which was

primarily between metal and chalcogen.

Specifically, there are four structures which are important in discussing MX compounds: NiAs, WC, MnP, and NaCl. A way of viewing these structures is given in Appendix C. An example of the NiAs-type structure is TiS. In this structure the sulfur has trigonal prismatic coordination symmetry; it is bonded to six Ti atoms at a distance of 2.48Å, which yields (Equation 16) a bond order of 0.63. The Ti has octahedral coordination symmetry, being bonded to six sulfur atoms. The shortest Ti-Ti distance, along the c axis, is 3.19Å corresponding to a bond order of 0.13.

Franzen suggested, as had Rundle for M(C,N,O) compounds, that the bonding electrons in NiAs resided primarily in metal-chalcogen bonds rather than in metal-metal bonds. Indeed, the metal-metal distances could be dictated entirely by strong metal-chalcogen interactions. For this reason the valences calculated from Pauling bond orders could be too high if metal-metal bond orders were included. The interatomic distances, bond orders, and valences for representative compounds having the NiAs-type, WC-type, and MnP-type structures are listed in Table 9. Every metal-metal bond order for these compounds is less than 0.20, indicating much less significant bonds than those bonds between metal and chalcogen. The metallic conductivity in monochalconides of these structures was therefore viewed by Franzen as arising from electrons delocalized in electron deficient metal-chalcogen bonds. The diamagnetic behavior of these compounds or

Table 9. Valences for some NiAs, WC, and MnP-type compounds of sulfur and selenium

Compound and structure-type	M-M distance (Å)	M-Ch distance (Å)	Bond order, n_{M-M}	Bond order, n_{M-Ch}	V_M	V'_M[a]	V_{Ch}
TiS(NiAs)	3.19(2)	2.48(6)	0.13	0.63	4.04	3.78	3.78
$VS_{1.1}$(NiAs)	2.92(2)	2.42(6)	0.16	0.54	3.56	3.24	3.24
HfS(WC)	3.43(2) 3.37(6)	2.60(6)	0.12 0.15	0.63	4.92	3.78	3.78
ZrS_{1-x}	3.43(6) 3.46(2)	2.63(6)	0.13 0.12	0.59	4.56	3.54	3.54
TiSe(MnP)	3.21(2)	2.52(1) 2.56(2) 2.70(2) 2.78(1)	0.12	0.89 0.78 0.45 0.33	4.25	4.01	4.01
$VS_{1.06}$(MnP)	2.94(2)	2.39(1) 2.52(2) 2.35(2) 2.34(1)	0.18	0.61 0.37 0.71 0.74	3.87	3.51	3.51

[a]Metal-metal bond orders not included.

their weak Pauli paramagnetism and interatomic distances were consistent with four electrons from both metal and chalcogen participating in bonding. Thus, four electrons in six bonding orbitals yielded bond orders of 2/3 for M-Ch bonds. In order to achieve six bonding orbitals on the chalcogen, Franzen proposed that chalcogen d orbitals were participating in the bonding.

Atomic coordination symmetry provided a further basis for this interpretation. For many monochalconides the chalcogens have trigonal prismatic coordination (NiAs, WC-types) or distorted trigonal prismatic coordination (MnP-type) suggesting that the bonding orbitals, e.g., d^3p^3 hybrids on the chalcogen, favor this coordination. Coordination other than trigonal prismatic for monochalconides can be understood in terms of the valence states of the metal. The trigonal prismatic symmetry is pictured as arising from the stability of four electron pairs delocalized over six bonding orbitals. For example, ScS has a maximum of three electron pairs delocalized over six orbitals, and, consequently, trigonal prismatic coordination of sulfur would not be expected. Rather, it seems that the lowest energy is obtained by s and p bonding as suggested by Rundle.

On the other side of the transition series Franzen suggested that the metals have too many electrons and not enough orbitals to form six electron-deficient bonds with the chalcogen. Zn, for example, has nine valence orbitals (one s, three p, and five d orbitals), of which it must use six orbitals and four electrons to provide for the stability of trigonal prismatic

coordination of, say, sulfur. This results in three orbitals not involved in Zn-S bonds, but Zn has eight electrons (12-4) to put into three orbitals which is incompatible with the exclusion principle. Thus, ZnS forms a structure in which the S coordination is tetrahedral, a symmetry consistent with s and p bonding orbitals.

Franzen also pointed out that monoxides are devoid of trigonal prismatic coordination symmetry for oxygen. He suggested that this fact could be understood by the inaccessibility of d orbitals for oxygen. As was mentioned previously, Caro (39) described some oxides and oxysalts in terms of the linkage of OM_4 polyhedra. Caro concluded that this structural feature was evidence for directional bonding in these compounds probably due to sp^3 hybridization for oxygen orbitals.

3. The bonding in Ti_2S

A qualitative description of the bonding in Ti_2S will now be given. The basis for this discussion is that Ti_2S can be viewed as a covalent compound following the suggestion by Slater, that the electrons are delocalized in directed orbitals to account for the metallic conductivity and the brittleness as suggested by Rundle, and that the interatomic distances may be correlated with bond order by Pauling's empirical equation.

It should be emphasized again that the coordination of sulfur is, for all three independent sulfurs, slightly distorted trigonal prismatic with additional coplanar metals perpendicular to and slightly removed from the faces of the prisms. One pos-

sible way to calculate bond orders in Ti_2S is to use the Pauling bond order equation based solely on interatomic distances. From this viewpoint S(1) is bonded to eight Ti atoms, S(2) to nine Ti atoms and S(3) to seven Ti atoms. The Ti atoms are bonded strongly to the sulfur atoms, but there is also extensive metal-metal bonding in Ti_2S. The interatomic distances and bond orders are listed in Table 8. The valences obtained for the six different Ti atoms and the three different sulfur atoms are listed in Table 10 under the column labeled "Non-directional, Covalent." The Ti valences are all greater than four; a valence of four is expected for Ti_2S, since one would expect the four outer electrons to be involved in bonding. The sulfur valences are also all greater than four whereas according to the view of bonding discussed above one would expect four valence electrons for sulfur to pair with the four electrons from Ti. These high valences could result from short, non-bonded distances as apparently is the case for β-W-type structures as pointed out by Geller (51). Thus, a second interpretation is possible by proposing that only certain directions are favorable for bonding due to the directed nature of the orbitals or hybrid orbitals.

The second interpretation of the bonding in Ti_2S is based on the premise that the Ti atoms situated at the corners of the trigonal prism are bonded to the sulfur at the center of that prism. The "waist" Ti atoms are not bonded to the sulfur in this scheme. The "waist" Ti atoms are, however, strongly bonded

Table 10. Atom valences for Ti_2S according to alternative bonding descriptions. Distances less than 3.17Å are considered.

Atom	Non-directional, covalent	Directional, trigonal prism, covalent
S(1)	4.47	3.56
S(2)	4.67	3.82
S(3)	4.49	3.92
Ti(1)	4.10	4.10
Ti(2)	4.53	4.38
Ti(3)	5.22	4.68
Ti(4)	4.62	3.24
Ti(5)	4.96	4.96
Ti(6)	4.36	4.10

to Ti atoms at the prism corners, e.g., Ti(3) to two Ti(6) and two Ti(2). The valences according to this directional approach to the bonding are listed in column three of Table 10. The valences for S are more reasonably between 3.5 and 4, while the valences for the Ti atoms, although still high, are generally lower than the non-directional valences. The high Ti valences obtained could still be due to short, non-bonded Ti-Ti distances.

In either interpretation the valences of the sulfur atoms, considering the approximate nature of Equation 16, are close to 4. This observation, along with the observed metallic conductivity, the Pauli paramagnetism, and the recurrence of the trigonal prismatic coordination symmetry, suggests that the proposal by Franzen (40) be extended to this metal-rich sulfide and that sulfur utilizes approximately four electrons and four to nine orbitals to form electron deficient, directional, covalent bonds. The participation in bonding of four to nine orbitals for sulfur is possible only if outer s or d orbitals are used on sulfur.

The proposal for participation by "outer" orbitals on sulfur should be met with stern requests for outer orbital energies and outer orbital sizes. The questions to be answered are: (a) are the outer orbitals, e.g., the d orbitals, low enough in energy to be used; and (b) even if the answer to (a) is "yes", are they of small enough size to give good overlap in bond formation? Information on orbital energies and sizes, however, are presently only available in approximate form, for band calculations have not been undertaken for Ti_2S or even for simpler

structures such as TiS. In an attempt to find some good numbers for energy levels and orbital extension one is usually left with values which either have been observed spectroscopically or have been calculated by the self-consistent field method.

Consider the experimental data. Spectroscopic evidence from Moore's (55) compilation are presented in Table 11. Table 11 not only has energy levels for the chalcogens and oxygen but also, for comparative purposes, other first and second row elements. There are several things which may be misleading about the information contained in Table 11. The first is that one electronic configuration has a manifold of terms associated with it, and consequently each configuration has terms over a range of energy. In the table the lowest term in the manifold was selected as representative of the configuration. The second possible confusion has to do with the applicability of these energy levels in the free atom case to the bond energies for a three-dimensional solid. There is no way to skirt the fact that one must analyze atoms or simple molecules for which data are available and extrapolate to cases involving combinations of such atoms, realizing that each atom will be perturbed by the nature of the combination.

It is common knowledge, for example, that Be is a metal, and therefore must have a Fermi energy such that a band is partially filled. Indeed, the closed shell of Be in the atomic ground state ($1s^2 2s^2$) would indicate insulator or semiconductor behavior. But in the solid the linear combinations of 2p or-

Table 11. Some spectroscopic energy levels, obtained from Moore's[a] compilation, for Li, Be, B, C, N, O, Si, P, S, and Se

Element	Term	Electronic configuration	Energy(ev)	Energy(cm^{-1})
Li	^2S	$1s^2 2s$	0	0
	^2P	$1s^2 2p$	1.85	14903
Be	^1S	$1s^2 2s^2$	0	0
	^3P	$1s^2 2s 2p$	2.73	21979
B	^2P	$1s^2 2s^2 2p$	0	0
	^2D	$1s^2 2s^2 3d$	6.79	54765
C	^3P	$1s^2 2s^2 2p^2$	0	0
	^3P	$1s^2 2s^2 2p 3s$	7.48	60334
	^3F	$1s^2 2s^2 2p 3d$	9.70	78199
	^3D	$1s^2 2s 2p^3$ (sp^3-hybrid)	7.95	64089
	^5S	$1s^2 2s 2p^3$	4.18	33735
N	^4S	$1s^2 2s^2 2p^3$	0	0
	^4P	$1s^2 2s^2 2p^2 3s$	10.3	83286

[a]Moore, C. E., National Bureau of Standards (U.S.), Circular 467 (1949).

Table 11 (Continued)

Element	Term	Electronic configuration	Energy(ev)	Energy(cm^{-1})
	^4D	$1s^2 2s^2 2p^2 3p$	11.8	94772
	^2F	$1s^2 2s^2 2p^2 3d$	13.0	104811
O	^3P	$1s^2 2s^2 2p^3 2p$	0	0
	^5S	$1s^2 2s^2 2p^3 3s$	9.15	73767
	^5P	$1s^2 2s^2 2p^3 3p$	10.7	86625
	^5D	$1s^2 2s^2 2p^3 3d$	12.1	97420
Si	^3P	$3s^2 3p^2$	0	0
	^3P	$3s^2 3p4s$	4.92	39683
	^3D	$3s3p^3$(sp^3-hybrid)	6.00	48399
	^3F	$3s^2 3p3d$	6.18	49850
P	^4S	$3s^2 3p^3$	0	0
	^4P	$3s^2 3p4s$	6.94	55939
	^4D	$3s^2 3p^2 4p$	8.11	65373
	^2F	$3s^2 3p^2 3d$	8.73	70391
S	^3P	$3s^2 3p^4$	0	0

Table 11 (Continued)

Element	Term	Electronic configuration	Energy(ev)	Energy(cm^{-1})
	^5S	$3s^2 3p^3 4s$	6.53	52623
	^5P	$3s^2 3p^3 4p$	7.87	63446
	^5D	$3s^2 3p^3 3d$	8.42	67878
Se	^3P	$4s^2 4p^4$	0	0
	^5S	$4s^2 4p^3 5s$	5.97	48182
	^5P	$4s^2 4p^3 5p$	7.35	59242
	^5D	$4s^2 4p^3 4d$	7.86	63370

bitals result in bonding states which are lower in energy than the atomic 2p state and thus the 2p band in the solid overlaps with the high-energy part of the 2s band resulting in many empty states above the Fermi energy and in metallic behavior. Callaway (56) states that recent energy band calculations indicate that the character of the electrons at the Fermi surface in Li, for example, is primarily p character. The data given in Table 11 for Li and Be show that the 2p atomic levels in these elements are 1.85 ev. and 2.73 ev., respectively, above the ground states. It is seen, therefore, how much band energies can be lowered from the related atomic energy levels.

Providing a reference in Table 11 is carbon, for it is commonly accepted that carbon utilizes one s and three p orbitals to form four sp^3 hybrid orbitals in tetrahedral configuration. The ground state of carbon is $1s^2 2s^2 2p^2 (^3P)$. To achieve the $1s^2 2s 3p^3$ configuration required for the hybrids, the energy expended is 4.2 ev. to the ^5S state (four unpaired electrons) or 8.0 ev. to the ^3D state (two unpaired electrons).

Consider sulfur in Table 11. Promotion of one 3p electron from the ground state configuration to the outer 4s orbital, 4p orbital, or 3d orbital requires 6.53, 7.87, or 8.42 ev., respectively. That these orbitals could be involved in bonding in order to achieve stronger metal-chalcogen bonds and thus more delocalization of electrons is reasonable when viewed in perspective with the energy requirement for carbon to adopt an sp^3 valence state configuration. On the basis of these atomic

spectral data it is concluded that selenium would be even more suitable for outer orbital participation in its bonding than sulfur.

Oxygen, on the other hand, has the d orbital 12.1 ev. above the ground state. It would appear that the amount of stability obtained by using the d orbital in the case of oxygen is not enough to offset the energy spent in promoting to the outer valence state. This interpretation is consistent with the fact that oxygen has never been found in trigonal prismatic coordination. For example, Ti_2O was found by Holmberg (57) to have the anti-$Cd(OH)_2$-type structure in which the oxygen atoms occupy the alternating layers of octahedral interstices perpendicular to the c axis of the hexagonal close-packed α-titanium structure. In the same system Holmberg (57) reported Ti_3O. It has a superstructure of the Ti_2O structure, i.e., the oxygen atoms in Ti_3O are octahedrally coordinated, and oxygen vacancies are ordered. As another example, nitrogen has not been observed in trigonal prismatic coordination, a fact again in line with the high promotion energies listed for N in Table II. Ti_2N was found by Holmberg (58) to have an anti-rutile structure in which the nitrogen atoms occupy one-half of the octahedral interstices in layers perpendicular to the c axis of α-titanium, although the Ti positions in α-titanium are somewhat distorted. A very interesting structural result, however, which will be discussed in Chapter VI, is that B, Si, Se, and P all have been observed to have trigonal prismatic coordination

as one of their various coordination symmetries. Again, the outer orbitals for these atoms have energies which are sufficiently close to the ground state to be accessible when a favorable bonding situation will balance the cost of the promotion.

A second way one may attempt to obtain good orbital energies and orbital sizes is to calculate them. Such a calculation was done by Craig and Zauli (59) for the molecular system SF_6. The calculation found self-consistent wavefunctions for the 3s, 3p, and 3d orbitals of sulfur based on an octahedral potential field of fluorine atoms. The results indicated a drastic contraction of the d orbitals of sulfur when occupied by two electrons, making d orbital overlap with fluorine orbitals more suitable for bonding. Furthermore, with regard to energies required to promote the ground state configuration s^2p^4 to sp^3d^2, they concluded that, "...the promotion energy into the sp^3d^2 configuration is likely to be available under conditions of molecule formation..."(60). These authors proposed that their calculations indicated that d orbital participation in the bonding of sulfur in SF_6 is permissible from both energy and orbital extension considerations.

Another calculation by the self-consistent-field method concerning the size and energy of d orbitals in various states of the sulfur atom was performed by Coulson and Gianturco (61). One part of their work concerned the calculation of the atomic energy E, the mean radius $\bar{r}$, and the radial maximum r_m for 3s,

3p, and 3d functions of sulfur for various spectroscopic terms. The results were (a) that $\bar{r}$ and r_m for both the 3s and 3p functions were fairly constant as one and then two d orbitals were included in the configuration, i.e., that the sizes of s and p orbitals were not sensitive to electrons being excited to d orbitals; (b) that the $\bar{r}$ for the 3d function decreased drastically from 4.00Å for the s^2p^3d configuration to 2.32Å, 1.90Å or 1.88Å for three different terms arising from the sp^3d^2 configuration; (c) that r_m suffered the same decrease as $\bar{r}$, e.g., from 3.34Å (s^2p^3d) to 1.42Å, 1.30Å or 1.20Å (sp^3d^2); and (d) that the energy required to promote one electron from a 3p to a 3d orbital was 7.27 ev., a value in fair agreement with the spectroscopic value of 8.42 ev. listed in Table 11, and the promotion energy to obtain two d electrons was 24.48 ev. Another part of Coulson and Gianturco's work was a calculation of E, $\bar{r}$, and r_m for various valence states and various hybrid states of sulfur. The results of these calculations were in agreement with their previous calculations, namely, that the d orbitals contract greatly when occupied by two electrons and the promotion energy for such a case, from the ground state, is ca. 25 ev. A third part of their work involved varying the charge on the sulfur. They found that the formal charge greatly affected the d orbital size, but had very little affect on s and p orbital sizes. Indeed, for a formal charge of +0.6, configuration $s^{0.9}p^{2.7}d^{1.8}$ decreased the $\bar{r}$ for 3d to 1.42Å, a mean radius which looks more like the mean radius of a valence or-

bital than of an "outer orbital."

The conclusions drawn from these studies were that d orbitals on sulfur are contractable by electron population and by positive formal charge on the sulfur and that the concomitant energy spent to involve the d orbitals in bonding could conceivably be compensated by bond formation in an appropriate coordination and with appropriate bonding partners.

Therefore, it is not contradictory to these calculations and spectroscopic observations to propose that trigonal prismatic coordination of d electron-rich Ti atoms with directional bond formation to a central sulfur could compensate for sulfur d orbital participation in the formation of the conduction band in Ti_2S.

Another bit of evidence in arguing for d orbital bonding by sulfur in augmented trigonal prismatic coordination is that this coordination was observed by Hoard (62) for Ta and Nb in K_2TaF_7 and K_2NbF_7, respectively. Extensive d orbital participation by the central atom would be expected in these cases.

4. Survey of metal-rich chalconides of Group IVB with 2:1 composition

a. Structures Let us now turn our attention to other metal-rich chalconide compounds of Group IVB which have 33 atomic percent chalcogen. Ti_2Se, Zr_2S and Zr_2Se are isostructural with Ti_2S, and Hf_2Se is isostructural with Hf_2S, which has a different structure than the Ti_2S-type. Lattice parameters for these metal-rich chalconides are listed in Table 12.

Table 12. Lattice parameters for M_2Ch compounds of Group IVB metals

Compound	Reference	Structure-type	Lattice parameters(Å)	$(r_{Ch}/r_m)_{Slater}$
Ti_2S	This work	Ti_2S	a=11.367±0.003 b=14.060±0.004 c= 3.326±0.001	0.714
Ti_2Se	(63)	Ti_2S	a=11.743±0.003 b=14.517±0.003 c= 3.457±0.009	0.821
Zr_2S	This work	Ti_2S	a=12.322±0.003 b=15.359±0.004 c= 3.508±0.001	0.645
Zr_2Se	(64)	Ti_2S	a=12.640±0.003 b=15.797±0.003 c= 3.602±0.001	0.742
Hf_2S	(65)	Hf_2S	a= 3.3736±0.0002 c=11.788±0.001	0.645
Hf_2Se	(63)	Hf_2S	a= 3.450±0.009 c=12.260±0.004	0.742

Ti_2Se and Hf_2Se were reported by Smeggil (63). A detailed characterization of Zr_2S is contained in this thesis in Chapter V. A refinement of the crystal structure of Zr_2Se was carried out by Franzen and Norrby (64) and the crystal structure of Hf_2S was reported by Franzen and Graham (65).

Hf_2S crystallizes in space group $P6_3/mmc$ with $\underline{a}$=3.37Å and $\underline{c}$=11.79Å. A view (after Franzen and Graham) of the (110) plane of Hf_2S showing the atoms drawn according to Slater's atomic radii is shown in Figure 46(f) in Appendix C. The crystallographically independent sulfur atom in Hf_2S is coordinated to six Hf atoms at the corners of a trigonal prism. The Hf atom is coordinated to three sulfur atoms and three Hf atoms in a distorted octahedron. There is, incidentally, extensive Hf-Hf bonding in Hf_2S, as can be seen by the overlap of the Hf atomic radii in the center of the (110) plane in Figure 46(f).

b. Valences The valences of Hf and S for Hf_2S, calculated using Equation 16, are 4.08 and 3.36, respectively.

The valences for each metal and chalcogen in the $M_2^{IV}Ch$ structures of the Ti_2S-type for which the positional parameters have been refined independently are listed in Table 13. The valences listed under (A) were calculated from Pauling's relationship without regard to directionality, while the valences under (B) were calculated based on directional bonding, i.e., excluding the waist metal-sulfur distances. Several observations may be made concerning these valences:

(1) The metal valences are generally too high in the (A)

Table 13. Comparison of valences of $M_2^{IV}CH$ compounds of the Ti_2S-type

	Ti_2S	Ave.	Ti_2Se	Ave.	Zr_2Se	Ave.
A. Non-directional, covalent						
M1	4.047	4.591	4.039	4.318	3.957	4.070
M2	4.553		4.116		4.118	
M3	5.182		4.858		4.350	
M4	4.555		3.823		3.830	
M5	4.911		4.966		4.385	
M6	4.297		4.109		3.782	
Ch1	4.431	4.524	4.962	5.020	4.111	4.384
Ch2	4.652		5.382		4.614	
Ch3	4.490		4.704		4.428	
B. Directed, trigonal prismatic, covalent						
M1	4.047	4.201	4.039	3.877	3.957	3.745
M2	4.400		3.887		4.060	
M3	4.636		4.248		3.985	
M4	3.161		2.340		2.591	
M5	4.911		4.966		4.385	
M6	4.050		3.782		3.490	
Ch1	3.512	3.744	3.976	4.133	3.465	3.733
Ch2	3.807		4.275		3.863	
Ch3	3.914		4.147		3.872	

list. An average metal valence of 4.1 in Zr_2Se in (A) is the most reasonable for a valence electron configuration of sd^3 for Zr.

(2) The average chalcogen valences for the three structures under either the directed or the non-directed interpretation are all above 3.7, a valence for the chalcogen which suggests the involvement of outer orbitals.

(3) Evidence favoring interpretation (A) is seen by focusing attention on M(4) which is the metal atom with the least distorted cubic coordination. But, according to interpretation (A), M(4) is also bonded to three additional sulfur atoms off three faces of the cube, i.e., M(4) is a waist atom to three different prisms. The valences calculated for M(4) according to interpretation (A), especially for Ti_2Se and Zr_2Se, are close to 4, as expected. Those valences calculated according to (B), however, are unreasonably low.

Additional trends in bond orders and valences are difficult to unravel at this time.

c. The Brewer-Engel correlation applied to Group IVB M_2Ch compounds The metal coordination is difficult to describe for the Ti_2S-type structures, but, as mentioned in the description of the Ti_2S structure, one can see a tendency for the metals to have cubic coordination, i.e., bonded to eight atoms at the corners of a distorted cube. Recall, for example in Figure 10, that Ti(4) has the least amount of distortion for this description of its coordination. Hf_2S and Hf_2Se, on the

other hand, have octahedral coordination of the metal atoms. In an attempt to understand the differences between the Ti_2S-type and the Hf_2S-type structures, Franzen, Smeggil, and Conard (66) viewed the structure-types in terms of a correlation proposed by Engel (67) and extended by Brewer (68, 69).

Engel (67) noted that the occurrence of the structures of metallic elements correlated with the number of valence electrons in s and p orbitals. For example, the structures of Na, Mg, Al, and Si are b.c.c., h.c.p., f.c.c., (body-centered cubic, hexagonal close-packed, face-centered cubic) and diamond, respectively, and the heats of atomization of the solid elements are 25.8(70), 35.3(70), 78.0(71), and 107.7(72) kcal/gram atoms, respectively, which indicates that the number of bonding electrons increases from one to four through Na to Si. Brewer's (68, 69) extensive study of the stability of alloy phases led him to formulate that the stability of a crystal structure of a metal or an alloy depended primarily on the average number of s and p electrons per atom:

$(sp)^1$ - $(sp)^{1.5}$ implied b.c.c. structure,

$(sp)^{1.7}$ - $(sp)^{2.1}$ implied h.c.p. structure,

$(sp)^{2.5}$ - $(sp)^3$ implied f.c.c. structure, and

$(sp)^4$ implied diamond structure.

Brewer also correlated the stability of b.c.c., h.c.p., and f.c.c. structures of metals with the promotion energies in gaseous atoms required to obtain excited states with one s or

p electron, two sp electrons, and three sp electrons, respectively. For example, considering Cr, Mo, and W, Brewer (69) tabulated the promotion energies for the lowest electronic configuration as in Table 14.

Table 14. Promotion energies in kcal/mole for the Group VI metals in the gaseous state. Ground states denoted by zeroes. (After Brewer (69), as obtained from Moore)

	$d^5s(^7S)$	$d^4s^2(^5D)$	$d^4sp(^7F)$
Cr	0	23	70
Mo	0	31	80
W	9	0	55

The promotion energies showed that the h.c.p., corresponding to the d^4sp configuration, would be unstable with respect to the b.c.c. structure (d^5s). The d^4s^2 state, Brewer pointed out, is not suitable for metallic bonding because the s electrons are paired and thus there would be only four bonding electron pairs instead of six bonding electron pairs as is the case for each of the other configurations.

For the Group IVB metals, which are of concern in the $M_2^{IV}Ch$ compounds, the promotion energies of the gaseous atoms to attain the two lowest excited states are listed in Table 15.

Table 15. Promotion energies in kcal/mole for the Group IV metals in the gaseous state. Ground states denoted by zeroes. (After Brewer (69), as obtained from Moore)

	$d^2s^2(^3F)$	$d^3s(^5F)$	$d^2sp(^5G)$
Ti	0	19	45
Zr	0	14	42
Hf	0	40	51

These excited states are close in energy, which correlates with the observation of both h.c.p. and b.c.c. structures of these metals. It is noted, however, that the promotion energy to attain the d^3s configuration for Hf is higher by a factor of two than the energies required to attain the same state for Ti or Zr. Thus the tendency for the metals in combination with chalcogens to form the Ti_2S-type structure correlates with the tendency for the metals to form the b.c.c. structure in the element which, in turn, correlates with the promotion energy to obtain the gaseous atoms in the sd^3 configuration.

A measure of the tendency for the elements to form the b.c.c. structure is the h.c.p.→b.c.c. transition temperature, which for Ti is 1155°K (73) for Zr is 1150°K(74) and for Hf is 2023°K (73). These values correlate with the promotion energies of the gaseous atoms to attain the first excited state (sd^3).

The fact that there is no cubic coordination of Hf in the Hf_2S-structure-type, and the fact that there are discernible cubic coordinations of the Ti and Zr atoms in the Ti_2S-type can be understood by the high promotion energy of Hf to attain the sd^3 configuration (which is correlated with b.c.c. coordination symmetry) relative to the promotion energies of Ti and Zr to attain the same sd^3 configuration.

F. Summary

The Ti_2S structure is not easily interpreted as a packing together of spheres, nor can the structure be viewed as interstitial sulfur atoms in the hexagonal close-packed or body-centered cubic structure of titanium. Ti_2Se, Zr_2S and Zr_2Se crystallize with the Ti_2S-type structure. Hf_2S and Hf_2Se crystallize with an entirely different structure, the Hf_2S-type.

The physical properties of this structure are alloy-like in nature.

Two descriptions of the chalcogen bonding have been presented for these compounds:

(1) The chalcogen is bonded to from seven to nine metal atoms, six of which form a distorted trigonal prism with one or more metal atoms adjacent to the faces of the prism. The description is based on covalent, electron-deficient interactions and Pauling bond orders.

(2) The chalcogen is bonded to six metal atoms in a slightly distorted trigonal prism. This description is based

on covalent, directional, electron-deficient interactions.

Both of the descriptions suggest that chalcogen outer orbitals are significantly involved in the formation of a conduction band, a suggestion which is reasonable in the light of recent energy level considerations and calculations of orbital sizes.

The metal atoms in the Ti_2S-type structure appear to have a tendency toward cubic coordination. The metal atoms in the Hf_2S-type structure have octahedral coordination. A possible rationale for understanding the difference in the metal atom environment in these two structures is found in the tendency for the structures of the elemental metals to be b.c.c., which correlates with the promotion energy required for gaseous atoms to attain the sd^3 electronic configuration.

III: THE CRYSTAL STRUCTURE OF $Nb_{21}S_8$

A. Introduction

1. Pertinent literature for the Nb-S system, S/Nb $\leq$ 1.0

The first systematic investigation of the phase relations in the Nb-S system was performed by Biltz and Köcher (75). For S/Nb $<$ 1.0 they reported a phase with homogeneity range of $0.5 \leqslant$ S/Nb $\leqslant 1.0$. Reinvestigations of the system were carried out by Jellinek, Brauer, and Müller (76), by Kadijk and Jellinek (77), by Ruysink, Kadijk, Wagner, and Jellinek (78), and by Kadijk (79). Kadijk (79) has characterized low and high temperature forms of $Nb_{1-x}S$ as having superstructures of the NiAs-type and the MnP-type structures, respectively, with a transition temperature of between 740-780°C. Another metal-rich phase in the Nb-S system was reported by Franzen, DeJong and Conard (80) to have a composition Nb_2S. Further work on this phase, including a complete structural analysis by Franzen, Beineke, and Conard (81), showed that the correct stoichiometry was $Nb_{21}S_8$. Table 16 lists the condensed phases in the metal-rich region of this system.

2. Purposes of this research

The investigation of $Nb_{21}S_8$ stemmed from a desire to describe more completely the chemistry of sulfur in combination with Groups IVB and VB transition metals. The purposes of the research in the Nb-S system were threefold: 1) to attempt to synthesize a niobium-rich sulfide using high temperature and,

Table 16. Condensed phases in the Nb-S system with $0 \lesssim S/Nb \lesssim 1.0$

Phase	Symmetry or space group	Lattice parameters	Comments	Reference
$Nb_{1-x}S$(high temp)	orthorhombic	a= 5.897(2)Å b= 3.326(1)Å c= 6.446(2)Å	superstructure of MnP-type	(77),(79)
$Nb_{1-x}S$(low temp)	hexagonal $P6_3mc$	a= 6.693Å c= 6.425Å	related to NiAs-type	(75),(77),(79)
$NbS_{0.9}$	$P6_3/mmc$	a= 3.33Å c= 6.39Å	NiAs-type	(75),(15)
(Nb_2S)			correct stoichiometry is $Nb_{21}S_8$	(80)
$Nb_{21}S_8$	I4/m	a=16.836(5)Å c= 3.352(1)Å		(81)
Nb	cubic, A2	a= 3.300Å		(82)

if successful, 2) to determine its crystal structure, and 3) to attempt to extend the proposals for chalcogen and metal bonding which resulted from studies of metal-rich Group IVB chalconides.

B. Sample Preparation and Analysis

The 99.92% niobium metal used in the preparation of $Nb_{21}S_8$ was obtained from the Stauffer Metals Company; a typical analysis of the metal is listed in Table 17. The 99.999% sulfur was obtained from the Gallard-Schlesinger Chemical Manufacturing Company.

Table 17. Typical spectroscopic analysis of niobium

Impurity	p.p.m.
O	113
N	175
C	110
Ta	$\sim$100
W	$\sim$200
Fe	20
Mo, Cr, Ni, Cu	$<$ 20
Mn, Mg, V, Zr	$<$ 20

The first preparation of $Nb_{21}S_8$ was accomplished by V. W. DeJong, but his sample was incorrectly characterized as Nb_2S by Franzen, DeJong, and Conard (80) due to the presence of $Nb_{1-x}S$ in

the sample. DeJong's sample was prepared using the high temperature techniques described in Chapter I. An annealing temperature of 1425°C was used, which was above the melting temperature, but the sample showed no visible interaction with the tungsten container. A composition analysis of this sample, performed by ignition of the sample to Nb_2O_5, determined the ratio of S/Nb to be 0.507±0.002. Analysis of this sample for oxygen content was performed by W. A. Stensland by the method of fast neutron activation analysis; the oxygen content was 4860±150 ppm or 0.4%. On the basis of the combustion of the sample and the fact that the oxygen impurity in the sample was small, the stoichiometry of the phase was reported as Nb_2S. The x-ray powder diffraction pattern was complex, but was indexed with a tetragonal unit cell, $\underline{a}$=16.794Å, and $\underline{c}$=3.359Å. The structural determination, reported in a later section, yielded the ratio of S/Nb=8/21=0.381. This result, along with the large difference between the density calculated from the known structure and the density determined using a one milliliter pycnometer, $D_{x\text{-}ray}$=7.71 g/cc, $D_{det'd}$=8.8 g/cc, indicated the presence of a contaminating phase.

In order to prepare pure $Nb_{21}S_8$, a series of samples with varying sulfur content was synthesized. The thermal histories of some of these samples are contained in Table 18. Guinier x-ray powder diffraction patterns were obtained for all samples. Combustion analyses for most samples were performed by D. Carlson using a slow-heating furnace with a maximum temperature

Table 18. Thermal history of some Nb-S samples (samples underlined have additional information in Table 19)

Starting material	Starting S/Nb ratio	Product	Description of product	Annealing temperature	Annealing time
Nb-S-II-2	>0.53	Nb-S-II-3	pellet	1350°C	2 hr.
Nb-S-II-3	ca. 0.53	Nb-S-II-4	sintered pellet	1370°C	3 hr.
Nb-S-II-4	-	Nb-S-II-5	melted	1440°C	2 hr.
Nb-S-II-5	-	Nb-S-II-6	melted	1500°C	1 hr.
Nb-S-III	0.53	Nb-S-III-1	sintered pellet	1390°C	1 hr.
Nb-S-III-1	-	Nb-S-III-1a.m.	arc-melted button	-	-
Nb-S-III-1a.m.	-	Nb-S-III-2	button	1340°C	2 hr.
Nb-S-III-2	0.45	Nb-S-III-3	melted	1500°C	1 hr.
Nb-S-III-3	-	Nb-S-III-4	melted	1500°C	decrease to 1400°C over 1 hr.
$Nb_{21}S_8$-1-1	0.49	$Nb_{21}S_8$-1-1	sintered pellet	1385°C	2 hr.
$Nb_{21}S_8$-1-1	-	$Nb_{21}S_8$-1-2	sintered pellet	1440°C	2 hr.
$Nb_{21}S_8$-1-2	-	$Nb_{21}S_8$-1-3	sintered pellet	1470°C	2 hr.
$Nb_{21}S_8$-1-3	-	$Nb_{21}S_8$-1-3a.m.	arc-melted button	-	-
$Nb_{21}S_8$-4	~0.50	$Nb_{21}S_8$-4-1	sintered pellet	1370°C	2 hr.
$Nb_{21}S_8$-4-1	-	$Nb_{21}S_8$-4-1a.m.	arc-melted button	-	-
Nb-S-V	0.35	Nb-S-V-1	sintered pellet	1390°C	2 hr.
Nb-S-V-1	-	Nb-S-V-1a.m.	arc-melted button	-	-

of 1000°C. The compositions and phase identification of some samples are listed in Table 19. As the composition of the samples decreased from S/Nb$\geq$ 0.5 to S/Nb=0.4, the intensities of six diffraction lines in the powder patterns were observed to decrease. These lines were absent from the powder pattern of sample Nb-S-V-1a.m., the composition of which was S/Nb=0.34, a value close to the calculated composition for $Nb_{21}S_8$, S/Nb=0.38. The fact that the composition was low for Nb-S-V-1a.m. was explained by a slight amount of Nb metal in the sample, as evidenced in the Guinier powder pattern. Also, the density of sample Nb-S-V-1a.m. was determined to be 7.8$\pm$0.1 g/cc, a value in good agreement with the x-ray density of 7.71 g/cc. It was concluded that Nb-S-V-1a.m. was predominantly $Nb_{21}S_8$ with slight contamination by Nb metal. Furthermore, it was concluded that a niobium sulfide with greater sulfur content than $Nb_{21}S_8$ was present in all samples except Nb-S-V-1a.m. Comparison with the recent results of Kadijk (79) showed that the more sulfur-rich contaminating phase in these samples was $Nb_{1-x}S$, orthorhombic form.

The specific procedure for the preparation of Nb-S-V-1a.m. ($Nb_{21}S_8$) was as follows. Niobium metal filings and sulfur were mixed in the ratio S/Nb=0.35 and heated in a sealed, evacuated Vycor tube at 450°C for two days. The product was pelletized and annealed at 1390°C for two hours in a tungsten crucible under high vacuum. The product of the high temperature treatment was arc-melted to yield $Nb_{21}S_8$ + Nb.

Table 19. Composition and phase identification for some Nb-S samples (see Table 18 for thermal histories)

Sample	Composition	Phases present
NbS-arc[a]	0.7	NbS(NiAs-type)
Nb-S-II-3	>0.5	$Nb_{21}S_8$, $Nb_{1-x}S$(h.t.)[b]
$Nb_{21}S_8$-1-3a.m.	0.53	$Nb_{21}S_8$, $Nb_{1-x}S$(h.t.)
Nb-S-II-6	0.51	$Nb_{21}S_8$, $Nb_{1-x}S$(h.t.)
$Nb_{21}S_8$-4-1a.m.	0.50	$Nb_{21}S_8$, $Nb_{1-x}S$(h.t.)
Nb-S-III-2	0.45	$Nb_{21}S_8$, $Nb_{1-x}S$(h.t.)
Nb-S-V-1a.m.	0.34	$Nb_{21}S_8$, Nb

[a]Fair, J. J., Department of Chemistry, Iowa State University of Science and Technology, Ames, Iowa. Studies on the Nb-S system. Private communication. 1967.

[b]Identified from powder data listed by Kadijk (79).

C. Properties of $Nb_{21}S_8$

$Nb_{21}S_8$ is a hard, brittle, lustrous solid. It melts at a temperature greater than 1470°C. Rough electrical measurements on an arc-melted button of $Nb_{21}S_8$ indicated that $Nb_{21}S_8$ is a good conductor. The density of $Nb_{21}S_8$ is 7.80±0.1 g/cc.

D. X-ray Examination of $Nb_{21}S_8$

1. Powder data

X-ray examination of $Nb_{21}S_8$ was performed using Guinier powder, Debye-Scherrer powder, Weissenberg single crystal, and single crystal orienter techniques, which were briefly described in Chapter I.

Using parameters obtained from rotation and Weissenberg data (see below), accurate lattice parameters were determined by a least squares refinement (8) of 2θ values from a Guinier powder diffraction pattern of sample Nb-S-V-1a.m. The final, refined lattice parameters for $Nb_{21}S_8$ were: tetragonal, a=16.836±0.005Å, c=3.352±0.001Å. The volume of the unit cell is 950Å^3. Table 20 lists the observed and calculated $\sin^2\theta$ values, 2θ values, d values, and the relative intensity of each reflection observed in the powder pattern.

2. Single crystal film data

Two single crystals from different samples were used in this investigation. The first crystal, selected from sample Nb-S-II-2, is shown mounted on a glass fiber in Figure 15(a). The crystal was needle-like with an approximately square cross-

Table 20. Guinier x-ray powder diffraction data for $Nb_{21}S_8$

$\underline{a}$=16.836±0.005, $\underline{c}$=3.352±0.001, tetragonal

hkℓ	I/I_o	$\sin^2\theta$(obs) x10^5	$\sin^2\theta$(calc) x10^5	2θ(obs)	2θ(calc)	d(obs)	d(calc)
350	10	7097	7115	30.90	30.94	2.891	2.888
231	5	8014	8000	32.89	32.86	2.721	2.723
260	5	8383	8373	33.66	33.64	2.660	2.662
141	5	8853	8838	34.62	34.59	2.589	2.591
170	80	10450	10466	37.72	37.75	2.383	2.381
501	100	10519	10514	37.85	37.84	2.375	2.375
521	70	11363	11352	39.40	39.38	2.285	2.286
370	10	12150	12139	40.80	40.78	2.210	2.211
800	1	13408	13397	42.96	42.94	2.104	2.105
451	1	13876	13864	43.74	43.72	2.068	2.069
820	1	14179	14234	44.24	44.33	2.045	2.042
480	1	16732	16745	48.29	48.31	1.883	1.882
002	10	21136	21128	54.74	54.73	1.675	1.676
590	1	22214	22185	56.24	56.20	1.634	1.635
132	1	23179	23216	57.56	57.61	1.600	1.599

Figure 15. Photographs of single crystals of $Nb_{21}S_8$ (X500): (top) single crystal from sample Nb-S-II-2; (center) single crystal from sample Nb-S-III-4 viewed perpendicular to fourfold crystallographic axis; (bottom) same crystal as in (center), viewed parallel to fourfold axis

section perpendicular to the needle axis; a short, fourfold crystallographic axis was coincident with the needle axis, and this axis was aligned on a Weissenberg camera as the rotation axis. Four levels of data were collected using MoK_α (λ=0.71069Å) radiation with a Zr filter. The Laue symmetry was determined to be 4/m and the general condition for diffraction was that $h+k+\ell = 2n$, which implied that the unit cell was body-centered. A layered structure was indicated by the observation that the hk0 and hk2 reciprocal lattice layers had the same relative intensities.

The number of formula units of $Nb_{21}S_8$ per unit cell, based on the measured density of 7.8 g/cc, was 2.0, i.e., 42 Nb atoms and 16 sulfur atoms per unit cell. Due to the indicated layering along the short axis (3.352Å) and the fact that extra conditions limiting possible reflections were not observed, the only atomic positions possible in the centrosymmetric space group I4/m, were the eightfold (h) and twofold (a) positions. Two $Nb_{21}S_8$ formula units were consistent with five Nb atoms in eightfold positions (h), one Nb atom in the twofold position (a), and two S atoms in eightfold positions (h).

Intensity data of the four Weissenberg levels were estimated by a multiple film technique. A linear resolution factor was applied to obtain unresolved K_α intensities. Lorentz and polarization correction factors were determined graphically (30). The absorption correction was made using a cylindrical approximation with cylinder radius of 8×10^{-4} cm., a value which was

estimated from photographs of the crystal (see Figure 15(a).

A three-dimensional Patterson function was synthesized for $Nb_{21}S_8$ using the hk0, hkl, hk2, and hk3 structure factors obtained from film intensities. The Patterson contained maxima only at z=0 and z=1/2 in agreement with the proposed atomic positions in I4/m. Since all atoms were located at either z=0 or z=1/2, the superposition method was applied to the z=0 section of the Patterson for $Nb_{21}S_8$. See Chapter II, Section C.1.a. for an explanation of the method. Images obtained by this method did not result in a refined structure. The reason for this failure is discussed in Section G of this chapter.

The film data were set aside and a more accurate method of data collection was employed, namely, measuring the intensities on a spectrogoniometer using a scintillation counter detector.

3. Single crystal counter data

The second crystal used in this study was selected from sample Nb-S-III-4 which was predominantly $Nb_{21}S_8$, and was aligned on a General Electric spectrogoniometer equipped with MoK_α radiation. Two photographs of the crystal (500X) are presented in Figure 15(b), and (c). The (b) view shows a face parallel to the fourfold crystallographic axis; the (c) view is parallel to the fourfold axis. Three standard reflections (12, 0, 0; 0, 12, 0 and 0, 0, 4) were used to generate all other reflection directions. The lattice parameters derived for $Nb_{21}S_8$ from the 2θ positions of these reflections were $\underline{a}$=16.843Å, $\underline{c}$=3.363Å, in reasonable agreement with the least squares refine-

ment of the powder data (see above).

The standard reflections were also used to identify and adjust tube intensity drift during the five-day data collection period. The tube drift is shown in Figure 16 which is a plot of the calibration factor versus time. The calibration factor was that factor required to normalize the intensities of the standards to their intensities obtained two days before the zero time on the plot. The increase of the calibration factor indicated a decrease in the intensity of the x-radiation from the tube. Since the tube remained in operation constantly, the cause for this drift was probably a defective electronic tube in the current stabilizer.

A brief discussion of the single crystal orienter was given in Chapter I. As mentioned in that section, an advantage of this method is that the crystal can be moved so as to position the diffracted radiation to be measured into the equatorial plane described by the counter, the crystal and the x-ray source. The three variables for the movement of the crystal are χ, ϕ, and θ. For $Nb_{21}S_8$ the hk0 reciprocal lattice net was aligned in the diffraction plane at $\chi=0$.

A total of 900 intensities were recorded for hk0 and hkl reflections. Of these 900, 557 were non-zero. All atoms were contained in planes at z=0 and z=1/2 (see above), and thus only hk0 and hkl zones were collected. The method by which individual intensities were recorded is shown for two actual reflections in Figure 17. A background, called the initial back-

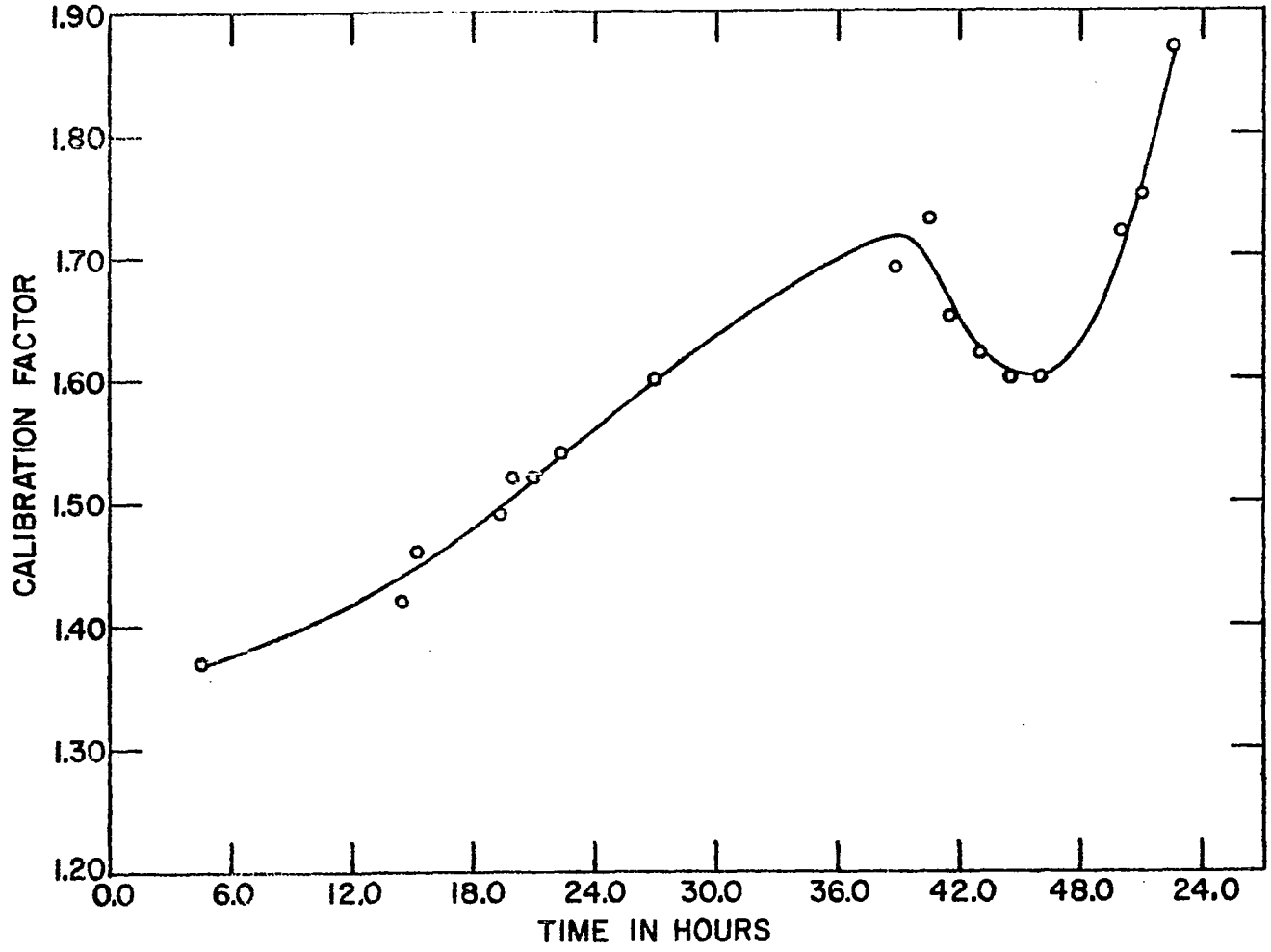

Figure 16. Plot of calibration factor vs. time for $Nb_{21}S_8$ data collection. The calibration factor was used to correct the X-ray tube intensity variation

Figure 17. Traces of counts vs. 2θ for two reflections of $Nb_{21}S_8$ obtained on the single crystal orienter, b_i and b_f are the initial and final background positions, respectively

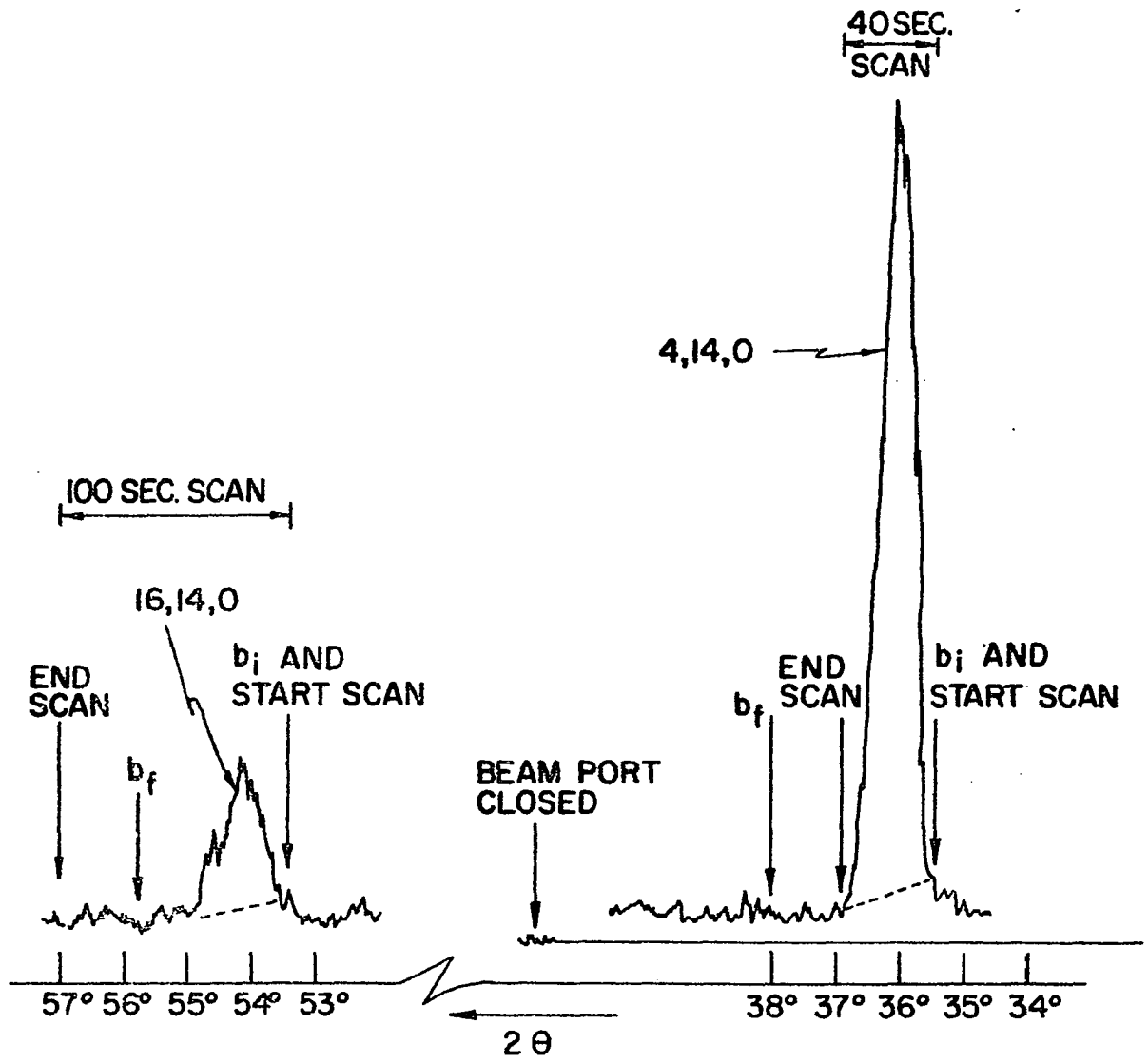
40 SEC. SCAN
4,14,0
100 SEC. SCAN
16,14,0
END SCAN
b_i AND START SCAN
b_f
BEAM PORT CLOSED
b_f
END SCAN
b_i AND START SCAN
57° 56° 55° 54° 53°
38° 37° 36° 35° 34°
2θ

ground, $\underline{b}_i$, was obtained by counting for at least 40 seconds at a constant 2θ setting. The scan was started at $\underline{b}_i$ and was taken at 2°/min. for whatever length of time was needed to insure that the entire peak was included. A second background called the final background, $\underline{b}_f$, was obtained by counting at a constant 2θ setting for at least 40 seconds. The $\underline{b}_i$ and $\underline{b}_f$ counts were averaged, normalized to the time of the scan, and subtracted from the integrated counts. Lorentz and polarization corrections were applied to all reflections. Absorption corrections were made with the use of a computer program, ABCOR, written by Busing and Levy (7) and adapted to the IBM 360/50 computer. A total linear absorption coefficient of 136.5 cm^{-1} was used in the calculation, and the equations of the planes describing the crystal, based on Figure 15(b) and (c), were:

$$\begin{aligned}
-0.19081x + 0.98163y &= 0.0026 \text{ cm.} \\
-0.83867x + 0.54464y &= 0.0033 \text{ cm.} \\
-0.5x - 0.86603y &= 0.0036 \text{ cm.} \\
+0.19081x - 0.98163y &= 0.0026 \text{ cm.} \\
0.92718x + 0.37461y &= 0.0027 \text{ cm.} \\
z &= 0.0014 \text{ cm.} \\
-z &= 0.0014 \text{ cm.}
\end{aligned} \qquad (17)$$

The transmission factors ranged from 0.43 to 0.55. No extinction corrections were made.

A three-dimensional Patterson function was synthesized from the magnitudes of the 557 non-zero structure factors which were derived from the counter intensities. The section at z=0, which was the same in gross features as the z=0 section syn-

thesized using film data, is shown in Figure 18.

Despite the fact that this map was sharper than the film data map, considerable work with the superposition method failed to yield a structure which would refine. This failure is discussed briefly in Section G.

E. Determination of the Structure

At the time when hope was dwindling for success in solving the $Nb_{21}S_8$ structure, Professor J. D. Dunitz,[1] who was a visiting lecturer at Iowa State University during the summer of 1966, suggested that the direct method might be used. The direct method was applied to the counter data and the structure was determined. Following is a brief discussion of the general approach to a centrosymmetric structure determination by the direct method. The last portion of this section is devoted to the specific application of the direct method to $Nb_{21}S_8$.

1. The direct method in crystallography

a. Unitary structure factors and sign determination

An excellent monograph on the direct method applied to crystallography was written by Woolfson (83) and most of this discussion is based upon Woolfson's presentation. The word "direct", used to modify "method", distinguishes an approach which uses definite mathematical relationships to determine the phase of a structure factor from approaches which are more intuitive

[1] Dunitz, J. D., Visiting lecturer, Institute for Atomic Research, Iowa State University of Science and Technology, Ames, Iowa. The direct method. Private communication. 1966.

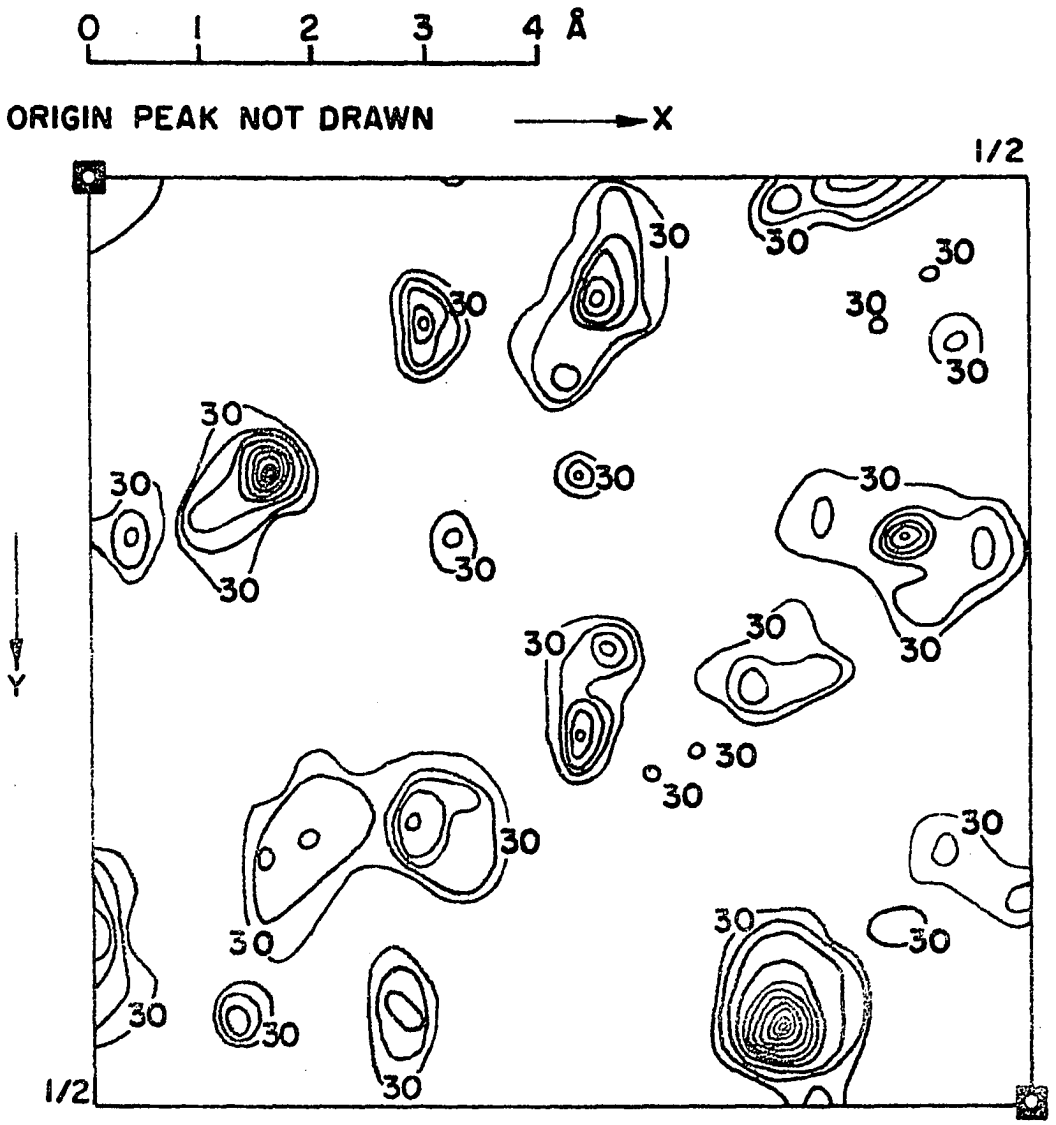

Figure 18. Patterson section (X, Y, 0) for $Nb_{21}S_8$ using counter data. Contours drawn in intervals of 30

in nature, such as image seeking by means of superpositions of Patterson maps. The direct method uses definite relationships, usually in the form of inequalities, to assign phases or to determine probabilities that structure factors have certain phases.

$Nb_{21}S_8$ is centrosymmetric; the discussion which follows is limited to this kind of structure. The structure factor can be written:

$$F(\underset{\sim}{H}) = \sum_{j=1}^{N} f_j \cos 2\pi \underset{\sim}{H} \cdot r_j, \tag{18}$$

in which the symbols have their usual meaning, as described in Chapter I. If all N atoms scatter in phase, then the $F(\underset{\sim}{H})$ would have its maximum possible value,

$$F(\underset{\sim}{H})_{max} = \sum_{j=1}^{N} f_j. \tag{19}$$

It is convenient to define another structure factor, termed the unitary structure factor, which is the ratio of $F(\underset{\sim}{H})$ to its maximum possible value:

$$U(\underset{\sim}{H}) = \frac{F(\underset{\sim}{H})}{F(\underset{\sim}{H})_{max}} = \sum_{j=1}^{N} \frac{f_j}{\Sigma f_j} \cos 2\pi \underset{\sim}{H} \cdot r_j$$

or

$$U(\underset{\sim}{H}) = \sum_{j=1}^{N} n_j \cos 2\pi \underset{\sim}{H} \cdot r_j, \tag{20}$$

where $n_j = f_j / \Sigma f_j$ is called the unitary scattering factor. Accordingly, $U(\underset{\sim}{H})$ must have a value between -1 and +1.

In order to derive the |U| values without knowing the structure, one must rely on knowledge concerning the distribution of U values or of F values. Wilson (84) showed that for a normal distribution of F values the probability of finding an F with a value between F and F+dF for a structure with a center of symmetry was

$$P(F)dF = \frac{\exp\left\{\frac{-|F|^2}{2\sum_{j=1}^{N} f_j^2}\right\}}{\left(2\pi \sum_{j=1}^{N} f_j^2\right)^{1/2}} dF \qquad (21)$$

or, in the case of unitary structure factors,

$$P(U)dU = \frac{\exp\left\{\frac{-|U|^2}{2\sum_{j=1}^{N} n_j^2}\right\}}{\left(2\pi \sum_{j=1}^{N} n_j^2\right)^{1/2}} dU. \qquad (22)$$

One of the assumptions used in the development of this probability function was that the scattering matter was randomly distributed throughout the unit cell. The extent to which this assumption is valid affects the applicability and success of the direct method in solving a particular structure. For $Nb_{21}S_8$, for example, the cell was large (1000Å^3) and niobium could be considered as the only scattering matter present; the sulfur scattering was assumed to be only a small perturbation on the niobium scattering.

Another assumption made in the application of the direct

method is with regard to the expression for $\langle U^2 \rangle$. The exact expression for U^2 is:

$$U^2(\underset{\sim}{H}) = \sum_{j=1}^{N} n_j^2 + \sum\sum_{n \neq m}^{NN} \cos 2\pi \underset{\sim}{H} \cdot (r_n - r_m). \qquad (23)$$

The assumption is that, on the average over groups of reflections there are as many negative as positive double summations and the entire second term becomes zero, leaving

$$\langle U^2 \rangle = \sum_{j=1}^{N} n_j^2. \qquad (24)$$

In general, the calculation of $|U|$ values is done by determining the functional form for the ratio between $\langle U^2 \rangle$ and $\langle I \rangle$ by averaging reflections contained in a certain volume shell of reciprocal space. The ratio, termed $\emptyset^2 = \langle U^2 \rangle / \langle I \rangle$, can then be applied to a specific intensity to find the $|U(\underset{\sim}{H})|$ for that reflection. The size of the volume shell for the averaging of the intensities is chosen so that enough intensities are averaged to be statistically meaningful and yet not so many are averaged so as to hinder the determination of a smooth function of $\emptyset^2$ or $\emptyset$ with $\sin\theta$.

There are basically two ways, related to one another, in which the $|U|$ values may be used toward sign determination. One way is by inequality relationships; the second is by probability relationships.

Harker and Kasper (85) developed relations between $|U|$ values in the form of inequalities. Details of the development, using Cauchy's inequality, may be found in Woolfson's (83) mono-

graph. The inequalities are:

$$(U_{\underset{\sim}{H}} + U_{\underset{\sim}{H}'})^2 \leq (1 + U_{\underset{\sim}{H}+\underset{\sim}{H}'})(1 + U_{\underset{\sim}{H}-\underset{\sim}{H}'}) \tag{25}$$

$$(U_{\underset{\sim}{H}} - U_{\underset{\sim}{H}'})^2 \leq (1 - U_{\underset{\sim}{H}+\underset{\sim}{H}'})(1 - U_{\underset{\sim}{H}-\underset{\sim}{H}'}). \tag{26}$$

In these inequalities $U_{\underset{\sim}{H}}$ is the unitary structure factor of a particular reflection which is described in reciprocal space by the vector $\underset{\sim}{H}$; $U_{\underset{\sim}{H}'}$ is another unitary structure factor indexed by $\underset{\sim}{H}'$; $U_{\underset{\sim}{H}+\underset{\sim}{H}'}$ is the unitary structure factor of the reflection whose index is the sum of the indices $\underset{\sim}{H}$ and $\underset{\sim}{H}'$. For example, if $\underset{\sim}{H}$=5,1,0 and $\underset{\sim}{H}'$=3,7,0, then $\underset{\sim}{H}+\underset{\sim}{H}'$=8,8,0. The inequalities are exact relationships. Sometimes, however, the inequality is satisfied for both choices of sign for a particular |U|, and thus is of no utility in unambiguous sign determination. By using |U| values which are sufficiently large, one usually can obtain sign information from the inequalities. Woolfson's (83) experience indicated that 10% of the |U| values must be greater than or equal to 0.4 in order for their phases to be completely determinable by inequalities.

For some structures the requirement that 10% of the structure factors have $|U| \geq 0.4$ is unreasonable. It is still possible to obtain signs for such structures, but the signs determined have a certain probability of being correct. The lower the |U| values used, the less probable is it that the determined sign is correct. From the Harker-Kasper inequalities, Equations 25 and 26, one can derive the expressions

$$S(\underset{\sim}{H})\ S(\underset{\sim}{H}')\ S(\underset{\sim}{H}+\underset{\sim}{H}') \approx +1 \qquad (27)$$

$$S(\underset{\sim}{H})\ S(\underset{\sim}{H}')\ S(\underset{\sim}{H}-\underset{\sim}{H}') \approx +1, \qquad (28)$$

which relate the phases of three relatively large structure factors. If two of the phases are known, the third may be assigned so that the triple product is equal to +1. Several attempts have been made to give a qualitative estimate of the probability that such a phase assignment was correct. The first of these attempts was by Zachariasen (86). More quantitative estimates have followed such as the one made by Cochran and Woolfson (87). These authors stated that the probability that the sign relationship, Equation 27, would hold was

$$P_+(\underset{\sim}{H},\underset{\sim}{H}') = \frac{1}{2} + \frac{1}{2}\tanh\left\{\frac{\epsilon_3}{\epsilon^3}\left|U_{\underset{\sim}{H}}U_{\underset{\sim}{H}'}U_{\underset{\sim}{H}+\underset{\sim}{H}'}\right|\right\} \qquad (29)$$

and

$$P_+(2\underset{\sim}{H}) = \frac{1}{2} + \frac{1}{2}\tanh\left\{\frac{\epsilon_3}{2\epsilon^3}\left|U_{2\underset{\sim}{H}}(U_{\underset{\sim}{H}}^2 - \epsilon)\right|\right\} \qquad (30)$$

where $\epsilon = \sum_{j=1}^{N} n_j^2$, $\epsilon_3 = \sum_{j=1}^{N} n_j^3$, and $P_+(\underset{\sim}{H},\underset{\sim}{H}')$ is the probability that the sign of $U(\underset{\sim}{H}+\underset{\sim}{H}')$ is the same as the sign of $U(\underset{\sim}{H})U(\underset{\sim}{H}')$.

The number of signs one needs to determine using the direct method is dependent on the number of structure factors one needs in order to synthesize a Fourier electron density map of the structure. Usually about 10% of the largest of the observed structure factors are sufficient to give fairly good resolution of most of the atom positions in a structure.

b. Determination of the origin of the unit cell For a centrosymmetric space group the structure factors which have

phases independent of the choice of origin are termed structure invariants. All other phases are dependent on the choice of origin and can be classified as to their dependence by the parities of the indices h, k, ℓ. The space group $P\bar{1}$, for instance, has eight independent centers of symmetry, any one of which may host the origin. In order to specify an origin, three phases other than structure invariants may be arbitrarily signed. But the phases so signed must be for structure factors which have different parity classes for h, k, and ℓ.

Hauptmann and Karle (88) state that for a primitive monoclinic space group there are eight possible origins, one of which may be specified by an arbitrary choice of phases for three structure factors having different parity classes of the Miller indices. For tetragonal space groups the number of independent origins is reduced to four due to symmetry, and thus two arbitrary signs may be assigned to specify the origin. Centering causes a further reduction in the number of independent origins. For example, a body-centered tetragonal cell has only two possible origins, one of which is selected by the arbitrary assignment of one phase.

2. Application of the direct method to $Nb_{21}S_8$

a. Derivation of |U| values The 880 intensities occurring at $\sin\theta < 0.7$, measured and corrected for Lorentz-polarization effects and absorption, were ordered as to their position in $\sin\theta$. Volume shells were selected in increments of 0.1 in $\sin\theta$. Table 21 lists the number of unobserved reflections

which were not systematically extinct, together with the smallest observed intensity within the region of interest or within adjacent regions. Table 22 lists the number of intensities and their sums for the seven regions of sinθ. The unobserved intensities were added to the sums listed in Table 22 by giving each intensity half the weight of the minimum intensity as listed in Table 21, the result of which is listed in Table 23 together with the $\langle I \rangle$ values for six $\langle \sin\theta \rangle$ values. The mean of the extreme values of sinθ was used instead of the mean of all sinθ values.

Table 21. List of unobserved reflections in regions of sinθ for $Nb_{21}S_8$. Minimum intensity observed in region or in neighboring region is listed in column 3. Systematically extinct reflections are not included

Sinθ region	N=number of unobserved reflections	Min. I(obs)	$\frac{\text{Min. I(obs)}}{2} \times N$
0.0-0.1	2	26.94	26.94
0.1-0.2	8	25.20	100.8
0.2-0.3	18	25.20	226.8
0.3-0.4	28	22.37	313.0
0.4-0.5	51	22.37	570.2
0.5-0.6	93	22.37	1039.7
0.6-0.7	129	30.25	1951.8
	$\Sigma N=329$		

Table 22. List of number of observed intensities and their sums for regions of sinθ for $Nb_{21}S_8$

sinθ region	N'=number of observed reflections	$\sum_{i=1}^{N'} I_i$
0.0-0.1	9	1105
0.1-0.2	55	185036
0.2-0.3	97	204893
0.3-0.4	127	148020
0.4-0.5	163	130372
0.5-0.6	198	80826
0.6-0.7	231	58726
	ΣN'=880	

Table 23. $\langle I \rangle$ and $\langle \sin\theta \rangle$ values for six regions of reciprocal space for $Nb_{21}S_8$

sinθ region	N'+N	$\sum_{j=1}^{N'+N} I_i$	$\langle \sin\theta \rangle$	$\langle I \rangle$
0.0-0.2	64	186141	0.1	2908
0.1-0.3	152	389929	0.2	2565
0.2-0.4	224	352913	0.3	1576
0.3-0.5	290	278382	0.4	959.9
0.4-0.6	361	211198	0.5	585.0
0.5-0.7	429	139552	0.6	325.2

The calculation of $\langle U^2 \rangle = \sum_{j=1}^{N} n_j^2$ is outlined in Table 24. $\langle U^2 \rangle$ was observed to be fairly constant over the range of sinθ considered. $\emptyset^2 = \langle U^2 \rangle / \langle I \rangle$ was obtained for each of the six $\langle \sin\theta \rangle$ and the plot of $\emptyset$ versus sinθ is shown as a smoothed

Table 24. The calculation of $\langle U^2 \rangle$ for $Nb_{21}S_8$

$\sin\theta$	$\sin\theta/\lambda$	f_{Nb}	f_S	$42f_{Nb}$	$24f_S$	All atoms $\sum_{j=1} f_j$	$\times 10^4$ n^2_{Nb}	$\times 10^5$ n^2_S	$42n_{Nb}{}^2$	$16n^2_S$	$\langle U^2 \rangle = \Sigma n_j{}^2$
0.2	0.282	28.85	9.95	1215	238	1453	3.94	4.57	0.0166	0.0011	0.0177
0.3	0.423	23.50	7.76	988	186	1174	4.00	4.37	0.0168	0.0010	0.0179
0.4	0.564	20.08	6.62	844	159	1003	4.00	4.35	0.0168	0.0010	0.0178
0.5	0.704	17.34	5.59	726	134	860	4.06	4.22	0.0170	0.0010	0.0180
0.6	0.845	15.62	4.89	655	117	772	4.09	4.02	0.0172	0.0010	0.0182
0.7	0.996	13.24	3.94	554	94.6	648.6	4.15	3.59	0.0174	0.0009	0.0183
0.8	1.13	11.43	3.27	480	78.5	558.5	4.20	3.44	0.0176	0.0008	0.0184
0.9	1.27	9.80	2.71	413	65.0	478.0	4.20	3.20	0.0176	0.0008	0.0184

curve in Figure 19. The |U| values obtained were corrected for the systematic extinction of half of the reflections due to body-centering. The $|U| \geq 0.38$ and one $|U| = 0.37$ are listed in Table 25, together with the $|F|_{obs}$ values. A projection of the reciprocal lattice, showing the hk0 and hkl reflections with $|U| > 0.37$, is shown in Figure 20.

b. Sign determination The triple product relationship

$$S(\underset{\sim}{H})S(\underset{\sim}{H}')S(\underset{\sim}{H}+\underset{\sim}{H}') \approx +1$$

was used to determine the signs of 47 structure factors of the 51 unitary structure factors which had $|U| \geq 0.37$.

Use was made of the fourfold symmetry, namely, $U(h,k,\ell) = U(\bar{k},h,\ell) = U(\bar{h},\bar{k},\ell) = U(k,\bar{h},\ell)$. Therefore,

$$S(hk\ell)S(\bar{k}h\ell)S(h-k,k+h,\ell) \approx +1, \qquad (31)$$

but since $S(hk\ell) = S(\bar{k}h\ell)$, then $S(h-k,k+h,\ell)$ must be positive. By this method eight signs were obtained which are listed in Table 26 with the probabilities associated with their being correct, as calculated according to Equation 30. These positive signs were used to find other positive signs by use of Equations 27 and 28. A total of nineteen phases were assigned as positive by this method.

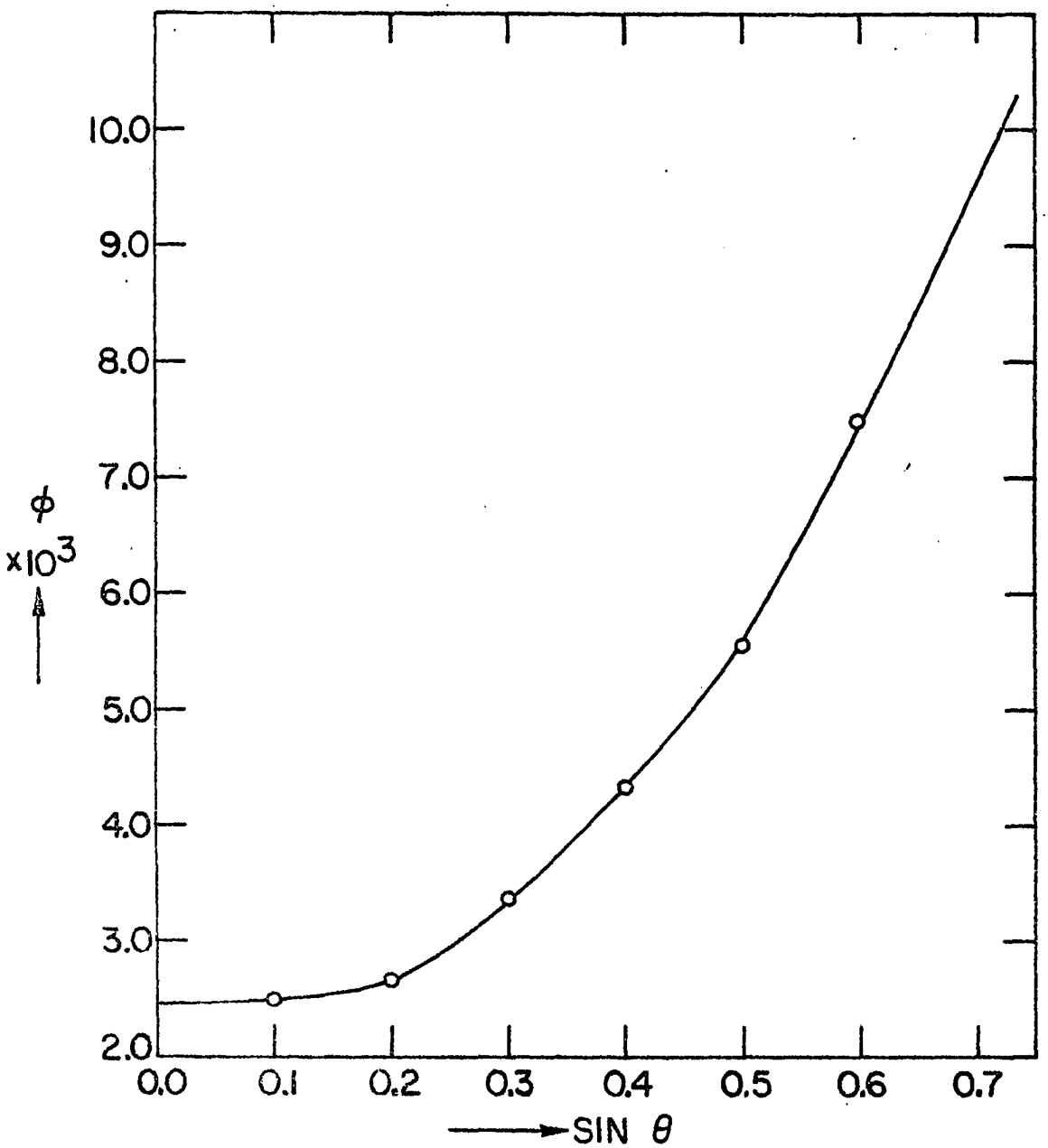

Figure 19. Plot of Ø vs. sin θ for $Nb_{21}S_8$ counter data

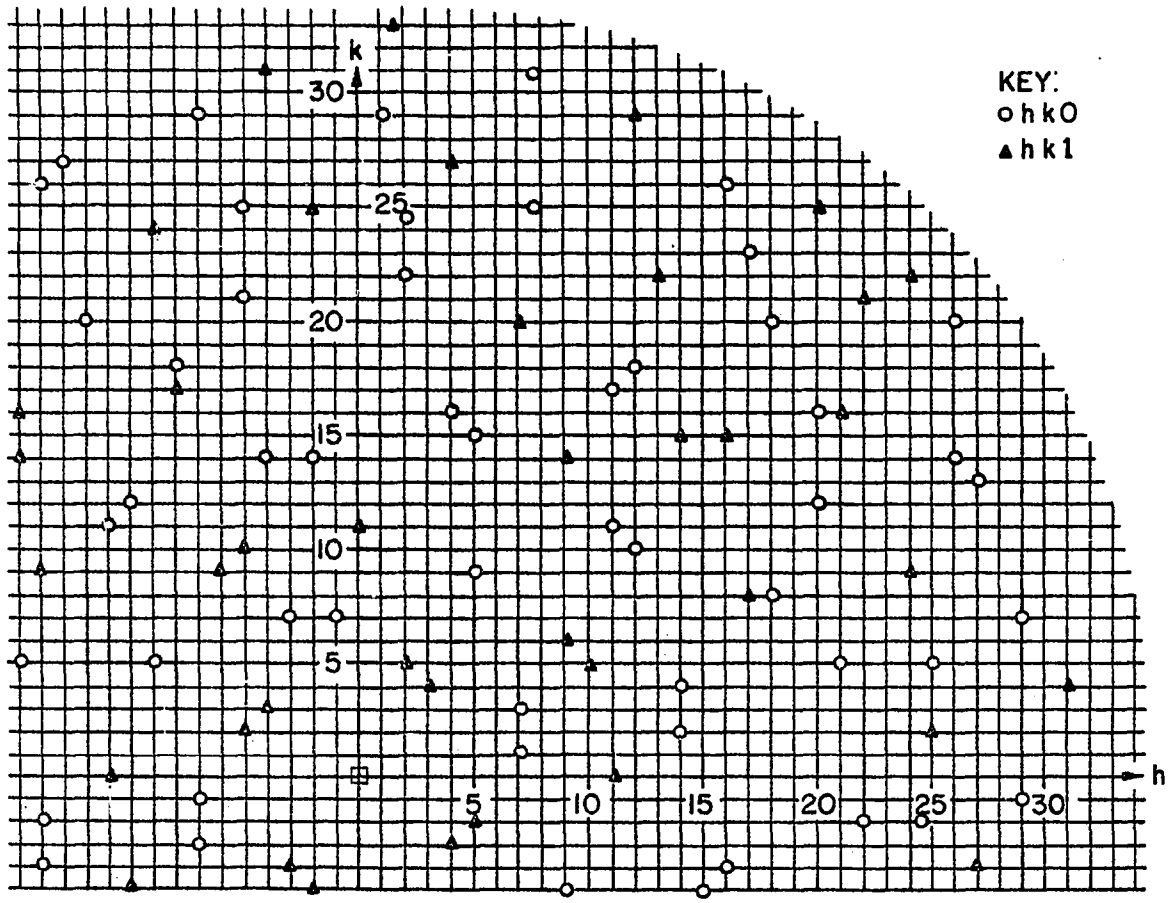

Figure 20. Projection of the reciprocal lattice of $Nb_{21}S_8$ showing $|U| \geq 0.37$

Table 25. List of reflections with $|U| \geq 0.37$ for $Nb_{21}S_8$

hkℓ	|U|	$\|F_o\|$	hkℓ	|U|	$\|F_o\|$
1,29,0	0.58	52	7,31,0	0.75	58
2,22,0	0.62	82	11,11,0	0.42	80
2,24,0	0.41	49	11,17,0	0.53	79
4,16,0	0.38	69	12,10,0	0.41	77
5,15,0	0.38	71	12,18,0	0.45	62
5, 9,0	0.46	115	14, 2,0	0.37	75
7, 1,0	0.41	116	14, 4,0	0.42	84
7, 5,0	0.47	130	16,26,0	0.63	51
7,25,0	0.71	75	17,23,0	0.47	42

Table 25 (Continued)

hkℓ	|U|	$\|F_o\|$	hkℓ	|U|	$\|F_o\|$
18, 8,0	0.45	69	7,20,1	0.62	84
18,20,0	0.55	55	9, 6,1	0.39	91
20,12,0	0.39	49	9,14,1	0.38	65
20,16,0	0.40	44	10, 5,1	0.39	89
21, 5,0	0.53	72	11, 0,1	0.56	129
25, 5,0	0.41	45	12,29,1	0.69	54
26,20,0	0.49	36	13,22,1	0.66	70
26,14,0	0.48	41	14,15,1	0.39	54
27,13,0	0.62	53	16,15,1	0.50	65
29, 7,0	0.42	36	17, 8,1	0.38	60
			20,25,1	0.52	39
			21,16,1	0.42	42
0,11,1	0.56	128	22,21,1	0.40	32
2, 5,1	0.61	169	24, 9,1	0.62	66
2,33,1	0.57	40	24,22,1	0.52	38
3, 4,1	0.49	138	25, 2,1	0.52	57
4,27,1	0.51	48	31, 4,1	0.49	38

Table 26. Determination of eight signs for $Nb_{21}S_8$ using Equation 31. Probabilities were calculated using Equations 29 and 30

hkℓ	h-k,k+h,0	h-k,k+h,0 sign	Probability, P_+
12,10,0	2,22,0	+	0.99
3, 4,1	7, 1,0	+	0.99
2, 5,1	7, 3,0	+	1.0
11, 0,1	11,11,0	+	0.99
4,16,0	20,12,0	+	0.92
21, 5,0	16,26,0	+	1.0
7,20,1	27,13,0	+	1.0

Table 26 (Continued)

hkℓ	2h,2k,2ℓ	2h,2k,2ℓ sign	Probability, P_+
7, 1,0	14, 2,0	+	0.95

Three other sets of structure factors were found: a set of 15 with the sign a, a set of five with the sign b, and a set of eight with the sign ab. For example, (13,22,1) + ($\bar{1}\bar{1}$,11,0) = (2,33,1). The triple product of signs is, with high probability, positive. The sign of 13,22,1 was a, and that of $\bar{1}\bar{1}$,11,0 was positive, which implies that 2,33,1 had a sign of a. Table 27 lists the reflections of each set of unknown signs. There was only one arbitrary choice of sign for the definition of an origin in this centered tetragonal cell (see above); the sign of 3,4,1 was chosen to be positive which, in effect, was a selection of a as positive.

There were, therefore, only two electron density maps synthesized from the known signs, one map with b positive, one with b negative. These two electron density maps are shown in Figure 21 for the z=0 section. These maps each contained more peaks, by about a factor of two, than could be explained on the basis of the cell content given by the density and lattice parameters. Of several attempts to solve the structure of $Nb_{21}S_8$ using these electron density maps and the Patterson map, the following

Table 27. Signs determined for 47 structure factors for $Nb_{21}S_8$

Sign	+	a	b	ab
Indices	2,22,0 7, 1,0 7, 3,0 14, 4,0 11,11,0 20,12,0 16,26,0 27,13,0 21, 5,0 0, 0,2 12,18,0 24,22,0 1,29,0 7,25,0 26,20,0 20,16,0 2,24,0 5,15,0 14, 2,0	3, 4,1 13,22,1 24, 9,1 11, 0,1 0,11,1 16,15,1 25, 2,1 17, 8,1 12,29,1 10, 5,1 20,25,1 9,14,1 21,16,1 2,33,1 14,15,1	4,27,1 2, 5,1 7,20,1 31, 4,1 9, 6,1	5, 9,0 26,14,0 18,20,0 12,10,0 11,17,0 7,31,0 29, 7,0 4,16,0
Total number in each set	19	15	5	8

scheme resulted in a structure which refined satisfactorily.

The strongest peak on the map with b negative and ab negative, i.e., the peak in the lower lefthand corner of Figure 21(a), was assumed to be an atom position x, y, 0. A corresponding Patterson peak occurred at 2x, 2y, 0. A superposition of the Z=0 section Patterson maps was performed with the origin of map B placed on 2x, 2y, 0 of map A and the origin of the resulting image placed at x, y, 0. A trial structure was thus obtained for the (x, y, 0) plane. This trial structure was

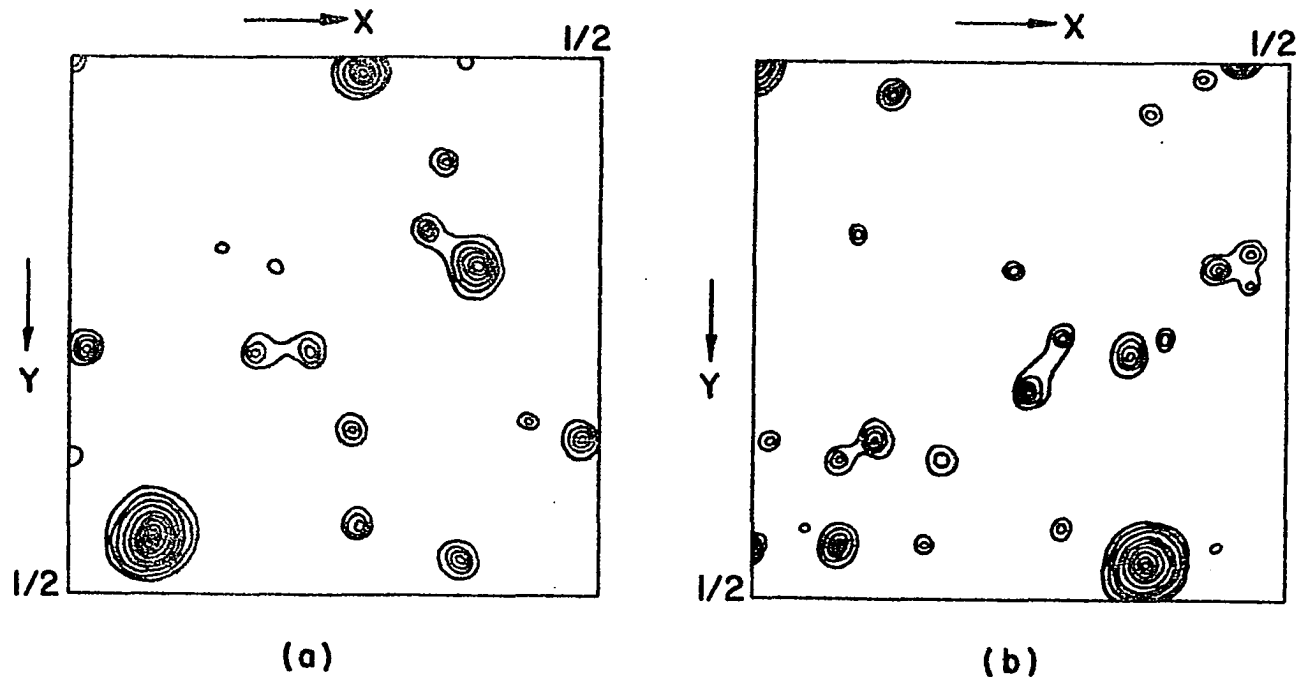

Figure 21. Two possible electron density maps for $Nb_{21}S_8$ obtained by choices of the sign of b. Forty-seven unitary structure factors were used in the Fourier synthesis, (a) b = negative; (b) b = positive

superimposed on the electron density map discussed above (b-, ab-) and a second trial structure was obtained from the coincident peaks. The second trial structure contained an atom at the origin and six other independent atom positions.

At this point in the structure determination, use was made of the known structural chemistry of lower transition metal sulfides (see discussion of Ti_2S structure), and the niobium and sulfur atoms were distributed among the six independent positions and the position at the origin in an attempt to obtain a structure in which there were six niobium atoms about each sulfur atom in a trigonal prism. There was an obvious hole in the structure which resulted from this distribution, and the placement of a niobium atom at this position completed the trigonal prism of niobium atoms located about one of the independent sulfur positions. This resulted in a final trial structure with a niobium in the twofold position at the origin, and five independent niobium atoms and two independent sulfur atoms in the eightfold positions x, y, 0.

3. Refinement

The final trial structure was refined by least squares computation (9) using atomic scattering factor tables given by Hansen, Herman, Lea and Skillman (35) and, after three cyles of refinement, a reliability index, defined by $R = \Sigma \left| |F_o| - |kF_c| \right| / \Sigma |F_o|$, of 0.12 was obtained.

The structure was further refined by least squares computation of the 14 positional parameters and eight isotropic tem-

perature factor coefficients, using a weighting scheme based on statistical counting errors. The weights were assigned by calculating a relative error in the observed structure factor for each reflection, namely, $\sigma_F = \sigma_I/2F(\overline{Lp})$ where σ_I is the estimated error in the intensity corrected for absorption, F is the observed structure factor and $\overline{Lp}$ is the Lorentz and polarization correction factor. The square of the error in intensity, σ_I^2, was taken to be the total counts plus the background counts plus the square of 5% of the total counts plus the square of 5% of the background counts plus an estimated error in the absorption correction. The "goodness of fit", defined by $\sum_i w_i(F_o-F_c)_i^2/n-s$, was equal to 1.35, where $\underline{w}$ is the weight $(1/\sigma_F)$ of the i^{th} reflection, $\underline{n}$ is the number of reflections and $\underline{s}$ is the number of variables. A final unweighted R = 0.063 was obtained. Table 28 lists the values obtained for the atomic positions and temperature factor coefficients. Table 29 lists the observed and calculated structure factors for all 557 observed reflections, and in addition, lists 60 unobserved reflections using parentheses to indicate F_{min} calculated using the background intensity. The unweighted R, including the unobserved reflections, was 0.086. Only the observed reflections were used in the least squares refinement.

Table 28. Final refined atomic parameters for $Nb_{21}S_8$

Atom	Wyckoff notation	x	y	B
Nb(1)	2(a)	0.0	0.0	0.36(5)
Nb(2)	8(h)	0.0813(1)	0.4502(1)	0.26(2)
Nb(3)	8(h)	0.2777(1)	0.0202(1)	0.58(3)
Nb(4)	8(h)	0.3843(1)	0.1851(1)	0.47(3)
Nb(5)	8(h)	0.1919(1)	0.1986(1)	0.54(3)
Nb(6)	8(h)	0.4509(1)	0.3643(1)	0.53(3)
S(1)	8(h)	0.1377(3)	0.0637(3)	0.30(7)
S(2)	8(h)	0.2126(3)	0.3644(3)	0.35(7)

For the purpose of checking the correctness of the refined structure, a difference Fourier synthesis was obtained using all 557 reflections. The synthesis showed the highest peaks, corresponding to about 0.8 electrons, in the z=0 section.

F. Description of the $Nb_{21}S_8$ Structure

Interatomic distances obtained from the final positional parameters and the associated bond orders calculated via Equation 16 are listed in Table 30. The Thermal Ellipsoid Plot computer program written by Johnson (10) was used with Slater's radii to draw the stereoscopic view of the structure along the c axis as illustrated in Figure 22. Special glasses are needed to see the structure in this drawing in three dimensions.

A complete schematic representation of the $Nb_{21}S_8$ structure, projected down the c axis, is shown in Figure 23. The radii of the circles representing the atoms are arbitrary and

Table 29. Complete list of observed and calculated structure factors for $Nb_{21}S_8$. Sixty unobserved reflections are included

K= 0,L= 0
H F(O) F(C)
2 53 54
4 27 31
6 109 116
8 230 -229
10 139 142
12 349 -351
14 100 105
16 235 241
18 42 -89
22 189 182
28 104 -87
30 133 -129
32 87 -71

K= 1,L= 0
H F(O) F(C)
7 493 631
9 50 48
15 339 321
17 141 142
21 171 164
27 145 -180
31 109 136

K= 2,L= 0
H F(O) F(C)
0 52 38
2 49 53
4 93 -83
6 523 -562
8 303 -274
10 33 -86
12 64 58
14 396 394
16 100 97
18 109 126
20 46 86
22 113 104

K= 3,L= 0
H F(O) F(C)
1 97 90
5 364 -376
7 681 696
9 182 169
13 45 -83
15 341 -335
17 93 86
23 141 136
25 102 -93
29 111 123
31 91 -69
33 145 146

K= 4,L= 0
H F(O) F(C)
0 23 31
2 32 27
4 89 96
6 87 84
8 412 406
10 165 178
12 41 56
14 443 432
16 107 114
20 294 -296
22 104 -108
24 86 75

K= 5,L= 0
H F(O) F(C)
3 37 17
5 415 397
7 92 -91
9 171 163
11 462 451
13 316 -311
17 65 -81
21 379 369
23 48 46
25 237 236
31 66 75

K= 6,L= 0
H F(O) F(C)
0 100 116
2 100 113
4 91 85
8 108 -105
10 193 194
12 122 -132
18 121 123
20 88 -86
22 148 -161
24 81 51
26 182 183
28 172 170
30 99 92
32 75 56

K= 7,L= 0
H F(O) F(C)
1 202 150
3 513 508
5 341 -317
7 58 67
11 111 -119
13 86 -90
17 126 122
21 98 81
25 160 158
27 168 -167
29 187 -181

K= 8,L= 0
H F(O) F(C)
0 236 -229
2 475 454
4 402 371
6 265 230
8 51 -51
10 61 52
12 130 131
18 361 359
20 86 -78
22 61 68
24 65 49
26 127 -112
28 132 136
32 101 107

K= 9,L= 0
H F(O) F(C)
1 143 -136
3 263 243
5 604 -598
7 361 -330
11 217 203
13 282 272
15 111 -106
17 311 295
19 236 232
25 67 73

K=10,L= 0
H F(O) F(C)
0 143 140
2 330 -319
4 207 199
6 322 293
8 197 -205
10 303 298
12 404 -390
14 118 -114
16 107 105
20 127 126
22 119 -110
26 128 111

K=11,L= 0
H F(O) F(C)
1 79 -79
3 71 70
5 173 172
9 127 118
11 420 428
13 263 261
19 203 -209
21 76 -76
23 97 -97
31 92 68

K=12,L= 0
H F(O) F(C)
0 356 -351
2 229 209
4 197 176
8 157 156
10 241 237
16 145 -142
18 215 215
20 260 238
24 52 68

K=13,L= 0
H F(O) F(C)
1 82 -85
3 66 66
5 54 -48
7 194 199
9 105 -135
13 127 131
15 154 -159
17 98 120
19 198 -187
21 64 -59
25 117 114
27 279 277
29 47 83

K=14,L= 0
H F(O) F(C)
0 124 125
2 122 118
6 157 156
8 39 -38
10 275 -273
16 164 -160
18 75 83
22 107 105
26 218 -225
30 47 -54

K=15,L= 0
H F(O) F(C)
1 115 109
3 366 363
5 176 157
7 136 -131
9 52 42
15 129 114
21 185 189
23 141 -149
27 46 89

K=16,L= 0
H F(O) F(C)
0 216 241
2 294 -275
4 363 -355
6 111 123
8 193 -199
10 196 192
14 149 139
16 180 183
20 231 242

K=17,L= 0
H F(O) F(C)
1 182 -178
3 104 97
5 82 77
7 124 126
9 161 -154
11 414 -395
13 199 195
21 80 87

K=18,L= 0
H F(O) F(C)
0 85 -89
2 93 95
4 178 -196
6 155 152
8 139 131
10 166 166
12 325 318
18 178 -184
20 83 -66
24 85 -81
26 99 -76
28 125 109

K=19,L= 0
H F(O) F(C)
7 286 267
9 99 101
13 141 148
15 48 -57
17 238 201
19 112 102

K=20,L= 0
H F(O) F(C)
2 201 -187
6 121 133
10 82 91
12 38 -48
14 142 157
18 287 -288
24 147 165
28 191 143

K=21,L= 0
H F(O) F(C)
1 113 115
3 112 -92
5 165 179
7 73 -86
11 47 -54
13 93 -96
21 115 150

K=22,L= 0
H F(O) F(C)
0 183 182
2 432 436
8 127 98
22 73 -52
24 252 244

K=23,L= 0
H F(O) F(C)
1 132 -126
3 65 -81
5 85 -84
7 77 76
9 88 85
13 117 107
17 220 219
23 113 83

K=24,L= 0
H F(O) F(C)
2 258 268
4 111 -86
8 153 -144
10 191 -199
16 79 100
18 72 61
22 57 76

K=25,L= 0
H F(O) F(C)
3 43 -24
9 395 410

K=26,L= 0
H F(O) F(C)
4 51 78
10 149 150
16 268 270

K=27,L= 0
H F(O) F(C)
9 135 138

K=28,L= 0
H F(O) F(C)
6 116 -98
10 45 -30
14 104 -91

K=29,L= 0
H F(O) F(C)
1 272 270
K=30,L= 0
H F(O) F(C)
0 147 -129
4 120 117
14 119 77

K=31,L= 0
H F(O) F(C)
1 97 78
7 307 -261

K=32,L= 0
H F(O) F(C)
6 81 92
8 109 134

K= 0,L= 1
H F(O) F(C)
1 52 51
3 94 -78
5 475 507
7 157 -147
11 678 709
15 203 199
17 203 -212
19 231 -248
23 212 -206
25 76 71
31 72 71
33 65 66

K= 1,L= 1
H F(O) F(C)
0 60 51
4 298 316
6 165 161
8 122 126
10 141 147
12 80 80
16 61 -63
18 307 311
20 238 245
24 116 -113
26 59 50

K= 2,L= 1
H F(O) F(C)
1 162 -167
3 323 323
7 281 280
9 68 -73
11 30 -30
13 79 -85
17 80 -93
19 63 -55
21 72 60
23 47 53
25 301 317
27 164 169
29 70 70

K= 3,L= 1
H F(O) F(C)
2 94 -72
4 169 169
6 163 169
10 294 -299
12 113 116
16 325 -323
18 265 266
20 43 -47
22 208 205
24 96 -31
26 200 -198
28 82 95
30 128 -132
32 92 106

K= 4,L= 1
H F(O) F(C)
1 146 147
3 122 118
5 212 201
7 121 119
11 59 68
13 179 184
15 138 -148
17 50 -33
19 189 199
21 141 131
23 152 -101
25 105 93
27 61 77
31 199 -193

K= 5,L= 1
H F(O) F(C)
2 887 -911
4 281 -262
6 219 213
8 200 -197
10 468 500
14 262 258
16 171 177
18 47 -31
20 215 218
26 94 88
32 149 94

K= 6,L= 1
H F(O) F(C)
5 40 49
7 112 -119
13 291 -295
15 64 83
21 240 247
23 156 -166
31 139 169

K=11,L= 1
H F(O) F(C)
15 172 178
17 79 80
21 107 107
23 73 -74
29 90 91

K= 7,L= 1
H F(O) F(C)
6 177 183
8 68 -75
10 172 170
12 198 -205
16 58 53
18 25 -3
20 53 51
24 147 162
30 65 -121

K=12,L= 1
H F(O) F(C)
11 134 -135
13 178 181
15 180 176
17 157 167
21 102 105
27 95 -113

K=13,L= 1
H F(O) F(C)
0 26 34
2 327 329
4 92 -294
6 210 -206
8 262 -266
10 99 -91
12 54 61
14 119 123
16 198 197
18 94 93
22 108 120
26 108 -106
28 107 119

K=14,L= 1
H F(O) F(C)
1 51 47
3 61 75
5 260 -269
7 212 218
9 342 347
13 52 58
15 238 -237
21 148 -156
29 65 70

K=15,L= 1
H F(O) F(C)
11 103 103
17 77 70
19 138 137
25 85 86

K=16,L= 1
H F(O) F(C)
10 224 235
12 114 -119
14 286 293
16 342 348
18 108 -96
22 132 -139

K=16,L= 1
H F(O) F(C)
1 85 88
5 187 190
9 147 152
11 105 105
13 104 -105
21 220 222
23 168 164
25 118 129

K=17,L= 1
H F(O) F(C)
0 213 -212
2 278 285
6 97 -83
12 115 -118
18 116 114
22 161 -163

K=18,L= 1
H F(O) F(C)
1 164 168
3 202 203
7 104 107
15 178 -182
17 131 129
23 143 146

K=19,L= 1
H F(O) F(C)
0 246 -248
2 115 118
6 227 232
12 180 168
14 60 63
18 133 134
24 55 56
26 79 -98

K=20,L= 1
H F(O) F(C)
1 54 -50
5 136 -132
7 443 -465
9 62 77
11 69 74
13 101 103
17 77 70
19 138 137
25 85 86

K=21,L= 1
H F(O) F(C)
2 130 -126
6 214 228
8 107 -106
10 166 176
14 129 -144
16 65 70
20 69 78
22 171 -154

K=22,L= 1
H F(O) F(C)
1 63 -74
3 103 99
5 73 87
11 68 80
13 368 371
15 72 73
23 112 -58

K=23,L= 1
H F(O) F(C)
0 202 -206
2 136 144
4 71 76
6 97 111
8 82 90
12 111 113
14 153 -165
18 88 82
20 138 154
22 85 98

K=24,L= 1
H F(O) F(C)
1 39 45
7 39 53
9 49 -47
13 73 72
15 129 -121
17 103 91
21 120 -128

K=25,L= 1
H F(O) F(C)
0 69 71
4 183 181
6 81 89
8 29 -27
12 73 -73
16 88 -83
18 45 -58
20 203 185

K=26,L= 1
H F(O) F(C)
1 50 57
9 60 57
11 86 66
15 113 89
17 32 -22

K=27,L= 1
H F(O) F(C)
0 30 35
4 254 -260
6 116 -117
12 62 70
16 64 91
18 72 61

K=28,L= 1
H F(O) F(C)
1 30 -41
5 68 78
11 133 -147

K=29,L= 1
H F(O) F(C)
2 53 81
4 131 -144
6 62 59
8 63 54
12 281 274
14 45 55

K=30,L= 1
H F(O) F(C)
1 77 80
5 70 80
7 71 64
9 149 157
11 74 -111

K=31,L= 1
H F(O) F(C)
0 71 71
2 110 -104

K=32,L= 1
H F(O) F(C)
1 124 112

K=33,L= 1
H F(O) F(C)

Table 30. Interatomic distances (±0.003Å) and bond orders in $Nb_{21}S_8$

Reference atom	Neighbor	Number of neighbors	Distance (Å)	Bond order
Nb(1)	S(1)	4	2.547	0.53
	Nb(6)	8	2.949	0.36
Nb(2)	S(2)	1	2.634	0.38
	Nb(2)	4	2.819	0.59
	Nb(4)	2	2.884	0.46
	Nb(3)	2	2.946	0.36
	Nb(2)	1	3.202	0.13
Nb(3)	S(1)	1	2.462	0.73
	S(2)	2	2.570	0.48
	Nb(4)	2	2.902	0.43
	Nb(2)	2	2.946	0.36
	Nb(6)	2	3.140	0.17
Nb(4)	S(2)	2	2.482	0.68
	Nb(5)	2	2.877	0.47
	Nb(2)	2	2.884	0.46
	Nb(3)	2	2.902	0.43
	Nb(6)	1	3.210	0.13
	Nb(5)	1	3.238	0.12
Nb(5)	S(1)	1	2.440	0.80
	S(2)	2	2.551	0.52
	S(2)	1	2.806	0.19
	Nb(4)	2	2.877	0.47
	Nb(5)	2	3.100	0.20
	Nb(6)	2	3.112	0.19
	Nb(4)	1	3.238	0.12
Nb(6)	S(1)	2	2.533	0.56
	S(1)	2	2.548	0.53
	Nb(1)	2	2.949	0.36
	Nb(3)	2	3.112	0.19
	Nb(5)	2	3.140	0.17
	Nb(4)	1	3.210	0.13
S(1)	Nb(5)	1	2.440	0.80
	Nb(3)	1	2.462	0.73
	Nb(6)	2	2.533	0.56
	Nb(1)	1	2.547	0.53
	Nb(6)	2	2.548	0.53
S(2)	Nb(4)	2	2.482	0.68
	Nb(5)	2	2.551	0.52
	Nb(3)	2	2.570	0.48
	Nb(2)	1	2.634	0.38
	Nb(5)	1	2.806	0.19

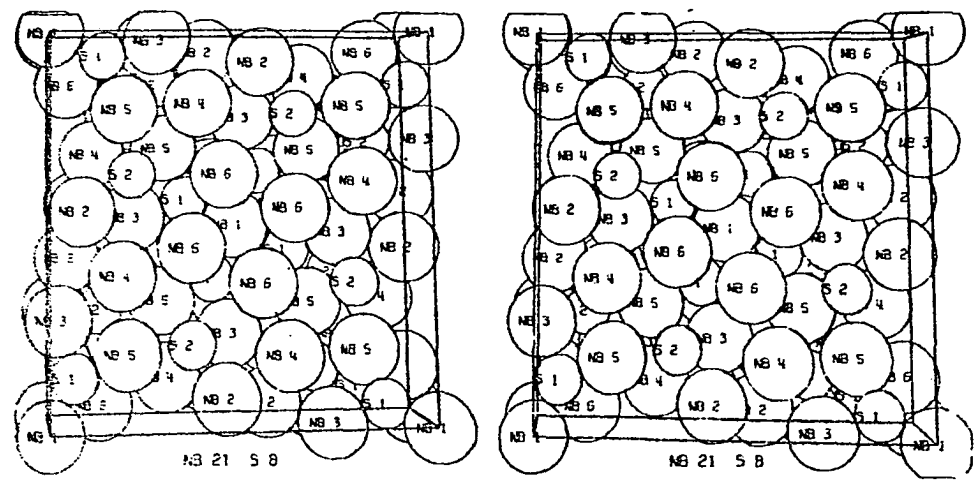

Figure 22. Stereoscopic illustration of the $Nb_{21}S_8$ structure viewed along the c axis. The box represents a unit cell

Figure 23. Projection along the c axis of approximately one and one-half unit cells of the $Nb_{21}S_8$ structure. Symmetry elements of I4/m are shown. Dashed lines show projected coordination polyhedra of the sulfur atoms. Bold-lined parallelogram contains structural similarities to Nb_2Se

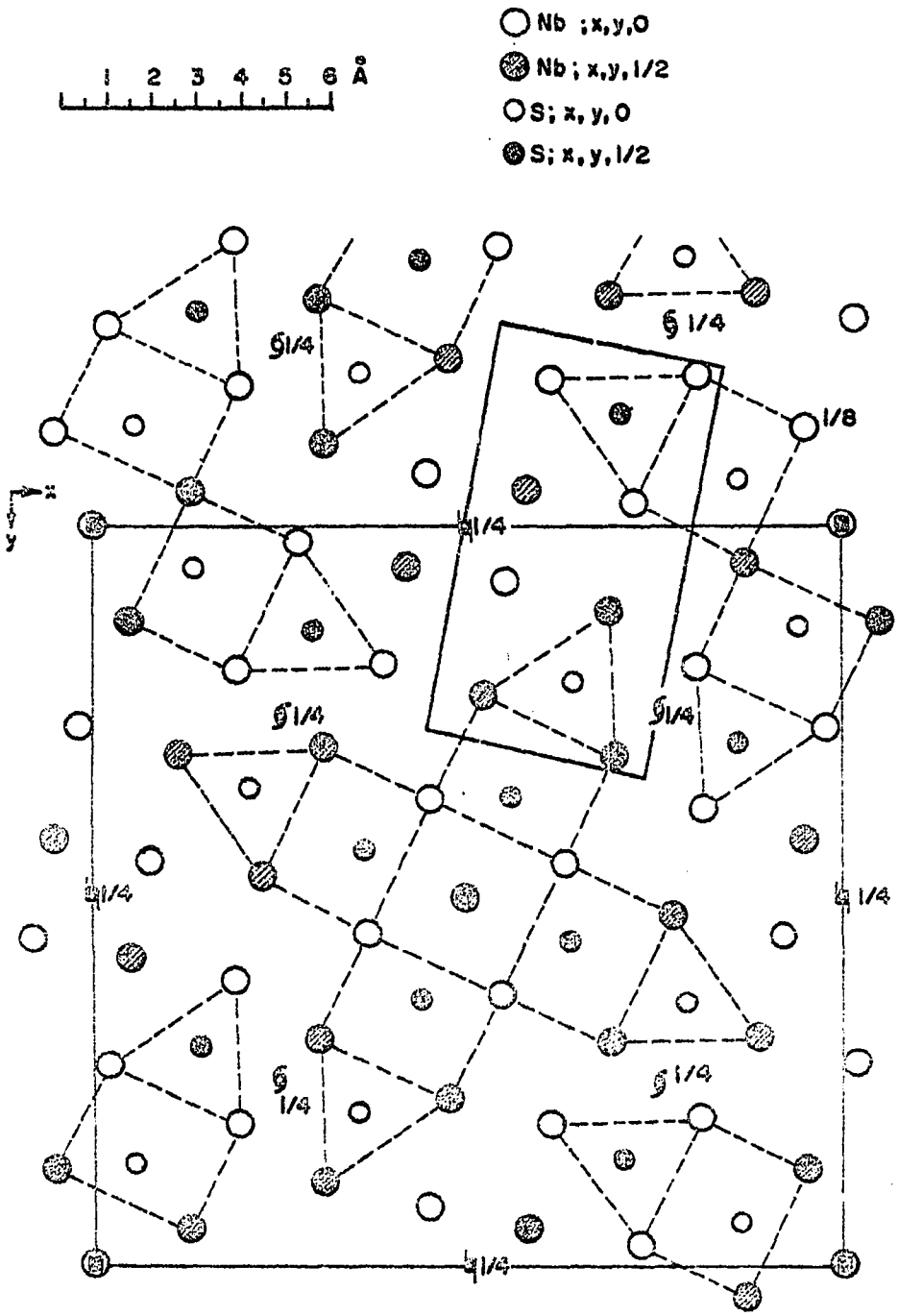
Nb ; x, y, 0
Nb ; x, y, 1/2
S; x, y, 0
S; x, y, 1/2
1 2 3 4 5 6 Å
z
y
1/4
1/8

very small so that the coordination may be more easily seen. Disregard for the present, the bold-lined parallelogram in the upper portion of the figure. The figure contains also the symmetry elements for space group I4/m. The $Nb_{21}S_8$ structure has atoms at z=0 and z=1/2. There are two crystallographically independent sulfur positions in this structure; each sulfur is coordinated to six Nb atoms at the corners of a slightly distorted trigonal prism. As discussed in Chapter II, Section D, and as shown in Figure 12, there are two possible ways a trigonal prism may be situated relative to a mirror plane: 1) with the threefold axis perpendicular to the mirror plane, and 2) with the threefold axis lying in the mirror plane. In projection these two situations are a triangle and a rectangle, respectively. Accordingly, it can be seen from Figure 22 and Figure 23 that, in $Nb_{21}S_8$, the coordination polyhedron of S(2) is of the first case and that of S(1) is of the second case. In addition, the trigonal prisms are augmented by metal atoms adjacent to the rectangular faces of the prisms in the same manner as was found for Ti_2S-type compounds. These augmented trigonal prisms for each sulfur position are shown in Figure 24.

The niobium coordination is not easy to describe. The most significant feature of the metal coordination, however, is that, as is the case with Ti atoms in Ti_2S, the Nb atoms in $Nb_{21}S_8$ have tendencies toward body-centered cubic coordination. Consider, for example, the coordination of the niobium at 1/2, 1/2, 1/2, i.e., in the center of the unit cell. It is located

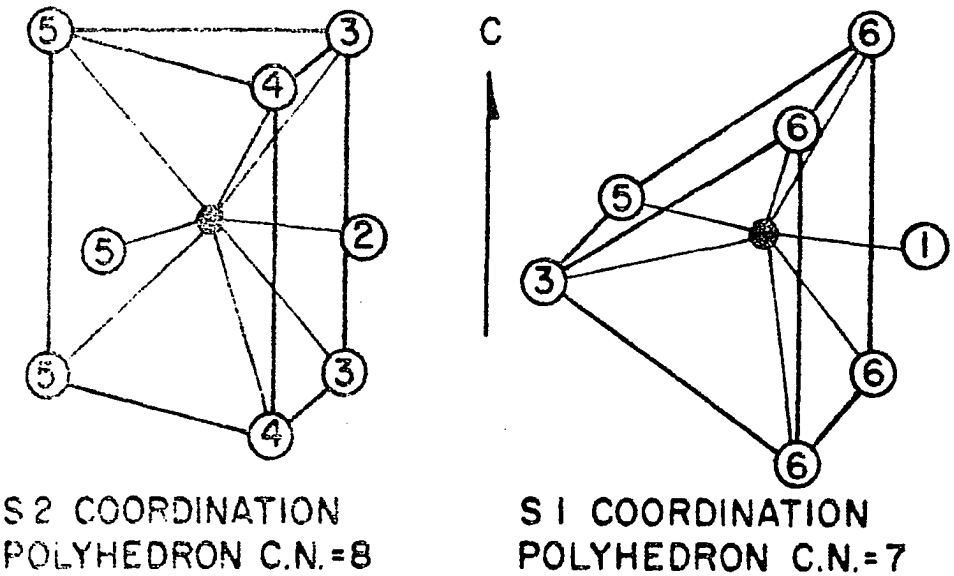

Figure 24. Coordination polyhedra of the two independent sulfur atoms in $Nb_{21}S_8$: (a) S(2), (b) S(1)

at the center of a slightly distorted cube of Nb atoms. In addition, there are sulfur atoms adjacent to the square faces of the cube.

G. Discussion

The discussion concerning the results of the crystal structure determination of $Nb_{21}S_8$ is presented in four parts: in the first a comparison of the refinements of the structure using two sets of data, one collected by visual estimation of intensity on film and one collected using scintillation counter scanning techniques, is given; the second part is a discussion of the failure of superposition techniques in yielding a refinable trial structure; the third is a discussion of the application of the direct method; and the fourth part presents a qualitative proposal for viewing the bonding in $Nb_{21}S_8$.

1. Comparison of film and counter data refinements

The refinement of the structure of $Nb_{21}S_8$ reported in the previous section used the data collected by a counter scanning technique. It is of interest to examine the structure factors obtained from the film work and to compare the refinements obtained from each. One-hundred-eleven zero and first level film data were used for four cycles of least squares computation (9) in refining two scale factors, an overall temperature factor, and fourteen atomic positional parameters. The positional parameters at the beginning of this refinement were those obtained from the last cycle of refinement using the counter data. The

results of the film data refinement are listed in Table 31 together with the counter data results. The overall temperature factor, B, was 0.88$\mathring{A}^2$ for the film data refinement. The standard deviations are listed in parentheses and refer to the last place in the fractional coordinate. The reliability index for the film data was 12.3%, to be compared with 6.3% obtained for the counter data.

Table 31. Comparison of refinements for $Nb_{21}S_8$ using film data and counter data

Atom	Wyckoff notation	Film data refinement x	Film data refinement y	Counter data refinement x	Counter data refinement y
Nb(1)	2(a)	0	0	0	0
(2)	8(h)	0.081(1)	0.452(1)	0.0813(1)	0.4502(1)
(3)	8(h)	0.277(1)	0.019(1)	0.2777(1)	0.0202(1)
(4)	8(h)	0.385(1)	0.186(1)	0.3843(1)	0.1851(1)
(5)	8(h)	0.193(1)	0.197(1)	0.1919(1)	0.1986(1)
(6)	8(h)	0.451(1)	0.366(1)	0.4509(1)	0.3643(1)
S (1)	8(h)	0.138(4)	0.063(4)	0.1377(3)	0.0637(3)
(2)	8(h)	0.213(4)	0.358(4)	0.2126(3)	0.3644(3)

The counter data, with about five times the number of reflections observed on the films, gave an order of magnitude improvement in the positional parameters and a reduction of about 1/2 of the R factor. The individual temperature factors for the counter data refinement are significantly lower than the overall temperature factor obtained using film data. This difference may be due to the fact that only an approximate ab-

sorption correction was made for the film data.

2. The failure of the superposition method in the structure determination of $Nb_{21}S_8$

The reason for the failure of the superposition method for the film data was initially thought to have been the inaccuracy of the data. A subsequent Patterson synthesized from data collected by counter techniques, although improving the resolution of the Patterson, also failed to give a suitable trial structure by superposition methods. In an attempt to discuss the subtle reasons for such failure in both these sets of data, it is interesting to view the differences between Ti_2S, a structure for which a suitable trial structure was obtained, and $Nb_{21}S_8$. Ti_2S is orthorhombic with two n-glides; $Nb_{21}S_8$ is body-centered tetragonal. The Patterson Ti-Ti peaks relative to the S-S peaks for Ti_2S are $(22)^2/(16)^2 \simeq 1.9$; the Patterson Nb-Nb peaks relative to the S-S peaks for $Nb_{21}S_8$ are $(41)^2/(16)^2 \simeq 6.5$. The atoms in Ti_2S are positioned relative to the n-glides such that the Patterson map at Z=0, i.e., the vector map of atoms with the same z coordinate is a combination of the real structure at the x,y,0 plane and the x,y,1/2 plane, but the two planes in the real structure are oriented differently with respect to each other, resulting in a resolution of the two structural layers in the Z=0 Patterson map. The $Nb_{21}S_8$ structure, on the other hand, has the real x,y,1/2 plane displaced by 1/2, 1/2, 1/2, (body-centering condition) to the x,y,0 plane. The Patterson Z=0 section contains the vector maps for both

structural layers, but they are coincident. The result of this fact is that the Nb-Nb vectors are dominant for $Nb_{21}S_8$, resulting in a superposition which contains a square array of Nb positions.

With enough work, however, a trial structure for $Nb_{21}S_8$ probably could have been obtained by vector shift methods. If superpositions had been performed on every peak on the Patterson, even the very small peaks, at least some atoms could have been located. For example, the strongest peak which was used as the basis for a superposition in the unitary map in Figure 21(a) was a very small peak in the Z=0 Patterson (see the lower left hand corner of Figure 18).

3. The direct method

After a structure has been solved using the direct method, an interesting question arises: how closely do the unitary structure factors calculated by the graphical method compare with their calculated values based on the known structure? This question concerns the validity of the approximations made in the calculation of $|U|$ values from the distribution of observed intensities.

The unitary structure factors were calculated for the known structure using the computer program ORFLS (9) but $\underline{n}_j$, the unitary scattering factors, were used instead of the atomic scattering factors, $\underline{f}_j$, as for the usual use of ORFLS. These unitary structure factors were used to calculate the $\emptyset$ factor for individual reflections, $\emptyset_{calc} = U_{calc}/I_{obs.}$, and the $\emptyset_{calc}$

values were plotted versus sinθ. The plot is reproduced in Figure 25, the Ø versus sinθ plot which was used to obtain the $|U|_{obs}$ values is included in the plot. The agreement between the experimental Ø values and the calculated Ø values is good. The calculated points are above the experimental line for sinθ values less than 0.4, whereas above this sinθ value, the calculated points occur both above and below the line. This suggests that the low angle unitary structure factors were slightly too small as calculated by the graphical method. In general, however, the graphical method did yield reliable |U| values for this particular structure, indicating that the approximation of cancellation of cross terms in Equation 23 was valid.

Another interesting question arises in applying the direct method: how low can the |U| values in the triple product relationship be before the probability that the sign of $U_{\underset{\sim}{H}\pm\underset{\sim}{H}'}$ is the same as the sign of $U_{\underset{\sim}{H}}U_{\underset{\sim}{H}'}$ falls below 90%? For $Nb_{21}S_8$ decreasing values of $|U_{\underset{\sim}{H}\pm\underset{\sim}{H}'}|$ were selected and are listed in Appendix D together with the $U_{\underset{\sim}{H}}$ and $U_{\underset{\sim}{H}'}$ values and the probability that the sign was correct. The results for $Nb_{21}S_8$ were that $|U_{\underset{\sim}{H}\pm\underset{\sim}{H}'}|$ may be as low as 0.15 and, provided the $|U_H|$, $|U_{H'}| > 0.30$, the probability will still be greater than 90%. For three equal |U| values they may be no less than 0.27 in order that the probability remain greater than 90%.

4. The bonding in $Nb_{21}S_8$

The physical properties of $Nb_{21}S_8$ and Ti_2S are similar, e.g., they are good conductors and highly brittle. Furthermore, the

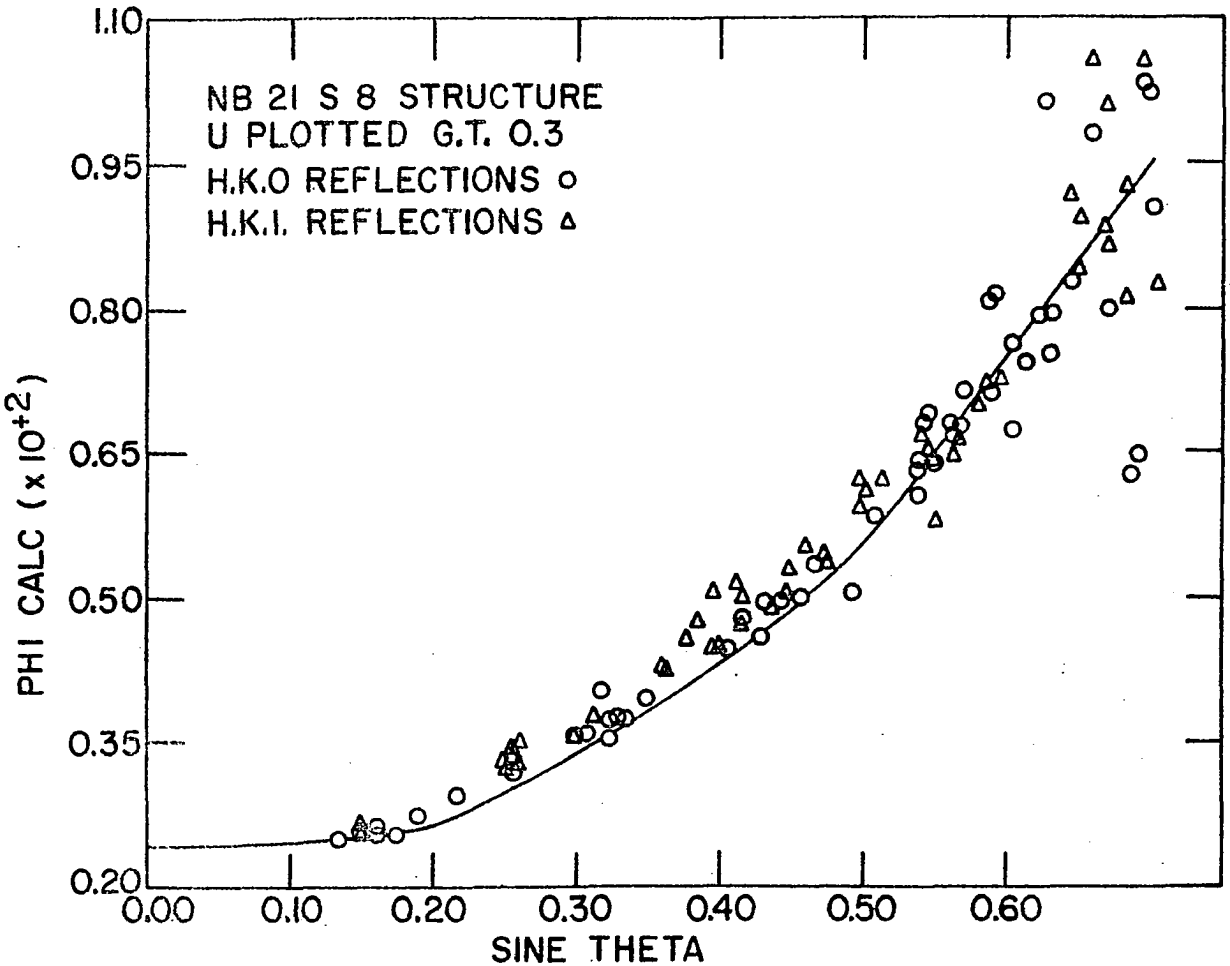

Figure 25. Plot of Ø vs. sin θ for $Nb_{21}S_8$, comparing the experimental Ø values (solid line) and the calculated Ø values for $|U| > 0.30$

coordination of sulfur, ubiquitous in Groups IVB and VB monochalconides and in Group IVB metal-rich chalconide compounds, is observed for both crystallographically independent sulfur atoms in $Nb_{21}S_8$. The similarity of physical properties and structural characteristics of these metal-rich compounds suggests that the bonding proposal for Group IVB metal-rich compounds could be extended to $Nb_{21}S_8$. This bonding interpretation for $Nb_{21}S_8$, as for Ti_2S, has bases in Slater's (38) suggestion that the bonding in solids may be viewed as covalent in the relationship between bond distance and bond order formulated by Pauling (41), in Rundle's (42) consideration of directed orbitals, and in the correlation noted by Brewer (68) and Engel (67) between structure and the number of s and p valence electrons/atom.

There are two interpretations which can be discussed with regard to $Nb_{21}S_8$. The first interpretation is based on the assumption that all bond orders are given approximately by the empirical relationship due to Pauling

$$D(n) = D(1) - 0.6 \log n. \qquad (16)$$

This relationship was discussed in Chapter II. The valences of niobium and of sulfur calculated according to this view are listed in column two of Table 32. The valences for the Nb atoms are reasonable if it is assumed that Nb has a maximum of five valence electrons, e.g., a valence configuration of sd^4. A valence of four for sulfur, together with the observed high conductivity of $Nb_{21}S_8$, suggests that outer orbitals on sulfur are participating in bonding, as was proposed by Franzen for the

monochalconides and extended to the metal-rich chalconides of Group IVB metals discussed in Chapter II.

Table 32. Atom valences for $Nb_{21}S_8$ according to alternative bonding descriptions

Atom	Valence based on an 7-fold, 8-fold coordination	Valence based on trigonal prismatic coordination only
Nb(1)	4.97	2.86
Nb(2)	4.50	4.12
Nb(3)	3.62	3.62
Nb(4)	4.31	4.31
Nb(5)	3.86	3.67
Nb(6)	3.74	3.74
S(1)	4.22	3.69
S(2)	3.93	3.36

The second proposal, based on the hypothesis that sulfur bonding in compounds of this type is directional in nature, considers that only the metals located at the corners of the trigonal prism are bonded to the sulfur atoms. The close sulfur to waist metal distances, according to this view, arise as a result of the strong metal-metal bonding of the waist metal to the four metals located at the corners of the prism face to which the waist metal is adjacent. The valences calculated using Equation 16 under this criterion are given in column three of Table 32. These valences are also in accord with sulfur utilizing outer orbitals in bonding to the niobium atoms in $Nb_{21}S_8$.

If one assumes that Nb uses all of its valence electrons in bonding in $Nb_{21}S_8$, then Nb(1) has an unreasonably low valence (2.9) based on the second interpretation for which the sulfur bonding is directed only to the corners of the prism. However, Nb(1) has a valence of 5.0 based on the augmented sevenfold coordination of S(1), see Figure 24. This comparison favors the interpretation that the metal atoms adjacent to the faces of the prism are bonded to the sulfur. Magnetic measurements to support the proposed diamagnetic (or Pauli paramagnetic) behavior of $Nb_{21}S_8$ have not been made.

The niobium coordination is complex, but the tendency for niobium to have cubic coordination is not surprising, since the only known elemental form of niobium has the b.c.c. structure. This fact is consistent with the Brewer-Engel (68) view in which the b.c.c. structure for Nb is correlated with the low-lying sd^4 electronic configuration for the gaseous Nb atom, as observed spectroscopically.

A survey of metal-rich Group VB compounds will be delayed until the discussion of the Nb_2Se structure in Chapter IV.

IV: THE CRYSTAL STRUCTURE OF Nb_2Se

A. Introduction

1. Survey of the Nb-Se system in the region $0 < Se/Nb < 1.0$

The only phase heretofore known to exist in the region $0 < Se/Nb < 1.0$ was Nb_5Se_4, a compound reported by Selte and Kjekshus (89) to be isostructural with Ti_5Te_4. The structure of the latter compound was reported by Grønvold, Kjekshus and Raaum (90). Nb_5Se_4 was reported to have tetragonal symmetry with a=9.871Å, c=3.4529Å.

2. Specific purposes of this research

The purpose of the present work was to investigate the metal-rich region of the Nb-Se system, using high temperature techniques, to ascertain whether a metal-rich selenide of niobium could be synthesized, and to determine whether its structure was in accord with the previously discussed ideas concerning bonding in Group IVB metal-rich compounds and in $Nb_{21}S_8$.

B. Preparation and Analysis of Sample

The niobium metal used in the synthesis of Nb_2Se was obtained from Dupont de Nemours & Company. The 99.999% selenium was obtained from Alfa Inorganics, Incorporated.

Nb_2Se was first observed by J. Graham,[1] but it was impos-

---

[1]Graham, J., Department of Chemistry, Iowa State University of Science and Technology, Ames, Iowa. Preparation of Nb_2Se. Private communication, 1967.

sible for him to characterize the new phase due to the quantity of Nb_5Se_4 also in his sample. Several single crystals from Graham's sample were investigated by x-ray diffraction techniques (see below). The preparation of pure Nb_2Se was not accomplished; in all preparations carried out in this work there was always slight contamination from either Nb metal or Nb_5Se_4. The most pure Nb_2Se was prepared following the general method outlined in Chapter I with an initial Se/Nb ratio of 0.53. The high temperature annealing treatment was performed at 1560°C for 20 minutes. There was evidence that, at this temperature, selenium vaporized extensively, and longer annealing periods resulted in significant contamination of Nb_2Se by Nb metal. Shorter time periods or lower temperatures, on the other hand, resulted in products which were primarily mixtures of Nb and Nb_5Se_4.

As evidenced by x-ray powder diffraction photographs, the most pure sample of Nb_2Se had a slight amount of Nb metal co-existing with it. A combustion analysis was performed on this sample and yielded Se/Nb=0.444 $\pm$ 0.001, a value in agreement with the fact that Nb metal was in the Nb_2Se sample. Three density determinations were carried out using a one milliliter pycnometer.

C. Physical Properties of Nb_2Se

Nb_2Se is a hard, brittle, lustrous solid. It melts at a temperature greater than 1560°C. Rough electrical conductivity measurements on a sintered pellet of Nb_2Se indicated that it is

a good conductor of electricity at room temperature. The density of Nb_2Se is 7.8 ± 0.1 g/cc.

D. X-ray Examination of Nb_2Se

1. Powder investigation

X-ray investigations of the powdered sample were performed using Debye-Scherrer and Guinier techniques. Using lattice parameters obtained from single crystal photographs (see below), accurate lattice parameters were obtained by a least squares refinement (8) of the 2θ values from a Guinier powder diffraction pattern of a sample containing Nb_2Se and Nb_5Se_4. The refined monoclinic lattice parameters were: $\underline{a}$=13.995±0.005Å, $\underline{b}$=3.430±0.002Å, $\underline{c}$=9.306±0.005Å, β=92.04±0.04°, ($\underline{b}$ axis unique). Table 33 lists the $\sin^2\theta$ observed, $\sin^2\theta$ calculated, and the relative intensity of each reflection, with the exception of lines associated with Nb_5Se_4 (see above).

2. Single crystal investigations

Two single crystals were studied in this work. The first crystal was aligned along the twofold axis of a monoclinic cell and Weissenberg layer photographs were obtained using CuK_α radiation. The general condition for reflection was observed to be h+k=2n. The possible space groups were C2, Cm, or C2/m ($\underline{b}$ axis unique). It was observed that h0ℓ and h2ℓ had approximately the same relative intensities as also did hlℓ and h3ℓ, indicating that all atoms were approximately in levels at y=0 and y=1/2. The intensities on the photographic record were

Table 33. Guinier x-ray powder diffraction data for Nb_2Se

Monoclinic, $\underline{a}$=13.995Å, $\underline{b}$=3.4298Å, $\underline{c}$=9.306Å, β=92.04°

hkℓ	I/I_o	$\sin^2\theta$(obs)	$\sin^2\theta$(calc)	2θ(obs)	2θ(calc)	d(obs)	d(calc)
001	5	0.00686	0.00686	9.50	9.50	9.300	9.300
002	5	0.02750	0.02744	19.09	19.07	4.645	4.650
$\bar{3}10$	25	0.07780	0.07774	32.39	32.38	2.762	2.763
$\bar{1}12$	50[a]	0.08028	0.08024	32.92	32.91	2.719	2.719
$\bar{3}11$	15	0.08553	0.08558	34.01	34.02	2.634	2.633
$\bar{3}12$	100	0.10327	0.10322	37.49	37.48	2.397	2.397
312	60	0.10729	0.10713	38.24	38.21	2.352	2.353
600)	80[a]	0.10968	0.10918	38.68	38.59	2.326	2.331
004)		0.10968	0.10973	38.68	38.69	2.326	2.325
$\bar{6}01$	15	0.11413	0.11408	39.49	39.48	2.280	2.281
204	5	0.12443	0.12448	41.31	41.32	2.184	2.183
$\bar{5}10$	5	0.12622	0.12627	41.62	41.63	2.168	2.168
$\bar{5}11$	5	0.13142	0.13148	42.51	42.52	2.125	2.124
$\bar{6}02$	5	0.13278	0.13272	42.74	42.73	2.114	2.114
$\bar{3}13$	50	0.13647	0.13653	43.36	43.37	2.085	2.085
$\bar{4}04$	50[a]	0.15355	0.15305	46.14	46.06	1.966	1.969
$\bar{6}03$	5	0.17654	0.17674	49.69	49.72	1.833	1.832
$\bar{3}14$	5	0.18385	0.18358	50.78	50.74	1.796	1.798
$\bar{8}01$	60[a]	0.19826	0.19840	52.88	52.90	1.730	1.729
$\bar{0}20$	50	0.20161	0.20175	53.36	53.38	1.715	1.715
$\bar{6}04$	10	0.21050	0.21114	54.62	54.71	1.679	1.676
$\bar{8}02$	10	0.21622	0.21637	55.42	55.44	1.656	1.656

[a]These diffraction lines are overlapped by Nb_5Se_4 diffraction lines.

estimated visually for two octants of the zero and first levels using multiple films. Lorentz and polarization corrections were determined graphically (30). Absorption corrections were made using a computer program written by Busing and Levy (7) with a linear absorption coefficient of 1070 cm^{-1}. The size of the crystal was determined by microphotographs to be approximately $10\mu \times 30\mu \times 10\mu$. A Patterson map of the data had maxima only at Y=0 and Y=1/2 in agreement with the proposed layering, but attempts to solve the structure using superposition techniques were unsuccessful.

The second single crystal of Nb_2Se was examined using a Hilger-Watts four-circle, automatic diffractometer coupled to an SDS 910/IBM 1401 computer, as described by Dahm, Benson, Nimrod, Fitzwater and Jacobson (6). MoK_α radiation (λ=0.7107Å), filtered by Zr, was used to measure the integrated intensities of 1563 reflections for $2\theta < 80^\circ$. The standard alignment reflections were: 0,2,0; 6,0,0; 0,0,4. Small corrections (less than 5%) for the non-linearity of the detector were applied to the six strongest intensities. Lorentz and polarization corrections were applied.

The single crystal is shown in the photographs (500X) in Figure 26. It was estimated that the planes describing the surface of the crystal were:

$$-0.97815x + 0.34202y - 0.42262z - 0.0015 = 0$$
$$0.96593y - 0.25882z - 0.0044 = 0$$
$$1.0x - 0.0030 = 0$$
$$-0.96593y + 0.25882z - 0.0044 = 0$$

Figure 26. Photographs (X500) of a single crystal of Nb_2Se

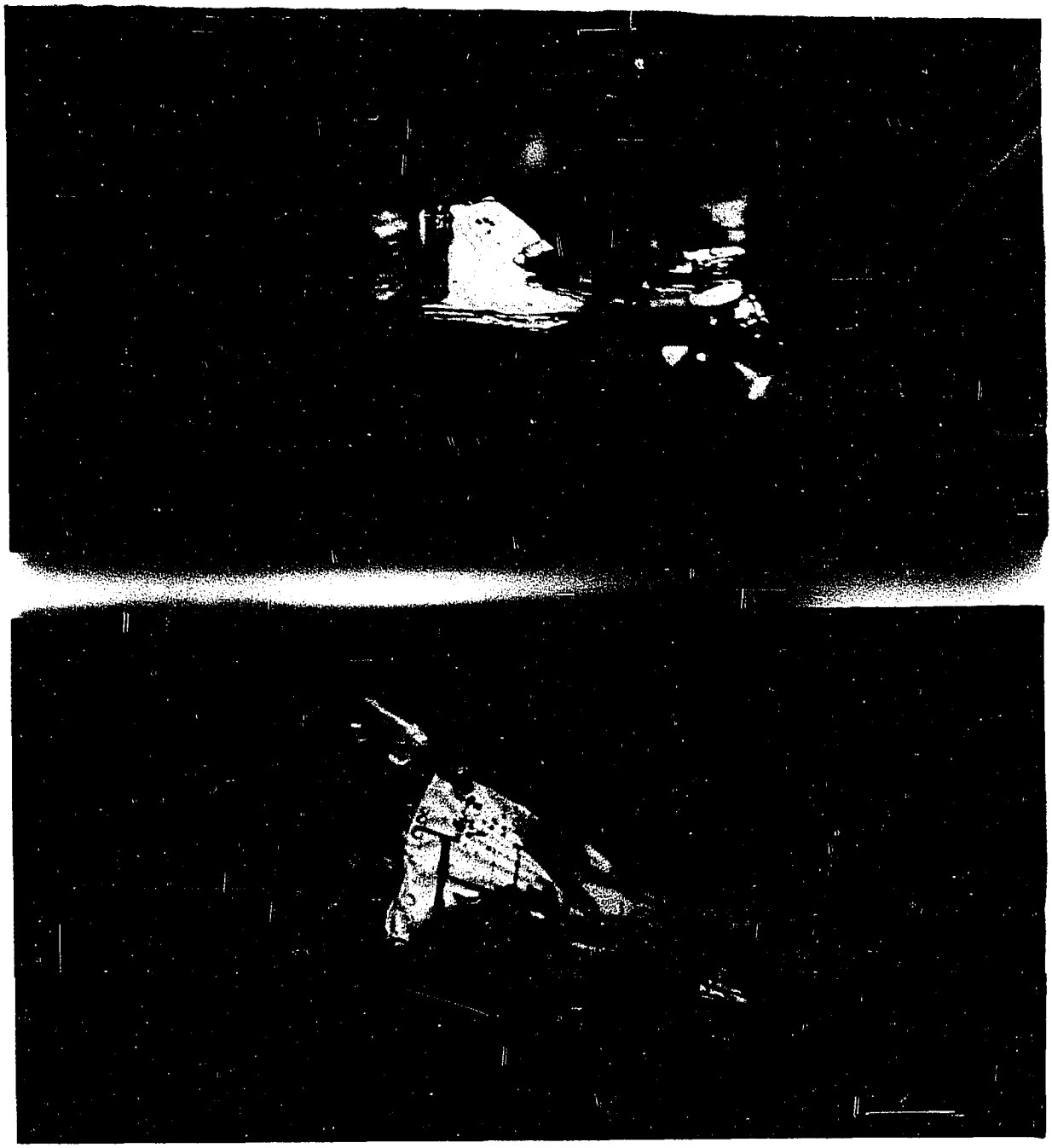

$$
\begin{aligned}
-1.0x \qquad\qquad\qquad\qquad &- 0.0030 = 0 \\
0.25882y + 0.96593z &- 0.0090 = 0 \\
-0.25882y - 0.96593z &- 0.0090 = 0 \\
-0.37358y + 0.81915z &- 0.0036 = 0. \qquad (32)
\end{aligned}
$$

Using this description of the crystal and the computer program ABCOR (7), an absorption correction was calculated for a linear absorption coefficient of 275 cm^{-1}.

The estimated error for each reflection was obtained from the following relationship:

$$\sigma^2(|F|) = \frac{A\overline{Lp}}{4}\left(\frac{I_B+I_T}{I_T-I_B}\right) + \frac{\overline{Lp}(I_T-I_B)}{4A}\,\sigma^2(A) + \left(\frac{I_T-I_B}{4\overline{Lp}}\right)A\sigma^2(\overline{Lp})$$

where A is the absorption factor, $\overline{Lp}$ is the Lorentz-polarization correction factor, I_T is the total count, I_B is the background count, $\sigma^2(A) = 0.0025$ and

$$\sigma^2(\overline{Lp}) = \left[\frac{\cos 2\theta(1+\cos^2 2\theta) - 2\sin^2 2\theta\cos 2\theta}{(1+\cos^2 2\theta)^2}\right]^2 \sigma^2(2\theta),$$

where $\sigma^2(2\theta) = 0.0004$.

E. Determination of the Structure of Nb_2Se Using Counter Data

1. Intensity distribution analysis

An intensity distribution analysis was performed on the three-dimensional data in an effort to determine whether the reciprocal lattice was centric or acentric. Wilson (84) showed that the mean value of the structure amplitudes for an noncen-

trosymmetric structure is greater than that for a centrosymmetric structure. Howells, Phillips and Rogers (91) developed a graphical method to aid in the distinction between centric and acentric intensity distributions. They showed that two functions could be written relating the fraction N(z) of reflections the intensities of which are equal to or less than a fraction, z, of the local average. These two theoretical functions are: $N(z) = 1-e^{-z}$ for accentric distributions and $N(z) = \text{erf}(1/2z)^{1/2}$ for centric distributions where "erf" is the error function. The functions are plotted in Figure 27; the upper curve is for a centric distribution, the lower curve for an acentric distribution. The values of N(z) for three ranges of $\sin\theta$ for all data of Nb_2Se are listed in Table 34, and the average N(z) values are plotted as a function of z in Figure 27. It was concluded from this comparison that the structure of Nb_2Se was centric or hypercentric, as discussed by Lipson and Woolfson (92), and that the space group was C2/m.

Table 34. N(z) values as functions of z for different ranges of $\sin\theta$ for Nb_2Se data

$\sin\theta$ range	z									
	0.1	0.2	0.3	0.4	0.5	0.6	0.7	0.8	0.9	1.0
0.1-0.2	0.38	0.42	0.52	0.52	0.59	0.63	0.65	0.66	0.69	0.75
0.2-0.3	0.35	0.46	0.52	0.55	0.58	0.60	0.63	0.68		
0.3-0.4	0.28	0.41	0.47	0.52	0.58					
Average N(z)	0.33	0.43	0.50	0.53	0.58	0.62	0.64	0.67	0.69	0.75

Figure 27. Plot of average N(z), the fraction of reflections whose intensities are equal to or less than a fraction, $\underline{z}$, of the local average vs. $\underline{z}$, for centric and acentric structures (lines) and for Nb_2Se (points)

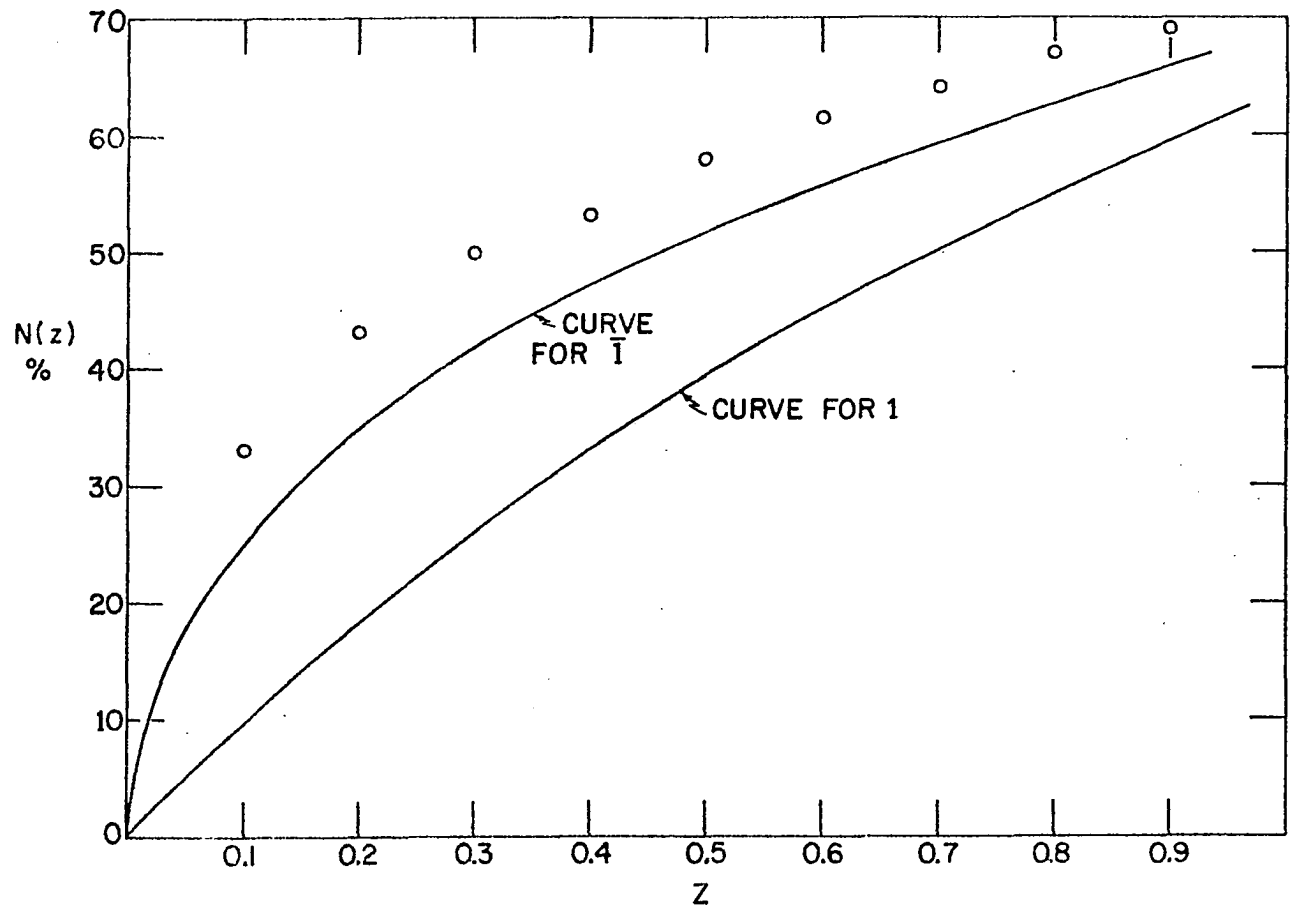
70
60
50
40
30
20
10
0
N(z)
%
CURVE
FOR $\bar{1}$
CURVE FOR 1
0.1
0.2
0.3
0.4
0.5
0.6
0.7
0.8
0.9
Z

2. Atom positions in C2/m

On the basis of the measured density and the volume of the cell, it was estimated that there were eight Nb_2Se formula units per unit cell. Sixteen Nb atoms and eight selenium atoms, occupying layers at y=0 and y=1/2 (see above), were consistent with the fourfold positions (i) x,0,z of C2/m.

3. Patterson trials

A three-dimensional Patterson was synthesized using h0ℓ and h1ℓ data. The Y=0 section is shown in Figure 28. Since the entire structure was contained in the Y=0 plane, superposition methods were used on the Y=0 Patterson, but no image so obtained refined satisfactorily using the largest structure factors. The image of the correct structure, however, was obtained by superposition techniques. Its failure to refine was the result of using only large structure factors in the least squares computation.

4. Direct method

The use of the direct method for the solution of the phase problem in crystal structure analysis was discussed in Section E,1, Chapter III. The application of the method for Nb_2Se was slightly different from the application in the case of $Nb_{21}S_8$.

The calculation of $\langle U^2 \rangle$ for various $\sin\theta/\lambda$ values is summarized in Table 35. A computer program, DIRE, was written to calculate Ø from the three-dimensional intensities and the $\langle U^2 \rangle$ values, taking account of differences in multiplicities of certain zones of data. The results of that calculation are listed

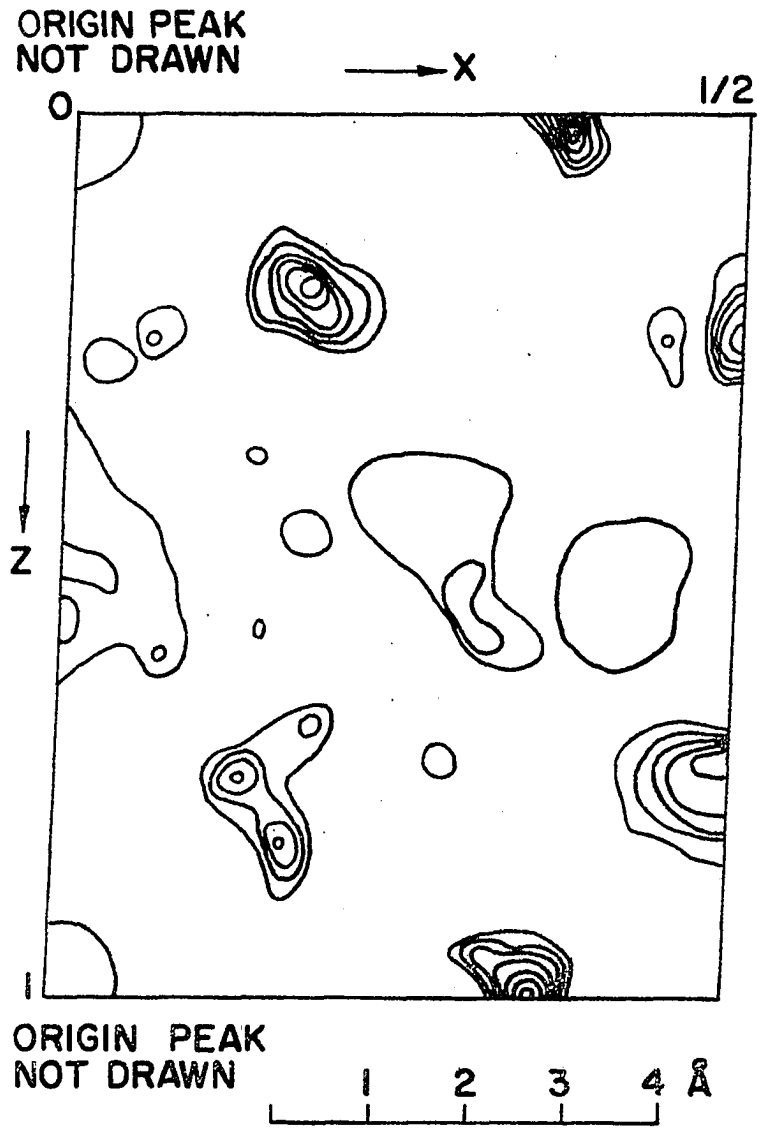

Figure 28. Patterson section (X, 0, Z) for Nb_2Se

Table 35. The calculation of $\langle U^2 \rangle$ for Nb_2Se

$\sin\theta/\lambda$	f_{Nb}	f_{Se}	$16f_{Nb}$	$8f_{Se}$	All atoms Σf_i	$x10^4$ n^2_{Nb}	$x10^4$ n^2_{Se}	$16n^2_{Nb}$	$8n^2_{Se}$	$\langle U^2 \rangle = \frac{}{\Sigma n_i^2}$
0.140	35.75	29.85	572.0	239.0	811.0	19.4	13.5	0.031	0.011	0.042
0.282	28.85	24.20	462.0	193.7	655.7	19.4	13.6	0.031	0.011	0.042
0.423	23.50	19.89	376.0	159.1	535.1	19.3	13.8	0.031	0.011	0.042
0.564	20.08	16.30	332.5	130.5	463.0	20.1	12.4	0.032	0.010	0.042
0.704	17.34	13.24	277.5	106.0	383.5	20.5	11.9	0.033	0.009	0.042
0.845	15.62	10.84	250.0	86.6	336.6	21.4	10.5	0.034	0.008	0.042
0.996	13.24	8.94	212.0	71.5	283.5	21.8	10.0	0.035	0.008	0.043
1.13	11.43	7.79	183.0	62.3	245.3	21.8	10.1	0.035	0.008	0.043
1.27	9.80	6.94	156.9	55.5	212.4	21.2	10.6	0.034	0.008	0.043

in Table 36. A plot of Ø versus sinθ is reproduced in Figure 29. Unitary structure factors were calculated according to the relationship $|U| = \emptyset \sqrt{I} \sqrt{2}$. There were 117 $|U| > 0.4$ for $h0\ell$ and $h1\ell$ data, or about 10% of all structure factors in these layers, including those structure factors which were zero due to systematic extinctions. Only the $h0\ell$ and $h1\ell$ data were used to assign signs, since the unitary structure factors were found to depend on $\underline{k}$ only so far as $\underline{k}$ was even or odd, i.e., $U(h0\ell) = U(h2\ell)$ and $U(h1\ell) = U(h3\ell)$, in agreement with the proposed layering in the $\underline{y}$ direction.

Table 36. Calculation of Ø for $\langle \sin\theta \rangle$ values for Nb_2Se

sinθ range	M=no. of reflections	$\sum_{i=1}^{M} I_i$	$\langle \sin\theta \rangle$	Ø
0.0 -0.05	1	1.72	0.05	0.150
0.05-0.10	6	11.35	0.10	0.072
0.10-0.15	26	250.2	0.15	0.061
0.15-0.20	45	553.3	0.20	0.080
0.20-0.25	80	274.6	0.25	0.084
0.25-0.30	116	899.3	0.30	0.083
0.30-0.35	175	871.4	0.35	0.099
0.35-0.40	206	775.1	0.40	0.108
0.40-0.45	291	1031.0	0.45	0.124
0.45-0.50	348	726.6	0.50	0.142
0.50-0.55	430	893.2	0.55	0.156
0.55-0.60	507	733.6		

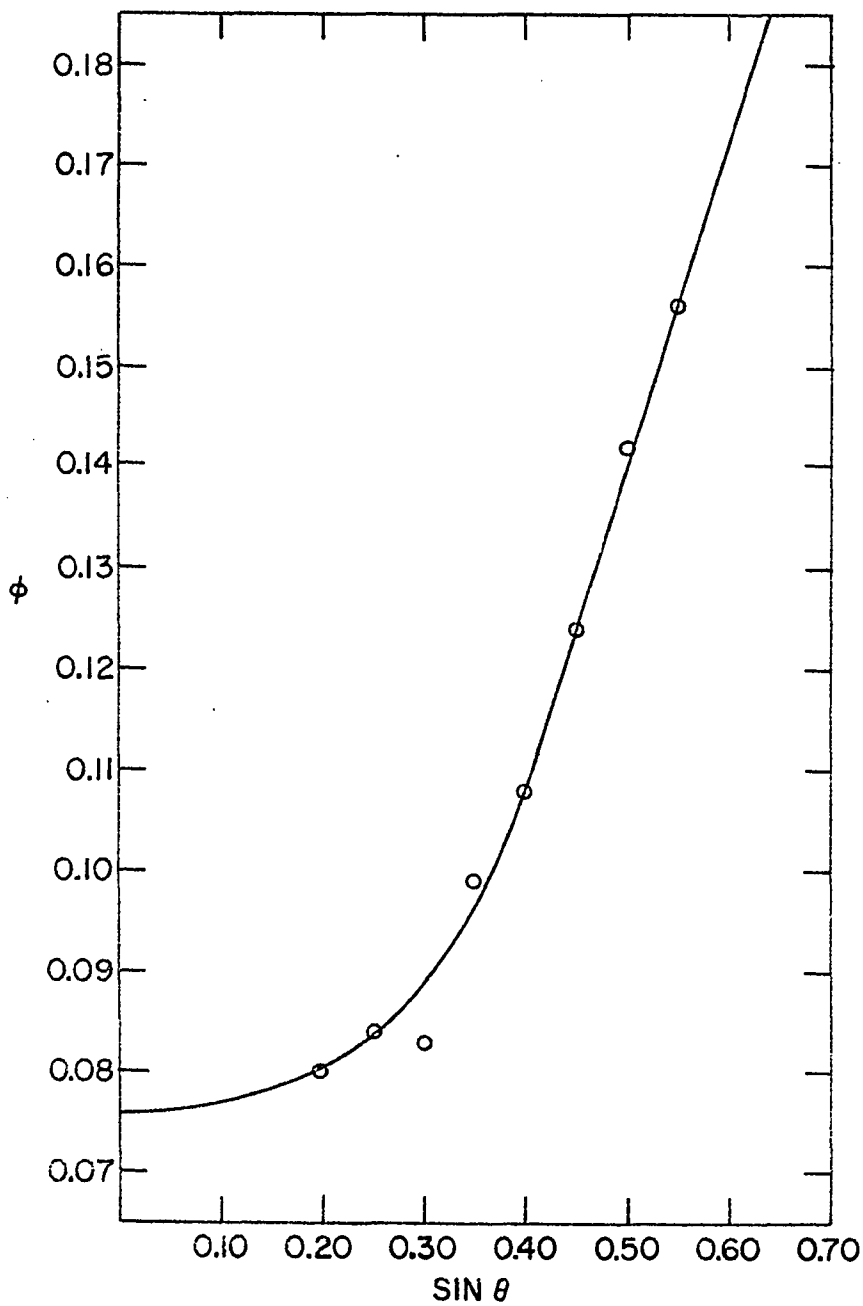

Figure 29. Plot of Ø vs. sin θ for Nb_2Se

A set of twelve signs was determined using the Harker-Kasper (85) inequalities, Equations 26 and 27, and the sign relationship $S(\underset{\sim}{H})S(\underset{\sim}{H}')S(\underset{\sim}{H}\pm\underset{\sim}{H}') =$ positive. This set of structure factors, together with the probability that the $S(\underset{\sim}{H}\pm\underset{\sim}{H}')$ is the same as the product of $S(\underset{\sim}{H})S(\underset{\sim}{H}')$, Equation 29, is listed in Table 37. There four structure factors which were assigned symbolic signs, a, b, c, and d.

Table 37. The set of twelve initial signs assigned for Nb_2Se

$(\underset{\sim}{H}\pm\underset{\sim}{H}')$	$\underset{\sim}{H}$	Sign of $\underset{\sim}{H}$	$\underset{\sim}{H}'$	Sign of $\underset{\sim}{H}'$	Sign of $(\underset{\sim}{H}\pm\underset{\sim}{H}')$	Sign of $\underset{\sim}{H}\pm\underset{\sim}{H}'$ for a=+ d=+	Probability that $S(\underset{\sim}{H})S(\underset{\sim}{H}')S(\underset{\sim}{H}\pm\underset{\sim}{H}')$=+
$\bar{6}01$					a	+	-
$\bar{3}12$					b	b	-
204					c	c	-
312					d	+	-
600	312	d	$\bar{3}12$	b	bd	b	100%
004	312	d	$\bar{3}12$	b	bd	b	100%
$\bar{3}13$	$\bar{6}01$	a	312	d	ad	+	100%
$\bar{6}05$	$\bar{6}01$	a	004	bd	abd	b	100%
$\bar{3}14$	$\bar{3}13$	ad	$\bar{6}01$	a	d	+	100%
$\bar{6}02$	$\bar{3}14$	d	312	d	+	+	99%
$\bar{9}13$	$\bar{3}13$	ad	600	bd	ab	b	100%
911	$\bar{6}01$	a	312	d	ad	+	100%

Hauptmann and Karle (88) showed that for a monoclinic primitive space group three linearly independent phases may be arbitrarily assigned to define the origin of the unit cell (see Section E,1,b, Chapter III). The centering condition for C2/m reduced the number of independent centers of symmetry to four

and thus reduced the number of arbitrary sign assignments to two. Accordingly, U(3,1,2) = $\underline{a}$ = +, and U($\bar{6}$,0,1) = $\underline{d}$ = + were assigned.

The triple product sign relationship proposed by Zachariasen, (86)

$$S(H) \approx S[\sum_{H'} S(H')S(H-H')], \qquad (33)$$

was used to extend the assignment of signs. For example, the sign of 6,0,4, S(6,0,4), was given by S(6,0,4)$\approx$ S[S(3,1,2)S(3,1,2) + S(6,0,0)S(0,0,4) + S($\bar{3}$,1,3)S(9,1,1)]$\approx$S[(+)(+) + (b)(b) +(+)(+)] which implied S(6,0,4) = +. This relationship was used to extend the determination of signs to all 117 structure factors with $|U| > 0.4$. There were two symbolic signs, $\underline{b}$ and $\underline{c}$. Four electron density maps were synthesized according to the possible choices of signs for $\underline{b}$ and $\underline{c}$; these maps are shown in Figure 30. All the maps had strong peaks in basically the same relative positions to other strong peaks.

Using the 117 reflections with $|U| > 0.4$, least squares refinements were carried out on the positional parameters inferred from each of the four different electron density maps, but none of the trial structures refined satisfactorily. The trial structure which had the best agreement between F_o and F_c, R=45%, was the same trial structure as had been obtained from superposition techniques of the Patterson. The structure was based on the $\underline{b}$-, $\underline{c}$+ map in Figure 30. Structure factors were assigned signs, using Equation 33, and were added to those originally used, in

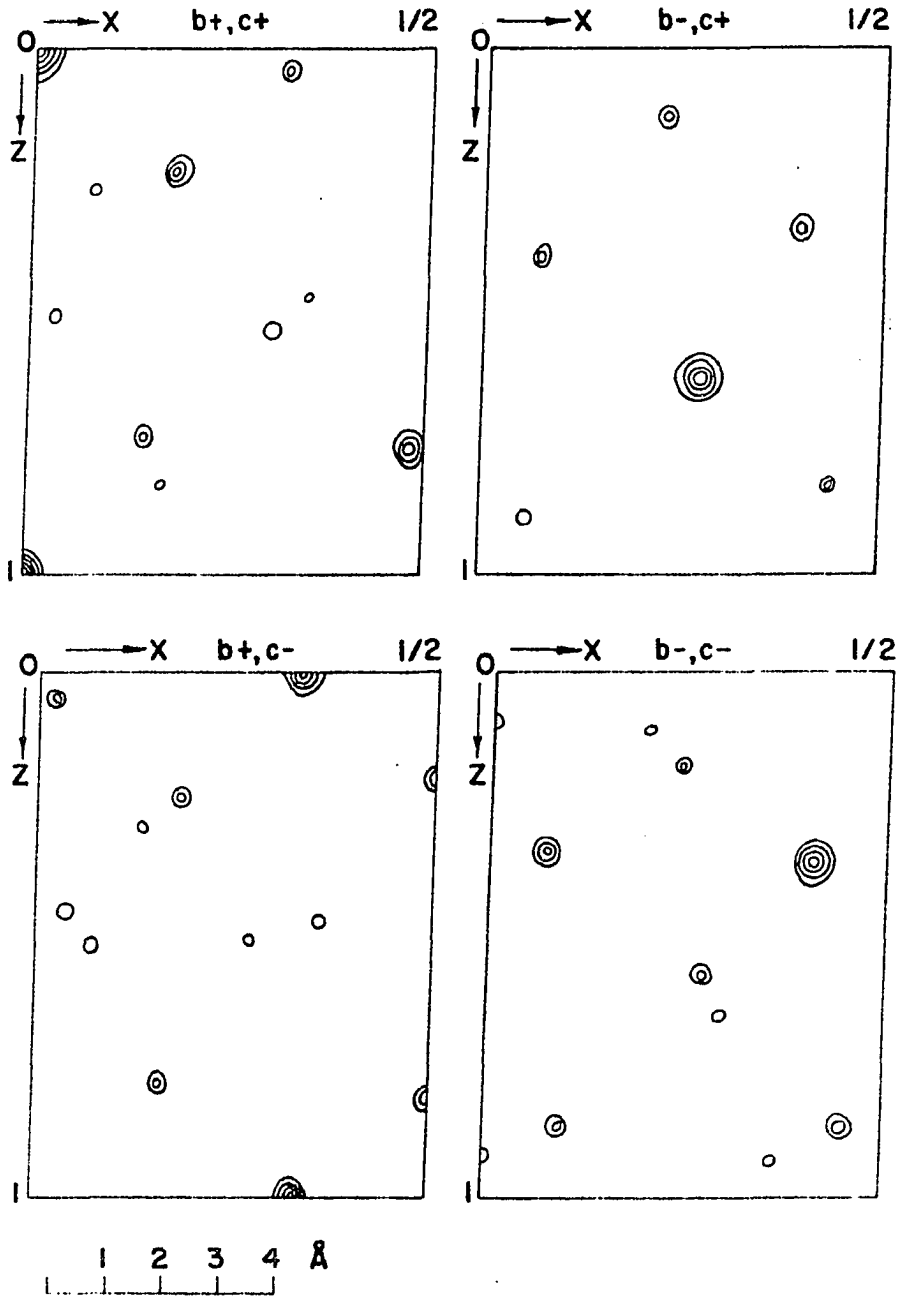

Figure 30. Four electron density maps for Nb_2Se synthesized using unitary structure factors as Fourier coefficients. Symbolic phases in the maps are: (a) b+, c+; (b) b-, c+; (c) b+ c-; (d) b-, c-

groups of 10-20, in repeated attempts to refine the trial structure and to obtain new electron density sections at y=0. For some of the additional reflections the | U | values were below 0.30, but in all cases the signs were only accepted with confidence for a 5:1 ratio of terms in Equation 33. After assigning 32 additional signs the trial structure refined to R=14%.

5. Refinement

Further refinement of positional parameters and isotropic thermal parameters of the six independent atoms of the structure was performed using ORFLS (9) with 578 reflections of the zero and first levels, and the 0,2,0 reflection. The h0ℓ and h1ℓ were accepted as "observed" provided that $\sigma(I)/I < 0.4$, where $\sigma(I)$ was obtained by counting statistics discussed previously. The atomic scattering factors used were those given by Hansen, Herman, Lea and Skillman (35); both real and imaginary components of anomalous dispersion (30) were included for Nb, -2.1 and 0.9, respectively, and for Se, -0.1 and 2.4, respectively. Weights were checked by fitting a straight line to a plot of $w(F_o-F_c)^2$ versus F_o^2. The weights were adjusted, using computer program OMEGA[1], so that a straight line of least squares fit had a slope of 0.01.

An unweighted R factor of 0.105 was obtained for the 578 reflections; the last cycle of the refinement showed that all

---

[1]Porter, S., Department of Chemistry, Iowa State University of Science and Technology, Ames, Iowa. Computer program OMEGA for weights check. Private communcation. 1968.

variable shifts were $<1\%$ of their estimated standard deviations. The final values of the variables are listed in Table 38. The standard deviation of an observation of unit weight or the "goodness of fit",

$$[\Sigma w\Delta^2/m-n]^{1/2}, \qquad (34)$$

was 1.03, where w is the revised weight of a single observation, Δ is $(F_o - F_c)$, m is the number of observations, 578, and n is the number of variables, 19. The list of observed and calculated structure factors are tabulated in Table 39. The reliability index, including the unobserved reflections, was 11.1%.

Refinement of the structure was also performed with anisotropic thermal parameters using all 1563 data. The anisotropic components of the thermal parameters are given in Table 38; $\beta_{12} = \beta_{23} = 0$ for atoms in x,0,z positions (37). The positional parameters obtained in this refinement were the same, within the standard deviations, as those listed in Table 38. In this case the R factor was 0.10 and the "goodness of fit", as defined by Equation 34, was 0.94. Refinements were also carried out in the noncentrosymmetric space groups. For both C2 and Cm the R factors were less than the corresponding refinement in C2/m. Table 40 compares the R factors for the different space groups. Hamilton (93) developed a criterion for judging the acceptability of one structure over another when the R factors differ and when different numbers of variables are used in the refinements. For Nb_2Se the hypothesis that the noncentrosym-

Table 38. Refined atomic parameters for Nb_2Se

Atom	Isotropic refinement			Anisotropic refinement			
	x	z	B(Å^2)	β_{11}	β_{22}	β_{33}	β_{13}
Nb(1)	0.2155(1)	0.1251(2)	0.43(3)	0.00049(4)	0.0080(8)	0.00128(9)	0.00022(4)
Nb(2)	0.0839(1)	0.3988(2)	0.39(3)	0.00048(4)	0.0064(8)	0.00115(9)	0.00028(4)
Nb(3)	0.4127(2)	0.3491(2)	0.58(4)	0.00063(4)	0.0076(8)	0.0020 (1)	0.00051(4)
Nb(4)	0.2568(1)	0.6228(2)	0.32(3)	0.00039(4)	0.0058(8)	0.00098(9)	0.00015(4)
Se(5)	0.1410(2)	0.8627(2)	0.44(4)	0.00058(5)	0.0065(8)	0.0015 (1)	0.00023(5)
Se(6)	0.4253(2)	0.8157(2)	0.54(4)	0.00060(5)	0.0077(8)	0.0018 (1)	0.00041(5)

Table 39. Observed and calculated structure factors for h0ℓ and hlℓ data for Nb_2Se

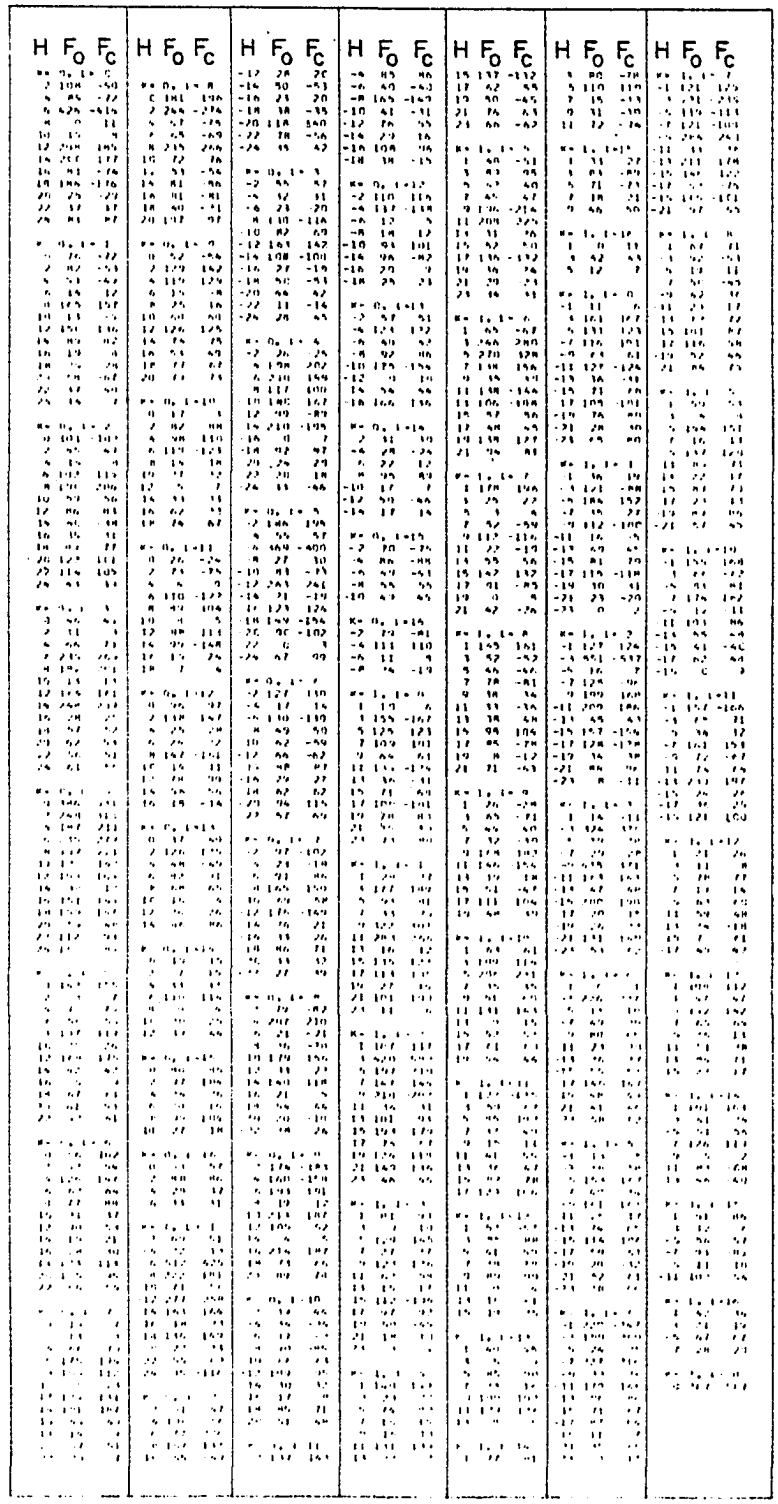

metric structure was correct rather than the centrosymmetric one could be rejected, according to Hamilton's criterion, at the 99.5% confidence level for both C2 and Cm.

Table 40. Comparison of R factors for three different refinements of the Nb_2Se structure

Space group	# reflections	# parameters	R factor
C2/m	1563	37	9.8
C2	1563	42	9.7
C2/m	578	19	11.1
Cm	578	23	11.0

For the purpose of checking the correctness of the refinement, a difference electron density synthesis was performed using 578 reflections of the zero and first levels. The map is shown in the y=0 section in Figure 31. Contours of this map are drawn in units of one electron per $\mathring{A}^3$; the atom positions are shown as dashed circles. This difference map had maxima corresponding to about two electrons at atomic positions.

F. Description of the Nb_2Se Structure

The ORTEP computer program written by Johnson (10) was used to draw the three-dimensional stereoscopic view of the Nb_2Se structure presented in Figure 32: the view is along the short b axis (the unique axis). Interatomic distances were

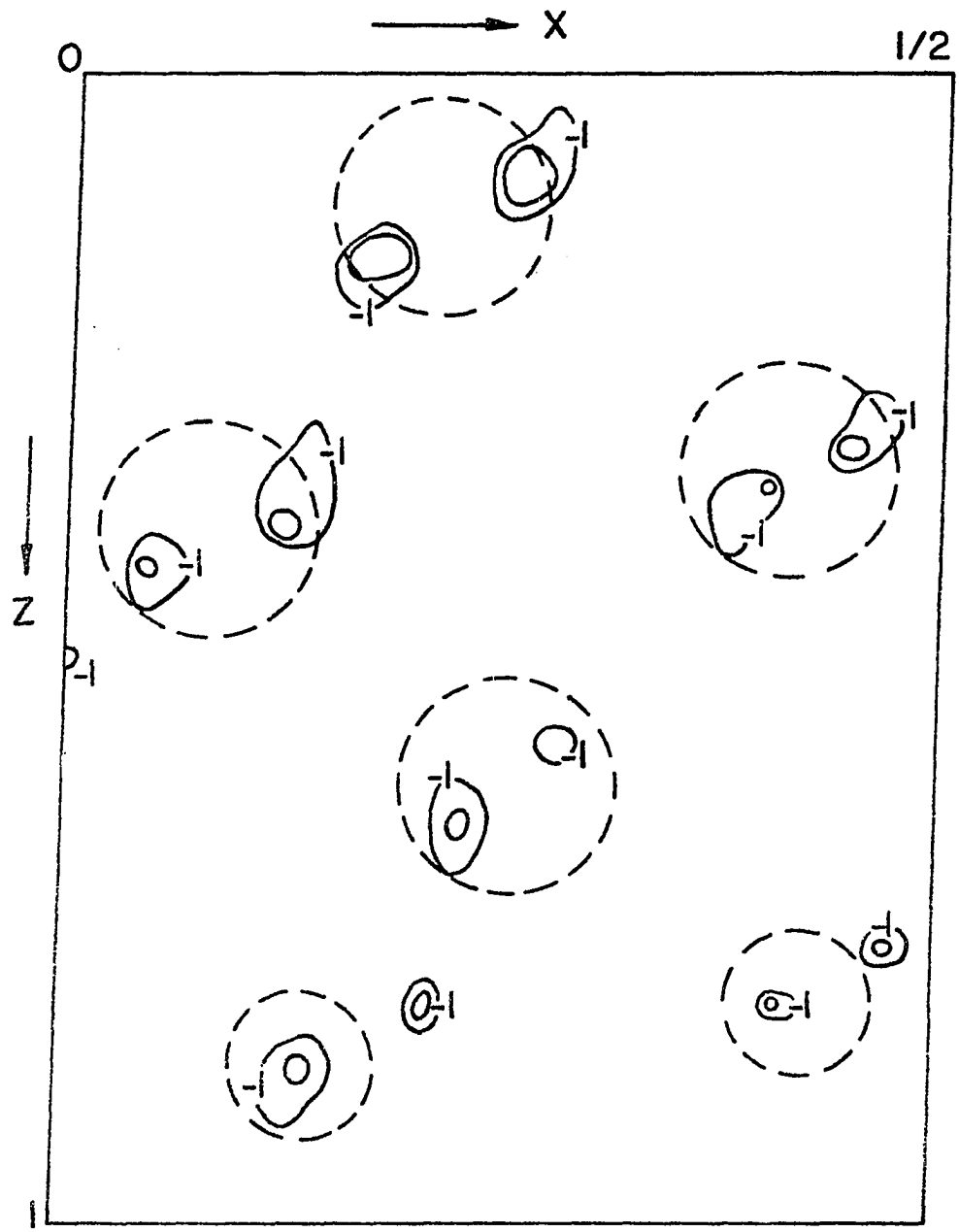

Figure 31. Difference electron density at y = 0 for the Nb_2Se structure. Contours are drawn in units of one electron. The atom positions are shown as dashed circles

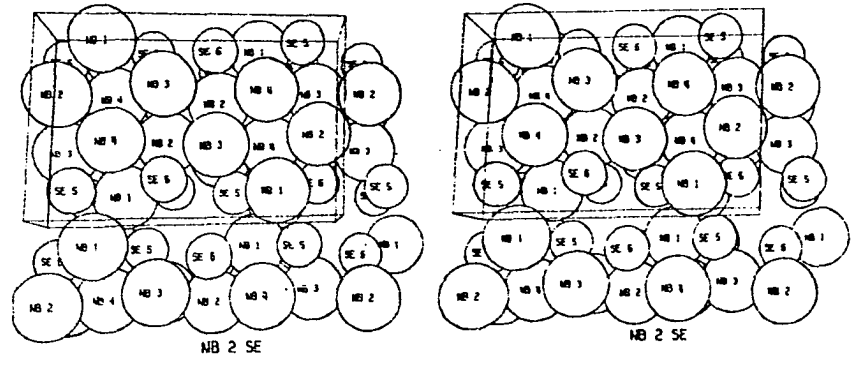

Figure 32. Stereoscopic illustration of the Nb_2Se structure viewed along the b axis

calculated using ORTEP; distances less than 3.42Å are listed in Table 41.

Table 41. Interatomic distances (±0.003Å) and bond orders in Nb_2Se. Distances less than 3.42Å are considered

Reference atom	Neighbor	No. of neighbors	Distance, Å	Bond order
Nb(1)	Se(5)	1	2.618	0.66
	Se(5)	2	2.642	0.60
	Se(6)	2	2.682	0.53
	Nb(4)	2	2.923	0.40
	Nb(1)	2	3.074	0.22
	Nb(2)	1	3.197	0.16
	Nb(3)	1	3.404	0.07
Nb(2)	Se(6)	2	2.630	0.63
	Nb(4)	2	2.826	0.56
	Nb(3)	2	2.904	0.43
	Nb(3)	2	2.967	0.33
	Nb(2)	1	3.060	0.23
	Nb(4)	1	3.138	0.18
	Nb(1)	1	3.197	0.16
Nb(3)	Se(5)	2	2.701	0.48
	Se(6)	1	2.782	0.36
	Nb(2)	2	2.904	0.43
	Nb(4)	2	2.947	0.35
	Nb(2)	2	2.967	0.33
	Nb(1)	1	3.404	0.07
	Nb(4)	1	3.411	0.07
Nb(4)	Se(5)	1	2.805	0.33
	Nb(2)	2	2.826	0.56
	Nb(4)	2	2.857	0.50
	Se(6)	1	2.911	0.21
	Nb(1)	2	2.923	0.40
	Nb(3)	2	2.947	0.35
	Nb(2)	1	3.138	0.18
	Nb(3)	1	3.411	0.07

Table 41 (Continued)

Reference atom	Neighbor	No. of neighbors	Distance, Å	Bond order
Se(5)	Nb(1)	1	2.618	0.66
	Nb(1)	2	2.642	0.60
	Nb(3)	2	2.701	0.48
	Nb(4)	1	2.805	0.33
Se(6)	Nb(2)	2	2.630	0.63
	Nb(1)	2	2.682	0.53
	Nb(3)	1	2.782	0.36
	Nb(4)	1	2.911	0.21

A projection of the Nb_2Se structure along the unique direction is shown in Figure 33. In this figure the radii of the atoms are drawn arbitrarily so as to make the coordination more easily visualized. For the present, disregard the bold-lined parallelogram in the middle of the projection.

One rather startling feature about Nb_2Se is the presence of regions in the structure which are empty. These void spaces are easily seen in the stereoscopic view in Figure 32; in Figure 33 the voids are centered on the twofold axes at the corners of the unit cell and on the twofold axes which lie at one-half of the unit cell in the $\underline{x}$ direction.

In the two previous structures, Ti_2S and $Nb_{21}S_8$, the chalcogen coordination was rather easy to describe, while the metal coordination was difficult to describe simply. The reverse is true for Nb_2Se: the metal coordination is rather

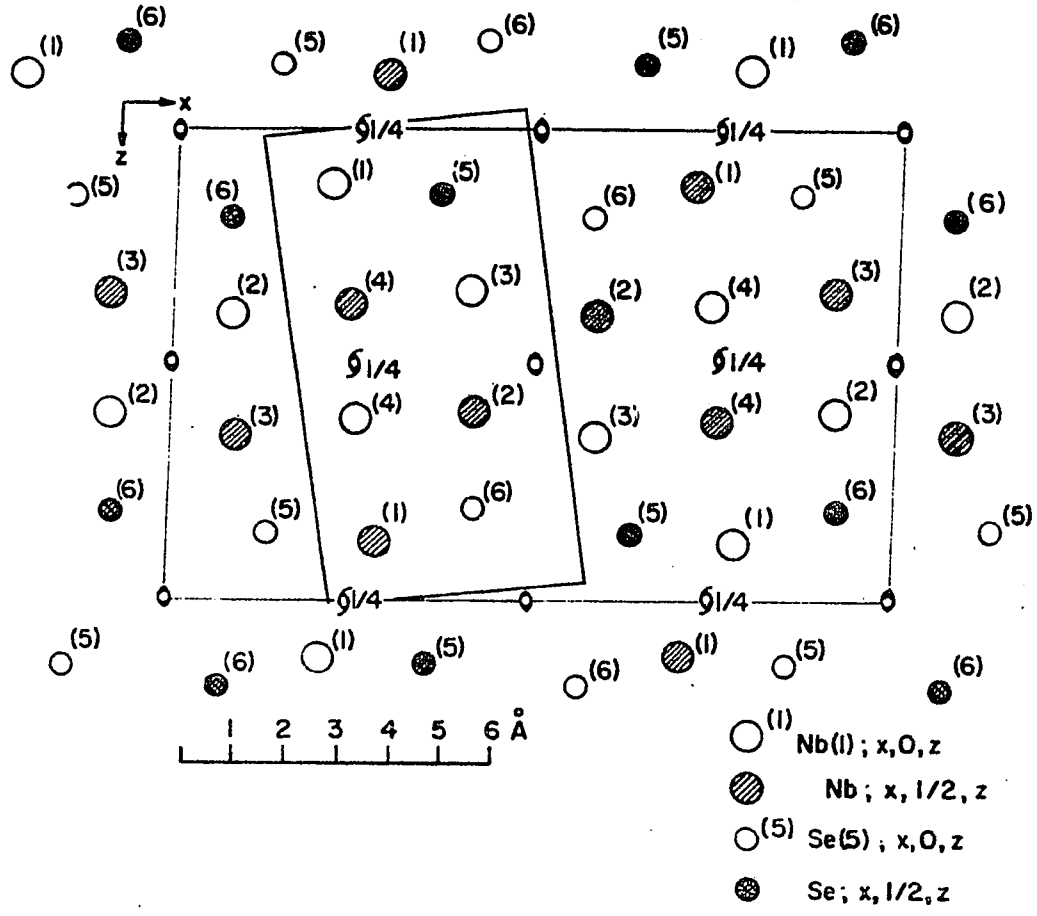

Figure 33. Projection of the Nb_2Se structure on (010). Symmetry elements of space group C2/m are shown. Light-lined large parallelogram delineates the unit cell of Nb_2Se. The bold-lined small parallelogram contains structural similarities to $Nb_{21}S_8$

easy to describe in terms of body-centered cubic coordination; the coordination of the Se atoms, on the other hand, is obscured by the presence of the voids.

Specifically, the coordination polyhedra of the four metals may be viewed as body-centered cubic: Nb(1) to 2Nb(1), 2Se(6), 2Nb(4) and 2Se(5); the cube in this case is quite distorted. For Nb(2) the cube is less distorted: 2Se(6), 4Nb(3) and 2Nb(4), and for Nb(3) the cube is described in 2Se(5), 2Nb(4) and 4Nb(2). Nb(4) has the least distortion of its cubic coordination: 2Nb(1), 2Nb(2), 2Nb(3) and 2Nb(4) at distances 2.83Å-2.95Å, very nearly equal to the closest Nb-Nb distance found in Nb metal, 2.86Å.

The two crystallographically independent Se atoms are bonded to the same number of Nb atoms, namely six, and both have equivalent environments although it is not simple to describe the coordination geometry. The selenium atoms can be viewed as belonging to non-bonded tetrahedra, sharing edges in the b direction. There is no selenium-selenium bonding in these tetrahedra; the closest Se-Se distance in Nb_2Se is 3.43Å, to be compared with the Slater (38) radius of 1.15Å.

It is possible to provide rather convincing evidence, however, that the selenium coordination in Nb_2Se is not entirely different from the trigonal prismatic coordination of chalcogens found in the Ti_2S-type structure and the $Nb_{21}S_8$-type structure. That evidence is presented in the next section.

G. Discussion

1. Apparent failure of superposition techniques in solving Nb_2Se

It was not possible to refine the trial structure obtained from the superposition of Patterson syntheses for Nb_2Se. This failure, however, was not the result of an incorrect trial structure, but rather was the result of an inadequate set of data used in the refinement. Apparently there was a certain number of reflections of a certain kind which were needed in order to make the refinement converge with respect to certain atomic positional parameters. If the refinement had been performed on the superposition trial structure using all 578 $h0\ell$ and $h1\ell$ data, the extra work of assigning signs by the direct method would not have been necessary.

2. A comparison between film data and automatic diffractometer data refinements

The film data collected were used to refine the positional parameters, individual isotropic temperature factor coefficients and two scale factors. The results of the film data refinement are listed in Table 42, together with the values from the refinement using automatic diffractometer data. The R factor for the refinement using the 184 film data for Nb_2Se was 20%, which is to be compared with 10% for the counter data.

Table 42. Comparison of film and counter data refinements of the Nb_2Se structure

Atom	Film[a] x	Film[a] z	Automatic counter x	Automatic counter z	Automatic counter B
Nb(1)	0.215(1)	0.124(2)	0.2155(1)	0.1251(2)	0.43(3)
(2)	0.085(1)	0.398(2)	0.0839(1)	0.3988(2)	0.39(3)
(3)	0.414(1)	0.347(2)	0.4127(2)	0.3491(2)	0.58(4)
(4)	0.257(1)	0.622(2)	0.2568(1)	0.6228(2)	0.32(3)
Se(5)	0.142(1)	0.861(2)	0.1410(2)	0.8627(2)	0.44(4)
(6)	0.424(1)	0.812(2)	0.4253(2)	0.8157(2)	0.54(4)

[a] B parameters not refined.

3. The direct method

As done previously for $Nb_{21}S_8$, the approximations used in the direct method were checked using the data for Nb_2Se. Unitary structure factors were calculated for the known structure of Nb_2Se and $\emptyset$ values for each reflection with $|U| > 0.4$ were calculated. Those $\emptyset$ values are plotted versus $\sin\theta$ in Figure 34, together with the $\emptyset$ versus $\sin\theta$ plot which was experimentally obtained by averaging procedures and by the assumption that $\langle U^2 \rangle = \sum_{j=1}^{N} n_j^2$. The agreement between the calculated points and the experimental points is generally good. At high $\sin\theta$ values, however, many of the calculated $\emptyset$ values lie above the experimentally obtained $\emptyset$ values represented by the line indicating that, for this structure, the $|U|$ values ob-

Figure 34. Plot of Ø vs. sin θ for Nb_2Se, comparing the experimental Ø values (solid line) and the calculated Ø values for $|U| > 0.40$

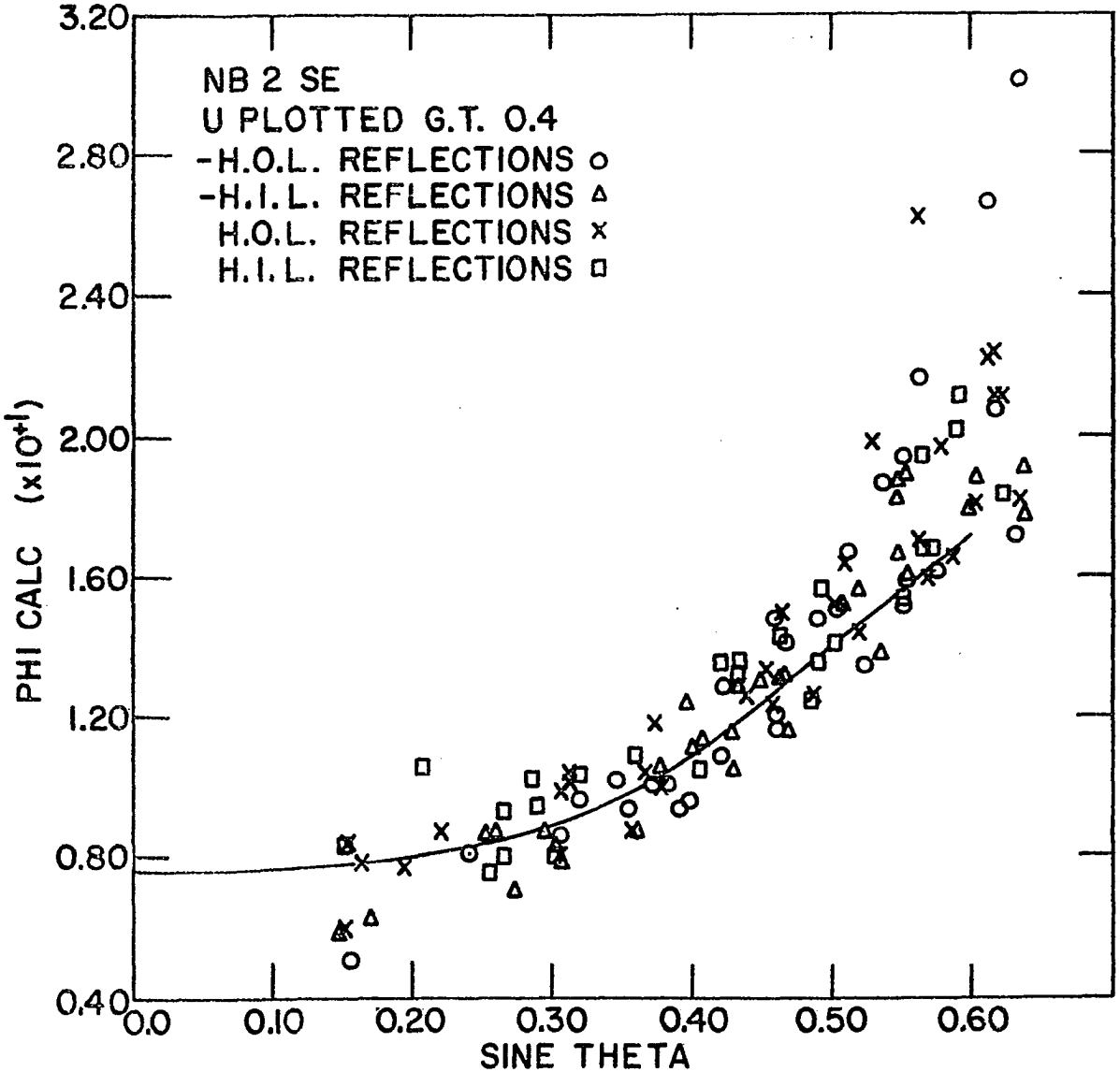
NB 2 SE
U PLOTTED G.T. 0.4
-H.O.L. REFLECTIONS
-H.I.L. REFLECTIONS
H.O.L. REFLECTIONS
H.I.L. REFLECTIONS
PHI CALC (x10+1)
3.20
2.80
2.40
2.00
1.60
1.20
0.80
0.40
0.0
0.10
0.20
0.30
0.40
0.50
0.60
SINE THETA

tained at high sinθ were underestimated. Indeed, this underestimation of |U| values could explain the fact that in order to refine a trial structure, $|U| > 0.3$ were accepted.

4. Discussion of the Se coordination in Nb_2Se

One might have expected, based on the bonding proposed for sulfur in $Nb_{21}S_8$, that selenium would behave as a "normal" chalcogen in a metal-rich niobium selenide, i.e., that selenium in Nb_2Se would have trigonal prismatic symmetry and high valence consistent with directional, delocalized, covalent bonding and with the participation of outer orbitals in the conduction band. The initial observation that the Nb_2Se structure appears to be different from $Nb_{21}S_8$ is examined below.

Nb_2Se can be compared with the $Nb_{21}S_8$ structure. The projections of the structures can serve to make a comparison. Figure 33 shows the Nb_2Se structure projected along its short axis (3.42Å); the bold-lined parallelogram is now to be considered. Figure 23 shows the $Nb_{21}S_8$ structure; the bold-lined parallelogram in that projection is also to be considered. There is a dramatic structural similarity between Nb_2Se and $Nb_{21}S_8$ contained in the parallelograms. By drawing the two structures such that the parallelograms are congruent, the projection of the atom positions in the structures are seen to be almost superimposed. Such a drawing is presented in Figure 35; the red portion of the drawing is the Nb_2Se structure in projection and the black portion is the $Nb_{21}S_8$ structure in projection.

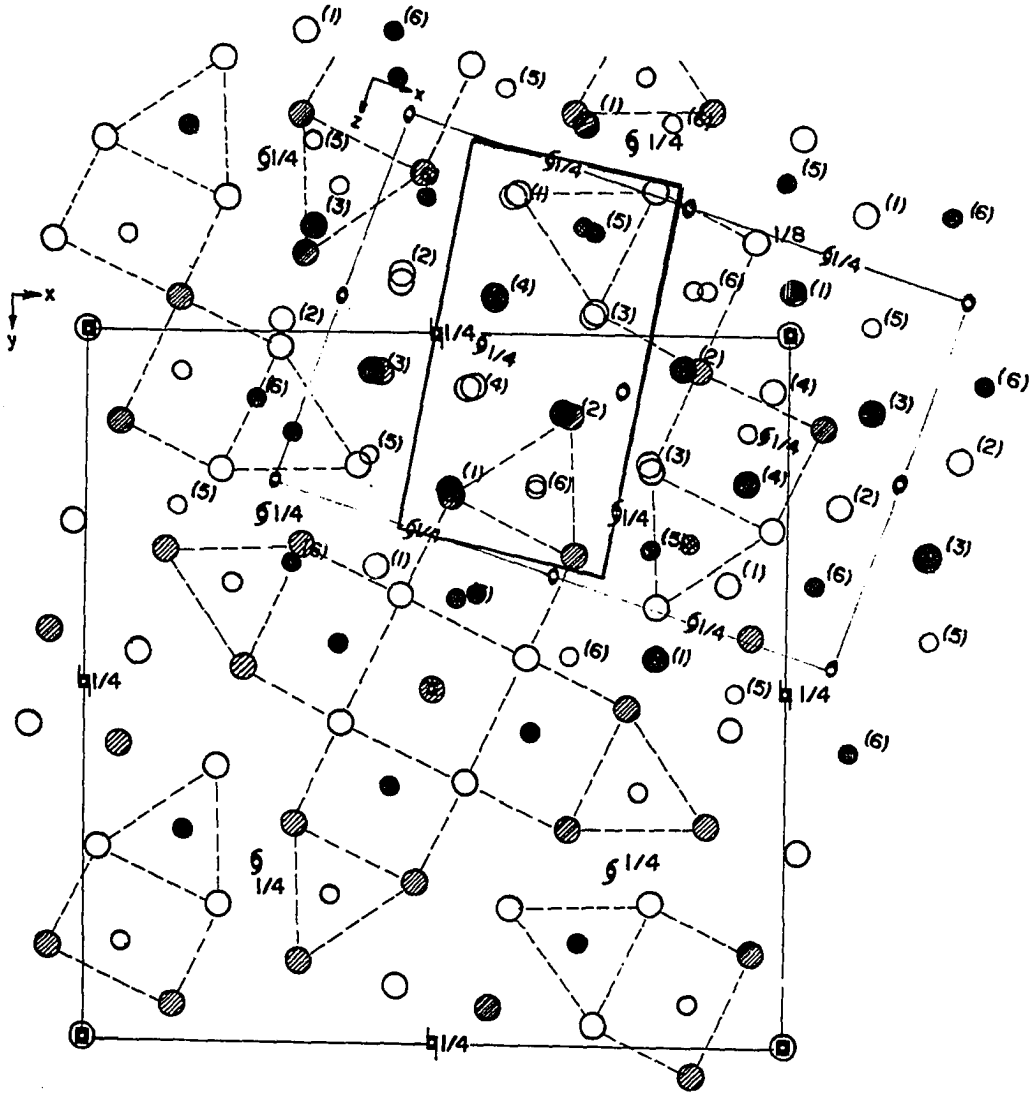

Figure 35. Superimposition of a portion of the projected $Nb_{21}S_8$ structure (black) with the projected Nb_2Se structure (red). The bold-lined parallelograms in Figures 23 and 33 are made congruent in this figure

There are two exceptions to the superimposition of the bold-lined parallelograms of Nb_2Se and $Nb_{21}S_8$: 1) the Nb atom at z= 1/2 in the lower right hand corner of the $Nb_{21}S_8$ parallelogram is missing in the Nb_2Se parallelogram, and 2) the Nb atom at z=0 in the upper right hand corner of the $Nb_{21}S_8$ parallelogram is missing in the Nb_2Se parallelogram. These two missing atoms in the Nb_2Se structure relative to the $Nb_{21}S_8$ structure are precisely where the void spaces occur in the Nb_2Se structure.

As discussed previously, and as shown by the dotted lines in the $Nb_{21}S_8$ projection, the coordination of S(2) in the $Nb_{21}S_8$ structure is trigonal prismatic with two augmenting Nb waist atoms adjacent to two rectangular faces of the prism. On the basis of the structural similarity between Nb_2Se and $Nb_{21}S_8$, it is possible to describe the two Se coordination polyhedra in Nb_2Se as fragments of augmented trigonal prisms. For example, the coordination of Se(5) is as follows: to 2Nb(1), 2Nb(3) and 2X (X=missing Nb) forming the trigonal prism, and to Nb(1) and Nb(4) located adjacent to the faces of the trigonal prism. The coordination of Se(6) is: to 2Nb(1), 2Nb(2), and 2X forming the prism, and to augmenting metal atoms Nb(3) and Nb(4).

5. The bonding in Nb_2Se

The observation of the structural similarity between the Nb_2Se structure and a portion of the $Nb_{21}S_8$ structure and the identification of fragments of augmented trigonal prismatic coordination polyhedra for Se in Nb_2Se suggests that the bonding interpretation for Nb_2Se is similar to that proposed for

$Nb_{21}S_8$ and for Group IVB metal-rich chalconides as well. It is proposed that non-bonded orbitals are directed into the void regions of the Nb_2Se structure whereas bonding orbitals occupy the same relative regions in the $Nb_{21}S_8$ structure.

The valences of Nb and Se in Nb_2Se are listed in Table 43. The average calculated valence of the chalcogen in this compound is about three, a significant reduction from the chalcogen valences in most other metal-rich chalconides. This reduction in calculated valence can be understood in terms of the non-bonded orbitals on the chalcogen directed toward the voids in the Nb_2Se structure.

Table 43. Valences of Nb and Se in Nb_2Se

Atom	Valence
Nb(1)	4.32
Nb(2)	4.47
Nb(3)	3.67
Nb(4)	3.52
Se(5)	3.15
Se(6)	2.89

The valence of Nb in this compound is lower than expected for a d^4s electronic configuration. The tendency is, however, for Nb to have the same coordination as found for the metal atoms in $Nb_{21}S_8$ and Ti_2S, namely, body-centered cubic. The occurrence of this coordination symmetry for Nb may be corre-

lated with the number of s electrons in the valence configuration which, as pointed out by Brewer (68), can be correlated with the promotion energy needed to attain the d^4s configuration in the gaseous Nb atom.

6. Survey of metal-rich chalconides of transition metal Groups IVB and VB

a. Structures The metal-rich chalconides of Group IVB metals with 33 atomic percent chalcogen were discussed in Chapter II: Ti_2S, Ti_2Se, Zr_2S, Zr_2Se, Hf_2S, Hf_2Se. Other metal-rich compounds of Group IVB are listed in Table 44.

Ti_3S was reported by Eremenko and Listovnichii (26) to have a structure related to the Ti_3P [ϵ (Fe-P-B)-type structure (27)]. In the latter structure the non-metal has augmented trigonal prismatic coordination symmetry. The Zr-S system is quite complex and will be discussed in detail in Part II of this work. ZrS_{1-x} has the WC-type structure (see Appendix C) over a wide range of stoichiometry, Zr_2S has the Ti_2S-type, and $Zr_{21}S_8$ has the $Nb_{21}S_8$-type structure; the structure of Zr_5S has not yet been solved. $ZrSe_{1-x}$ and $ZrTe_{1-x}$ were reported to have the WC-type structures by Hahn and Ness (94, 95).

The Ti_5Te_4 structure is an important type of structure. Ti_5Te_4 has a narrow range of homogeneity and, although it exists with roughly the same atomic ratio as the defect chalconides with the WC-type structure, its structure is very different from the WC-type. The tetragonal structure of Ti_5Te_4 is shown in projection in Figure 36.

Table 44. Classification of known metal-rich chalconides of Group IV and V metals

	Structure-type	Class[a]	Average chalconide coordination number	Average chalconide valence	Reference
Ti_2S	Ti_2S	I	7.7	4.5	(24), this work
Ti_2Se	Ti_2S	I	7.7	-	(63)
Zr_2S	Ti_2S	I	7.7	-	This work
Zr_2Se	Ti_2S	I	7.7	4.3	(63)
Hf_2S	Hf_2S	I	6	3.4	(65)
Hf_2Se	Hf_2S	I	6	-	(63)
Ti_3S	(Ti_3P?)	II	-	-	(26)
Zr_5S	?	II	-	-	This work
$Zr_{21}S_8$	$Nb_{21}S_8$	II	7.5	-	This work
α-V_3S	α-V_3S	II	8	5.0	(99)
β-V_3S	β-V_3S	II	8	5.0	(99)
$Nb_{21}S_8$	$Nb_{21}S_8$	II	7.5	4.1	(81), this work
Ta_6S	Ta_6S	II	-	-	(104), (63)

[a]Defined in text.

Table 44 (Continued)

	Structure-type	Class[a]	Average chalconide coordination number	Average chalconide valence	Reference
V_5S_4	Ti_5Te_4	III	6	-	(96)
V_5Se_4	Ti_5Te_4	III	6	-	(97)
V_5Te_4	V_5Te_4	III	6	-	(98)
$NbS_{x(x=?)}$	?	III	-	-	This work
Nb_5Se_4	Ti_5Te_4	III	6	-	(89)
Nb_2Se	Nb_2Se	III	6	3.0	This work
Nb_5Te_4	Ti_5Te_4	III	6	-	(89)
Ta_2S	Ta_2S	III	5	3.0	(103), (63)
Ti_5Te_4	Ti_5Te_4	IV	6	3.9	(90)
ZrS_{1-x}	WC	IV	6	3.5	(106)
$ZrSe_{1-x}$	WC	IV	6	-	(94)
$ZrTe_{1-x}$	WC	IV	6	-	(95)

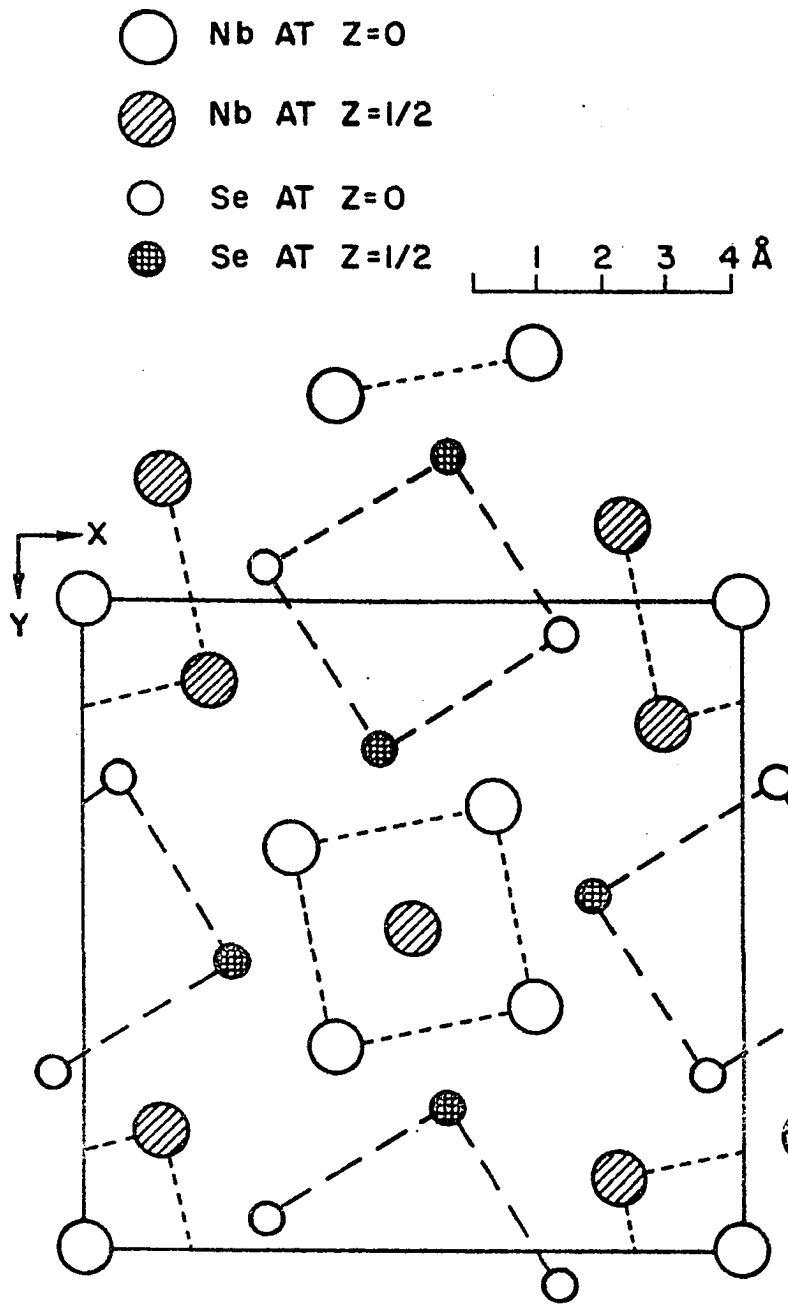

Figure 36. Projection of Ti_5Te_4-type structure on (001). Nb_5Se_4 crystallizes with this structure

Nb_2Se and $Nb_{21}S_8$ are also listed in Table 42 together with other known Group VB metal-rich chalconides. One finds a number of Group VB compounds with the Ti_5Te_4 structure: V_5S_4 (96), V_5Se_4 (97), Nb_5Se_4 (89), and Nb_5Te_4 (89), while V_5Te_4 (98) exists in a related monoclinic form. V_3S exists in two forms, α and β (99), both related to the Ni_3P structure (100) which, in turn, is related to the Fe_3P (101) and Ti_3P (102) structures. The coordination of sulfur in V_3S is distorted augmented trigonal prismatic. The metal has a tendency toward b.c.c. coordination in V_3S. The structures of Ta_2S and Ta_6S are complex; these structures were solved by Franzen and Smeggil (103, 104) and were recently discussed in detail by Smeggil (63). It is significant to note that Ta_2S has void regions in its structure and has low coordination and low valence for sulfur while, on the other hand, the more tantalum-rich sulfide, Ta_6S, has no such void regions and has distorted trigonal prismatic coordination of the sulfur.

b. Comparison of structures and classification of compounds The structural similarity between $Nb_{21}S_8$ and Nb_2Se was demonstrated in Section 4. Nb_2Se also has structural features which can be compared with Nb_5Se_4 (Ti_5Te_4-type structure, see Figure 36). There are void regions in both structures in the vicinity of the chalcogen; that is, in Nb_2Se and Nb_5Se_4 the chalcogen atoms are located in non-bonded clusters. In fact, the selenium coordination polyhedra are the same for both structures. The same remarks are applicable to the iso-

structural compounds, V_5S_4, V_5Se_4 and Nb_5Te_4. The Ta_2S structure also exhibits void regions in the structure around which the sulfur atoms are located in a non-bonding fashion.

Chalcogen valences, calculated via Pauling's relationship, are presented in Table 44 for Group VB compounds in which the interatomic distances are well known. These valences suggest that a distinction is possible between those compounds which have fairly high chalcogen valence (between 4 and 5) and those compounds which have lower chalcogen valences (ca. 3).

The facts that (a) the Ti_2S-type structure is found extensively in Group IVB compounds yet not at all in Group VB compounds, (b) there are seven known compounds of Group VB metals which display low coordination numbers, low valences of the chalcogen and have clusters of non-bonded chalcogens, while there is only one such compound (Ti_5Te_4) in the Group IVB metals, and (c) other than the aforementioned seven compounds, Group VB compounds are more metal-rich than the Ti_2S-type structure, suggest that the following classification may be made. CLASS I refers to Group IVB metal-rich chalconides with chalcogen/metal (Ch/M) = 0.5, which form with high chalcogen coordination numbers (six to nine). CLASS II refers to the Group IVB and VB compounds with $Ch/M < 0.5$ and with high chalcogen coordination numbers. CLASS III refers to other Group VB compounds which have $1.0 > Ch/M \geq 0.5$ and low chalcogen coordination numbers (five to six). CLASS IV refers to those Group IVB compounds which have $1.0 > Ch/M > 0.5$. In addition, the structures of CLASS III

compounds exhibit regions containing non-bonded chalcogen clusters and regions with extensive metal-metal bonding.

The coordination numbers and valences of the chalcogen atoms in the various classes strongly suggest an electron concentration interpretation of the differences and similarities of these compounds. All CLASS I compounds have approximately the same valence electron concentration. The valence electron concentration (v.e.c.) is increased if the stoichiometry is unchanged, but a Group VB metal replaces a Group IVB metal. Since no Group VB metal-rich chalconides with 2:1 composition are isostructural with Group IVB metal-rich chalconides with 2:1 composition, this increase in v.e.c. appears to result in compounds unstable either with respect to disproportionation into a still lower chalconide (forming a CLASS II compound) and a higher chalconide, or with respect to a structure type in which the chalcogen contributes fewer electrons to the conduction band of the solid (forming a CLASS III compound).

PART II. THE METAL-RICH REGION OF THE ZIRCONIUM-SULFUR SYSTEM

V. THE METAL-RICH REGION OF THE Zr-S SYSTEM

A. Introduction

1. Survey of the metal-rich region of the Zr-S system

The first systematic study of the Zr-S system was performed by Strotzer, Biltz and Meisel (1) in 1939. In the region $0 < S/Zr < 1.5$ they reported a phase with variable composition $ZrS_{1.5}$ - $ZrS_{1.2}$ and two more metal-rich phases, $ZrS_{0.75}$ and $ZrS_{0.33}$. Hägg and Schönberg (14) reinvestigated the system in 1954 and reported a tetragonal ZrS and a subsulfide of unknown composition. It was suggested by Jellinek (15), in a critical review of transition metal sulfide chemistry, that the tetragonal ZrS reported by Hägg and Schönberg was actually ZrOS which has the PbFCl-type structure (105).

Hahn, Harder, Mutschke and Ness (106) also reinvestigated the Zr-S system. They prepared a phase labeled Zr_3S_4 which they proposed was cubic, a=10.25Å. On the basis of powder diffraction intensities, Hahn, et al., proposed that the sesquisulfide phase, $Zr_{1-x}S$, was a superstructure of the NaCl-type in which half of the metal sites were fully occupied and half were statistically occupied. They reported the range of homogeneity of this phase to be $Zr_{1.5}$-$ZrS_{0.9}$, which included the ideal 1:1 compound, ZrS, which they found to have the NaCl-type structure,

$\underline{a}$=5.25Å. Hahn, et al. (106) found a phase with the WC-type structure which was deficient in sulfur content relative to ZrS. The WC-type phase was labeled ZrS_{1-x} and its range of composition was reported as x=0.2 to 0.5. These workers, upon annealing samples with S/Zr = 0.8 in silica tubes at high temperature for several weeks, found a tetragonal phase, Zr_4S_3, but this phase was subsequently shown by Jellinek and Hahn (107) to be ZrSiS, which was a result of sample interaction with the preparative tube at temperatures greater than 1000°C.

McTaggert and Wadsley (108) found the range of stoichiometry for $Zr_{1-x}S$ to be $ZrS_{1.6}$ - $ZrS_{0.9}$, but proposed a primitive cubic cell of 10.25Å, rather than a face-centered cell, to index their powder pattern.

Bracuti (109) confirmed Hahn's work, finding a sesquisulfide which was indexed on a cubic basis, $\underline{a}$=10.28Å, while the 1:1 compound was found to have the NaCl-type structure. The same partial ordering of metal atoms was derived by Bracuti from powder diffraction data. Jellinek (15) expressed the opinion, however, that the distinction between cubic and rhombohedral symmetry for the superstructure phase, $Zr_{1-x}S$, was only possible in a single crystal study, and that since a rhombohedral phase had been proposed by Hahn and Ness (94) for $Zr_{1-x}Se$, such a study was needed for the sulfide phase.

Steiger (110) also prepared some zirconium sulfide samples. He observed $Zr_{1-x}S$, a cubic sublimate ZrS, and the WC-type ZrS_{1-x}. The phases observed in prior investigations and in the

present one are listed in Table 45, together with pertinent crystallographic data.

2. Specific purposes of research

The purposes of this research were: 1) to characterize the equilibrium phases in the Zr-S system below S/Zr = 1.5, 2) to obtain single crystals of all phases observed and to determine their structures, and 3) to determine the symmetry and the nature of the ordering of defects in $Zr_{1-x}S$.

B. Experimental Methods

1. Sample preparation

a. Chemicals used The Zr metal used in the preparation of zirconium sulfides was obtained from the Ames Laboratory; a typical analysis of the metal is given in Table 46. The sulfur used was 99.999% pure, obtained from the Gallard-Schlesinger Chemical Manufacturing Company. The preparation of samples was performed using high temperature techniques as described in Chapter I.

Table 45. Condensed phases in the metal-rich region of the Zr-S system

Phase	Range of solid solution	Symmetry or space group	Lattice parameters (Å)	Comments	References
$Zr_{1-x}S$	$ZrS_{1.5}$-$ZrS_{0.9}$	cubic	$\underline{a}$=10.25	Zr vacancies ordered	(106)
	ZrS_{1-6}-$ZrS_{0.9}$	cubic, $P4_132$ or $P4_332$	$\underline{a}$=10.25		(108)
		cubic	$\underline{a}$=10.28	Zr vacancies ordered	(109), also (1), (15)
$Zr_{0.77}S$		monoclinic, C2/m	$\underline{a}$=10.35 $\underline{b}$=10.31 $\underline{c}$= 7.33 $\underline{\beta}$=135.06	Zr vacancies ordered superstructure of NaCl-type	This research
ZrS		cubic	$\underline{a}$= 5.25	NaCl-type	(106)
		cubic	$\underline{a}$= 5.12	NaCl-type	(109)
		cubic	$\underline{a}$= 5.15	NaCl-type	(110)
		cubic, Fm3m	$\underline{a}$= 5.16	NaCl-type	This research
ZrS_{1-x}	$ZrS_{0.8}$-$ZrS_{0.5}$	hexagonal, $P6_3/mmc$	$\underline{a}$= 3.436 $\underline{c}$= 3.435	WC-type	(106)
		hexagonal	$\underline{a}$= 3.429 $\underline{c}$= 3.455	WC-type	(110)
	$ZrS_{0.8}$-$ZrS_{0.6}$	hexagonal	$\underline{a}$= 3.4301 $\underline{c}$= 3.4505	WC-type	This research

Table 45 (Continued)

Phase	Range of solid solution	Symmetry or space group	Lattice parameters(Å)	Comments	References
Zr_2S		orthorhombic, Pnnm	$\underline{a}$=12.322 $\underline{b}$=15.359 $\underline{c}$= 3.508	Ti_2S-type structure	This research
$Zr_{21}S_8$		tetragonal, I4/m	($\underline{a}\cong$16.4) ($\underline{c}\cong$ 3.2)	$Nb_{21}S_8$-type structure	This research
Zr_5S		tetragonal, $I4_1/amd$	$\underline{a}$= 9.752 $\underline{c}$=19.216	structure determination underway	This research

Table 46. Typical spectroscopic analysis of the Zr metal used in zirconium sulfide preparations

Impurity	Level
Fe	27
C	33
Al	<25
Ti	8
N	10
Mg	25
Assay 99.987%	

b. The formation of W_2Zr As mentioned in Chapter I, the study of the Zr-S system, using a W crucible to contain the sample during high temperature treatment, was complicated by the formation of W_2Zr. The structure of W_2Zr was determined by Claassen and Burgers (111) to be the $MgCu_2$-type structure, cubic, a=7.61Å.

W_2Zr was observed to form under two particular conditions in this research: 1) W_2Zr was observed as a residue remaining in the bottom of a W crucible after a melted sample of Zr_5S was removed from the crucible with hot HNO_3; 2) W_2Zr was observed to form on the W lid of a Zr lined W crucible during high temperature annealing treatments at 1100°C-1550°C of samples consisting of Zr_2S and ZrS_{1-x}. The prevention of the formation of W_2Zr using a Zr liner in a W crucible was successful for samples with composition $S/Zr < 0.5$.

2. Analyses of samples

a. Phase analysis A partial list of equilibrated samples, together with their method of preparation, is contained in Table 47. Phase analysis was performed using the Debye-Scherrer and Guinier powder diffraction methods. All phases were identified in powder patterns with the exception of $Zr_{21}S_8$, which was observed only as a single crystal (see below).

b. Chemical analysis The S/Zr ratios listed in Table 47 were determined by combustion of the sulfide samples, contained in Pt crucibles, to ZrO_2. This determination was based on the assumption that only Zr and S were present in the samples. The oxygen content in the filed metal was determined by R. K. Winge of the Ames Laboratory, using the d.c. carbon arc method, to be 1000-1400 ppm.

c. Microprobe analysis One sample (Zr-S-XV-1) was subjected to microprobe analysis, performed by F. Laabs of the Ames Laboratory. This method of analysis is based on x-ray emission from the sample upon electron impact. Phase homogeneity, identification of elements present, and atomic weight composition of the sample are determined. The results of this analysis for the Zr-S-XV-1 sample are presented below.

3. Density determinations

Densities were determined using a 1 ml. pycnometer and either powdered sample or small chunks of samples. Water was used to determine the volume of the pycnometer and to cover the sample for volume displacement measurements. For powdered

Table 47. Partial list of equilibrated zirconium sulfide samples

Sample	Annealing temperature	Phases present	S/Zr	Comments
Zr-S-XIX-3	1200°C	Zr_5S+Zr		
Zr-S-XIX-3a.m.	arc-melted	Zr_5S+Zr		
Zr-S-XVIII-1	1175°C	Zr_5S	0.196	
Zr-S-XVIII-1a.m.	arc-melted	Zr_5S		Single crystal study of Zr_5S.
Zr-S-XV-1	1300°C	$(Zr_{21}S_8)$+Zr_2S		Single crystal study of $Zr_{21}S_8$. Two phases observed by microprobe analysis.
Zr-S-XIV-1	1400°C-melted	Zr_2S+Zr		Single crystal study of Zr_2S
Zr-S-XXII-3a.m.	arc-melted	Zr_2S+ZrS_{1-x}	0.4	
Zr-S-X-1	1340°C	ZrS_{1-x}+Zr_2S		
Zr-S-X-2	1600°C-melted	ZrS_{1-x}	0.66	
Zr-S-I-4	1700°C	ZrS_{1-x}+Zr		Single crystal study of ZrS_{1-x}.
Zr-S-I-10	1650°C	ZrS_{1-x}+Zr	0.81	
Zr-S-III-3a.m.	arc-melted	ZrS+ZrS_{1-x}	1.08	The S/Zr was in error.
Zr-S-III-5a.m.#2	arc-melted	ZrS		Single crystal study of ZrS.

Table 47 (Continued)

Sample	Anneling temperature	Phases present	S/Zr	Comments
Zr-S-IV-1	1500°C	$Zr_{1-x}S+ZrS_{1-x}$	1.14	
Zr-S-II-2a.m.	arc-melted	$Zr_{1-x}S$	1.301	Single crystal study of $Zr_{0.77}S$.

samples the pycnometer containing the sample was evacuated prior to the addition of water in order to eliminate the formation of small air bubbles in the powder.

C. Results

1. Crystallographic data for Zr_5S

Two crystals were examined by x-ray diffraction of the phase in the Zr-S system which coexists in equilibrium with Zr at 1200°C. The composition of the phase was S/Zr=0.196±0.003 or Zr_5S.

The first crystal investigated was twinned, but was successfully aligned along a 13.2Å rotation axis using a Weissenberg camera. Zero and first level Weissenberg photographs were taken with CuK_α radiation. The extinction conditions were consistent with space group Fddd(#70). The lattice parameters, as obtained from the Weissenberg film, were $\underline{a}$=18.8Å, $\underline{b}$=13.5Å, and $\underline{c}$=13.5Å, but the powder diffraction pattern was not indexable using these parameters. In an attempt to remount this crystal on a goniometer for further study, it was lost.

A second crystal was selected from Zr-S-XVIII-1a.m. It was single and was aligned along a 9.9Å rotation axis. Both the first and second level Weissenberg photographs taken with CuK_α radiation had plane net symmetry $C_{2\ell}$. The axes in the plane net were 9.8Å and 19.8Å. The general conditions for diffraction were:

$h+k+\ell = 2n$

$(h0\ell)\ h+\ell = 2n$

$00\ell\ \ \ell = 8n$

$(h00)\ \ h = 2n$

Due to the fact that the rotation axis of the second crystal was approximately $\sqrt{2}$ times the rotation axis of the first crystal and, furthermore, since the rotation axis was approximately equal to one of the axes perpendicular to it, tetragonal symmetry was suspected. A Laue photograph was obtained with the 19.8Å axis directed toward the x-ray beam; this photograph had 4/mmm symmetry, thus confirming tetragonal symmetry. Precession photographs were taken of the zero level hk0 reciprocal lattice plane and displayed fourfold symmetry with axis length 9.8Å and extinction conditions h,(k) = 2n.

The two possible centrosymmetric space groups are I4/mmm (#139) and $I4_1/amd$ (#141). The latter space group is the more probable one based on the observed extinctions in the 00ℓ reflections, $\ell = 8n$.

The first crystal had been aligned along the face-diagonal of the body-centered tetragonal cell, but the fourfold axis for this crystal was 18.8Å, whereas the fourfold axis for the second crystal was 19.8Å. These axes, however, were difficult to measure accurately; an average value for the c parameter from the two crystals was calculated to index the powder diffraction pattern.

The Guinier powder diffraction pattern was indexed and the lattice parameters were refined by least squares computation using LCR-2 (8). The final parameters were $\underline{a}=9.732\pm0.001$, $\underline{c}=19.216\pm0.003$. Table 48 lists all observed diffraction lines, their intensities, indices, and calculated and observed values of 2θ and $\sin^2\theta$. Two fuzzy, broad lines were not indexed. These lines could not be indexed as Zr or Zr_2S diffraction lines.

Table 48. Guinier x-ray powder diffraction data for Zr_5S

CuK_α radiation, Tetragonal, $\underline{a}= 9.752\pm0.001$Å, $\underline{c}=19.216\pm0.003$Å
$V=1830$Å^3

hkℓ	I/I_o	$\sin^2\theta$(obs) x10^5	$\sin^2\theta$(calc) x10^5	2θ(obs)	2θ(calc)
2,2, 4	25	7551	7561	31.90	31.92
3,2, 1	15	8272	8272	33.43	33.43
1,0, 7	80	8499	8495	33.90	33.89
3,1, 4	80	8823	8809	34.56	34.53
3,2, 3	100	9570	9554	36.04	36.01
4,0, 0	50	9990	9984	36.85	36.84
	5	10428		37.68	
4,0, 2	15	10621	10626	38.04	38.05
4,1, 1	15	10771	10767	38.33	38.31
2,1, 7	5	11006	10995	38.75	38.73
4,2, 0	10	12466	12477	41.35	41.37
2,0, 8	10	12784	12779	41.90	41.89
3,0, 7	5	13504	13486	43.12	43.09
4,1, 5	10	14657	14620	45.02	44.96
4,2, 4	5	15073	15048	45.69	45.65
2,2, 8	15	15261	15273	45.99	46.01
4,3, 1		15773	15760	46.80	46.78
5,0, 1	10	15773	15760	46.80	46.78
4,0, 6		15773	15766	46.80	46.79
4,0, 8	10	20252	20266	53.49	53.51
	Fuzzy	22498		56.63	
5,0, 7	15	23460	23467	57.94	57.95
4,3, 7		23460	23467	57.94	57.95
5,3, 4	10	23756	23786	58.34	58.38
3,0,11	15	25053	25053	60.07	60.07
5,4, 1	15	25721	25737	60.95	60.97

Table 48 (Continued)

hkℓ	I/I_o	$\sin^2\theta(obs) \times 10^5$	$\sin^2\theta(calc) \times 10^5$	2θ(obs)	2θ(calc)
4,2,10	20	28569	28545	64.02	64.59
6,3, 3	30	29496	29520	65.79	65.82
6,0, 8	5	32752	32743	69.82	69.81
1,1,14		32752	32743	69.82	69.81
2,0,14	10	33969	33986	71.30	71.32
5,0,11	15	35023	35040	72.57	72.59
4,3,11		35023	35040	72.57	72.59

The density of Zr_5S (Zr-S-XVIII-1a.m.) was determined four times: 6.87 g/cc, 6.66 g/cc, 6.63 g/cc and 6.47 g/cc, which averaged to 6.6±0.2 g/cc. This density and the volume of the unit cell were consistent with between 70 and 80 $ZrS_{0.2}$ formula units per unit cell.

2. Study of $Zr_{21}S_8$

a. Single crystal study $Zr_{21}S_8$ was not conclusively identified in powder diffraction patterns, although some diffraction lines not indexed in the diffraction patterns of Zr_5S and Zr_2S might have been $Zr_{21}S_8$ diffraction lines. The evidence for the existence of $Zr_{21}S_8$ was based on a single crystal diffraction pattern and on microprobe analytical results.

Several crystals were selected from sample Zr-S-XV-1 which was predominantly Zr_2S. One of these crystals was successfully aligned along a 3.2Å rotation axis and a Weissenberg zero layer photograph was taken using CuK_α radiation. The relative inten-

sities and the positions of the diffraction spots on the film were almost identical to the zero layer photograph of $Nb_{21}S_8$. It was concluded that the zirconium sulfide was isostructural with $Nb_{21}S_8$ and, accordingly, the composition was assigned $Zr_{21}S_8$. The lattice parameters obtained from the Weissenberg photograph were not accurate: $a \cong 16.4\text{Å}$, $c \cong 3.2\text{Å}$.

b. Microprobe results In the absence of identification of $Zr_{21}S_8$ in the powder diffraction pattern of Zr-S-XV-1, it was felt that more careful analysis of the sample was necessary. Several small chunks of the sample were mechanically polished and were analyzed by the microprobe method.

There were two distinct phases observed in the microprobe study by F. Laabs. One phase was present only to a very minor extent and was located near the surface of the bulk sample. This minor phase was also observed to have a higher weight percent Zr than the predominant phase. These observations were consistent with the formation of a Zr-rich phase resulting from the vaporization of a sulfur-rich species. Precise weight percents of Zr and S, which were the only species detected in the sample, were not obtained due to x-ray absorption and imprecise knowledge of sulfur content in reference samples.

3. Crystallographic data for Zr_2S

The diffraction lines of an unknown phase were observed together with the diffraction lines of Zr in sample Zr-S-XIV-1 which had melted at 1400°C. A single crystal was selected from this sample and was aligned along a 3.3Å axis on a Weissenberg

camera. Zero and first layer photographs had mmm diffraction symmetry and the relative intensities of the diffraction spots were approximately the same as those of Ti_2S. It was concluded that the structure of the zirconium sulfide phase was the same as Ti_2S and, accordingly, the composition was designated as Zr_2S.

Using approximate lattice parameters from the layer photographs, accurate parameters were determined from the Guinier powder diffraction data of sample Zr-S-XV-1 by least squares computation using LCR-2 (8). The refined parameters for Zr_2S were: $\underline{a}=12.322\pm0.003$Å, $\underline{b}=15.359\pm0.004$Å, $\underline{c}=3.508\pm0.001$Å. The observed diffraction lines for Zr_2S are listed in Table 49. Included in this table are the observed and calculated 2θ and $\sin^2\theta$ values and the calculated intensities. The intensities were calculated using a computer program written by Yvon, Jeitschko and Parthé (11). There were four lines in the pattern which were not indexed. These lines were not attributable to Zr, Zr_5S, or ZrS_{1-x} and, since one of the lines, namely $\sin^2\theta$ =0.22410, was evident in the powder pattern of Zr_5S, it was concluded that these four lines were $Zr_{21}S_8$ diffraction lines, but all efforts to index them on a tetragonal basis failed.

The calculated density of Zr_2S was 6.42 g/cc. The melting point of Zr_2S was observed to be less than 1400°C.

4. Study of ZrS_{1-x}

ZrS_{1-x} has a fairly wide range of solid solution. No definite range was established in this work, but S/Zr=0.66 was ob-

Table 49. Guinier x-ray powder diffraction data for Zr_2S

Orthorhombic, CuK_α radiation $\underline{a}=12.322\pm0.003$Å, $\underline{b}=15.359\pm0.004$Å, $\underline{c}=3.508\pm0.001$Å

hkℓ	$(I/I_o)_{obs}$	$(I/I_o)_{calc}$	$\sin^2\theta$(obs)	$\sin^2\theta$(calc)	2θ(obs)	2θ(calc)
1,4,0	5	7.6	4362	4415	24.11	24.26
1,1,1	10	9.5	5477	5462	27.07	27.03
4,0,0	10	14	6261	6252	28.98	28.96
4,1,0	5	6.9	6521	6504	29.59	29.55
	5		6708		30.02	
4,2,0	2	4.4	7268	7259	31.28	31.26
2,2,1	50	27	7391	7391	31.55	31.55
2,5,0	10	6	7849	7849	32.54	32.54
3,0,1	50	57	8344	8340	33.58	33.57
4,3,0	30	15	8529	8514	33.96	33.93
3,1,1	30	17	8602	8587	34.11	34.08
	5		8848		34.61	
0,6,0	25	21	9092	9052	35.10	35.02
1,4,1	60	62	9244	9234	35.40	35.38
3,2,1	10	4	9350	9345	35.61	35.60
	40		9714		36.32	
3,5,0	40	46	9797	9807	36.48	36.50
5,1,0	30	30	10016	10021	36.90	36.91
2,4,1	100	100	10407	10407	37.64	37.64
3,3,1	90	79	10610	10600	38.02	38.00
2,6,0		10	10610	10616	38.02	38.03
5,2,0	25	18	10767	10777	38.31	38.33
0,5,1	50	40	11121	11110	38.96	38.94
4,1,1	10	11	11347	11325	39.37	39.33
1,5,1	5	1.6	11502	11497	39.65	39.64
5,3,0	35	5	12070	12031	40.66	40.59
4,2,1		25	12070	12076	40.66	40.67

Table 49 (Continued)

hkℓ	$(I/I_o)_{obs}$	$(I/I_o)_{calc}$	$\sin^2\theta$(obs)	$\sin^2\theta$(calc)	2θ(obs)	2θ(calc)
4,5,0	25	7	12564	12541	41.52	41.48
3,6,0		5	12564	12570	41.52	41.53
1,7,0	20	16	12720	12715	41.79	41.78
5,4,0	30	15	13779	13791	43.58	43.60
5,1,1	30	15	14830	14843	45.30	45.32
6,3,0	15	2	16317	16330	47.65	47.67
1,8,0	15	11	16479	16485	47.90	47.91
2,8,0	5	2	17667	17660	49.71	49.70
4,7,0	10	1	18588	18575	51.08	51.06
0,0,2	50	41	19244	19279	52.04	52.09
6,3,1	10	2	21128	21150	54.73	54.76
2,9,0	20	10	21939	21939	55.86	55.86
	15		22410		56.51	
6,6,0	20	12	23091	23120	57.44	57.48
7,2,1	40	14	24962	24977	59.95	59.97
1,9,1	30	13	25561	25584	60.74	60.77
7,3,1	25	24	26203	26234	61.58	61.62
5,7,1	30	9	26913	26913	62.50	62.50
6,6,1	30	10	27980	27940	63.87	63.82
0,6,2	20	8	28341	28333	64.33	64.32
3,9,1	20	14	28719	28711	64.81	64.80
3,5,2	30	19	29083	29083	65.27	65.27
5,1,2	20	13	29305	29305	65.55	65.55

served to be in a single phase region. The lattice parameters for sample Zr-S-X-2 were obtained from LCR-2 (8): $\underline{a}$=3.4301±0.0008Å, $\underline{c}$=3.4505±0.0012Å. The Guinier powder data for this refinement are listed in Table 50.

Table 50. Guinier-x-ray powder diffraction data for ZrS_{1-x}

$\underline{a}$=3.4301Å, $\underline{c}$=3.4505Å, Hexagonal, CuK_α radiation

hkℓ	I/I_o	$\sin^2\theta$(obs)	$\sin^2\theta$(calc)	2θ(obs)	2θ(calc)
0,0,1	5	0.04992	0.04984	25.82	25.80
1,0,0	30	0.06734	0.06725	30.08	30.06
1,0,1	70	0.11703	0.11709	40.01	40.02
1,1,0	100	0.20168	0.20168	53.37	53.37
1,1,1	10	0.25182	0.25151	60.24	60.20
1,0,2	15	0.26650	0.26642	62.16	62.17
2,0,1	40	0.31854	0.31878	68.72	68.75
1,1,2	20	0.40100	0.40100	78.58	78.58

A single crystal of ZrS_{1-x} was selected from sample Zr-S-I-4 and was aligned along the hexagonal $\langle \bar{1}10 \rangle$ direction. Weissenberg layer photographs indicated that the WC-type determined by Hahn, et al. (106) for ZrS_{1-x} was correct.

5. Study of ZrS

a. Preparation The preparation of pure ZrS was performed using the general methods outlined in Chapter I with specific details as follows: 1) The elements (S/Zr = 1.3) reacted at 400°C in an evacuated and sealed Vycor tube to yield a mixture of ZrS_2 and ZrS_3 coating unreacted Zr metal filings.

2) The Zr, ZrS_2, ZrS_3 mixture was annealed at 1600°C for two hours. The product of the annealing was a mixture of $Zr_{1-x}S$ and ZrS_{1-x}. 3) The annealing treatment was repeated at 1300°C for four hours. 4) The $Zr_{1-x}S$, ZrS_{1-x} mixture was melted in an arc-melter. ZrS was obtained without contamination by ZrS_{1-x} after several repetitions of this step. The sample was labeled Zr-S-III-5a.m.-#2.

b. Crystallographic data A very sharp and clear Debye-Scherrer powder diffraction pattern of Zr-S-III-5a.m.-#2 was completely indexed on a face-centered cubic lattice: a=5.16Å. A complete list of all diffraction lines is contained in Table 51. There were two faint lines which caused some confusion. Initially the lines were indexed on a primitive cubic unit cell, a=5.16Å; these lines later were determined to be the two most intense diffraction lines (2,0,0 and 2,2,0) due to CuK_β radiation (λ=1.39Å).

Six crystals were investigated by Weissenberg and precession techniques. All six crystals were interpreted on a face-centered cubic (f.c.c.) cell of ca. 5.2Å. The sixth crystal, suitable for intensity collection, was aligned along a fourfold axis and three Weissenberg layer photographs were taken using CuK_α radiation. Intensities were estimated visually on multiple films, graphical $\overline{Lp}$ corrections were applied, transmission factors for the film were determined and applied, and a linear resolution of $K_{\alpha_1} - K_{\alpha_2}$ was assumed. No absorption corrections were made due to the crystal's small size, as evidenced in

Table 51. Debye-Scherrer x-ray powder diffraction data for ZrS

a=5.16Å, cubic, CuK_α radiation					
hkℓ	I/I_o	$\sin^2\theta$(obs)	$\sin^2\theta$(calc)	2θ(obs)	2θ(calc)
1,1,1	40	0.06681	0.06707	30.02	29.96
*	5	0.07313		31.38	
2,0,0	100	0.08958	0.08908	34.83	34.73
**	1	0.14620		44.96	
2,2,0	80	0.17941	0.17814	50.12	49.93
3,1,1	15	0.24623	0.24495	59.50	59.33
2,2,2	15	0.26828	0.26719	62.39	62.25
4,0,0	10	0.35690	0.35632	73.37	73.30
3,3,1	10	0.42411	0.42308	81.27	81.15
4,2,0	50	0.44643	0.44539	83.85	83.73
4,2,2	50	0.53505	0.53444	94.02	93.95
3,3,3 5,1,1)	5	0.60139	0.60122	101.70	101.68
4,4,0	15	0.71281	0.71257	115.19	115.16
5,3,1	10	0.77967	0.77938	124.01	123.97
4,4,2 6,0,0)	40	0.80188	0.80167	127.14	127.11
6,2,0	40	0.89071	0.89076	141.39	141.40
6,2,2	50	0.97951	0.97980	163.54	163.66

*P of 200.

**P of 220.

Figure 37 which shows a photograph (X500) of the ZrS crystal mounted on a glass fiber. The dimensions of the crystal were $30\mu \times 30\mu \times 60\mu$.

The symmetry of the crystal, as evidenced by the diffraction pattern, was cubic, space group Fm3m (NaCl-type). Structure factors were calculated according to the NaCl-type structure and the R factor for the ten most reliable reflections was 4%; the R factor for all fifteen independent reflections was 20%. In view of the fact that no absorption corrections were made and that the intensities were visually estimated, this agreement was acceptable, and thus it was concluded, in agreement with previous workers (106, 109, 110), that ZrS has the NaCl-type structure.

6. Study of $Zr_{1-x}S$, x=0.33

a. Preparation and x-ray diffraction data A sample was prepared in the single phase region of $Zr_{1-x}S$ in a manner similar to that used for ZrS except that for $Zr_{1-x}S$ a starting S/Zr = 1.5 was used. The product of the preparation was labeled Zr-S-II-2a.m. and was analyzed by combustion to have a ratio S/Zr = 1.301. The density was found to be 4.8 ± 0.1 g/cc.

The powder diffraction pattern was initially indexed on a f.c.c. basis with a lattice parameter approximately double that of ZrS, namely a=10.28Å. The powder data suggested that $Zr_{0.77}S$ was a superstructure of the NaCl-type structure.

A single crystal was selected from the $Zr_{0.77}S$ sample after many attempts. A photograph of that crystal is shown in

Figure 37. Photograph (X500) of a single crystal of ZrS

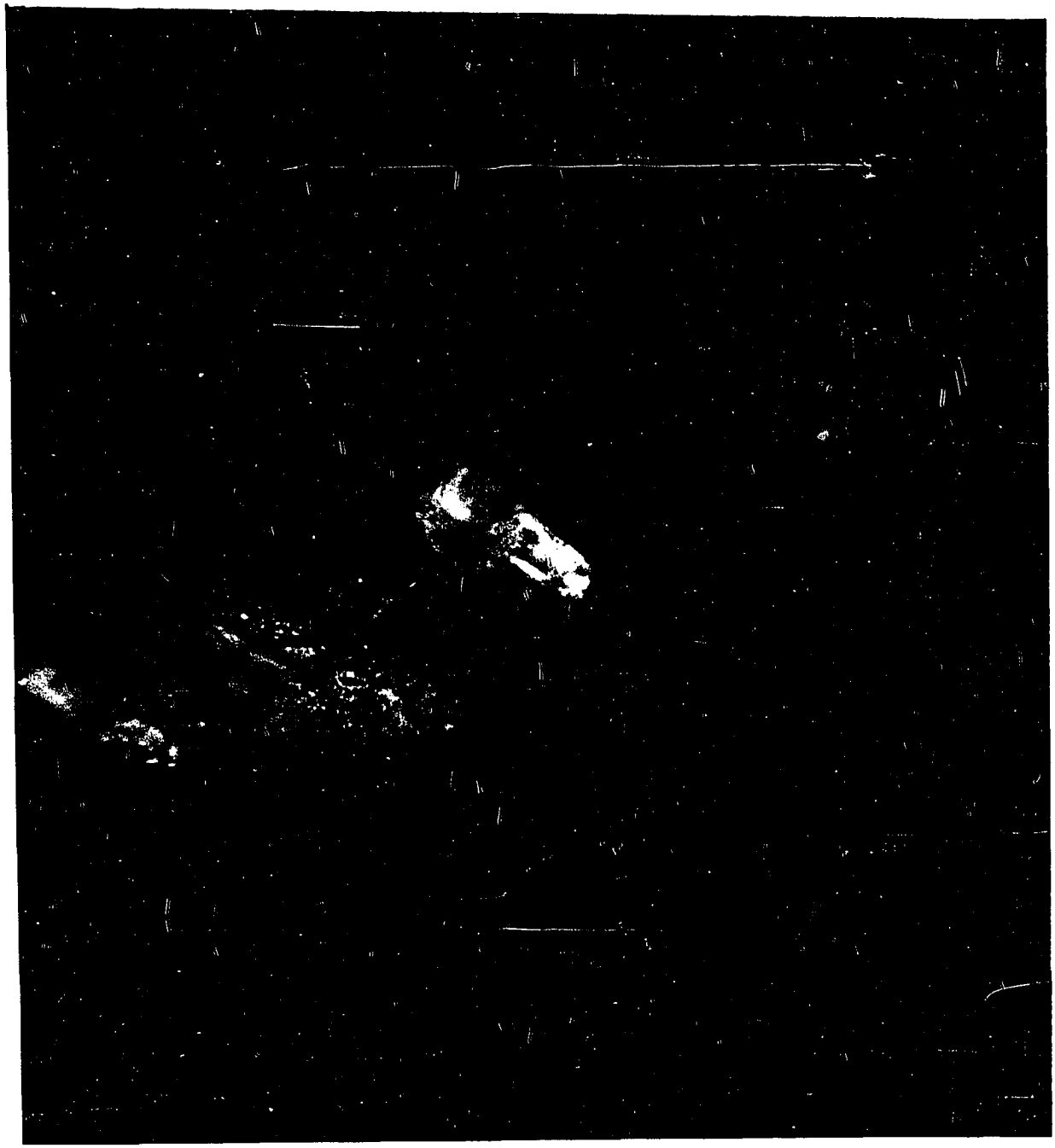

Figure 38. The details on the photograph of the crystal are blurred due to slight vibrations of the glass fiber on which the crystal was glued. The shape of the crystal was fairly regular; its size was approximately 70 x 70 x 120 microns. The crystal was aligned for data collection on a General Electric x-ray spectrogoniometer with a scintillation counter detector.

On the basis of previous work (106, 109, 15) it was considered that the symmetry of the $Zr_{1-x}S$ phase might be either cubic (four threefold axes) or rhombohedral (one threefold axis). In order to distinguish between these two symmetries, scans were recorded for the proposed cubic reciprocal lattice rows hhh, $\bar{h}hh$, $\bar{h}h\bar{h}$, and $hh\bar{h}$. The four scans are shown in Figure 39. The arrows on the topmost scan indicate the starting points for obtaining integrated peak intensities, the results of which are placed in parentheses below the indices of each peak on all scans. Absorption corrections were not applied to these particular integrated intensities, but, as can be seen from the measured intensities of the even-even-even parity reflections (the NaCl-type sublattice reflections), the error in these intensities due to absorption is less than 10%.

The conclusions reached upon analysis of the scans shown in Figure 39 were as follows:

1) There was no observed distortion of the NaCl sublattice, i.e., reflections (2,2,2), (4,4,4), (6,6,6), and (8,8,8) occurred at the same 2θ values for all four reciprocal lattice scans.

Figure 38. Photographs (X500) of a single crystal of $Zr_{1-x}S$, $x = 0.33$. Dimensions are approximately $70\mu \times 70\mu \times 120\mu$

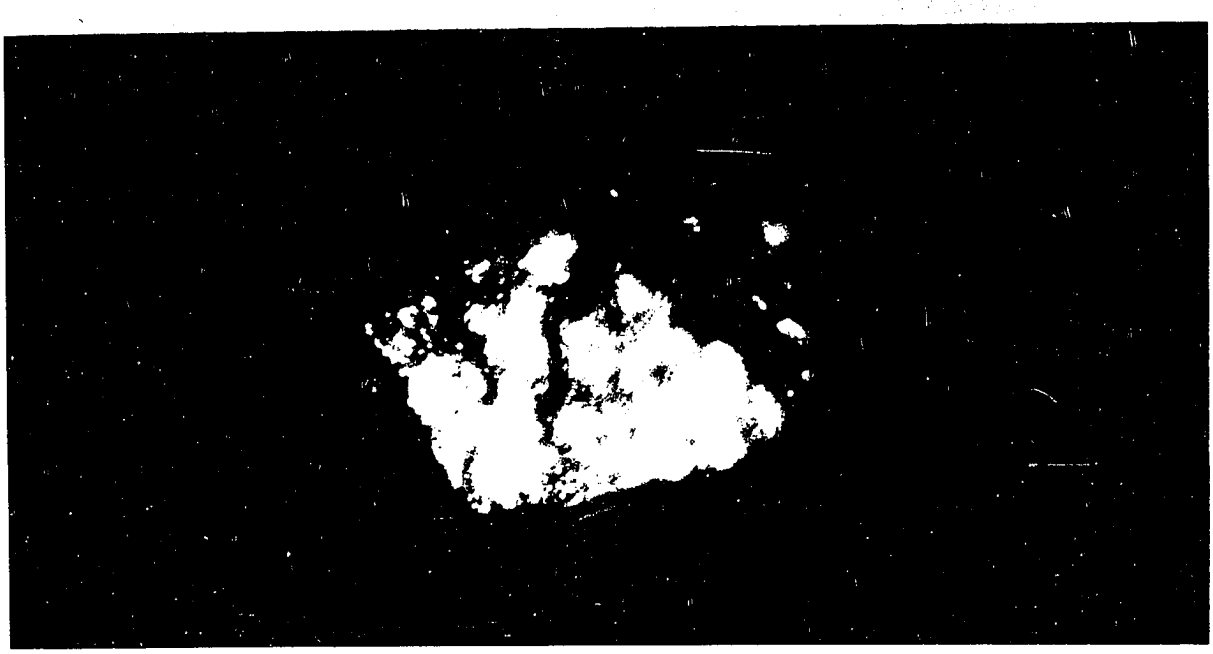

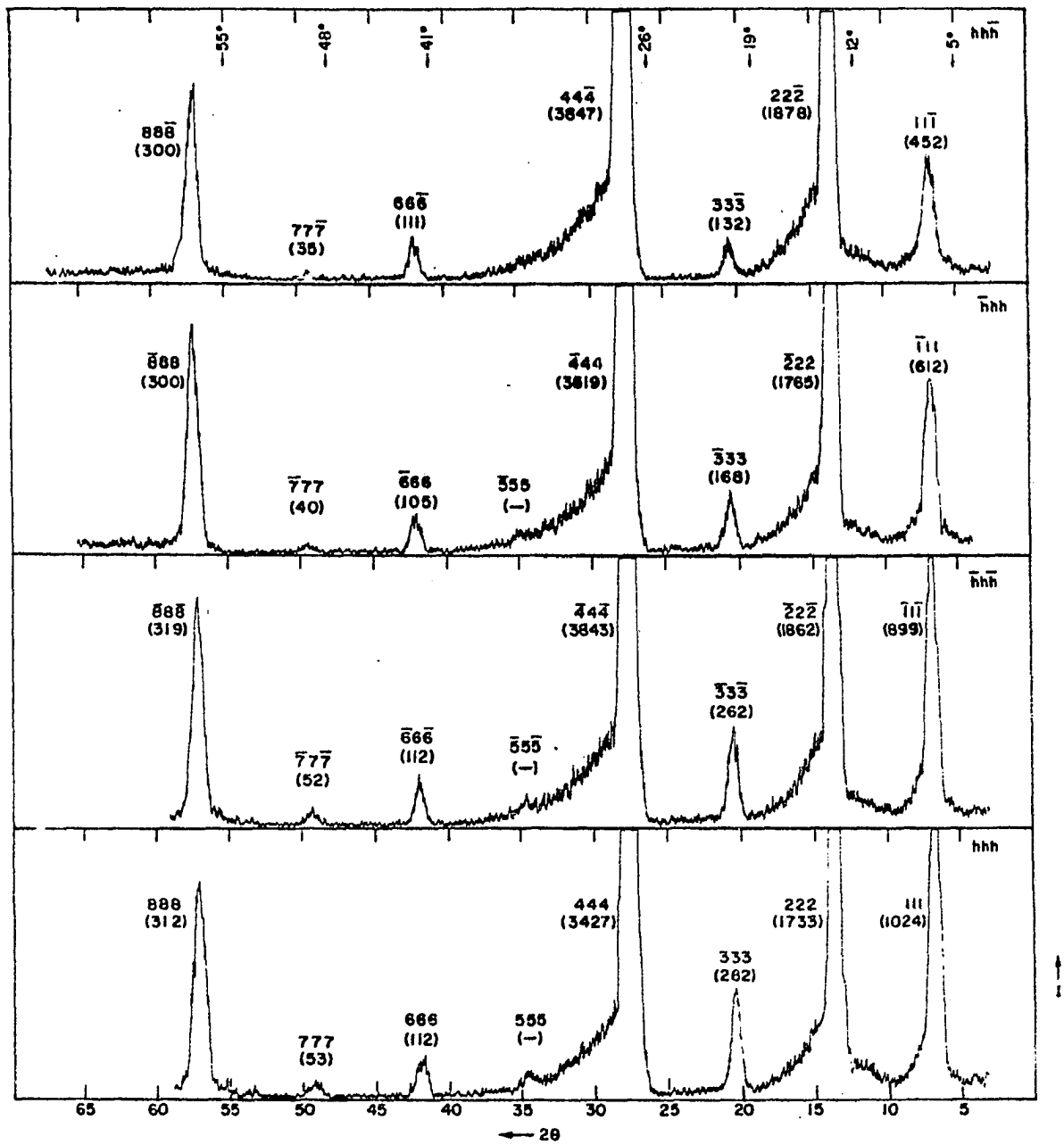

Figure 39. Two-theta scans of "cubic" reciprocal lattice row (hhh̄), (h̄hh), (h̄hh̄), and (hhh) of $Zr_{0.77}S$. Integrated intensities of peaks are given in parentheses

2) The superstructure peaks had small intensities relative to the substructure (NaCl) peaks. Compare, for example, $3,3,\bar{3}$ (132 counts) with $4,4,\bar{4}$ (3847 counts).

3) The substructure (NaCl) intensities were consistent with cubic symmetry within the relative errors in counting. This fact also indicated that absorption was not great for this crystal.

4) The superstructure intensities showed 2/m diffraction symmetry, i.e., $(\bar{h}hh) = (hh\bar{h})$ and $(hhh) = (\bar{h}h\bar{h})$ within the uncertainties due to errors in counting. The rather poor fit for these equalities of the (1,1,1) type reflections was probably due to their close position to the primary x-ray beam.

The crystal data for $Zr_{0.77}S$ are presented in Table 52. The density calculated by assuming that the only defects present were Zr vacancies, an assumption consistent with Hahn, et al. (106), was 4.91 g/cc, in good agreement with the observed density of 4.8 ± 0.1 g/cc. The positions for the NaCl-type structure in space group C2/m-#12 are also listed in Table 52. There are six crystallographically independent Zr positions in the unit cell, four positions with twofold multiplicity and two positions with fourfold multiplicity. All six of these positions are fixed in the space group C2/m. There are four positions for the sulfur atoms; each position has fourfold multiplicity. Lattice parameters were obtained from a least squares computation (8) of Guinier powder data which was indexed on a end-centered monoclinic unit cell. The results were: $\underline{a}=10.29$

Table 52. Crystal data for $Zr_{0.77}S$

Space group: C2/m (monoclinic)

Single crystal lattice parameters: $\underline{a}$= 10.35Å
$\underline{b}$= 10.31Å
$\underline{c}$= 7.33Å
β=135.06°
V=554Å^3

Density: measured: 4.80±0.1 g/cm^3
calculated assuming only Zr vacancies: 4.91 g/cm^3

Positions for filled NaCl-type structure in C2/m.
(1/2, 1/2, 0) +

2	Zr in (a);	0, 0, 0
2	Zr in (b);	0,1/2, 0
2	Zr in (c);	0, 0,1/2
2	Zr in (d);	0,1/2,1/2
4	Zr in (e);	1/4,1/4, 0;1/4,3/4, 0
4	Zr in (f);	1/4,1/4,1/2;1/4,3/4,1/2
16		

4	S in (g);	0, y, 0; 0, $\bar{y}$, 0 with y $\cong$ 1/4
4	S in (h);	0, y,1/2; 0, $\bar{y}$,1/2 with y $\cong$ 1/4
4	S in (i);	x, 0, z; $\bar{x}$, 0, $\bar{z}$ with x $\cong$ 1/4, z $\cong$ 0
4	S in (i);	x, 0, z; $\bar{x}$, 0, $\bar{z}$ with x $\cong$ 1/4, z $\cong$ 1/2
16		

± 0.09Å, $b=10.29\pm0.03$Å, $c=7.26\pm0.01$Å, $\beta=134.9\pm0.1^{\circ}$. The list of powder data for $Zr_{1-x}S$ appears in Table 53.

Table 53. Guinier x-ray powder diffraction data for $Zr_{0.77}S$

$a=10.29$Å, $b=10.29$Å, $c=7.26$Å, $\beta=134.9^{\circ}$
Monoclinic, CuK_{α} radiation

hkℓ	I/I_o	$\sin^2\theta$(obs)	$\sin^2\theta$(calc)	2θ(obs)	2θ(calc)
$\bar{1}$,1,1	10	0.01666	0.01686	14.83	14.92
$\bar{1}$,1,2	10	0.06197	0.06176	28.83	28.78
$\bar{2}$,2,2	20	0.06738	0.06738	30.09	30.09
0,0,2	100	0.08992	0.08968	34.90	34.85
$\bar{1}$,3,2	5	0.10669	0.10659	38.13	38.11
$\bar{1}$,1,3	5	0.15086	0.15148	45.71	45.81
0,4,2	50	0.17894	0.17867	50.05	50.10
$\bar{1}$,3,3	5	0.19687	0.19631	52.68	52.60
$\bar{2}$,2,4	10	0.24698	0.24706	59.60	59.61
$\bar{4}$,4,4	40	0.26974	0.26959	62.58	62.56

A total of 283 three-dimensional single crystal data were collected manually using the General Electric spectrogoniometer with filtered MoK_{α} radiation. For the data collection, standard reflections (0,4,0), (0,0,2), and ($\bar{4}$,0,2) were used to generate the diffracting positions for all other reflections using program SCO-6. These standard reflections were also used to calibrate the tube intensity. The calibration curve obtained from integrated scans of these standards for the time of the data collection is shown in Figure 40.

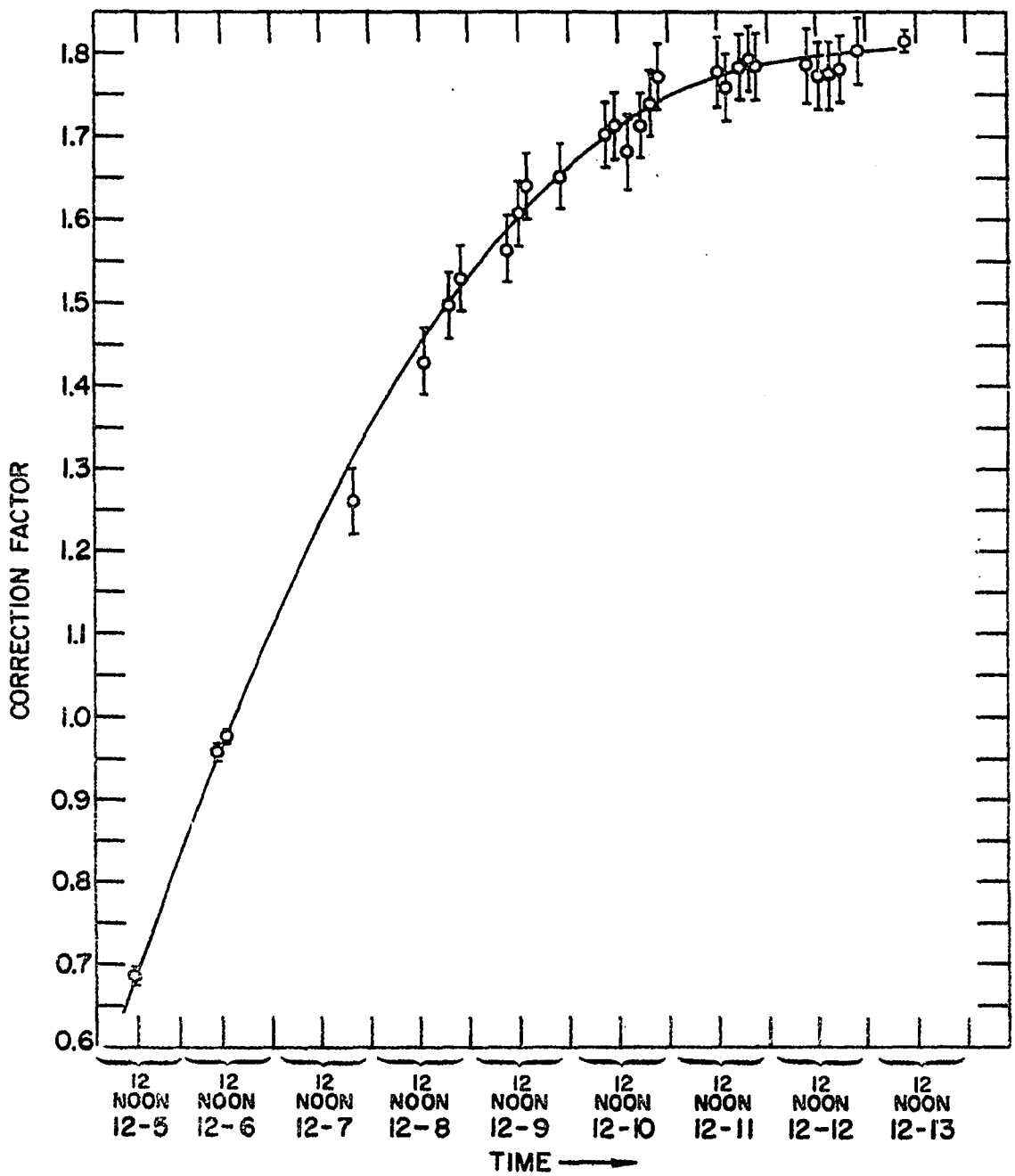

Figure 40. Plot of calibration factor vs. time for $Zr_{0.77}S$ data collection. The calibration factor was used to correct the x-ray tube intensity variation

The highest integrated intensities were obtained for the (0,0,1) monoclinic peak, but the peak was very broad, about six degrees in 2θ. Donald Lokken[1] suggested that this peak might be caused by white radiation from the very strong substructure peak (0,0,2). This suggestion was found to be correct; the profile of MoK_α radiation, Zr filtered, showed a white streak or peak at about $\lambda_{K_\alpha}/2$. Reflections which displayed this characteristic were deleted. One hundred sixty-seven reflections had non-zero intensities: 165 were superstructure intensities, and two were substructure or fundamental intensities. Lorentz and polarization corrections were applied. Absorption corrections, although not large, were made using ABCOR (7) with a linear absorption coefficient of 66.7 cm^{-1}. The 167 F_{obs} are listed according to their parities in Table 54. The fundamental reflections observed were (0,0,2) and $(\bar{2},2,2)$; they are Type 5 parity.

b. The determination of the crystal structure of $Zr_{0.77}S$

Due to the fact that the positional parameters of the zirconium positions are fixed by symmetry (see Table 52), it was possible to obtain the six occupation parameters for these positions by the solution of six simultaneous linear equations. The quantities required to obtain these six equations were the structure factors for each of the six parities corrected for thermal

---

[1]Lokken, D., Department of Chemistry, Iowa State University of Science and Technology, Ames, Iowa. White radiation. Private communication. 1969.

Table 54. Parity conditions for observed structure factors of $Zr_{0.77}S$ and calculation of $\overline{F'_{obs}}$

Type of parity	Conditions on h, k, ℓ	N=no. of struc. fac.	$N \sum_i \frac{Fi}{2k(f_{Zr})_i}$	$\overline{F'_{obs}}$	Mean error
1	odd, odd, even	80	50.90	0.64	0.02
2	odd, odd, odd	71	67.65	0.95	0.03
3	even, even, odd [h/2, k/2 both even or both odd]	4	- 1.59	-0.40	0.05
4	even, even, odd [h/2 odd, k/2 even or h/2 even, k/2 odd]	4	0.94	0.24	0.05
5	even, even, even [h/2, k/2 both even or both odd]	2	11.64	5.82	0.58
6	even, even, even [h/2 even, k/2 odd or h/2 odd, k/2 even]	6	- 2.05	-0.34	0.07

motion, the atomic scattering factors, and the contribution to diffraction from sulfur. Sulfur in the undistorted (NaCl) positions makes no contribution to reflections other than fundamentals. The structure factors so corrected were denoted by F'_{obs}.

The first step in the calculation of the six average $\overline{F'_{obs}}$ values was to obtain $\overline{F'_{obs}}$ for Type 5 reflections, i.e., the substructure structure factor independent of $\sin\theta/\lambda$. In order to correct for thermal motion a Wilson (112) plot of

$$\ell n \frac{\overline{F^2}}{\overline{f^2}} \text{ vs. } \frac{\sin^2\theta}{\lambda^2}$$

was made for the superstructure data. The plot is shown in Figure 41, $B=1.19\text{Å}^2$. The scale factor was determined from the two fundamentals by comparing F_{obs} with F_{calc} based on the known composition $Zr_{0.77}S$. The $\sin\theta/\lambda$ independent $\overline{F'_{obs}}$ values were defined to be

$$\overline{F'_{obs}} = \frac{1}{N} \sum_{i=1}^{N} \frac{F_i}{2k(f_{Zr})_i} \qquad (35)$$

where the F_i is the i^{th} relative observed structure factor corrected for thermal motion, $\underline{k}$ is the scale factor, $(f_{Zr})_i$ is the scattering factor of Zr at the Bragg angle of the i^{th} reflection, and the average is over the structure factors of a certain parity type. The $\overline{F'_{obs}}$ values and their mean errors, for each parity type, are listed in columns 5 and 6, respectively, in Table 54.

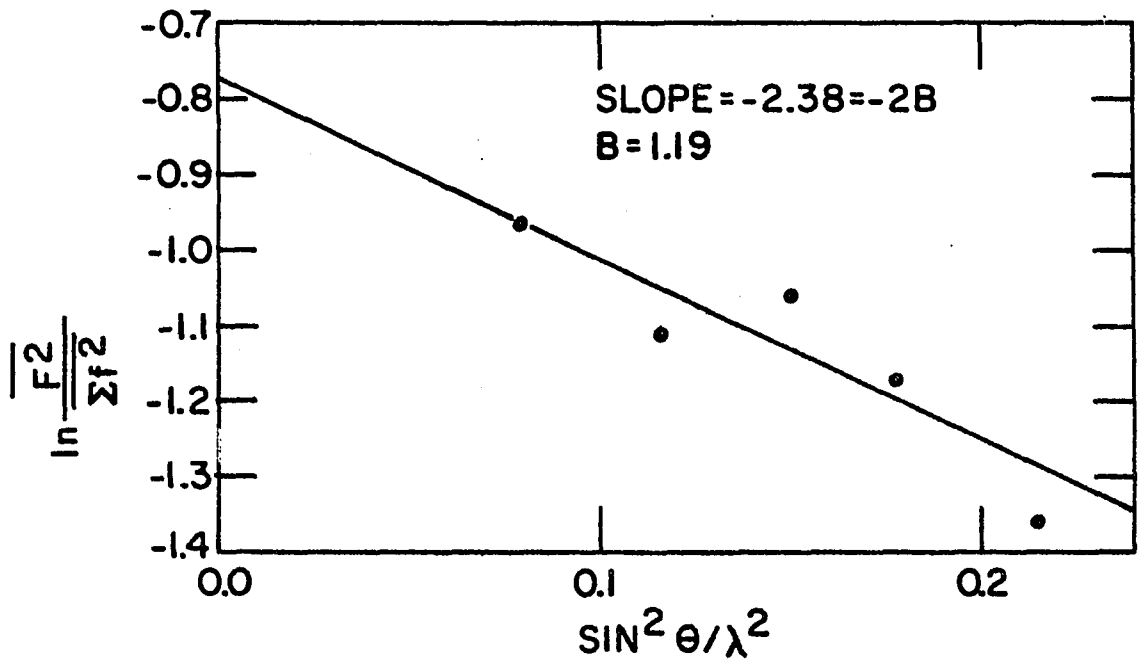

Figure 41. Wilson plot for the superstructure data of $Zr_{0.77}S$

The six equations for each of the $\overline{F'_{obs}}$ in terms of the percent occupancies of Zr sites, a, b, c, d, e, and f for the six parity types were:

$$\overline{F'}(1) = a - b + c - d \tag{36}$$

$$\overline{F'}(2) = a - b - c + d \tag{37}$$

$$\overline{F'}(3) = a + b - c - d + 2e - 2f \tag{38}$$

$$\overline{F'}(4) = a + b - c - d - 2e + 2f \tag{39}$$

$$\overline{F'}(5) = a + b + c + d + 2e + 2f \quad \text{(sulfur contribution considered)} \tag{40}$$

$$\overline{F'}(6) = a + b + c + d - 2e - 2f \tag{41}$$

where a, b, c, d, e, f are the percent occupancies of Zr sites (a), (b), (c), (d), (e), (f) in space group C2/m, and the numbers in parentheses following $\overline{F'}$ refer to the parity types listed in Table 54. The equations above were solved for the six occupancy parameters:

$$a = \tfrac{1}{4}\overline{F'}(1)+\tfrac{1}{4}\overline{F'}(2)+\tfrac{1}{8}\overline{F'}(3)+\tfrac{1}{8}\overline{F'}(4)+\tfrac{1}{8}\overline{F'}(5)+\tfrac{1}{8}\overline{F'}(6) \tag{42}$$

$$b = -\tfrac{1}{4}\overline{F'}(1)-\tfrac{1}{4}\overline{F'}(2)+\tfrac{1}{8}\overline{F'}(3)+\tfrac{1}{8}\overline{F'}(4)+\tfrac{1}{8}\overline{F'}(5)+\tfrac{1}{8}\overline{F'}(6) \tag{43}$$

$$c = \tfrac{1}{4}\overline{F'}(1)-\tfrac{1}{4}\overline{F'}(2)-\tfrac{1}{8}\overline{F'}(3)-\tfrac{1}{8}\overline{F'}(4)+\tfrac{1}{8}\overline{F'}(5)+\tfrac{1}{8}\overline{F'}(6) \tag{44}$$

$$d = -\tfrac{1}{4}\overline{F'}(1)+\tfrac{1}{4}\overline{F'}(2)-\tfrac{1}{8}\overline{F'}(3)-\tfrac{1}{8}\overline{F'}(4)+\tfrac{1}{8}\overline{F'}(5)+\tfrac{1}{8}\overline{F'}(6) \tag{45}$$

$$e = \tfrac{1}{8}\overline{F'}(3)-\tfrac{1}{8}\overline{F'}(4)+\tfrac{1}{8}\overline{F'}(5)-\tfrac{1}{8}\overline{F'}(6) \tag{46}$$

$$f = -\tfrac{1}{8}\overline{F'}(3)+\tfrac{1}{8}\overline{F'}(4)+\tfrac{1}{8}\overline{F'}(5)-\tfrac{1}{8}\overline{F'}(6). \tag{47}$$

The percent occupancies are listed in Table 55. The errors, listed in Table 55, were calculated by a propagation of errors treatment as derived by Birge (113):

$$R_a^2 = \sum_i \left(\frac{\partial a}{\partial \overline{F'}(i)}\right)^2 R^2_{\overline{F'}(i)}, \qquad (48)$$

where R_a is the error in the quantity $\underline{a}$, $\overline{F'}(i)$ is the i^{th} $\overline{F'}$; and $R_{\overline{F'}(i)}$ is the error associated with the i^{th} $\overline{F'}$ value.

Table 55. Percent occupancies of Zr sites in $Zr_{0.77}S$

Zr site, Wyckoff notation	% occupancy	Error
a	107	±8
b	27	±8
c	63	±8
d	79	±8
e	69	±7
f	85	±7

A least squares refinement (9) was then performed on the sulfur positions using the occupancies of Zr sites, the overall B, and the $\underline{k}$, as obtained above. The scattering factors used were those calculated by Hansen, et al. (35), corrected for anomalous dispersion (30). The final sulfur positional parameters are listed in Table 56. The reliability index on completion of the refinement was 18.5% including ten unobserved superstructure structure factors; R was 16% excluding the unob-

served reflections. A list of observed and calculated structure factors is given in Table 57.

Table 56. Sulfur positional parameters and average S coordination in $Zr_{0.77}S$. The sulfur coordination in the NaCl-type structure is 6.0

Sulfur site Wyckoff notation	Parameter	Value	Error	#Zr near neighbors
g	y	0.254	0.001	4.50
h	y	0.2489	0.0009	4.42
i	x	0.252	0.001	4.14
	z	-0.003	0.002	
i	x	0.253	0.001	4.46
	z	0.507	0.002	

Table 57. Observed and calculated structure factors for $Zr_{0.77}S$

K = 0																			
H	L	FO	FC	1	3	48	43	7	0	24	24	-1	5	28	24	3	2	28	22	1	1	56	44
4	1	18	-15	-1	3	50	39	5	0	28	20	-3	5	60	44	-1	2	34	27	-1	1	46	43
-8	1	0	-11	-3	3	61	57	3	0	34	38	-5	5	30	30	-3	2	25	28	-3	1	50	43
0	2	507	503	-5	3	51	40	1	0	55	39	-7	5	56	44	-5	2	27	19	-5	1	34	35
-2	3	0	13	-7	3	46	41	-1	0	38	39	-9	5	38	25	-7	2	19	23	1	2	23	22
-6	6	0	-10	-9	3	31	25	-3	0	42	38	-1	6	0	19	3	3	27	17	-1	2	28	28
				1	4	22	16	-5	0	18	20	-3	6	28	18	1	3	28	33	-3	2	32	29
				-1	4	33	27	-7	0	36	24	-5	6	22	21	-1	3	38	28	-5	2	16	21
				-3	4	23	28	5	1	41	35	-7	6	21	23	-3	3	43	41	-7	2	41	24
K = 1				-5	4	36	26	3	1	48	41	-9	6	28	16	-5	3	41	28	1	3	50	36
H	L	FO	FC	-7	4	28	29	1	1	72	59	-7	7	51	36	-7	3	37	31	-1	3	30	33
5	0	27	19	-1	5	31	22	-1	1	67	59					-1	4	25	21	-3	3	58	44
3	0	53	38	-3	5	45	43	-3	1	71	58					-5	4	22	19	-5	3	31	33
1	0	51	41	-5	5	38	29	-5	1	48	43		K = 4			-7	4	20	22	-7	3	39	35
-1	0	58	41	-7	5	49	43	-7	1	33	33	H	L	FO	FC	-1	5	26	16	-1	4	19	23
-3	0	37	38	-9	5	30	23	5	2	16	13	-6	0	0	-10	-3	5	30	33	-3	4	23	23
-5	0	28	19	-1	6	23	18	3	2	22	28	0	1	0	-21	-7	5	29	33	-5	4	22	22
-7	0	21	23	-5	6	20	21	1	2	35	28	0	3	24	-16	-9	5	23	17	-7	4	31	24
5	1	29	33	-7	7	43	35	-1	2	35	38												
3	1	51	40					-3	2	51	39		K = 5				K = 6				K = 8		
1	1	68	59					-5	2	25	27	H	L	FO	FC	H	L	FO	FC	H	L	FO	FC
-1	1	88	61		K = 2			-7	2	42	29	7	0	27	19	0	1	18	11	-2	0	0	-11
-3	1	65	58	H	L	FO	FC	1	3	59	44	3	0	35	28	-6	5	0	-12				
-5	1	49	41	2	1	19	-20	-1	3	45	41	1	0	28	27						K = 9		
-7	1	29	32	0	2	20	-17	-3	3	71	57	-1	0	36	27		K = 7			H	L	FO	FC
3	2	34	28	-2	2	175	152	-5	3	43	42	-3	0	27	28	H	L	FO	FC	1	0	22	15
1	2	22	27	0	3	0	11	-7	3	52	43	3	1	35	29	5	0	21	17	-3	0	25	17
-1	2	52	38	-4	5	0	9	1	4	21	17	1	1	39	40	3	0	33	29	-1	1	30	22
-3	2	36	40					-1	4	28	28	-1	1	46	39	1	0	32	28	-3	1	31	23
-5	2	35	26					-3	4	34	29	-3	1	41	40	-1	0	29	28	-1	3	25	16
-7	2	26	29		K = 3			-5	4	24	27	-5	1	35	30	-3	0	36	29	-3	3	32	25
3	3	29	23	H	L	FO	FC	-7	4	32	29	-7	1	20	24	3	1	32	34	-5	3	28	16

A Fourier electron density synthesis using only superstructure structure factors had maxima corresponding to the percent occupancies of Zr sites. A difference Fourier synthesis showed no appreciable maxima.

c. Description of the crystal structure of $Zr_{0.77}S$

A perspective drawing of the structure is presented in Figure 42. The monoclinic cell is shown by heavy lines and the NaCl-type ZrS cells are shown as thin-lined cubes. The atomic labels in the drawing are consistent with the labels in Table 52.

As can be seen from Table 55 there are, within the errors stated, four different Zr occupancies. The calculated composition for this structure, based on the Zr occupancies, is $Zr_{0.72}S$, which is in reasonable agreement with the observed composition of $Zr_{0.77}S$. The differences between the sulfur positions with regard to coordination are not great; the number of Zr near neighbors to each sulfur, obtained by summing the site occupancies of Zr, are listed in Table 56.

D. Discussion

1. Coordination polyhedra

In this work the existence of three compounds with narrow homogeneity ranges in the region $0 \leqslant S/Zr \leq 0.5$ was established. Two of the compounds, $Zr_{21}S_8$ and Zr_2S, were found to be isostructural with $Nb_{21}S_8$ and Ti_2S, respectively. The coordination of the sulfur atoms in both of these structures is augmented

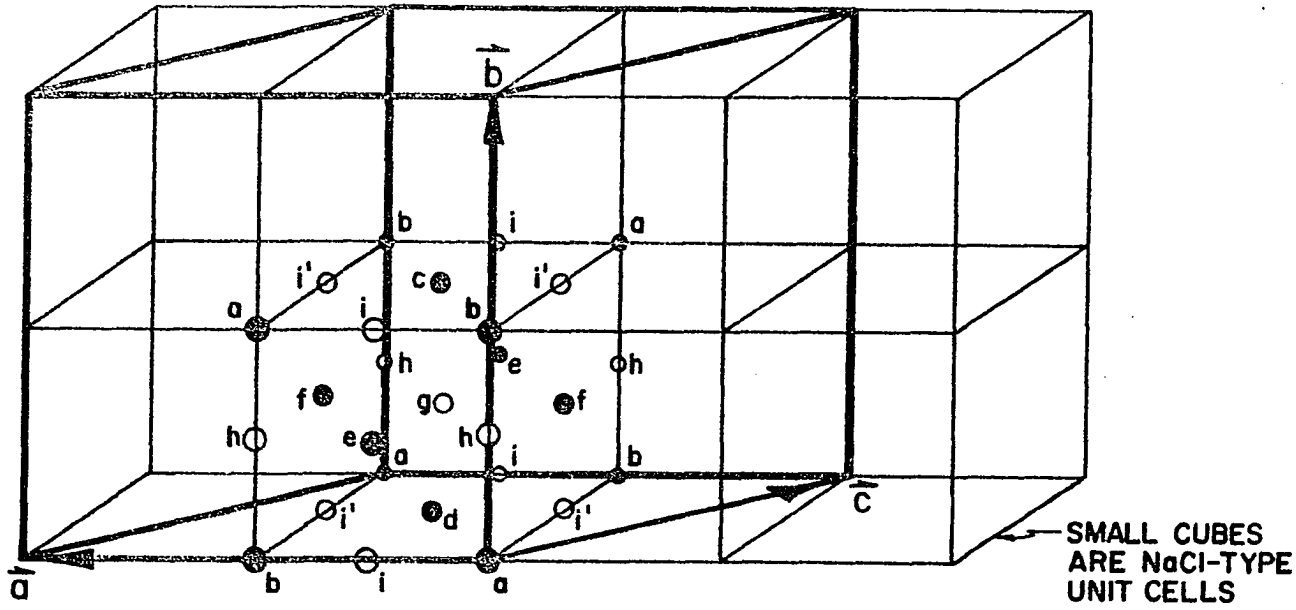

Figure 42. A perspective drawing of the structure of $Zr_{0.77}S$. The monoclinic cell is shown by heavy lines; the NaCl-type ZrS cells are shown as thin-lined cubes

trigonal prismatic; the metal atom coordination in these structures has a tendency to be cubic. The coordination symmetry and the physical properties of these compounds are consistent with the proposal that the bonding is covalent, directional, and electron-deficient as discussed previously for Ti_2S and $Nb_{21}S_8$.

The structure of ZrS_{1-x}, in which the defects are distributed randomly, is WC-type, the same as HfS (114). The WC-type structure is illustrated in Figure 46(b), Appendix C. Both metal and non-metal have trigonal prismatic coordination symmetry. The metal-metal distance in ZrS_{1-x} and HfS is 3.43Å, corresponding to a Pauling bond order of about 0.08. The bonding is, therefore, primarily between metal and chalcogen, e.g., bond orders of 0.59 for Zr-S bonds in ZrS_{1-x} and 0.63 for Hf-S bonds in HfS. Accordingly, the valence of S in ZrS_{1-x}, assuming Zr sites filled, is 3.54 and the valence of Hf and S in HfS is 3.78. The high valences for sulfur in these compounds together with trigonal prismatic symmetry suggests that participation by sulfur in the bonding in ZrS_{1-x} is similar to that given previously for more metal-rich chalconides. The difference in bonding between ZrS_{1-x} and Zr_2S, for example, seems to be primarily in the amount of zirconium-zirconium bonding and the degree of sulfur coordination.

The structure of ZrS (1:1 composition) is the NaCl-type in which the coordination of both metal and chalcogen is octahedral, as shown in Figure 46(e), Appendix C. This structure will be

discussed below.

2. The $Zr_{0.77}S$ structure

The structure of $Zr_{0.77}S$ reported here is, to a good approximation, a superstructure of the ZrS structure (NaCl-type), whereby superstructure is meant a structure for which the space group of the atom positions, termed the substructure space group, is different from the space group of the structure due to the incomplete occupancy of one or more atom positions (six positions in $Zr_{0.77}S$, with four empirically different occupancies). The monoclinic structure of $Zr_{0.77}S$ is a superstructure of ZrS insofar as the shifts of atomic positions in the monoclinic cell from what they are in the cubic cell are insignificant, as can be seen to be very nearly the case from the data in Tables 52 and 56. The relatively small shifts in the sulfur positions (4σ or less in every case) indicate that the assumption made previously, that scattering by sulfur contributed negligibly to other than even-even-even parity reflections, was valid. All available evidence (1, 106, 108, 109, 110) suggests that the composition Zr/S = 0.77 falls in a one-phase region which contains Zr/S $\cong$ 1.0 and Zr/S $\cong$ 0.66 as limiting compositions.

The long-range forces which order the zirconium vacancies in three dimensions in $Zr_{0.77}S$ are at this time not well understood. Solid state research in defect characterization and theory is presently very active, primarily in transition metal oxide systems, e.g., TiO, VO and FeO. It is hoped that consid-

eration of $Zr_{1-x}S$ will contribute to that research.

3. The existence of an uncharacterized higher sulfide of zirconium

A sample which has an initial ratio of S/Zr equal to 1.5 was annealed at 1230°C for one hour. In the unequilibrated product three sets of diffraction lines were observed in the Debye-Scherrer powder patterns: 1) ZrS_{1-x} lines, 2) $Zr_{1-x}S$ lines, and 3) lines which could not be indexed on bases of either ZrS_2, ZrS_3, ZrOS or any metal-rich phase. These lines were located at the following $\sin^2\theta$ values:

0.02062

0.02192

0.02744

0.03740

0.05011

These diffraction lines may arise from an uncharacterized sulfide with S/Zr > 1.5.

4. Some metal-rich oxides of zirconium and titanium

The crystal structure of Zr_3O was determined by Holmberg and Dagerhamn (115). Like the structures of Ti_2O and Ti_3O discussed in Chapter II, Zr_3O is a superstructure of the hexagonal close-packed metal structure. The oxygen atoms at the ideal composition are completely ordered in 1/3 of the octahedral interstices. The valence of oxygen in Zr_3O, based on Pauling bond orders, is 3.12, a valence consistent with Rundle's (42) view of octahedral coordination (see Chapter I) in which

oxygen uses s and p orbitals to form six directional bonds of approximate order 1/2.

ZrO, like ZrS, has the NaCl-type structure (116). This similarity, however, is not expected in terms of the bonding proposal that sulfur is potentially different from oxygen when in combination with transition metals due to the availability of outer orbitals.

TiO has the NaCl-type structure in which approximately 15% of Ti and O vacancies are randomly distributed (117, 118). A low temperature form of TiO was observed by means of electron diffraction by Watanabe, Castles, Jostsons, and Malin (119) to have a monoclinic ordering of the titanium and oxygen vacancies. Another ordered structure with tetragonal symmetry was observed by Watanabe, et al. (120) at the composition $TiO_{1.25}$ to be stable over a narrow range of composition and to have an arrangement of vacancies different from that in the low temperature form of TiO. A third ordered structure of TiO_x was observed (121) at the intermediate composition $TiO_{1.19}$ and appears to be a mixture of the ordered monoclinic and tetragonal structures.

5. The stability of ZrS having the NaCl-type structure

ZrS is an anomaly, along with ZrSe, in the chemistry of Groups IVB and VB transition metal chalconides inasmuch as they are the only known chalconide compounds of the aforementioned metals with Ch/M < 1.3 which have octahedral coordination symmetry of the chalcogen. Possible considerations to explain this structural difference are offered in this discussion. The

discussion is partitioned as follows: 1) a consideration of distances and valences, observed and calculated, respectively, for various NaCl MX compounds (M = Group IVB transition metals, X = C, N, O, S); 2) a consideration of radius ratio arguments in an attempt to explain ZrS; and 3) a consideration of valence electron concentration and orbital availability in MX compounds.

(1) Table 58 lists the carbides, nitrides, oxides and sulfides of Group IVB metals having the NaCl-type structure. The vacancy concentration, the cell size, the metal-metal distances, and the metal-nonmetal distances are listed. The valences were calculated using Pauling's relationship, Equation 16, in which Pauling's (41) single bond radii were used: O=0.66Å, N=0.70Å, C=0.77Å, S=1.04Å. As is quite evident in Table 58 the metal-metal distances are fairly long, much longer than in the respective elemental solids. This fact was observed by Rundle (42), as discussed in Chapter I, and is consistent with his proposal that the bonding in these compounds is primarily between metal and non-metal atoms and that a bonding scheme must take account of that strong interaction. From Rundle's viewpoint the 2s and 2p orbitals on the non-metal can be used to form sp orbitals, with additional bonding utilizing the residual p orbitals. Thus, 1/3 of the bonds are electron pair bonds and 2/3 are half bonds (bond order 1/2). In MX compounds, therefore, for the six equivalent (by "resonance") bonds formed, each one has an order of 2/3. For only p orbital participation, however, the order of each bond is 1/2. All valences calculated

via Equation 16 are roughly in agreement with Rundle's scheme, that is, the valences are between three and four (1/2 x 6 = 3; 2/3 x 6 = 4). Accordingly, the bond orders and valences for ZrS suggest that both s and p orbitals on the sulfur are involved in bonding to six zirconium atoms.

Table 58. MX(NaCl-type) compounds of Group IV metals. Vacancy concentration, metal-metal and metal-nonmetal distances and valences are listed

Compound	a(Å)	Vac.[a] conc.	Distances(Å) M-M	M-X	Valences[b] V_M	V_X	References
TiC	4.32	2 %	3.16	2.16	4.47	4.47	(122)
TiN	4.24	4 %	3.00	2.12	3.92	3.92	(123)
TiO	4.18	15 %	2.96	2.09	2.76	2.76	(118)
ZrC	4.68	3.5%	3.31	2.34	3.65	3.65	(122)
ZrN	4.58	3.5%	3.24	2.29	3.42	3.42	(123)
ZrO	4.58		3.24	2.29	3.00	3.00	(116)
ZrS	5.16		3.65	2.58	4.25	4.25	This work
HfC	4.63	4 %	3.27	2.31	3.90	3.90	(124)
HfN	4.52		3.20	2.26	3.78	3.78	(125)

[a]Obtained from Denker (54).

[b]Valences are corrected for vacancy concentration.

The metal-rich region of the zirconium-sulfur system, it appears, demonstrates two possible bonding modes for sulfur. The first is that sulfur promotes valence electrons to outer d orbitals, which, in turn, results in enough energy in bonding directionally with zirconium to make up for the energy needed to achieve the promoted state. This bonding for sulfur is characterized by trigonal prismatic symmetry and high valence as, for example, is present in Zr_2S. The second bonding mode is that sulfur uses s and p valence orbitals without promotion to outer orbitals. In this case it would seem that the sulfur energetically prefers octahedral symmetry. The energy differences between these two cases may be subtle and are explored more fully in the third section of this discussion.

Bilz (53) presented a qualitative MO scheme for NaCl-type structures of transition metals. According to this view, ZrS, with ten electrons in molecular orbitals, either (a) has two electrons in a non-bonding 3s level of sulfur, six electrons in T_{1u} bonding orbitals and two electrons in the 5s Zr non-bonding orbital, or (b) has two electrons in an A_{1g} bonding orbital, six electrons in T_{1u} bonding orbitals, and two unpaired electrons in the non-bonding 4d orbitals on Zr. Such unpairing of d electrons in case (b) would lead to paramagnetic susceptibility which has been observed for isoelectronic TiO. No magnetic measurements have been performed on ZrS.

(2) A second way the stability of ZrS might be understood is by the geometry of packing the atoms together. This view

has been promoted with success for "interstitial" compounds, i.e., compounds which have one component in a close-packed structure and another component in interstices of that structure. The requirement for stability for such "interstitials" is that the hole formed by the bonding, spherically symmetric atoms be large enough to accept a spherically symmetric smaller atom. The NaCl-type structure has been described as close-packed metal atoms with non-metal atoms in the octahedral holes. Hägg (52) suggested that the criterion for "interstitial" compounds to form was that $0.41 < r_x/r_m < 0.59$, where r_x is the radius of the interstitial atom and r_m is the radius of the metal atom. For example, TiC fits this criterion, $r_x/r_m=0.5$, using Slater's atomic radii.

A radius ratio consideration of the Group IVB stoichiometric sulfides leads to two rather disturbing, related facts:

(a) The radius ratios of the three compounds TiS, ZrS, and HfS, are all greater than the upper limit proposed by Hägg, namely, 0.71, 0.65, 0.65, respectively. ZrS is the only of the three with the NaCl-type structure. Indeed, from geometrical considerations alone, it would appear that ZrS and HfS should be isostructural.

(b) The ZrS structure has fairly long metal-metal distances and therefore is poorly described as a structure in which the Zr atoms are close-packed.

Thus, while the interstitial concept has been successful in describing many NaCl-type compounds, it appears that it is

not suitable for application to ZrS.

(3) In another attempt to understand ZrS, one might consider the series of compounds ZrS, ZrP, and ZrSi. In this series the number of valence electrons varies. ZrP was found by Irani and Gingerich (126) to have two forms, α-ZrP (slightly phosphorus deficient) which has the NaCl-type structure and β-ZrP (1:1) which has the TiP-type structure. The β-ZrP structure has one-half of the phosphorus atoms with octahedral coordination and one-half in trigonal prismatic coordination. Schachner et al. (127) determined ZrSi to have the FeB-type structure in which the X component has augmented trigonal prismatic coordination. In the ZrSi structure there is extensive Si-Si bonding, since the augmenting atoms adjacent to the rectangular faces of the prism are Si atoms (this is to be contrasted with the augmented trigonal prismatic coordination for sulfur in Zr_2S, for example, for which the augmenting atoms are metals).

In changing the valence electron concentration (v.e.c.) of the X component it appears that the coordination symmetry of the X component undergoes a change from fully octahedral in ZrS to partially trigonal prismatic in β-ZrP to completely trigonal prismatic in ZrSi. By changing the non-metal constituent from silicon to phosphorus to sulfur one could consider the changes of three atomic parameters. The first parameter is the valence electron concentration which increases in going from Si to S. The second and third effects are somewhat more

subtle. The second effect is that the excited state promotion energies for the three gaseous atoms are ordered Si < P > S (see Table 11) and the third effect is that the outer d orbitals for sulfur in a $s^2p^3d^1$ configuration (61), for example, are not contracted as much as the outer d orbitals of the phosphorus atom which, in turn, does not have the d orbitals contracted as much as does the silicon atom (128). Consequently, the ordering of the overlap between non-metal d orbitals and metal orbitals is Si > P > S. It is the contention here that the result of the combination of the second and third effects makes it possible to consider the bonding availability of outer d orbitals to be best for silicon, poorer for phosphorus, and poorer yet for sulfur. The word "bonding" is emphasized because availability of orbitals, in this contention, does not merely result from a low promotion energy, but rather results from a combination promotion energy and bonding energy. In other words, the sulfur d orbitals are not as good bonding atomic orbitals as the P d orbitals, because the sulfur orbitals are more diffuse even though, from a strictly energetic viewpoint, the sulfur d's are more likely to be used in bonding than the P d's because of their lower promotion energy. Thus, trigonal prismatic symmetry in MX compounds of Zr correlates with the bonding availability of d orbitals on the X components and thus correlates with an increase in d character of the conduction band in these solids.

Support for this idea is given by a consideration of the monocarbides of the Group VIB metals. CrC does not exist as such, but is stabilized by a small amount of Ti and has the NaCl-type structure (129). MoC has various forms, two of which are NaCl-type (130) and WC-type (131). WC, of course, has the WC-type structure. The valence electron concentration is the same for these compounds, but the d orbital availability is relatively more enhanced for W with respect to Cr. The stability of the WC structure in this group can be viewed as arising from a greater participation of d orbitals in the conduction band from both metal and non-metal. Likewise, the d orbital participation in $Ti_{0.3}W_{0.7}C$ is diminished and this solid solution has the NaCl-type structure (132).

This last case is complicated by the variance of the v.e.c. Denker (54) has pointed out that in TiC (v.e.c.=8) a bonding band is almost completely filled. He argues that TiN (v.e.c.= 9) and TiO (v.e.c.=10) fill antibonding d states, a proposal in agreement with the lower melting points and hardness of TiN and TiO. The Fermi level in hypothetical NaCl-type WC, it could be argued, would be so high in the antibonding band that the structure would be unstable with respect to the WC-type structure. According to Denker's view, ZrS is isoelectronic with TiO in which the Fermi level lies across antibonding bands.

E. Summary

Three heretofore unknown intermediate compounds in the Zr-S system were prepared and identified: Zr_5S, $Zr_{21}S_8$, and Zr_2S. These compounds have very narrow ranges of composition. $Zr_{21}S_8$ has the $Nb_{21}S_8$-type structure. Zr_2S has the Ti_2S-type structure. Both these structures have augmented trigonal prismatic coordination symmetry of sulfur.

The ZrS_{1-x} phase was confirmed as having the WC-type structure with random distribution of vacancies over a fairly wide range of composition.

ZrS was determined by single crystal methods to have the NaCl-type structure. The occurrence of the octahedral coordination of sulfur in ZrS is rationalized in terms of valence electron concentration and the lack of involvement of d orbitals in the formation of valence bands.

$Zr_{1-x}S$, previously proposed as having either a cubic or rhombohedral superstructure of the NaCl-type by powder diffraction methods, was determined by single crystal methods to have long-range monoclinic ordering of Zr vacancies at the composition $Zr_{0.77}S$.

VI. PROPOSALS FOR FURTHER RESEARCH

A. General Survey of Metal-rich Borides, Silicides, and Phosphides

The previous chapters of this thesis reported work performed on metal-rich chalconide compounds of Groups IVB and VB transition metals. It is interesting, in attempting to find an appropriate way of viewing the bonding in these compounds, to compare the features of metal-rich chalconides with features exhibited by metal-rich phosphides, silicides, and borides. Several outstanding surveys of the crystal chemistry of these compounds have been published. Nevitt (133), in a review of the alloy chemistry of transition elements, discussed silicides. Nowotny (132) surveyed the known alloy chemistry of borides, carbides, nitrides, aluminides, and silicides. Rundqvist's (101) review of binary transition metal phosphides is an excellent compilation of data reported to 1962. In 1965, Rundqvist collaborated with Aronsson and Lundström (134) to compile structures and properties of binary borides, silicides, and phosphides. More recently, Hulliger (135) has provided an extensive survey of the crystal chemistry of the chalconides and pnictides of the transition metals.

One general impression, which results from a survey of the structural features of metal-rich borides, silicides, pnictides and chalconides, is unavoidable. The impression is that the non-metal coordination polyhedra, over wide ranges of composi-

tion and with different transition metals, are strikingly similar--trigonal prismatic or augmented trigonal prismatic. To be sure, the augmenting atoms in the cases of boron and silicon polyhedra are, in many cases, boron and silicon atoms, respectively, and thus, in some borides and silicides, there is extensive boron-boron and silicon-silicon bonding. Also, silicon has a tendency to have square anti-prismatic coordination in many metal-rich silicides, but this coordination is not very much different from trigonal prismatic. The comparison between square anti-prismatic and trigonal prismatic coordination can be viewed in terms of the splitting of degenerate d orbitals under the influence of a crystal field, as is diagramed in Hulliger's (135) review. The d orbital splitting is slightly more severe for the square anti-prism field relative to the trigonal prism field; both fields result in a stabilization of one d orbital relative to the degenerate level. The deviations from an ideal coordination symmetry are interesting in their own right, but perhaps more fundamental to the understanding of the ubiquity of the trigonal prismatic coordination of the non-metal atoms is to attempt to investigate and understand the possible chemical reasons for the stability of that coordination. As the factors which stabilize trigonal prismatic coordination become evident it might then be possible to understand the reasons for distortions of trigonal prismatic coordination symmetry.

The three reviews mentioned above basically try to view the stability of structures in terms of geometrical considerations of packing or "size effects" of atoms or ions. With this kind of approach it is possible to systematize the structural chemistry of many hundreds of compounds, and it is not the intention of this thesis to degrade the arguments which consider the sizes of atoms as being important. Certainly the sizes of atoms, in considering orbital extension, as discussed in Chapter II, is one of the more important aspects of orbital overlap and chemical bonding. However, it is the intention of this thesis to suggest that electronic effects and the directionality, energy, and spacial extension of combinations of appropriate atomic orbitals might be a more appropriate way to systematize and to understand the chemistry of the metal-rich compounds with which the present work is concerned.

In view of the general remarks above, it is proposed that further research involve the careful and systematic characterization of trends in bond distances, coordination symmetry, valence electron concentration, and orbital participation in transition metal-rich boron, silicon, phosphorus, and chalcogen compounds. For this kind of investigation it would be necessary to know the structures and some physical properties of all stable phases in the systems of interest.

B. Specific Proposals

Specifically, research activities which might provide a more complete view of metal-rich compounds are as follows.

1. Proposal #1

Investigate the Ti-S system in the region between Ti and Ti_2S. Recent work by Eremenko and Listovnichii (26) indicates that the metal-rich region of this system may be as complex as the metal-rich region of the Zr-S system.

2. Proposal #2

Investigate the selenides and tellurides of the Groups IVB and VB transition metals.

(a) It would be particularly interesting in this work to attempt to synthesize Hf_2Te. The Hf-Te system, below the 1:1 stoichiometry, has not been adequately investigated, but, on the basis of valence electron concentration and orbital bonding availability, one is tempted to propose that Hf_2Te would be isostructural with Hf_2S and Hf_2Se. It would also be interesting to attempt to measure the amount of d orbital participation by the chalcogen in such a structure. Hf_2Te offers that possibility. Hf^{177} and Te^{125} are both Mössbauer active (136, 137), thus enabling Mössbauer spectra to be observed for both kinds of atomic sites. The most severe problem to be overcome in the Hf-Te system is probably a preparative one. At the high temperatures needed to prepare such a metal-rich phase,

the vapor pressure of tellurium is high. Thus, a technique might be used to prevent the loss of tellurium, e.g., a closed tungsten crucible, which has been used successfully for the preparation of some metal-rich selenides by Smeggil (63) and Strachan[1].

(b) Another interesting study would be the V-Se system. According to the classification of Groups IVB and VB metal-rich chalconides presented in Chapter IV, V_2Se, if stable, would be a CLASS III compound, that is, it would be similar to Nb_2Se and Ta_2S in which the chalcogen contributes fewer bonding electrons than do the chalcogens in CLASS I and II compounds. Indeed, the similarity between the V-S and Nb-S systems and the fact that Nb_2Se is stable suggest that the attempt to prepare and characterize V_2Se would be worthwhile.

3. Proposal #3

Investigate the Th-S system. It has been observed by Dwight (138) that the alloying behavior of Th closely resembles the alloying behavior of the Ti Group IVB metals. Since the Ti_2S-type structure is alloy-like, it would be interesting to try to prepare Th_2S, for example, using high temperature techniques.

---

[1]Strachan, D. M., Department of Chemistry, Iowa State University of Science and Technology, Ames, Iowa. Metal-rich selenide preparations. Private communication. 1969.

4. Proposal #4

Continue the investigation of the Zr-S system. Some areas of interest which were uncovered and/or unanswered in the present research, as discussed in Chapter V, are as follows:

(a) The determination of the crystal structure of Zr_5S. It would be surprising if Zr_5S did not exhibit trigonal prismatic coordination of the sulfur atoms.

(b) The preparation of $Zr_{21}S_8$ in pure form. It would be worthwhile to establish the exact T vs. X phase relations in this region of the Zr-S system.

(c) The establishment of the range of homogeneity and the lattice parameter variations of ZrS_{1-x} (WC-type).

(d) The study of additional compositions in the one phase region $Zr_{1-x}S$. It would be interesting to look at various single crystals of different compositions in an effort to determine the nature of the ordering of defects with changing composition.

(e) The determination of good densities for the 1:1 composition, ZrS, in an effort to determine the number of vacancies present in the NaCl-type lattice. This determination could be compared with other MX compounds which crystallize with the rocksalt structure and which, in some cases, are massively defective at the 1:1 composition, e.g., TiO.

(f) The characterization of the unknown phase which appears to be more sulfur-rich than $Zr_{1-x}S$, as was evidenced

by some unindexable diffraction lines from samples which were in the ZrS-ZrS_2 composition range.

(g) The determination of magnetic susceptibilities for the metal-rich zirconium sulfides.

(h) The calculation of overlap integrals for ZrS in an effort to determine more quantitatively whether Zr-Zr bonding is significant in the ZrS structure.

5. Proposal #5

Initiate careful studies of the Zr-Se and Zr-Te systems in the metal-rich regions. One might expect that the ordering of vacancies in $Zr_{1-x}S$, $Zr_{1-x}Se$, and $Zr_{1-x}Te$ would be similar. Recent powder diffraction experiments performed by Salomons and Wiegers (139) showed that $Zr_{1-x}Se$ could be indexed on a rhombohedral basis. The work reported in Chapter V on $Zr_{1-x}S$ showed the diffraction symmetry of $Zr_{0.77}S$ to be monoclinic. The symmetries of $Zr_{1-x}Se$ and $Zr_{1-x}Te$ should be determined with single crystal studies.

6. Proposal #6

In attempting to more fully characterize the physical properties of metal-rich compounds it would be interesting to conduct quantitative measurements of magnetic and electrical properties on such compounds as Ti_2S, $Nb_{21}S_8$, and Nb_2Se.

This thesis has been concerned with the interpretation of metal-rich structures on the basis of covalent, electron-deficient interactions between energetically available and sizably favorable atomic orbitals. Some results have suggested that

valence electron concentration may be a significant factor in the stabilization of certain structures. In an attempt to determine the significance of valence electron concentration, several predictions can be made and research proposed to check them.

7. Proposal #7

One might be tempted to view the stability of M_3S phases as the result of competition between d orbital participation on the metal or d orbital bonding availability for non-metals and the number of valence electrons per atom. For example, Ti_3Si has the Ti_3P-type structure (140) and V_3Si has the Cr_3O-type structure (141), which can be viewed as having the non-metal surrounded by twelve metal atoms in an icosahedral arrangement. The Ti_3P-type has augmented trigonal prismatic coordination of the non-metal. The distortion of V_3Si might be understood by the fact that the d orbitals for V are less available for bonding, relative to the s and p orbitals, than they are for Ti due to the increase in nuclear charge without concomitant shielding. Brewer (69) discussed the stability of the Cr_3O-type (Cr_3Si-type) structure in terms of a distortion of the d orbitals of the metal to allow better overlap of d orbitals along the direction of close contact of other metal atoms. He pointed out that as the d orbitals become relatively more exposed in the fourth and fifth transition series, strong d electron bonding can occur without this distortion and thus other structure-types are stable.

It would seem, even though the outer d orbitals are energetically available for silicon, that silicon promotes to an excited valence state only when its d orbitals will have good overlap with metal d orbitals. One can then consider increasing the valence electron concentration (substitute P for Si) while, at the same time, decreasing the availability of outer orbitals on the non-metal--consider the Ti_3P (Ti_3P-type structure) (142) and V_3P (Ti_3P-type structure) (142). The occurrence of the Ti_3P structure for both Ti_3P and V_3P suggests that the increase in valence electron concentration, from Ti_3Si to Ti_3P and from V_3Si to V_3P, in spite of the greater promotion energy needed to achieve an excited state for phosphorus relative to silicon, stabilizes the augmented trigonal prismatic coordination of phosphorus. Two final considerations in this series of compounds are Ti_3S and V_3S. As was discussed in Chapter V, for the series of compounds ZrSi, ZrP, and ZrS, the changes in atomic orbitals from P to S are subtle. It is suggested in the present work, however, that the phosphorus d orbitals are more available for bonding that the sulfur d orbitals primarily because of orbital size considerations. Indications are that Ti_3S has the Ti_3P-type structure (26). V_3S is known to have a structure which may be viewed as exhibiting features between the Cr_3O-type and Ti_3P-type structures (99). These observations suggest that silicon has too few valence electrons to promote to an excited state when in combination with vanadium. Phosphorus apparently has enough valence electrons and is able

to adopt an excited valence configuration. Sulfur, however, even though having more valence electrons than phosphorus, has less bonding availability of excited valence states than phosphorus so that sulfur, in V_3S, adopts a coordination which is half-way between that coordination adopted for silicon and phosphorus in V_3X compounds. If this argument has some validity, then one would expect to find a $V_3(P,Si)$ with the V_3S-type structure since, according to the argument presented, it would appear possible to achieve the same balance between valence electron concentration and outer orbital availability in $V_3(P, Si)$ as seems to be present in V_3S.

It is interesting to note that Nb_3Si and Ta_3Si both have the Ti_3P-type structure (140), while V_3Si has the Cr_3O-type structure. This difference can be understood in terms of the increased availability of niobium and tantalum d orbitals for bonding with the silicon outer d orbitals as compared with the vanadium d orbitals which are relatively compact.

8. Proposal #8

It would be interesting to study the series of compounds ZrS, Zr_2SC, and ZrC. The structure-types of these compounds are, respectively, NaCl, H-phase, and NaCl. The Zr_2Sc structure was determined by Kudielka and Rohde (20) and is of the Cr_2AlC-type of H-phase type. The Zr_2SC structure is interesting because the sulfur has trigonal prismatic coordination while the carbon has octahedral coordination. It could be argued, however, that the carbon finds the octahedral site more favor-

able because of its small size. A similar study could be performed with more equal-sized constituents. For example, consider the series, ZrP (NaCl) (126), Zr_2PS (?), and ZrS (NaCl). It would be interesting to determine if phosphorus and sulfur have coordination preferences in Zr_2PS. Any preference or absence thereof might be correlated with differences in bonding availability of the outer orbitals of these non-metals.

9. Proposal #9

A generalization can be made regarding the occurrence of metal-rich phosphides as compared with metal-rich sulfides: there are more transition metal-rich phosphides than metal-rich sulfides. This is particularly true as the d orbitals of the metal constituent become more populated, i.e., as the metal constituent varies from left to right in a transition series. This observation might be understood in terms of the greater participation in bonding of d orbitals of phosphorus relative to sulfur.

(a) As compared with the Fe-P and Co-P systems, the Ni-P system is quite complex. For example, the following phases have been observed: Ni_3P (Fe_3P-type) (100), $Ni_{2.55}P$ (143), $Ni_{12}P_5$ (144), Ni_2P (Fe_2P-type) (145), Ni_5P_4 (143), and NiP (143). It is possible that the Ni-S system is also more complex than the Fe-S or Co-S system. Phases reported in the metal-rich region of the Ni-S system are $Ni_{3\pm x}S_2$ (146), Ni_3S_2 (147), $Ni_4S_{3\pm x}$ (148), Ni_6S_5 (146), Ni_7S_6 (135), and Ni_9S_8

(148). All of these phases, however, have compositions S/Ni greater than 0.6. It would be worthwhile to investigate this system with increased metal content using high temperature preparative techniques.

(b) The Pd-S system (149) is complex in the metal-rich region: Pd_4S (150), Pd_3S (151), and $Pd_{2.2}S$ exist. Likewise, the reported phases in the Pd-Se system (149) are $Pd_{6-7}Se$, Pd_4Se (150), $Pd_{2.8}Se$, and $Pd_{17}Se_{15}$ (152), and in the Pd-Te system (149) are Pd_4Te, Pd_3Te, Pd_5Te_2, and Pd_2Te. In contrast, there have been no reports of metal-rich platinum chalconides. The lack of stability of metal-rich platinum chalconides cannot be understood in terms of valence electron concentration, orbital availability effects, or geometrical factors. It would be worthwhile, therefore, to attempt to prepare metal-rich compounds in the Pt-S, Pt-Se, and Pt-Te systems.

10. Proposal #10

Another interesting observation in metal-rich boron-phosphorus chemistry is that Fe_3B does not exist, but is stabilized by a small amount of phosphorus (134). There are two major differences between boron and phosphorus: a) outer d orbitals are more available for bonding on phosphorus than on boron, and b) phosphorus has more valence electrons than does boron. It would be interesting to study the Fe-B-Si system in the composition range Fe_3B to Fe_3Si, and to compare the results to the Fe_3

(P,B) data. By the addition of silicon, instead of phosphorus, to Fe_3B, one might look for structural features stabilized by increased d orbital bonding (Si compared with P) and/or decreased valence electron concentration (Si compared with P). On the other hand, it would be equally interesting to study the Fe-B-S system, comparing, once again, the results with the Fe (P, B) data. The addition of sulfur rather than phosphorus to Fe_3B would allow one to observe structural features which were stabilized by decreased d orbital bonding (S relative to P) and/or increased valence electron concentration (S relative to P).

11. Proposal #11

Co_3P has not been observed. Depending upon the conclusion reached in experiments dealing with Proposal #10, one could add sulfur or silicon to attempt to stabilize $Co_3(P,S)$ or $Co_3(P,Si)$. This kind of study might provide insight into the relative importance of various competing factors which lead to the stabilization of metal-rich structures.

12. Proposal #12

It would be interesting, in view of the similarities between $Nb_{21}S_8$ and Nb_2Se (see Chapter IV), and also in view of their differences, to study the extent of solubility of Se in $Nb_{21}S_8$ and of S in Nb_2Se. This study might provide a way of understanding more clearly the apparently subtle factors which stabilize a CLASS II compound over a CLASS III compound in the Nb-S system and a CLASS III compound instead of a CLASS II com-

pound in the Nb-Se system (see Chapter IV for the definition of CLASS). The outstanding differences between atomic S and Se seem to be in orbital sizes and in slight differences in relative atomic orbital energy levels.

BIBLIOGRAPHY

1. Strotzer, E. F., Biltz, W. and Meisel, K., Z. anorg. allg. Chem., 242, 249 (1939).

2. Bartram, S. F., Ph.D. Thesis, Rutgers University, New Brunswick, New Jersey, 1958.

3. Buerger, M. J., Crystal Structure Analysis, 1st edition, John Wiley and Sons, Inc., New York, N. Y., 1960.

4. Stout, G. H. and Jensen, L. H., X-ray Structure Determination, 1st edition, The Macmillan Company, New York, N. Y., 1968.

5. Hambling, P. G., Acta Cryst., 6, 98 (1953).

6. Dahm, D. J., Benson, J. E., Nimrod, D. M., Fitzwater, D. R. and Jacobson, R. A., U. S. Atomic Energy Report IS-1701 [Iowa State Univ., Ames, Institute for Atomic Research], 1967.

7. Busing, W. R. and Levy, H. A., Acta Cryst., 10, 180 (1957).

8. Williams, D. E., U. S. Atomic Energy Report IS-1052 [Iowa State Univ., Ames, Institute for Atomic Research], 1964.

9. Busing, W. R., Martin, K. O. and Levy, H. A., Oak Ridge National Laboratory Report ORNL-TM-305 [Oak Ridge National Laboratory, Tennessee], 1962.

10. Johnson, C. K., Oak Ridge National Laboratory Report ORNL-3794 [Oak Ridge National Laboratory, Tennessee], 1965.

11. Yvon, K., Jeitschko, W. and Parthé, E., A Fortran IV Program for the Intensity Calculation of Powder Patterns (1969 version), School of Metallurgy and Materials Science, University of Pennsylvania, Philadelphia, Pennsylvania, 1969.

12. Biltz, W., Ehrlich, P. and Meisel, K., Z. anorg. allg. Chem., 234, 97 (1937).

13. Hahn, H. and Ness, P., Z. anorg. allg. Chem., 302, 17 (1959).

14. Hägg, G. and Schönberg, N., Arkiv Kemi, 7, 371 (1954).

15. Jellinek, F., Arkiv Kemi, 20, 447 (1963).

16. Abendroth, R. P. and Schlechten, A. W., Trans. Met. Soc. AIME, 215, 145 (1959).

17. Filonenko, N. E. and Kudryavtsev, V. I., Doklady Akad. Nauk SSSR, 88, 891 (1953).

18. Brown, J. F., Clark, W. D. and Parker, A., Metallurgia, 56, 215 (1957).

19. Frick, C. and Rohde, H., Arch. Eisenhüttenw., 31, 419 (1960).

20. Kudielka, H. and Rohde, H., Z. Kristallogr., 114, 447 (1960).

21. Franzen, H. F. and Gilles, P. W., J. Chem. Phys., 42, 1033 (1965).

22. Franzen, H. F., Ph.D. Thesis, University of Kansas, Lawrence, Kansas, 1962.

23. Stone, G. D., M.S. Thesis, University of Kansas, Lawrence, Kansas, 1963.

24. Owens, J. P., Conard, B. R. and Franzen, H. F., Acta Cryst., 23, 77 (1967).

25. Nylund, A., Acta Chem. Scand., 20, 2393 (1966).

26. Eremenko, V. N. and Listovnichii, V. E., Mater. Seminara, 1st, Kiev (1965). Original not available; abstracted in Chem. Abs., 69, 100519u (1969).

27. Rundqvist, S., Acta Chem. Scand., 16, 1 (1962).

28. Hahn, H. and Harder, B., Z. anorg. allg. Chem., 288, 241 (1956).

29. Schönberg, N., Acta Metallurg., 2, 427 (1954).

30. International Tables for X-ray Crystallography. K. Lonsdale, editor, Kynoch Press, Birmingham, 1952.

31. Hughes, E. W., J. Amer. Chem. Soc., 63, 1737 (1941).

32. Patterson, A. L., Phys. Rev., 46, 372 (1934).

33. Buerger, M. J., Vector Space and Its Application in Crystal-Structure Investigation, John Wiley and Sons, Inc., New York, 1959.

34. Harker, D., J. Chem. Phys., 4, 381 (1936).

35. Hansen, H. P., Herman, F., Lea, J. D. and Skillman, S., Acta Cryst., 17, 1040 (1964).

36. Hughes, E. W., J. Amer. Chem. Soc., 63, 1742 (1941).

37. Levy, H. A., Acta Cryst., 9, 679 (1956).

38. Slater, J. C., J. Chem. Phys., 41, 3199 (1964).

39. Caro, P. E., J. Less-Common Metals, 16, 367 (1968).

40. Franzen, H. F., J. inorg. nucl. Chem., 28, 1575 (1966).

41. Pauling, L., The Nature of the Chemical Bond, 3rd edition, Cornell University Press, Ithaca, N. Y., 1960.

42. Rundle, R. E., Acta Cryst., 1, 180 (1948).

43. Wasastjerna, J. A., Soc. Sci. Fennica Comm. Phys.-Nat., 1: 1 (1923). Original not available; abstracted in Chem. Abs., 18, 1238 (1924).

44. Goldschmidt, V. M., Trans. Faraday Soc., 25, 253 (1929).

45. Pauling, L., Proc. Roy. Soc. (London), A, 114, 181 (1927).

46. Zachariasen, W. H., Z. Kristallogr., 81, 1 (1932).

47. Slater, J. C., Quantum Theory of Molecules and Solids, Volume 2, McGraw-Hill Book Company, Inc., New York, N. Y., 1963.

48. Sanderson, R. T., J. inorg. nucl. Chem., 28, 1553 (1966).

49. Moody, G. J. and Thomas, J. D. R., J. Chem. Soc. 1964, 1417 (1964).

50. Rundle, R. E., "Theories of Bonding in Metals and Alloys", in Intermetallic Compounds, J. H. Westbrook, Ed., John Wiley and Sons, Inc., New York, N. Y., 1967, Chapter 2.

51. Geller, S., Acta Cryst., 9, 885 (1956).

52. Hägg, G., Z. Physik. Chem. (Leipzig), 12B, 33 (1931).

53. Bilz, H., Z. Physik, 153, 338 (1958).

54. Denker, S. P., J. Less-Common Metals, 14, 1 (1968).

55. Moore, C. E., National Bureau of Standards (U. S.), Circular 467 (1949).

56. Callaway, J., Energy Band Theory, Academic Press, Inc., New York, N. Y., 1964, p. 150.

57. Holmberg, B., Acta Chem. Scand., 16, 1245 (1962).

58. Holmberg, B., Acta Chem. Scand., 16, 1255 (1962).

59. Craig, D. P. and Zauli, C., J. Chem. Phys., 37, 601 (1962).

60. Craig, D. P. and Zauli, C., J. Chem. Phys., 37, 608 (1962).

61. Coulson, C. A. and Gianturco, F. A., J. Chem. Soc. 1968, 1618 (1968).

62. Hoard, J. L., J. Amer. Chem. Soc., 61, 1252 (1939).

63. Smeggil, J. G., Ph.D. Thesis, Iowa State University of Science and Technology, Ames, Iowa, 1969.

64. Franzen, H. F. and Norrby, L. J., Acta Cryst., B24, 601 (1968).

65. Franzen, H. F. and Graham, J., Z. Kristallogr., 123, 133 (1966).

66. Franzen, H. F., Smeggil, J. and Conard, B. R., Mat. Res. Bull., 2, 1087 (1967).

67. Engel, N., Ingenïören, M101 (1939). Original not available; summarized in English in Powder Metallurgy Bulletin, 7, 8 (1954).

68. Brewer, L., "Thermodynamic Stability and Bond Character in Relation to Electronic Structure and Crystal Structure", in Electronic Structure and Alloy Chemistry of the Transition Elements, P. A. Beck, Ed., Interscience, New York, N. Y., 1963.

69. Brewer, L., "Prediction of High Temperature Metallic Phase Diagrams", in High Strength Materials, V. F. Zackay, Ed., John Wiley and Sons, Inc., New York, N. Y., 1965.

70. JANAF (Joint Army Navy Air Force) Tables. The Dow Chemical Company, Midland, Michigan, 1962.

71. JANAF (Joint Army Navy Air Force) Tables. The Dow Chemical Company, Midland, Michigan, 1965.

72. JANAF (Joint Army Navy Air Force) Tables. The Dow Chemical Company, Midland, Michigan, 1966.

73. Hultgren, R., Orr, R. L., Anderson, P. D. and Kelley, K. K., Selected Values of Thermodynamic Properties of Metals and Alloys, John Wiley and Sons, Inc., New York, N. Y., Supplement, 1966.

74. Hultgren, R., Orr, R. L., Anderson, P. D. and Kelley, K. K., Selected Values of Thermodynamic Properties of Metals and Alloys, John Wiley and Sons, Inc., New York, N. Y., Supplement, 1967.

75. Biltz, W. and Köcher, A., Z. anorg. allg. Chem., 237, 369 (1938).

76. Jellinek, F., Brauer, G. and Müller, H., Nature, Lond., 185, 376 (1960).

77. Kadijk, F. and Jellinek, F., to be published; cited by Ruysink, A. F. J., Kadijk, F., Wagner, A. J. and Jellinek, F., Acta Cryst., B24, 1614 (1968).

78. Ruysink, A. F. J., Kadijk, F., Wagner, A. J. and Jellinek, F., Acta Cryst., B24, 1614 (1968).

79. Kadijk, F., Ph.D. Thesis, The State University, Groningen, The Netherlands, 1969.

80. Franzen, H. F., DeJong, V. W. and Conard, B. R., J. inorg. nucl. Chem., 28, 3052 (1966).

81. Franzen, H. F., Beineke, T. A. and Conard, B. R., Acta Cryst., B24, 412 (1968).

82. Edwards, J. W., Speiser, R. and Johnston, H. L., J. Appl. Phys., 22, 424 (1951).

83. Woolfson, M. M., Direct Methods in Crystallography, Clarendon Press, Oxford, 1961.

84. Wilson, A. J. C., Acta Cryst., 2, 318 (1949).

85. Harker, D. and Kasper, J. S., Acta Cryst., 1, 70 (1948).

86. Zachariasen, W. H., Acta Cryst., 5, 68 (1952).

87. Cochran, W. and Woolfson, M. M., Acta Cryst., 8, 1 (1955).

88. Hauptmann, H. and Karle, J., Solution of the Phase Problem, I. The Centrosymmetric Crystal: ACA Monograph No. 3, The Letter Shop, Wilmington, 1953.

89. Selte, K. and Kjekshus, A., Acta Chem. Scand., 17, 2560 (1963).

90. Grønvold, F., Kjekshus, A. and Raaum, F., Acta Cryst., 14, 930 (1961).

91. Howells, E. R., Phillips, D. C. and Rogers, D., Acta Cryst., 3, 210 (1950).

92. Lipson, H. and Woolfson, M. M., Acta Cryst., 5, 680 (1952).

93. Hamilton, W. C., Acta Cryst., 18, 502 (1965).

94. Hahn, H. and Ness, P., Z. anorg. allg. Chem., 302, 37 (1959).

95. Hahn, H. and Ness, P., Z. anorg. allg. Chem., 302, 136 (1959).

96. Furuseth, S., Selte, K. and Kjekshus, A., Acta Chem. Scand., 19, 95 (1965).

97. Røst, E. and Gjertsen, L., Z. anorg. allg. Chem., 328, 299 (1964).

98. Røst, E., Gjertsen, L. and Haraldsen, H., Z. anorg. allg. Chem., 333, 301 (1964).

99. Pedersen, B. and Grønvold, F., Acta Cryst., 12, 1022 (1959).

100. Aronsson, B., Acta Chem. Scand., 9, 137 (1955).

101. Rundqvist, S., Arkiv Kemi, 20, 67 (1962).

102. Knausenberger, M., Brauer, G. and Gingerich, K. A., J. Less-Common Metals, 8, 136 (1965).

103. Franzen, H. F. and Smeggil, J. G., Acta Cryst., in press.

104. Franzen, H. F. and Smeggil, J. G., submitted for publication in Acta Cryst.

105. McCullough, J. D., Brewer, L. and Bromley, L., Acta Cryst., 1, 287 (1948).

106. Hahn, H., Harder, B., Mutschke, U. and Ness, P., Z. anorg. allg. Chem., 292, 82 (1957).

107. Jellinek, F. and Hahn, H., Naturwissensch., 49, 103 (1962).

108. McTaggert, F. K. and Wadsley, A. D., Australian J. Chem., 11, 445 (1958).

109. Bracuti, A. J. J., Ph.D. Thesis, Rutgers University, New Brunswick, New Jersey, 1958.

110. Steiger, R. P., Ph.D. Thesis, University of Iowa, Iowa City, Iowa, 1968.

111. Claassen, A. and Burgers, W. G., Z. Kristallogr., A86, 100 (1933).

112. Wilson, A. J. C., Nature, 150, 152 (1942).

113. Birge, R. T., Am. J. Phys., 7, 351 (1939).

114. Franzen, H. F. and Graham, J., J. inorg. nucl. Chem., 28, 377 (1966).

115. Holmberg, B. and Dagerhamn, T., Acta Chem. Scand., 15, 919 (1961).

116. Schönberg, N., Acta Chem. Scand., 8, 1460 (1954).

117. Erhlich, P., Z. anorg. allg. Chem., 247, 53 (1941).

118. Andersson, S., Collen, B., Kuylenstierna, U. and Magnéli, A., Acta Chem. Scand., 11, 1641 (1957).

119. Watanabe, D., Castles, J. R., Jostsons, A. and Malin, A. S., Acta Cryst., 23, 307 (1967).

120. Watanabe, D., Terasaki, O., Jostsons, A. and Castles, J. R., J. Phys. Soc. Japan, 25, 292 (1968).

121. Watanabe, D., Terasaki, O., Jostsons, A. and Castles, J. R., "Electron Microscope Study on the Structure of Low Temperature Modification of Titanium Monoxide Phase", paper presented at the Solid State Chemistry Advanced Study Institute, Scottsdale, Arizona, April, 1969. To be published in Proceedings of that Institute, L. Eyring and M. O'Keeffe, editors (1969).

122. Elliott, R. O., J. Phys. Chem., 62, 630 (1958).

123. Vainshtein, E. Ye., Verkhoglyadova, T. S., Zhurakovskii, Ye. A. and Samsonov, G. V., Physics of Metals and Metallography, 12(3), 52 (1961).

124. Benesovsky, F. and Rudy, E., Planseeber. Pulvermet., 8, 66 (1960).

125. Rudy, E. and Benesovsky, F., Monatsh. Chem., 92, 415 (1961).

126. Irani, K. S. and Gingerich, K. A., J. Phys. Chem. Solids, 24, 1153 (1963).

127. Schachner, H., Nowotny, H. and Kudielka, H., Monatsh. Chem., 85, 1140 (1954).

128. Webster, B. C., J. Chem. Soc. 1968, 2909 (1968).

129. Bloom, D. S. and Grant, N. J., Trans. AIME, 188, 41 (1950).

130. Clougherty, E. V., Lothrop, K. H. and Kafalas, J. A., Nature, 191, 1194 (1961).

131. Kuo, K. and Hägg, G., Nature, 170, 245 (1952).

132. Nowotny, H., "Alloy Chemistry of Transition Element Borides, Carbides, Nitrides, Aluminides, and Silicides," in Electronic Structure and Alloy Chemistry of the Transition Elements, P. A. Beck, Ed., Interscience, New York, N. Y., 1963.

133. Nevitt, M. V., "Alloy Chemistry of Transition Elements," in Electronic Structure and Alloy Chemistry of the Transition Elements, P. A. Beck, Ed., Interscience, New York, N. Y., 1963.

134. Aronsson, B., Lundström, T. and Rundqvist, S., Borides, Silicides, and Phosphides, John Wiley and Sons, Inc., New York, N. Y., 1965.

135. Hulliger, F., Structure and Bonding, 4, 83 (1968).

136. Wertheim, G. K., Science, 144, 253 (1964).

137. Unland, M. L., J. Chem. Phys., 49, 4514 (1968).

138. Dwight, A. E., Nature, 187, 505 (1960).

139. Salomons, W. and Wiegers, G. A., The system zirconium-selenium, unpublished results, Groningen, The Netherlands, 1969.

140. Schubert, K., Raman, A. and Rossteutscher, W., Naturwissensch., 51, 506 (1964).

141. Alekseevskii, N. E., Savitskii, E. M., Baron, V. V. and Efimov, Yu. V., Doklady Akad. Nauk SSSR, 145, 82 (1962). Original not available; abstracted in Chem. Abs., 57, 15951g (1962).

142. Lundström, T., Acta Chem. Scand., 17, 1166 (1963).

143. Larsson, E., Arkiv Kemi, 23, 335 (1965).

144. Rundqvist, S. and Larsson, E., Acta Chem. Scand., 13, 551 (1959).

145. Blaugher, R. D., Holm, J. K. and Yocom, P. N., J. Phys. Chem. Solids, 26, 2037 (1965).

146. Liné, G. and Huber, M., Compt. Rend. Acad. Sci. Paris, 256, 3118 (1963). Abstracted in English in Chem. Abs., 59, 1156a (1963).

147. Kullerud, G. and Yund, R. A., J. Petrol, 3, 126 (1962). Original not available; abstracted in Chem. Abs., 57, 2908h (1962).

148. Kuznetsov, V. G., Eliseev, A. A., Shpak, Z. S., Palkina, K. K., Sokolova, M. A. and Dmitriev, A. V., Vopr. Met. i Fiz. Poluprov., 159 (1961). Original not available; abstracted in Chem. Abs., 56, 5444g (1962).

149. Grønvold, F. and Røst, E., Acta Chem. Scand., 10, 1620 (1956).

150. Grønvold, F. and Røst, E., Acta Cryst., 15, 11 (1962).

151. Røst, E. and Vestersjø, E., Acta Chem. Scand., 22, 819 (1968).

152. Geller, S., Acta Cryst., 15, 713 (1962).

153. Thorn, R. J. and Winslow, G. H., Recent Developments in Optical Pyrometry, ASME unpublished paper No. 63-WA-224, 1963.

APPENDIX A: PYROMETER CALIBRATION

The pyrometer used in this work was calibrated using the technique of sectored disks described by Thorn and Winslow (153). The freezing point of Cu was used as the standard for the pyrometer temperature scale. Another temperature was established from the standard temperature, S_o, by heating a W crucible with a blackbody hole to some unknown temperature, T_1, such that S_o was obtained when the blackbody was viewed through a rotating sectored disk of known transmissivity. By removing the sectored disk an additional point on the pyrometer scale, S_1, was determined. By repetition of this procedure, using S_1 as the reference, higher S values were obtained. The corrections between the true temperatures calculated via Wien's equation and the pyrometer temperature scale were obtained for temperatures in the range 1000-1900°C. These corrections for the three optical pyrometer scales are plotted in Figure 43.

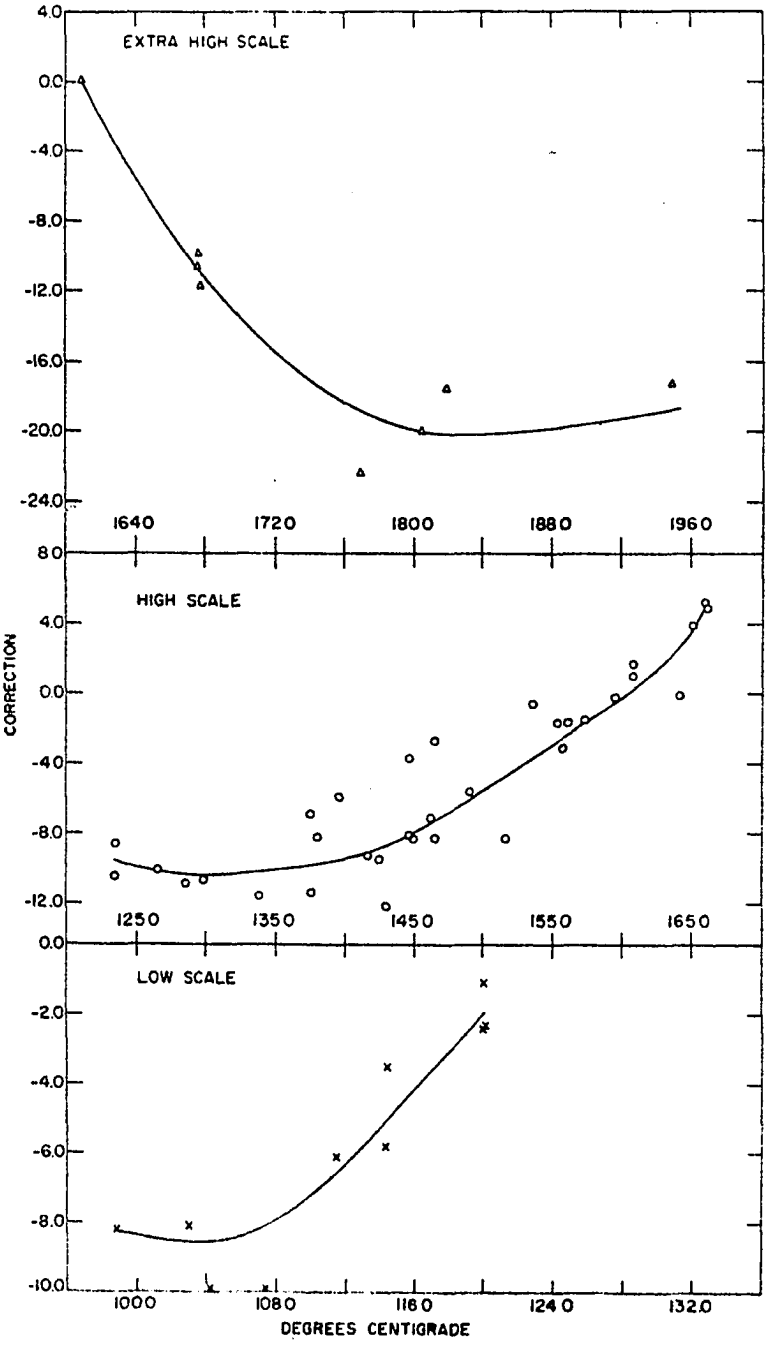

Figure 43. Plots of correction temperature vs. observed temperature for three scales, LOW, HIGH, XHIGH, of Leeds and Northrup optical pyrometer

APPENDIX B: SLATER AND PAULING RADII

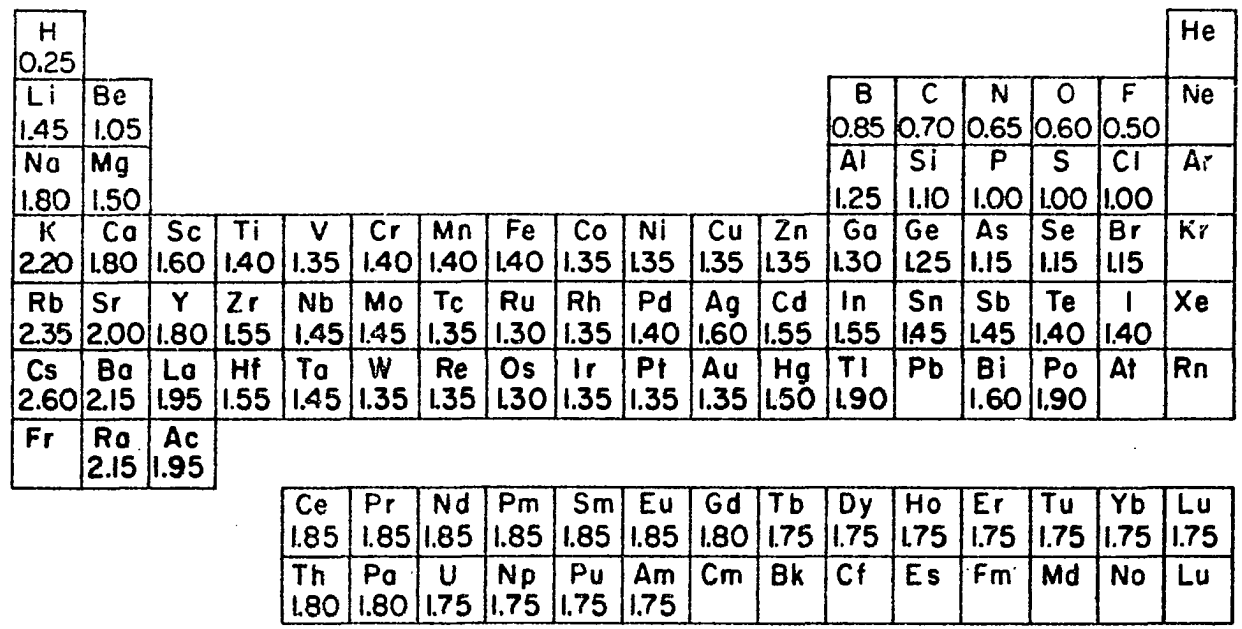

Figure 44. Tabulation of Slater's (39) atomic radii (in Å)

H																	He
Li 1.22	Be 0.89											B 0.80	C	N	O	F	Ne
Na 1.57	Mg 1.36											Al 1.25	Si 1.17	P 1.10	S 1.04	Cl	Ar
K 2.02	Ca 1.74	Sc 1.44	Ti 1.32	V 1.22	Cr 1.19	Mn 1.18	Fe 1.17	Co 1.16	Ni 1.15	Cu 1.18	Zn 1.21	Ga 1.25	Ge 1.24	As 1.21	Se 1.17	Br	Kr
Rb 2.16	Sr 1.91	Y 1.62	Zr 1.45	Nb 1.34	Mo 1.29	Tc 1.27	Ru 1.25	Rh 1.25	Pd 1.28	Ag 1.34	Cd 1.38	In 1.42	Sn 1.42	Sb 1.39	Te 1.37	I	Xe
Cs 2.35	Ba 1.98	La 1.69	Hf 1.44	Ta 1.34	W 1.30	Re 1.28	Os 1.26	Ir 1.26	Pt 1.30	Au 1.34	Hg 1.39	Tl 1.44	Pb 1.50	Bi 1.51	Po	At	Rn
Fr	Ra	Ac															

Ce 1.65	Pr 1.64	Nd 1.64	Pm 1.63	Sm 1.62	Eu 1.85	Gd 1.62	Tb 1.61	Dy 1.60	Ho 1.58	Er 1.58	Tu 1.58	Yb 1.70	Lu 1.56
Th 1.65	Pa	U 1.43	Np	Pu	Am	Cm	Bk	Cf	Es	Fm	Md	No	Lu

Figure 45. Tabulation of Pauling's (41) metallic radii (in Å)

APPENDIX C: NiAs, WC, MnP, NaCl, AND Hf_2S STRUCTURE TYPES

The NiAs-type, WC-type, MnP-type, and NaCl-type structures may be viewed, for descriptive purposes, as the stacking of hexagonal plane nets of atoms in different sequences along the sixfold axes of the nets. The projections of three possible hexagonal nets are shown in Figure 46(a). For example, for one kind of atom, the stacking sequence ...ABABA... is the hexagonal close-packed structure and the sequence ...ABCABC... is the cubic close-packed structure. In the latter case the sixfold axis is destroyed, but a threefold axis remains.

The (110) plane of the hexagonal cell is shown as a heavy line in Figure 46(a); it is seen that this plane contains all the atom positions A, B, and C, and thus a drawing of this plane shows the complete structure. Such a drawing of the (110) plane is shown for the illustration of the WC-type structure in Figure 46(b). The stacking sequence is ...AB'AB'..., where the prime indicates that a different kind of atom occupies the B site relative to the A site. From Figure 46(a) it is seen that the B' site is in a trigonal prismatic environment, three A sites below and three A sites above. The A sites are also in a trigonal prismatic environment of B sites, three above and three below. Figure 46(b) is drawn specifically for ZrS_{1-x} using Slater's atomic radii.

The NiAs-type structure, shown in Figure 46(c), is related to the WC-type. The sequence for NiAs is ...AB'AC'A... Again

Figure 46. Stacking sequences for the WC-type, NiAs-type, MnP-type, NaCl-type, and Hf_2S-type structures (a) Hexagonal plane nets A, B, and C drawn in projection. Heavy line shows the (110) plane of the hexagonal cell; (b) ZrS_{1-x} (WC-type structure) drawn on the (110) plane. Stacking sequence is ...AB'AB'... Radii of atoms are those according to Slater; (c) TiS (NiAs-type structure) drawn on the (110) plane with stacking sequence ...AB'AC'A ...; (d) projection of the MnP-type structure onto the orthorhombic (010) plane. Dotted circles indicate the ideal NiAs positions; (e) ZrS (NaCl-type structure) drawn on the hexagonal (110) plane with stacking sequence ...AC'BA'CB'A...; (f) Hf_2S structure [after Franzen and Graham (74)] drawn on the (110) plane. Stacking sequence is ..BA'BCA'C...

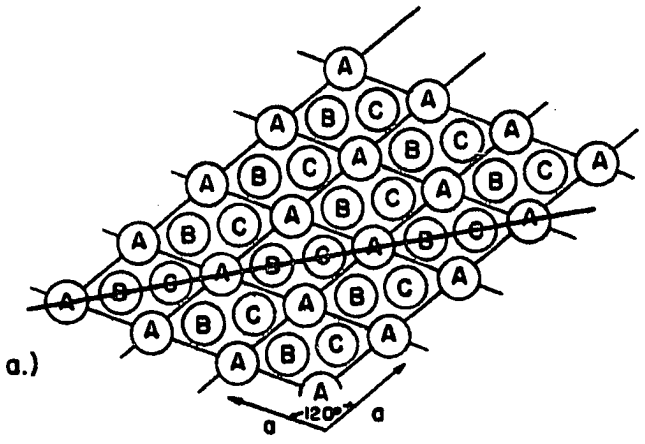
a.)
A
120°
a
a

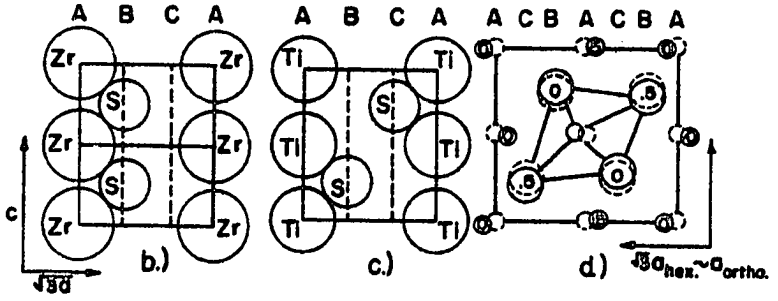
A B C A
Zr
Si
c
√3a
b.)
A B C A
Ti
Si
c.)
A C B A C B A
O
Si
d.)
√3a hex. ~ a ortho.

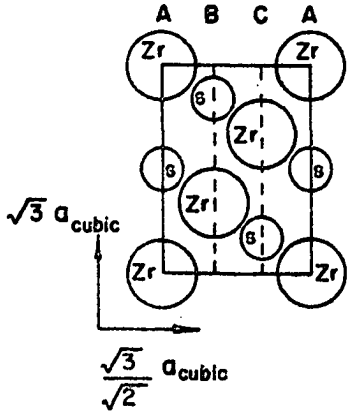
A B C A
Zr
Si
√3 a cubic
√3/√2 a cubic
e.)

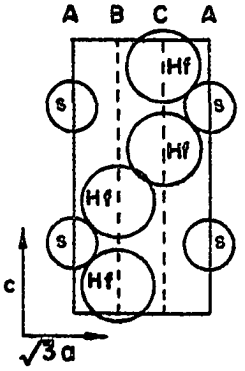
A B C A
Hf
Si
c
√3a
f.)

the B' site is in a trigonal prismatic environment, but the A site has octahedral coordination, three B' sites and three C' sites. The TiS structure is drawn to illustrate the (110) plane of the NiAs structure-type.

The MnP-type structure can be viewed as an orthorhombic distortion of the NiAs-type structure. Figure 46(d) shows a projection of the MnP-type structure onto the orthorhombic (010) plane. The numbers on the atom positions indicate the fractional unit cell distance above the (010) plane of the orthorhombic cell. The dashed circles represent the ideal NiAs positions.

The NaCl-type structure can be viewed in the (110) cubic plane which is equivalent to the (110) hexagonal plane. The stacking sequence is ...AC'BA'CB'A... In this structure each atom is octahedrally surrounded by dissimilar atoms. ZrS is illustrated in Figure 46(e) using Slater's radii.

The Hf_2S structure is shown in Figure 46(f). The stacking sequence is ...BA'BCA'C... The A' site is in a trigonal prismatic environment of either B sites or C sites. The B site has octahedral coordination to three C sites above and three A' sites below. The C site is equivalent to the B site with regard to coordination geometry.

APPENDIX D: $Nb_{21}S_8$ PROBABILITIES

The application of the triple product relationship for sign determination for $Nb_{21}S_8$ is continued from Chapter III in Table 59.

The indices for reflections $\underset{\sim}{H} \pm \underset{\sim}{H}'$ are in column 1 of Table 59, the $|U|$ values for $\underset{\sim}{H} \pm \underset{\sim}{H}'$ are in column 2. Columns 3 and 4 and columns 5 and 6 contain the indices and $|U|$ values for $\underset{\sim}{H}$ and $\underset{\sim}{H}'$, respectively. Column 7 contains the probability that $U_{\underset{\sim}{H} \pm \underset{\sim}{H}'}$ be the same sign as $U_{\underset{\sim}{H}} U_{\underset{\sim}{H}'}$, as calculated by Equation 29. Column 8 lists whether the $S(\underset{\sim}{H} \pm \underset{\sim}{H}') = S(\underset{\sim}{H})S(\underset{\sim}{H}')$ in the final refined structure agrees or disagrees with the assignment of the sign of $(\underset{\sim}{H} \pm \underset{\sim}{H}')$ by means of the triple product relationship.

There are several observations to be noted regarding Table 59: 1) For $|U_{\underset{\sim}{H} \pm \underset{\sim}{H}'}|$ greater than 0.3 and probabilities equal to or greater than 98%, all signs obtained by the triple product relationship agreed with the calculated signs.

2) For one relationship, in which the $|U_{23,7,0}|$ equaled 0.0 and for which the probability that $S(\underset{\sim}{H} + \underset{\sim}{H}') = S(\underset{\sim}{H})S(\underset{\sim}{H}')$ equaled 50%, the derived sign was incorrect.

3) For reflection 30,3,1, derived to have a negative sign with 100% probability, the derived sign was incorrect. The $|U_{30,3,1}| = 0.30$.

4) The sign of reflection 8,2,0 was obtained from three different triple product relationships. The probability that the sign was negative was 97% in two cases and was correct in those cases, whereas the probability that the sign was positive

Table 59. The sign determination of structure factors of $Nb_{21}S_8$ using unitary structure factors of low absolute magnitude. The probability that the sign is corrected as calculated according to Equation 29 is also tabulated

Column 1	Column 2	Column 3	Column 4	Column 5	Column 6	Column 7	Column 8 Agree	Column 8 Disagree
7, 9, 1	0.394	11, 0, 1	0.566	18, 8, 0	0.455	100%	Yes	
11, 5, 0	0.385	18, 8, 0	0.455	7, 3, 0	0.467	100%	Yes	
17, 9, 0	0.380	2,22, 0	0.617	$\bar{11}$, 5, 0	0.385	100%	Yes	
20, 4, 0	0.380	7,20, 1	0.616	$\bar{11}$, 0, 1	0.559	100%	Yes	
32, 5, 1	0.380	0,11, 1	0.559	$\bar{5}$,21, 0	0.528	100%	Yes	
33, 3, 0	0.380	5,15, 0	0.377	$\bar{8}$,18, 0	0.455	100%	Yes	
21,10, 1	0.371	11, 5, 0	0.385	10, $\bar{5}$, 1	0.391	100%	Yes	
7,19, 0	0.370	18, 8, 0	0.455	11,$\bar{11}$, 0	0.421	100%	Yes	
18, 1, 1	0.368	14, 4, 0	0.423	$\bar{4}$, $\bar{3}$, 1	0.495	100%	Yes	
26, 3, 1	0.368	21, 5, 0	0.528	$\bar{5}$, 2, 1	0.609	100%	Yes	
9,30, 1	0.366	11, 5, 0	0.385	$\bar{2}$,25, 1	0.522	100%	Yes	
28, 6, 0	0.365	9,14, 1	0.379	$\bar{15}$,14, 1	0.388	100%	Yes	
31,10, 1	0.363	27,13, 0	0.623	$\bar{4}$, 3, 1	0.495	100%	Yes	
3,15, 0	0.358	21,16, 1	0.418	18, 1, 1	0.368	100%	Yes	
3, 7, 0	0.352	17, 9, 0	0.380	20,16, 0	0.401	100%	Yes	
24,20, 0	0.351	21,16, 1	0.418	3, 4, 1	0.495	100%	Yes	
16, 3, 1	0.351	18, 8, 0	0.455	2, $\bar{5}$, 1	0.609	100%	Yes	
27, 1, 0	0.350	20, 4, 0	0.380	7, $\bar{3}$, 0	0.352	99%	yes	
6, 2, 0	0.350	24,22, 0	0.516	$\bar{18}$,20, 0	0.545	100%	Yes	
23,16, 1	0.347	24, 9, 1	0.625	$\bar{1}$, 7, 0	0.414	100%	Yes	
22, 9, 1	0.347	20, 4, 0	0.380	2, 5, 1	0.609	100%	Yes	
10,24, 0	0.341	7,20, 1	0.616	$\bar{3}$, 4, 1	0.495	100%	Yes	
27, 7, 0	0.337	22, 9, 1	0.347	$\bar{5}$, 2, 1	0.609	100%	Yes	
2,28, 0	0.337	17,23, 0	0.469	$\bar{15}$, $\bar{5}$, 0	0.377	100%	Yes	
26, 6, 0	0.336	22, 9, 1	0.347	4, $\bar{3}$, 1	0.495	100%	Yes	
15, 3, 0	0.335	26, 3, 1	0.368	11, 0, 1	0.566	100%	Yes	
22,17, 1	0.333	11,17. 0	0.534	11, 0, 1	0.566	100%	Yes	

Table 59 (Continued)

Column 1	Column 2	Column 3	Column 4	Column 5	Column 6	Column 7	Column 8	
							Agree	Disagree
21,15, 0	0.332	18, 8, 0	0.455	3, 7, 0	0.352	100%	Yes	
2, 8, 0	0.330	27,13, 0	0.623	25, 5, 0	0.412	100%	Yes	
16, 7, 1	0.329	21,16, 1	0.418	5, 9, 0	0.457	100%	Yes	
23, 0, 1	0.328	25, 5, 0	0.412	2, 5, 1	0.609	100%	Yes	
0,30, 0	0.328	2,25, 1	0.522	2, 5, 1	0.609	100%	Yes	
28,18, 0	0.327	21,15, 0	0.332	7, 3, 0	0.467	100%	Yes	
4,25, 1	0.327	21,10, 1	0.371	4,14, 0	0.423	100%	Yes	
0, 5, 1	0.327	11, 5, 0	0.385	11, 0, 1	0.566	100%	Yes	
7,12, 1	0.326	24,20, 0	0.351	17, 8, 1	0.384	99%	Yes	
15,14, 1	0.323	24,20, 0	0.351	9, 6, 1	0.390	99%	Yes	
20,23, 1	0.323	18, 1, 1	0.368	2,22, 0	0.617	100%	Yes	
23,18, 1	0.320	21,10, 1	0.371	2, 8, 0	0.330	99%	Yes	
27, 2, 1	0.320	23, 7, 0	0.0	2, 5, 1	0.609	50%		Yes
1,32, 1	0.318	27, 1, 0	0.350	5, 2, 1	0.609	100%	Yes	
18, 3, 1	0.317	32, 5, 1	0.380	14, 2, 0	0.368	99%	Yes	
2,17, 1	0.316	2,28, 0	0.337	0,11, 1	0.559	100%	Yes	
20, 1, 1	0.315	4,14, 0	0.423	16,15, 1	0.502	100%	Yes	
13,10, 1	0.314	3,16, 1	0.351	7, 3, 0	0.467	100%	Yes	
14,30, 0	0.311	15, 3, 0	0.335	1,27, 0	0.350	98%	Yes	
11,28, 1	0.311	16, 3, 1	0.351	5,25, 0	0.412	99%	Yes	
19, 9, 0	0.311	24, 9, 1	0.625	5, 0, 1	0.324	100%	Yes	
0,19, 1	0.310	16, 4, 0	0.382	3, 4, 1	0.495	100%	Yes	
18,18, 0	0.309	11,17, 0	0.534	7, 1, 0	0.414	100%	Yes	
22, 3, 1	0.306	17,23, 0	0.469	20, 1, 1	0.315	100%	Yes	
2,16, 0	0.306	14, 4, 0	0.423	2, 6, 0	0.350	100%	Yes	
6,21, 1	0.305	7,20, 1	0.606	14,26, 0	0.475	100%	Yes	
2,13, 1	0.303	16,15, 1	0.502	14, 2, 0	0.368	100%	Yes	
15, 1, 0	0.302	20,16, 0	0.401	5,15, 0	0.377	100%	Yes	
21,24, 1	0.301	3, 4, 1	0.495	18,20, 0	0.545	100%	Yes	
30, 3, 1	0.30	3, 4, 1	0.495	6,26, 0	0.336	100%		Yes
19,13, 0	0.30	7, 1, 0	0.414	20,18, 0	0.545	100%	Yes	

Table 59 (Continued)

Column 1	Column 2	Column 3	Column 4	Column 5	Column 6	Column 7	Column 8 Agree	Column 8 Disagree
18,12, 0	0.30	$\overline{5}$,10, 1	0.391	13,22, 1	0.659	100%	Yes	
14,23, 1	0.30	3, 4, 1	0.495	$\overline{20}$,18, 0	0.545	100%	Yes	
10,26, 0	0.30	18, 8, 0	0.455	$\overline{8}$,18, 0	0.455	100%	Yes	
30, 3, 1	0.30	18, 8, 0	0.455	$\overline{21}$,22, 1	0.400	100%	Yes	
8, 2, 0	0.21	20,12, 0	0.391	12,10, 0	0.405	97%	Yes	
8, 2, 0	0.21	14, 4, 0	0.423	6, 2, 0	0.350	97%		
8, 2, 0	0.21	$\overline{6}$,26, 0	0.366	2,28, 0	0.337	95%		Yes
8,12, 0	0.15	26,20, 0	0.488	18, 8, 0	0.455	97%	Yes	
8,12, 0	0.15	$\overline{8}$,18, 0	0.455	0,30, 0	0.328	93%		Yes
	0.27		0.27		0.27	90%		

was 95% and was incorrect.

5) The sign of reflection 8,12,0 was obtained from two different triple product relationships. The assignment of a positive sign was 97% probable and was correct. The assignment of a negative sign was 93% probable and was incorrect.

These results suggest that for a structure like $Nb_{21}S_8$ the triple product relationship should be used with $|U|$ greater than 0.3 and that signs should be accepted only when their probabilities, calculated according to Equation 29, are greater than 98%.